1134

THE M. W. KELLOGG COMPANY
a subsidiary of Pullman Incorporated

PB 211 431

MWKLG-RED-72-1271

REVIEW OF THE DRY LIMESTONE INJECTION PROCESS

TASK #3 FINAL REPORT FOR PHASE 1

Submitted to
ENVIRONMENTAL PROTECTION AGENCY
AIR POLLUTION CONTROL OFFICE
DIVISION OF PROCESS CONTROL ENGINEERING

Contract No CPA 70-68

May 1, 1972

Reproduced by
NATIONAL TECHNICAL
INFORMATION SERVICE
U S Department of Commerce
Springfield VA 22151

RESEARCH & ENGINEERING DEVELOPMENT

BIBLIOGRAPHIC DATA SHEET

1. Report No. APTD-1136

2.

3. Recipient's Accession No. PB-211 431

4. Title and Subtitle
Review of the Dry Limestone Injection Process
Task # 3 Final Report for Phase 1

5. Report Date May 1972

6.

7. Author(s)

8. Performing Organization Rept. No. MWKLG-RED-72-1271

9. Performing Organization Name and Address
The M. W. Kellogg Company
Research & Engineering Development
Piscataway, N. J.

10. Project/Task/Work Unit No.

11. Contract/Grant No. CPA 70-68

12. Sponsoring Organization Name and Address
ENVIRONMENTAL PROTECTION AGENCY
Office of Air Programs
Division of Control Systems

13. Type of Report & Period Covered Final

14.

15. Supplementary Notes

16. Abstracts The concept reviewed involves injection of the pulverized additive stone directly into the radiation section of the boiler proper to effect the vapor phase calcination and sulfation reactions. The basic objective was to provide an independent assessment of the status of the Dry Limestone Process Technology and to up-date the design bases to reflect any additional process information. All available information was reviewed on the Dry Limestone Injection Process and pertinent correlations and equipment design recommendations were derived wherever possible. The emphasis was placed on the evaluation of data from in situ calcination-sulfation studies taken in flow reactors designed to simulate commercial boilers. The correlation approach was developed for a "shrinking core" model, i.e., where SO_2 gas must diffuse through a reaction product layer ($CaSO_4$) to reach the shrinking inner core of available reactant (CaO). Attempts were made to test the reaction system model against data obtained in other flow reactor studies. Efforts were also made to compare the model with some initial test data from the Shawnee boiler using Limestone 2061. An analysis was made of process effects on the operability of a standard pulverized coal-fired boiler. Available information was reviewed for the obvious important equipment performance parameters, e.g., effect of additives on slagging characteristics, efficiency of dust removal equipment, and sluice water quality control.

17. Key Words and Document Analysis. 17a. Descriptors

Air pollution control equipment
Limestone
Additives
Design criteria
Calcium inorganic compounds
Sulfates
Chemical reactions
Temperature
Sulfur dioxide
Coal
Boilers
Water pollution

17b. Identifiers/Open-Ended Terms

17c. COSATI Field/Group 13B

18. Availability Statement Unlimited

19. Security Class (This Report) UNCLASSIFIED

20. Security Class (This Page UNCLASSIFIED

21. No. of Pages 280

22. Price $3.00

FORM NTIS-35 (REV. 3-72)

USCOMM-DC 14952-P72

RESEARCH AND ENGINEERING DEVELOPMENT

REVIEW OF THE DRY LIMESTONE
INJECTION PROCESS

TASK #3 FINAL REPORT FOR PHASE I

Submitted to
ENVIRONMENTAL PROTECTION AGENCY
AIR POLLUTION CONTROL OFFICE
DIVISION OF PROCESS CONTROL ENGINEERING
Contract No. CPA 70-68

APPROVED: Arlin G. Sliger
Project Director

Warren C. Schreiner
Manager
Chemical Engineering Development

Director
Development Engineering Department

R & ED 20 LAB. 3-68

THE M. W. KELLOGG COMPANY
A DIVISION OF PULLMAN INCORPORATED

Research & Engineering Development

Page No. ____________

Report No. RED-72-1271

REVIEW OF THE DRY LIMESTONE INJECTION PROCESS

TASK #3 FINAL REPORT FOR PHASE I

EPA- OAP-DCS CONTRACT NO. CPA 70-68

May 31, 1971

Staff: J.A. Bellott, G.M. Drissel, C.J. Royce, L.J. Scotti, A.G. Sliger

Period Covered: September 1970 to May 1971

L. O. No. 4092

Distribution:	Copy No.		**Copy No.**
OAP		L. E. Scholer	
L. C. Axelrod		W. C. Schreiner	
A. B. Cassidy		F. H. Shipman	
C. W. Crady		A. G. Sliger	
A. L. Dowling		M. J. Wall	
J. B. Dwyer		T. H. Wasp	
A. N. Holmberg		R.I.D. (4)	
R. H. Multhaup			
J. J. O'Donnell			

AUTHORS: A G Sliger
A. G. Sliger

J.A. Bellott

G M Drissel
G.M. Drissel

C. J. Royce
C.J. Royce

L. J. Scotti
L.J. Scotti

MWKLG-RED-72-1271

REVIEW OF THE DRY LIMESTONE INJECTION PROCESS

TASK #3 FINAL REPORT FOR PHASE I

CONTRACT NO. CPA 70-68

Submitted to
ENVIRONMENTAL PROTECTION AGENCY
OFFICE OF AIR PROGRAMS
DIVISION OF CONTROL SYSTEMS

by
THE M. W. KELLOGG COMPANY
RESEARCH & ENGINEERING DEVELOPMENT
PISCATAWAY, N.J.

May 31, 1971
Rev. December 14, 1971

ic

REVIEW OF THE DRY LIMESTONE INJECTION PROCESS

PHASE I FINAL REPORT

TABLE OF CONTENTS

Page No.

I. INTRODUCTION 1

II. SUMMARY AND CONCLUSIONS 6

III. RECOMMENDATIONS 11

IV. DISCUSSION OF RESULTS 12
  A. Pilot Plant Sulfation Data 12
    1. Battelle Studies 12
      a. Battelle Reactor Design and Conditions of Operation 12
      b. Battelle Data 14
    2. Babcock and Wilcox Studies 21
      a. Data for Limestone Additives 22
      b. Data with Dolomites 27
    3. Peabody Coal Studies 34
      a. Description of Reactor and Conditions of Operation 34
      b. Test Results 35
    4. Shawnee Plant Data 39
  B. Bench Scale Sulfation Data 42
    1. OAP Research Studies 42
    2. TVA Studies 45

TABLE OF CONTENTS

Page No.

IV. DISCUSSION OF RESULTS (Cont'd)

C. Evaluation of Process Models 55
  1. Kellogg Shrinking Core Model 55
    a. Theory and Development 55
    b. Model Parameters and Constants 63
      (1) Effect of Initial SO_2 Concentration 65
      (2) Effect of Temperature 74
      (3) Effect of Limestone Surface Area 74
      (4) Effect of Particle Size 74
      (5) Comparisons with Other Data 77
  2. OAP Model 83
    a. General Model Development 83
    b. Evaluation of Model Constants 95
  3. Wen Model 104
  4. MIT Model 113
D. Calcination Studies 117
  1. Particle Heat-up Calculations 117
  2. Deadburning Studies 122
  3. Battelle Calcination Data 125
  4. TVA Calcination Data 132
E. Gas-Particle Mass Transfer 135
  1. Kellogg Calculations 135
  2. Comparison with Other Studies 148
  3. Comparison with Initial SO_2 Reaction Rates 149

TABLE OF CONTENTS

Page No.

IV. DISCUSSION OF RESULTS (Cont'd)

F. Thermochemical and Physical Property Data 152
  1. Thermodynamic Data 152
  2. Stone Property Data 155
    a. R.D. Harvey Report 155
    b. G.H. McClellan Report 164
G. Process Effects on Equipment Performance 170
  1. Electrostatic Precipitator Efficiency Studies 170
    a. Summary 170
    b. Discussion of Test Results 171
  2. Coal Ash Deposition Studies 179
    a. Summary 179
    b. Fused-Slag Deposits 183
    c. Bonded Deposits 184
  3. Water Quality Control Studies 187

V. REFERENCES 197

APPENDICES

A. Thermochemical Values for Basic Reactions in Flue Gas Sulfur Fixation 201

B. Summary of Experimental Studies of SO_2 Removal Systems 217

C. Shrinking Core Model Development 230

LIST OF TABLES

Table No.	Title	Page No.
1	DRY LIMESTONE PROJECT - TEST RESULTS USING REVISED CALCULATIONS SHAWNEE STEAM PLANT	40
2	SURFACE AREAS OF CALCINED AND HYDRATED COLBERT COUNTY LIMESTONE CALCULATED FROM PORE VOLUMES	49
3	OAP MODEL SYSTEM PARAMETERS FOR DIFFERENT STONES	87
4	A COMPARISON OF THE OAP MODEL TO THE BENCH SCALE DATA FOR A HIGH PURITY DOLOMITE	88-89
5	VALUES OF APCO MODEL CONSTANTS OBTAINED BY NON-LINEAR REGRESSION ANALYSIS USING THE BATTELLE DATA	101
6	DATA KEY FOR WEN'S MODELING STUDIES	106
7	THE EFFECT OF TEMPERATURE ON REACTION PARAMETERS AND EFFECTIVE STRUCTURAL PROPERTIES OF CALCINE 9	114
8	PROPERTIES OF LIMESTONE NUMBER 2061 SET I, 70/140 MESH PARTICLE SIZE RANGE	123
9	BATTELLE CALCINATION DATA (No SO_2 Present) - LIMESTONE NO. 2061	128
10	BATTELLE CALCINATION DATA (In Situ Sulfation) - LIMESTONE NO. 2061	129
11	EFFECT OF INJECTION TEMPERATURE ON SURFACE AREA	131
12	TVA CALCINATION CORRELATION PREDICTIONS ACTIVATION ENERGY 30 KCAL/GM MOL	133
13	MASS TRANSFER CALCULATIONS	139
14	COMPARISON OF SOLIDS CONCENTRATION	144
15	EQUILIBRIUM CONCENTRATION OF SO_2 VERSUS TEMPERATURE	153

LIST OF TABLES (Cont'd)

Table No.	Title	Page No.
16	PETROGRAPHIC DESCRIPTION AND SOURCE OF SAMPLES	156
17	MINERALOGY OF TYPE SAMPLES IN WEIGHT PERCENTAGE	157
18	CHEMICAL ANALYSES IN WEIGHT PERCENTAGE	158
19	TRACE ELEMENT ANALYSES OF TYPE CARBONATE ROCKS DETERMINED BY NEUTRON ACTIVATION METHODS	159
20	RESULTS OF QUANTIMET STUDIES OF THE PORE STRUCTURE OF CARBONATE ROCK TYPES	160
21	GRAIN-SIZE DISTRIBUTION	160
22	DESCRIPTION OF THE CALCINES	161
23	SO_2 SORPTION CAPACITY OF TYPE SAMPLES AND STATISTICAL LINEAR CORRELATION COEFFICIENTS BETWEEN SO_2 SORPTION AND VARIOUS CHEMICAL ELEMENTS AND PETROGRAPHIC PROPERTIES	163
24	CORRELATION OF POROSIMETER AND SCANNING ELECTRON MICROSCOPE MEASUREMENTS	165
25	SURFACE AREAS OF CALCINES CALCULATED FROM POROSIMETER MEASUREMENTS	166-167
26	PROPERTIES OF SULFATION PRODUCTS	168
27	RESULTS OF ANALYSIS OF ASH POND EFFLUENT FROM TYPICAL PLANTS	190
28	SLUICE WATER QUALITY - NORMAL PLANT OPERATION	191
29	SLUICE WATER QUALITY - LIMESTONE INJECTION	192
30	SLUICE WATER QUALITY - NORMAL PLANT OPERATION	195
31	SLUICE WATER QUALITY - LIMESTONE INJECTION	195

LIST OF FIGURES

Figure No.	Title	Page No.
1	TEMPERATURE PROFILE IN DISPERSED PHASE REACTOR	13
2	EFFECT OF TEMPERATURE AND RESIDENCE TIME ON FRACTIONAL CONVERSION OF CaO	16
3	EFFECT OF TEMPERATURE AND RESIDENCE TIME ON FRACTIONAL CONVERSION OF CaO	17
4	EFFECT OF SO_2 CONCENTRATION AND RESIDENCE TIME ON FRACTIONAL CONVERSION OF CaO	18
5	EFFECT OF TEMPERATURE AND RESIDENCE TIME ON FRACTIONAL CONVERSION OF CaO	19
6	EFFECT OF TEMPERATURE AND RESIDENCE TIME ON FRACTIONAL CONVERSION OF CaO	20
7	EFFECT OF STOICHIOMETRY ON SO_2 REMOVAL	24
8	EFFECT OF SO_2 CONCENTRATION ON SO_2 REMOVAL	26
9	EFFECT OF RESIDENCE TIME ON CaO UTILIZATION	27
10	EFFECT OF STOICHIOMETRY ON SO_2 REMOVAL	28
11	EFFECT OF STOICHIOMETRY ON SO_2 REMOVAL	29
12	EFFECT OF STOICHIOMETRY ON SO_2 REMOVAL	30
13	EFFECT OF RESIDENCE TIME ON CaO UTILIZATION	32
14	EFFECT OF RESIDENCE TIME ON CaO UTILIZATION	33
15	EFFECT OF STOICHIOMETRY ON SO2 REMOVAL	36
16	EFFECT OF RESIDENCE TIME ON CaO UTILIZATION	37
17	SORPTION OF SO_2 FROM SIMULATED STACK GAS BY CALCINE OF -24+28 MESH COLBERT LIMESTONE	46

LIST OF FIGURES (Cont'd)

Figure No.	Title	Page No.
18	PORE VOLUMES OF COLBERT LIMESTONE, -24+28 MESH	47
19	EFFECT OF PARTICLE SIZE ON THE REACTION OF CALCINED LIMESTONE WITH SO_2 AND O_2	50
20	EFFECT OF SO_2 AND O_2 ON REACTION VELOCITY WITH -24+28 MESH COLBERT LIMESTONE	52
21	EFFECT OF CALCINATION CONDITIONS ON REACTIVITY OF CALCINE	54
22	MODEL SOLUTION FOR DIMENSIONLESS ABSORPTION RATE	61
23	MODEL SOLUTION FOR DIMENSIONLESS CUMULATIVE SO_2 PICK-UP	62
24	THE DEPENDENCY OF THE SHRINKING CORE MODEL K ON SO_2 CONCENTRATION	66
25	SHRINKING CORE MODEL PREDICTIONS FOR LIMESTONE 2061--74 MICRON PARTICLES	67
26	SHRINKING CORE MODEL PREDICTIONS--74 MICRON PARTICLES	69
27	SHRINKING CORE MODEL PREDICTIONS--74 MICRON PARTICLES	70
28	SHRINKING CORE MODEL PREDICTIONS--74 MICRON PARTICLES	71
29	SHRINKING CORE MODEL PREDICTIONS--74 MICRON PARTICLES	72
30	EFFECT OF TEMPERATURE PROFILE ON THE SHRINKING CORE MODEL PREDICTION	73
31	EFFECT OF TOTAL PARTICLE SURFACE ON THE SHRINKING CORE MODEL PREDICTION	75
32	SHRINKING CORE MODEL PREDICTIONS FOR LIMESTONE 2061--50 MICRON PARTICLES	76
32-A	SHRINKING CORE MODEL PREDICTIONS FOR LIMESTONE 2061--EFFECT OF PARTICLE SIZE	78

LIST OF FIGURES (Cont'd)

Figure No.	Title	Page No.
33	SHRINKING CORE MODEL PREDICTIONS-- 50 MICRON PARTICLES	79
34	SHRINKING CORE MODEL PREDICTIONS-- 50 MICRON PARTICLES	80
35	SHRINKING CORE MODEL PREDICTIONS-- 50 MICRON PARTICLES	81
36	FRACTIONAL CALCINE CONVERSION VERSUS TIME	91
37	EFFECT OF TIME AND TEMPERATURE OF CALCINATION ON REACTIVITY OF CALCINES	93
38	REACTION RATE VERSUS TEMPERATURE	105
39	DIFFUSION EFFECT UPON REACTION RATE	108
40	REACTION RATE VERSUS PARTICLE SIZE	109
41	REACTION RATE CONSTANT VERSUS GRAIN RADIUS	110
42	REACTION RATE VERSUS RECIPROCAL TEMPERATURE	112
43	PARTICLE HEAT-UP TIME FOR LIMESTONE	121
44	BATTELLE CALCINATION DATA - LIMESTONE NO.2061	126
45	SO_2 CONVERSION VERSUS STOICHIOMETRIC CaO FOR VARIOUS PARTICLE DIAMETERS	138
46	HEAT TRANSFER TO CLOUDS OF PARTICLES IN AIR	142
47	PARTICLE-GAS MASS TRANSFER CALCULATIONS SO_2 REMOVAL VERSUS ADDITIVE INJECTION RATE	146
47-A	INITIAL REACTION RATE VERSUS B.E.T. SURFACE AREA OF CALCINE	150
48	GAS VOLUME FLOW VERSUS PRECIPITATOR COLLECTION EFFICIENCY	172

LIST OF FIGURES (Cont'd)

Figure No.	Title	Page No.
49	ELECTROSTATIC PRECIPITATOR COLLECTION EFFICIENCY VERSUS PERCENT OF RATED CAPACITY	175
50	RATIO OF ESP AREA WITH ADDITIVES TO ESP AREA WITHOUT ADDITIVES VERSUS PERCENT OF RATED CAPACITY	176
51	THEORETICAL TOTAL ASH BURDEN AND SLUICE FLOW - LIMESTONE INJECTION	189
52	WATER QUALITY OF RECEIVING STREAM AT CRITICAL PLANT LOAD AND STREAM FLOWS	194

I. INTRODUCTION

The M. W. Kellogg Company has undertaken a review of the Dry Limestone Injection Process under OAP* Contract No. CPA 70-68 (Task Order #3, Phase I). The Dry Limestone Process referred to in this particular study is the process scheme developed and evaluated in the TVA conceptual design study report prepared for OAP and issued in 1968. This concept involves injection of the pulverized additive stone directly into the radiation section of the boiler proper to effect the vapor phase calcination and sulfation reactions. The resulting reaction products and unreacted stone are collected with the fly ash in the dust removal equipment downstream of the boiler. The increased quantity of particulates and changes in electrical properties (resistivity) have been reported to result in a substantial (~2 to 3-fold) increase in the size of electrostatic precipitator dust collection equipment under normal operation. Solids disposal problems are also aggravated and boiler deposition problems have been reported. Details of the initial specific process design conditions and assumptions can be obtained directly from the TVA design report.

The basic objective of the Kellogg Task Order was to provide an independent assessment of the status of the Dry Limestone Process Technology and to up-date the design bases used in the TVA study to reflect any additional process information developed since that time. Unfortunately, the timing of the Kellogg study was not ideal, as an OAP full scale test program to evaluate the process has been in progress at the TVA Shawnee Steam Plant (Unit No. 10) simultaneously with the Kellogg effort and is still continuing. The TVA plant test data are included as much as possible but programs were not sufficiently complete to permit incorporation of all their results into the Kellogg evaluation. Therefore, the approach taken in the present study was to

*or a precursor

review all available information on the Dry Limestone Injection Process and to derive pertinent correlations and equipment design recommendations wherever possible.

The Kellogg task effort was initiated in September, 1970 by assimilating all OAP and contractor reports, published articles and other technical information pertinent to the subject process. A review of this material revealed that a substantial experimental effort had been devoted to studies of the basic process chemistry and parameters which affect the limestone physical properties in numerous reaction systems. Most of this work, however, had been carried out in small scale equipment with long term exposure of the stone to calcination and subsequent sulfation conditions. A reasonable degree of success was achieved in developing reaction models to fit the laboratory data for a specific experimental configuration, e.g., reactor type, temperature, etc. However, a comparison of results from different bench scale studies was not particularly satisfactory. This observation is believed attributable to differences in experimental test conditions, particularly with precalcined stones, and the resultant effects on stone properties and sorption characteristics.

It was decided at this point in the project review that the bench scale data taken with relatively long residence times would not be applicable to the actual boiler injection system. Investigators had found that different reaction mechanisms seemed to be controlling in studies taken over a wide range of residence times, and time-temperature effects on critical limestone physical properties (e.g., internal surface area pore volume, etc) were a major factor limiting reaction rates. The emphasis in the Kellogg study, therefore, was placed on the evaluation of data from in situ calcination-sulfation studies taken in flow reactors designed to simulate commercial boilers. Pilot plant data for flow reactors were obtained from the studies of Battelle, Babcock and Wilcox, Peabody Coal and Ishihara. It was again found that a comparison of results from these investigators exhibited wide discrepancies. Attempts to resolve these variations were unsuccessful because of the generally incomplete status of reported test data, e.g., insufficient analyses to permit verification of material balances and incomplete information on additive properties to permit comparisons between different stone types. Kellogg concluded that the Battelle test data should be used to develop correlations for the reaction system since it exhibited a high degree of internal consistency, and the pilot studies used the same stone (Fredonia Valley Limestone No. 2061), and had equivalent residence times and similar time-temperature relationships as the initial screening Shawnee tests.

A number of feasible gas-solid reaction models have been proposed by various investigators to describe the SO_2-CaO system kinetics. The correlation approach used by Kellogg in this study was developed for a "shrinking core" model, i.e., where SO_2 gas must diffuse through a reaction product layer ($CaSO_4$) to reach the shrinking inner core of available reactant (CaO). This concept was favored because it has plausible physical and theoretical significance for the system of interest. The specific shrinking core model developed by Kellogg with the assistance of Kellogg's consultant, Prof. R. L. Pigford

(Univ. of California), assumes that a combined diffusional resistance limits the overall reaction rate. Kellogg developed constants for the proposed model to fit the Battelle data with Limestone No. 2061, and a high degree of correlation was obtained with different additive particle sizes and at different reactor operating conditions.

Attempts were then made to test the Kellogg reaction system model against data obtained in other flow reactor studies. This effort was not fruitful, mainly because of the scatter in available experimental information and a lack of complete stone physical property data. Efforts were also made to compare the model with some initial test data from the Shawnee boiler using Limestone 2061. The experimentally measured CaO conversions were substantially lower (factor of 2-3) than predicted. In these particular tests, the additive was injected at a boiler plane corresponding to high gas temperatures (>2300°F), and it is probable that the occurrence of stone deadburning gave rise to low lime utilization. It is also quite possible that other parameters in the full scale boiler, e.g., limestone distribution problems (see Section IV A.4.) and mass transfer effects, could be the reason for the apparent inability to duplicate pilot plant results. One expects that additional insight should be developed from tests currently in progress using a boiler plane corresponding to lower gas temperatures, i.e., ~2100°F gas temperature. It is believed that the Kellogg model is as accurate as any proposed to describe the CaO-SO_2 reaction system; however, further verification against full scale boiler tests is obviously required.

The remaining effort in the overall Kellogg review of the Dry Limestone Injection Process entailed an analysis of process effects on the operability of a standard pulverized coal-fired boiler. Available information was reviewed for the obvious important equipment performance parameters, e.g., effect of additives on slagging characteristics, efficiency of dust removal equipment, and sluice water quality control. The results of this particular study were disappointing in that much of the equipment performance know-how has not been studied in sufficient detail or exists mainly as proprietary information, with little useful published design data. For example, published studies of coal ash deposition tendencies give directional effects of certain parameters; however, no quantitative correlation is available to predict operability ranges for ash-limestone mixtures.

The boiler operability questions are critical and must be resolved before the Dry Limestone Injection Process can ever be installed commercially as a continuous control process. It is hoped that detailed equipment design information will be obtained from the TVA Shawnee tests on an actual boiler. The preliminary Shawnee test data that were available as of this writing exhibited considerable scatter, apparently partly explainable from problems of controlling the boiler operation. Initial full scale data on the electrostatic precipitator showed wide variation in the effect of limestone additive on collection efficiency and dust resistivity. The long term demonstration tests planned for the latter part of 1971 should resolve the data discrepancies and provide useful information in other areas concerning boiler operability.

II. SUMMARY AND CONCLUSIONS

A. A comparison of $CaO-SO_2$ reaction system data from various pilot plant studies shows a wide divergence in results. The following represent typical CaO utilizations measured for approximately the same reaction conditions, e.g., 1850°F injection temperature, 2.0 second gas residence time, stoichiometric ratio (CaO/SO_2) of unity and 74-105M particle size calcite:

Battelle Studies	10-15% CaO utilization
Babcock & Wilcox studies	10-30% CaO utilization
Peabody Coal Studies	20-40% CaO utilization

The discrepancy is believed attributable to differences in reactor configuration, experimental techniques, operating conditions, different types of stone, etc. The Battelle flow reactor data were chosen for modeling work on the basis of completeness of information and best degree of internal consistency and closest simulation of Shawnee test conditions with regard to time-temperature. Available data from Shawnee indicate utilizations in the range reported by Battelle.

B. A "shrinking core" diffusion-reaction model was developed and pertinent constants were derived to fit the available Battelle data with Fredonia Valley Limestone No. 2061. A good fit was obtained for the following experimental conditions: 50-74M average particle size; 1600°F-2100°F gas temperature; 0.025-0.95 mol % SO_2 in inlet gas. The reaction system modeling approach is similar to models developed by Dr. Wen and MIT in other OAP sponsored studies.

C. The Kellogg model could not be adequately tested against data from other pilot plant studies because of incomplete stone physical property data. Attempts to test this model against initial full scale TVA Shawnee tests with Limestone No. 2061 showed much lower measured CaO conversions, possibly due to high additive injection temperatures (>2300°F) and resultant deadburning.

D. The extensive bench scale studies of the $CaO-SO_2$ system revealed major effects of the calcination time-temperature relationships on stone properties and sorption characteristics. Reaction models developed from the bench scale studies could not be extrapolated to the actual flow system because of the much greater available B.E.T. surface area from in situ calcination-sulfation at low residence times (1-2 seconds). The time-temperature-surface area relation is not known and probably it will never be possible to determine this relation for a commercial system. The shrinking core model groups these variables together so the relation per se is not needed.

E. Limestone calcination studies showed that a high degree of calcination (60-70%) could be achieved in approximately 0.2 seconds at temperatures of 1900-2100°F in the actual boiler system. It was concluded that the calcination step is relatively fast in the overall sequence, hence it was decided to develop a model based on sulfation only since it appeared that such a model might adequately describe the system. Battelle and Dr. Wen are developing simultaneous calcination/sulfation models.

F. The effect on SO_2 absorption of major process variables is indicated as follows:

1. Additive properties - - numerous additives with a wide range of properties have been tested but no correlations relating additive properties to SO_2 removal have been developed. However, excellent correlations between initial reaction rate and surface area exist.

2. Temperature - - conflicting results from different investigations with some showing increased SO_2 absorption as temperature increases while others show no effect. If the temperature is high enough to cause deadburning, however, the removal efficiency falls off in all cases. Temperature above about 2300°F generally produce deadburning with the severity increasing with temperature. Time-temperature relationships are important as described in D. above.

3. Particle size/specific surface - - decreasing particle size and increasing specific surface apparently increases SO_2 removal to a point and then further changes have little effect. The point at which decreasing the particle size affects SO_2 absorption is not clearly defined, however, ranging from about 50 microns down to about 10 microns. Determination of the actual particle size is difficult and fragmentation or aggregation of the particles in the reaction zone may be a factor such that below a certain size, the size of the particles taking part in the reaction are independent of initial size.

4. SO_2 Concentration - - The apparent rate of reaction is dependent on SO_2 concentration and sulfate loading on the calcine, but further work is required in this area to better define the mechanism. It should be noted, however, that the existing shrinking core model is valid with respect to the most recent Battelle data available when the present work was done.

5. O_2 - - the majority of investigators have found that increasing the oxygen concentration (i.e., increasing excess air) generally increases the SO_2 absorption within the range studied (0.2% to 6%) but other factors (e.g., sulfate loading, alteration of time/temperature) have a significant effect. No correlations for O_2 effect on SO_2 absorption have been developed.

6. Pore size - - data have been obtained which indicate that pore diameter of the absorbent is a

significant factor in both absorption capacity and rate. The total SO_2 sorption capacity increases with increasing pore size and has been correlated with pore areas greater than 0.3 microns. The rate of reaction increases with decreasing pore size until a critical pore diameter of about 0.1 micron is reached.

G. Mass transfer predictions based on generalized theory revealed that the diffusional resistance in the gas-to-solid transfer process can be a major factor in the overall sulfation reaction. The mass transfer process effects could not be derived from the Battelle pilot reactor studies owing to the use of unrealistically low stone injection rates. The problem requires additional experimental investigation, involving actual boiler tests supplemented by gas-solid mass transfer studies at a low particle Reynolds number.

H. The effect of limestone addition on the stack gas dust resistivity and electrostatic precipitator (ESP) collection efficiency was investigated. Initial TVA tests on the Shawnee plant precipitator indicated considerable scatter in the measured precipitator efficiency as shown below:

ESP Efficiency w/Additive	Gas Flow Capacity (% Design)	Required ESP Area Factor to Maintain Baseline Outlet Loading (Area with Additive/Base Case Area)
87-91%	76-82%	1.1-1.4
68-88%	94-106%	1.3-2.25

It is evident that additional ESP test data are required to determine a more reliable design efficiency value in the presence of limestone. OAP has contracted Cottrell Environmental Systems to perform additional testing on the effects of limestone addition on solids collection efficiency.

I. A review of available information on the effects of boiler additives on coal ash deposition tendencies indicates directional trends but no general quantitative correlations. It appears that the ash sintering strength will be lowered in the presence of limestone, which should minimize problems resulting from the build-up of bonded deposits on tube surfaces. There also appears to be a relationship between tendency to deposit and tube temperature regime. Again, it will be necessary to obtain more useful design information from the full scale plant test program.

J. Preliminary test data from Shawnee have shown that water quality control problems will be a critical consideration in limiting the applicability of the Dry Limestone Injection Process. A 10-30 fold increase in the total dissolved solids content of the ash sluice water has been measured with limestone injection, along with an increase in disposal pond pH resulting from the hydration of excess CaO.

III. RECOMMENDATIONS

A. Final conclusions regarding applicability of the Dry Limestone Injection Process to full scale utility boilers should await completion of the Shawnee test program. The following items are of particular importance:

1. Additional data must be generated and evaluated when stone injection plane A-A corresponding to the reported optimum injection temperature of approximately 2100°F gas temperature is being used. The Shawnee test program should be designed to obtain data on different additive types with different average particle sizes at the injection location.

2. Additional information must be generated to permit a more reliable assessment of effects on the following equipment performance considerations:

    - Electrostatic Precipitator Efficiency
    - Boiler Operability and Deposition Problems
    - Sluice Water Quality Control Problems

B. The shrinking core model developed by Kellogg to describe the CaO-SO_2 reaction system should be tested by correlation with injection plane A-A data.

C. To use the Kellogg reaction model, or other proposed models with a theoretical basis, the available limestone internal surface area generated in the calcination-sulfation processes must be known. Recent studies in the Battelle test reactor have provided some data on B.E.T. surface area for in situ calcination conditions. It is recommended that additional studies be undertaken to generate similar data for other stone types.

D. Theoretical predictions indicate that gas-to-particle mass transfer can contribute a major resistance in the overall sulfation reaction process. A test program should be developed, either for the full scale boiler or a pilot flow reactor, to measure transfer coefficients in the actual system at low particle Reynolds numbers.

IV. DISCUSSION OF RESULTS

A. Pilot Plant Sulfation Data

1. Battelle Studies

a. Battelle Reactor Design and Conditions of Operation

The Battelle dispersed-phase reactor consisted of a vertical tube with a gas-fired burner at the bottom. Limestone was injected through one of a series of ports in the bottom portion of the reactor, was carried upward by the flue gas stream, and was subsequently extracted through another of a series of ports in the upper part of the reactor. Very low particle dispersions, on the order of 1 to 2 particles per cubic foot of flue gas, were used in order that each particle might experience an environment of essentially constant SO_2 concentration. This situation, of course, may not exist in commercial boilers where possible interparticle effects and significant SO_2 concentration gradients may affect the efficiency of the mass transfer operation.

The SO_2 concentration in the flue gas was continuously monitored by an IR analyzer, and temperatures throughout the reaction system were continuously monitored by a multipoint recorder. Gas temperatures at the top, middle and bottom of the reactor were recorded to provide an indication of vertical temperature gradients while the wall temperatures indicated temperatures usually 100° to 200°F cooler than the centerline temperatures. Figure 1, from the Battelle final report (1), shows a typical temperature profile along and normal to the axis of the

FIGURE I

TEMPERATURE PROFILE IN DISPERSED-PHASE REACTOR

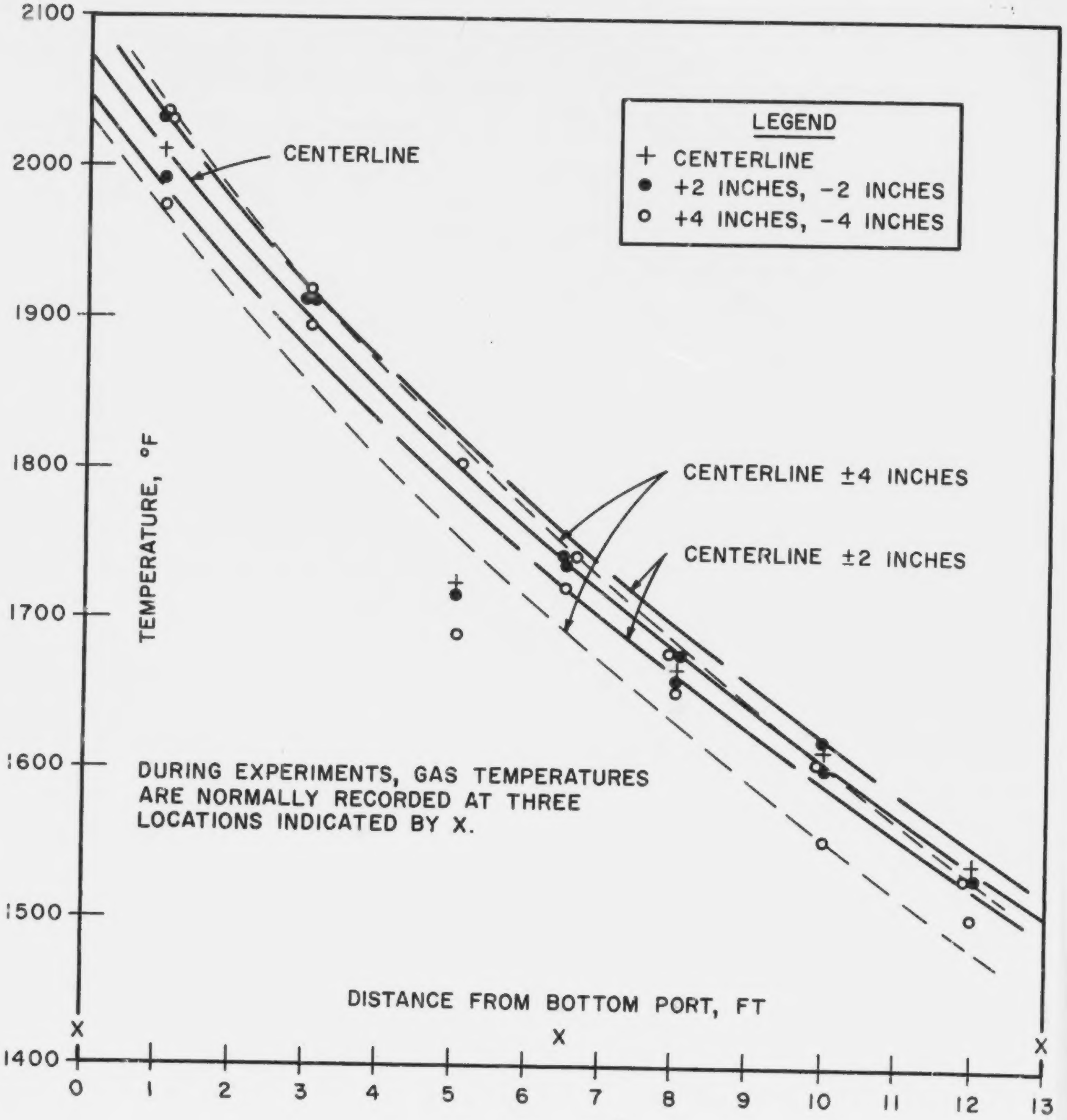

dispersed-phase reactor. The profiles in either direction appear to be fairly flat. Velocity gradients along the reactor were also measured and found to be nearly flat over the cross-section. In Battelle's residence time calculation, both the known temperature gradient and the flow profile were considered. Detailed test data received directly from Battelle showed revised residence times which were slightly different than the values presented in the Battelle final report.

Limestone 2061 (Fredonia Valley White), with an analysis of 90.17 percent $CaCO_3$, was used exclusively by Battelle in their recent studies. In all but one calcination run, the particle size range utilized was -140+200 U.S. Standard mesh (74-105 microns). Battelle's data were reported in terms of CaO utilization based on chemical analysis of the reacted stone. The samples were first hydrated after which a thermogravimetric analysis determined the carbonate and hydroxide content while total sulfur was determined by colorimetry. Battelle did not attempt a material balance over the reactor in order to check the consistency of their solids analysis data, although the success of such an attempt may be seriously limited in this case by the extremely low stoichiometric ratios (approximately 7 to 14 percent) employed.

b. Battelle Data

Sulfation data for the Battelle dispersed-phase reactor appear in the Battelle final report entitled "Investigation of The Reactivity of Limestone and Dolomite for Capturing SO_2 From Flue Gas"$^{(1)}$. These data were plotted as fractional CaO conversion versus residence time, and the results can be seen in Figure 2 through Figure 6 for reported mean temperatures ranging from 1600°F to 2148°F. Although one might anticipate increased CaO conversion with increased temperature over the entire range of residence times studied, there is no distinct evidence of this effect within the Battelle data. The higher temperature runs do, however, exhibit higher initial rates of reaction as demonstrated by the slope of the curve at time equal to zero. The Battelle data plots do show that reactor time-temperature effects are critical in controlling CaO conversion, and the higher temperature results undoubtedly reflect some degree of stone dead-burning.

Also included on Figure 3 are data showing the effect of O_2 concentration on CaO conversion. As can be seen from the curves, increasing the oxygen concentration from 0.4% to 6% increases the conversion, other conditions being constant. For example, at 1.5 seconds residence time and a temperature of about 1715°F, CaO conversions are 5.5%, 7.1% and 8.7% for oxygen concentrations of 0.4%, 3.0% and 6% respectively. Thus, it appears that increasing the amount of excess air in the boiler has the potential of increasing SO_2 removal.

Figure 4 is an excellent illustration of the effect of initial SO_2 gas concentration on overall CaO conversion. Higher SO_2 concentrations do indeed effect more efficient utilization of the limestone. Some of the apparent scatter within the Battelle data could be attributed to variations in reaction temperature profiles between different test runs. In spite of these apparent anomalies, however, considerable weight has been given to the Battelle data in the development of a reaction system model since the dispersed-phase reactor studies do reasonably simulate the Shawnee boiler and since the same limestone (No. 2061) was used in both tests.

FIGURE 2

EFFECT OF TEMPERATURE AND RESIDENCE TIME ON FRACTIONAL CONVERSION OF CaO

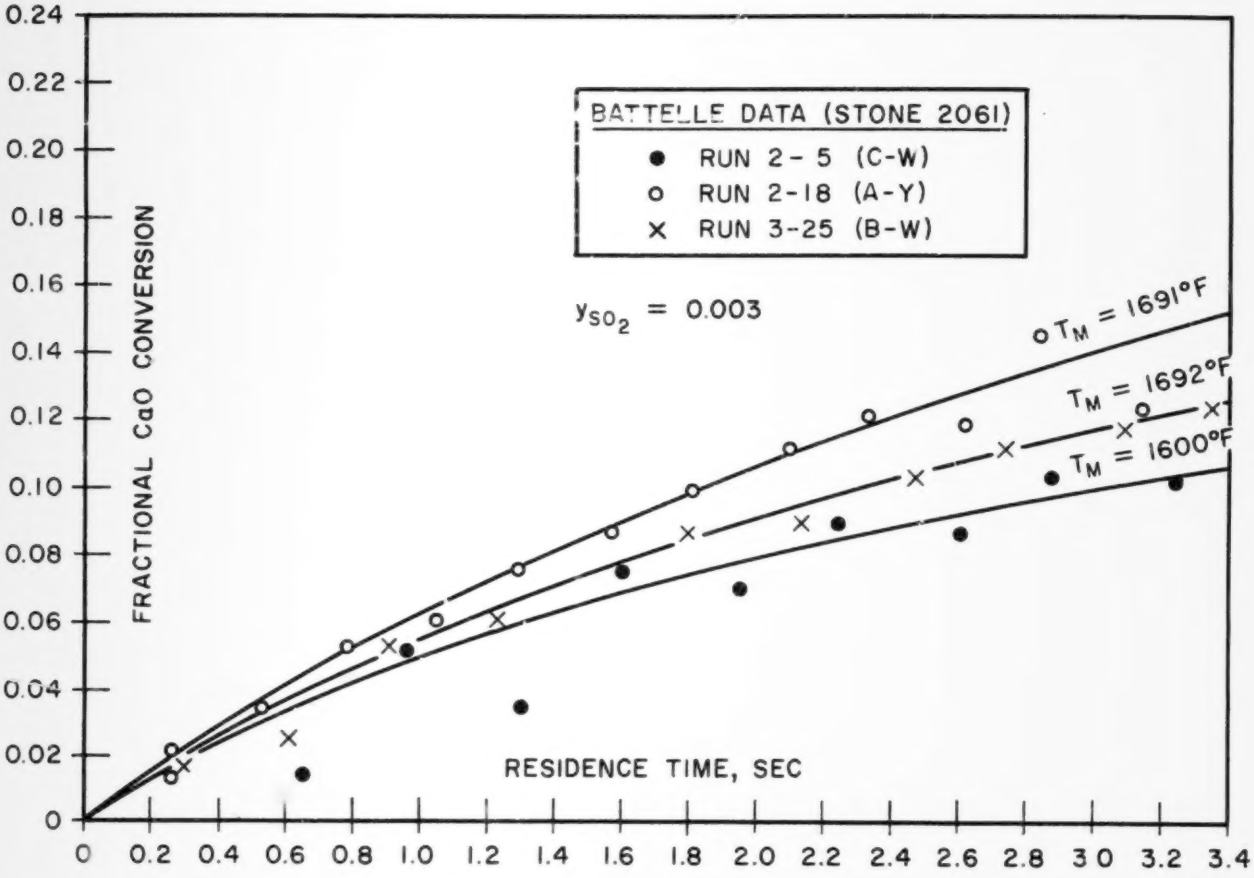

FIGURE 3

EFFECT OF TEMPERATURE AND RESIDENCE TIME ON FRACTIONAL CONVERSION OF CaO

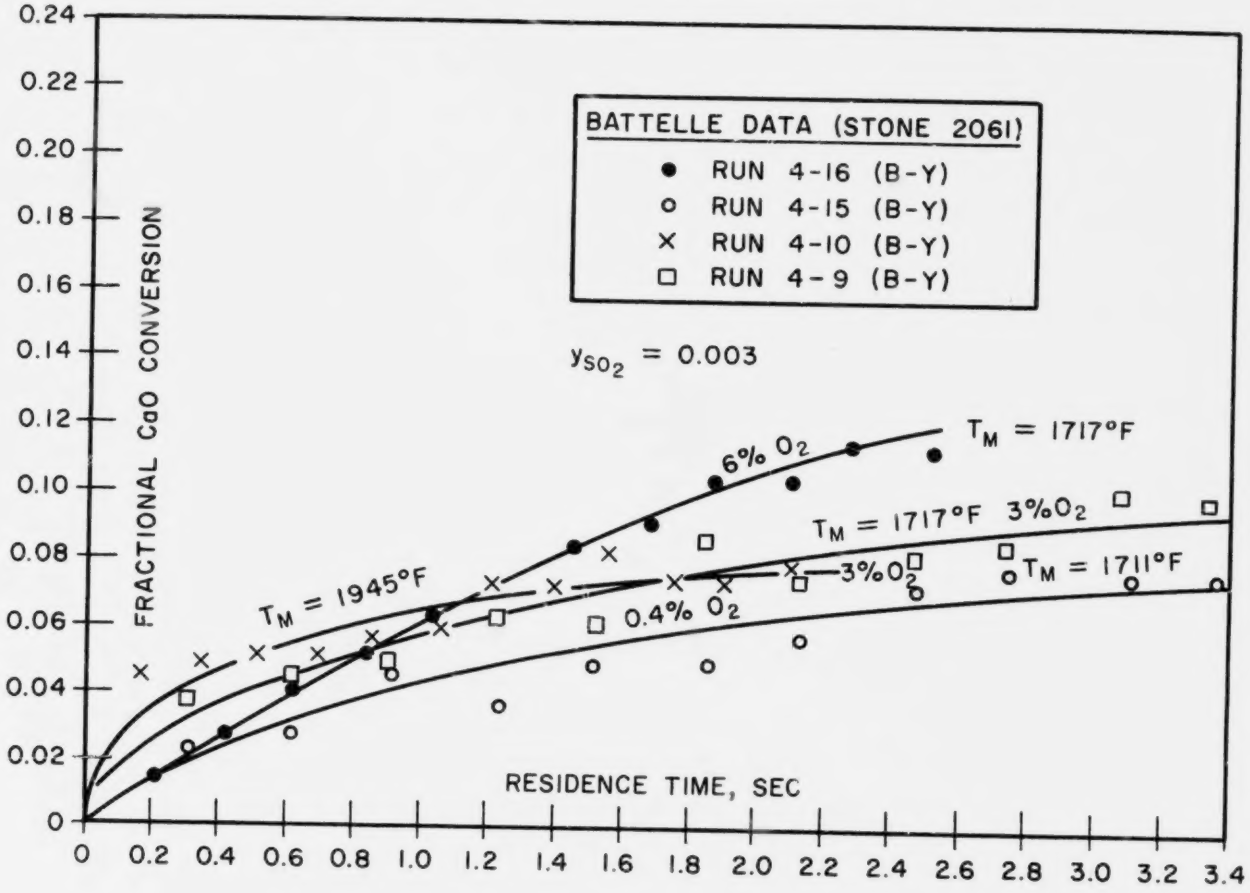

FIGURE 4

EFFECT OF SO_2 CONCENTRATION AND RESIDENCE TIME ON FRACTIONAL CONVERSION OF CaO

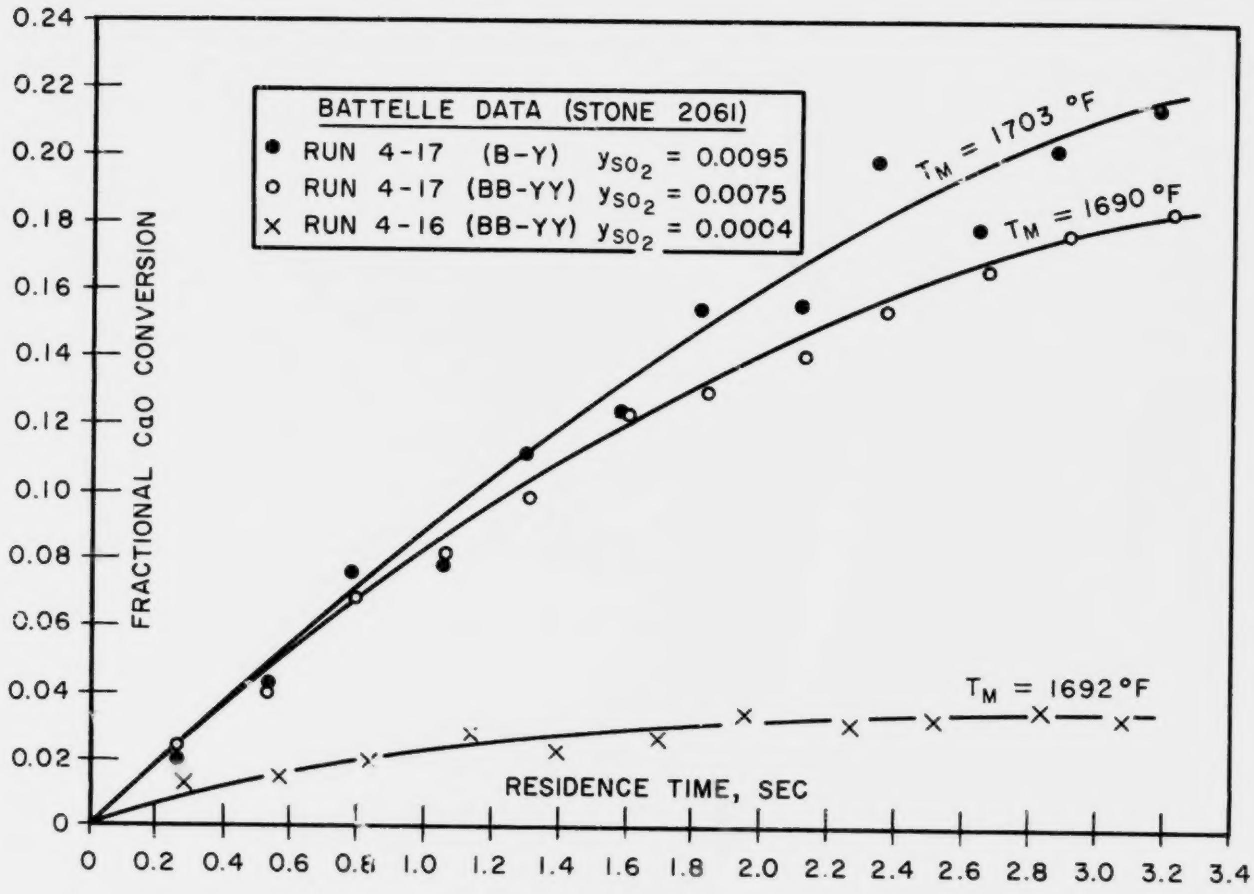

FIGURE 5

EFFECT OF TEMPERATURE AND RESIDENCE TIME ON FRACTIONAL CONVERSION OF CaO

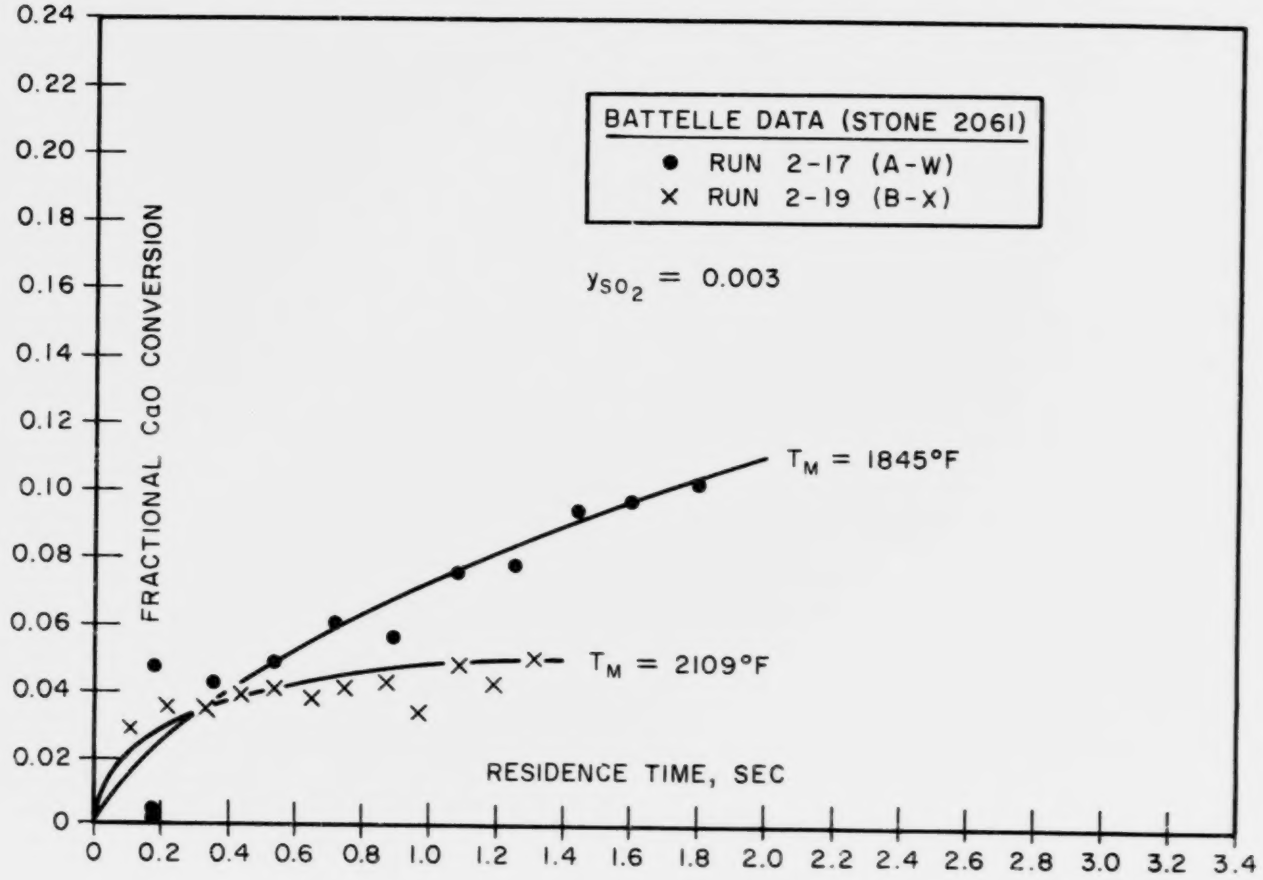

FIGURE 6

EFFECT OF TEMPERATURE AND RESIDENCE TIME ON FRACTIONAL CONVERSION OF CaO

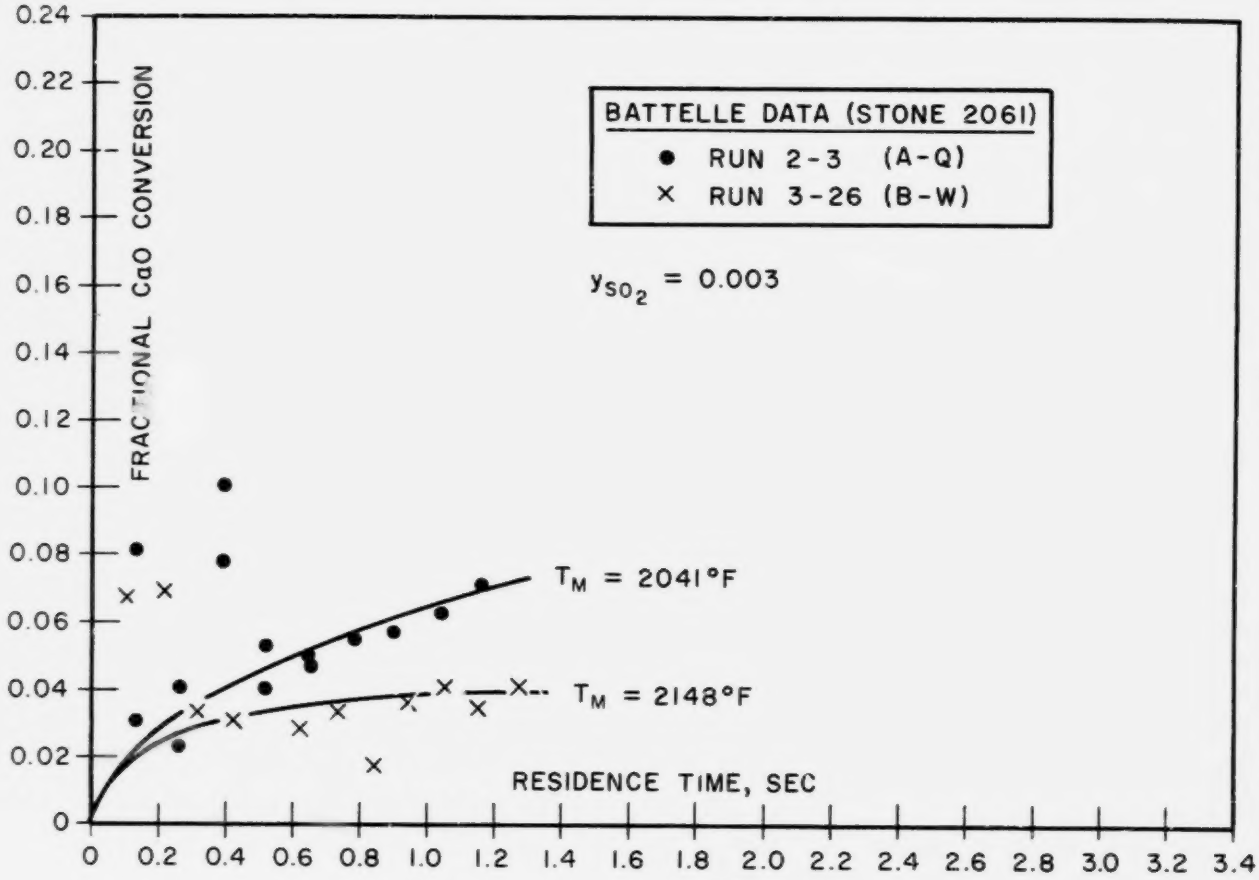

2. Babcock and Wilcox Studies

The Babcock and Wilcox (B & W) dispersed-phase reactor consisted of a vertical reaction chamber followed by a vertical heat exchanger which cooled the gases down to exit conditions. Both coal and limestone were fed into the top of the downflow reactor through separate injection ports. Residence times in the reactor were varied by (1) altering the coal firing rate, or (2) changing the vertical position and/or angle of the limestone injection port. The latter method, however, introduces the additional effect of temperature. The following injection ports along with their respective average injection temperatures were used with the B & W reactor:

Port A	2700°F
Port 1	2300°F
Port 2	1900°F
Port 3	1700°F
Port 4	1500°F

(It should be noted, however, that according to B & W the quantity of air used to convey the additive was large enough to reduce the flue gas temperature by about 400°F).

The reaction zone was assumed to extend from the point of injection down to the point in the vertical heat exchanger at which the temperature was approximately 1400°F. Most of the B & W data were taken from runs which utilized either injection port A or port 1. The data are reported in terms of stoichiometry and SO_2 removal which is determined by IR monitoring. Although wet chemical and X-ray analyses were made for most of the reacted-additive-fly ash mixtures, the reported SO_2-removal data are based on gas-phase analysis. No material balances are reported. The analyses of the solids apparently were made only to determine if there was any reaction between coal ash and additive. Had natural balances been determined, perhaps some of the inconsistencies within the data could have been explained.

The B & W study(2) made use of a large variety of limestones and dolomites, but only the limestones with a Ca content exceeding 87 percent were considered for analysis along with the dolomites. In some cases, the limestones and dolomites were precalcined to yield greater surface areas, or hydrated to give even larger surface areas. Greater surface was also effected by utilization of marls--limestones with characteristically high surface areas.

a. Data for Limestone Additions

An attempt to correlate SO_2 removal with specific external surface (cm^2/gm)* of the raw limestones proved unsuccessful because of the wide scatter of the data. A plot of SO_2 removal versus total external surface (obtained from both specific surface and stoichiometry) also revealed no apparent correlation for a specific set of operating conditions. For any fixed residence time, however, runs made with stones of very high specific external surface areas, representing the marls (~15,000 cm^2/gm), the hydrates (~17,000 cm^2/gm) and, in some cases, the calcines (~8,000 cm^2/gm), did exhibit higher SO_2 removals than those made with raw limestones (specific surfaces ranging from approximately 3,000 to 4,000 cm^2/gm) of larger average particle size.

---

*The reader is reminded that the specific surface measured by B & W represents only the outside surface of the limestone particles and should be related to particle size distribution of the stone and not internal surface area.

The effect of residence time on SO_2 removal was also explored. Since, at any one injection port, there existed insufficient data over an appreciable residence time range, this correlation had to be attempted using data from both injection ports A and 1. The result indicated a trend of increased SO_2 removal with increased residence time, but too much scatter was inherent in the data for any conclusive correlation. An explanation for some of the scatter may lie in the above mentioned temperature effect between the two injection ports.

Stoichiometry appeared to correlate well with SO_2 removal for limestone injection at port A and for coal firing rates ranging from 6.0 lb/hr down to 4.4 lb/hr (approximately 1.7 to 2.4 seconds residence time). Figure 7 illustrates this correlation. No particular trend was obtained, however, from similar data at higher coal rates representing shorter residence times. The stoichiometry range covered by the Battelle studies is also included in Figure 7 to illustrate the narrow range used in these tests and to show the difference in stoichiometry between the Battelle and B & W tests.

FIGURE 7

EFFECT OF STOICHIOMETRY ON SO_2 REMOVAL

LIMESTONE > 87% CaO — B AND W DATA

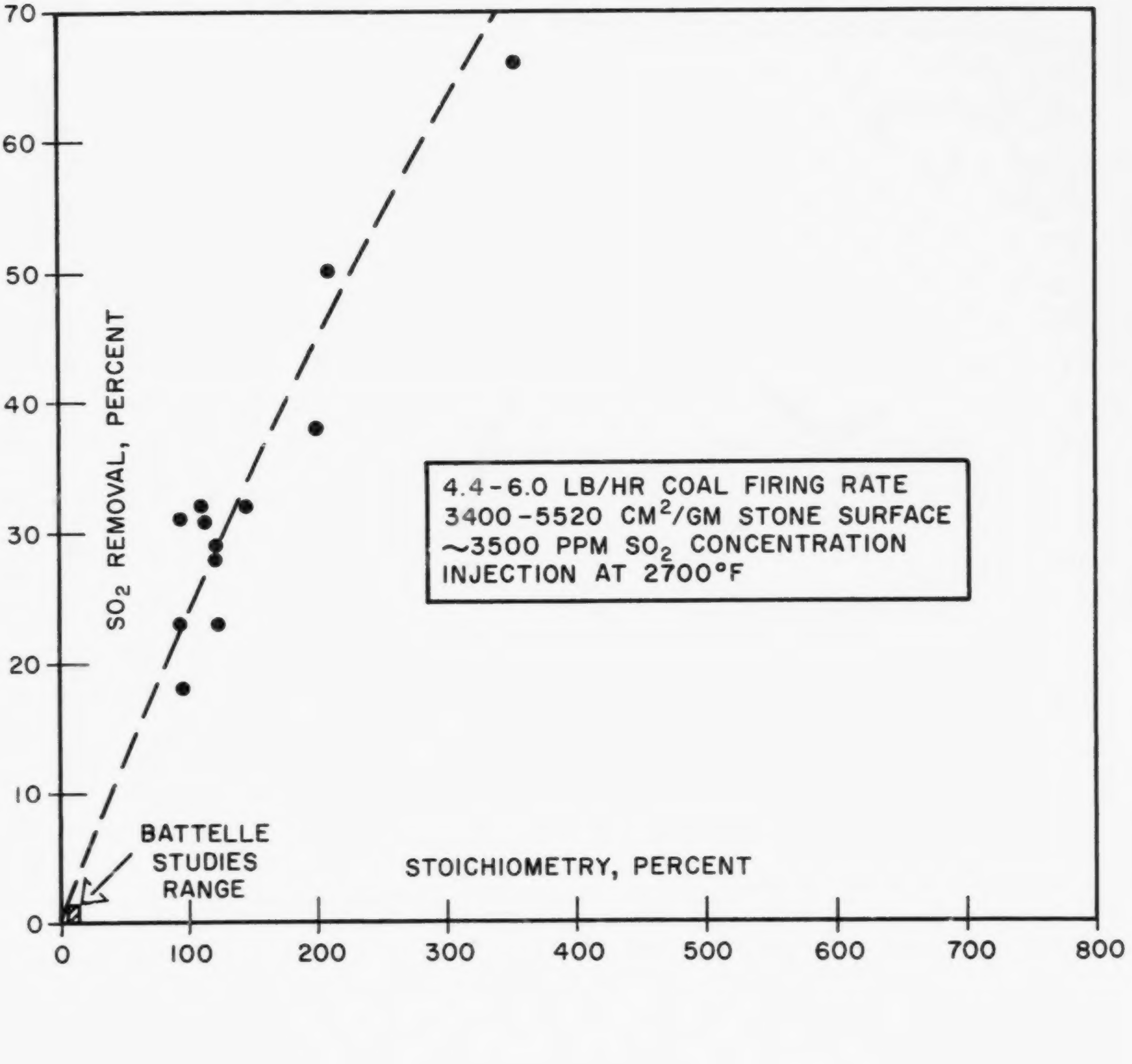

Figure 8 is a plot of initial SO_2 concentration in the gas phase correlated against SO_2 removal for limestone injected through port A. Although the data are scattered, the graph indicates increased SO_2 removal with increased SO_2 concentration. This trend was compared with the correlation provided by Battelle in their final report. For a comparable residence time (approximately 1.2 seconds), the effect of initial SO_2 concentration on SO_2 pickup is approximately the same for both the Battelle and the B & W studies.

The SO_2 removal data were converted to CaO utilization terms (determined from the ratio of SO_2 removal to stoichiometric fraction) for purposes of comparison with the Battelle data. Only the B & W data for runs with stoichiometric rates varying between 80 and 100 percent were considered. Figure 9 shows CaO utilization as a function of residence time for the B & W limestone data, and for Battelle data on a run in which the average temperature was approximately 1850°F (one of the best Battelle runs in terms of CaO utilization). Both sets of data cover runs in which the initial SO_2 concentration ranged between 3000 and 3500 molar ppm. From the graph, it is apparent that the B & W data for approximately 100 percent stoichiometry show significantly greater CaO utilization than do the Battelle data for which the Ca/S stoichiometry did not exceed about 14 percent. The validity of an analogy such as this, however, is questionable owing to the following differences between the two reactor conditions:

(1) The temperatures in the Battelle reactor ranged from about 2450°F to 1600°F, whereas that of B & W maintained a reaction temperature

FIGURE 8

EFFECT OF SO_2 CONCENTRATION ON SO_2 REMOVAL

LIMESTONE > 87% CaO — B AND W DATA

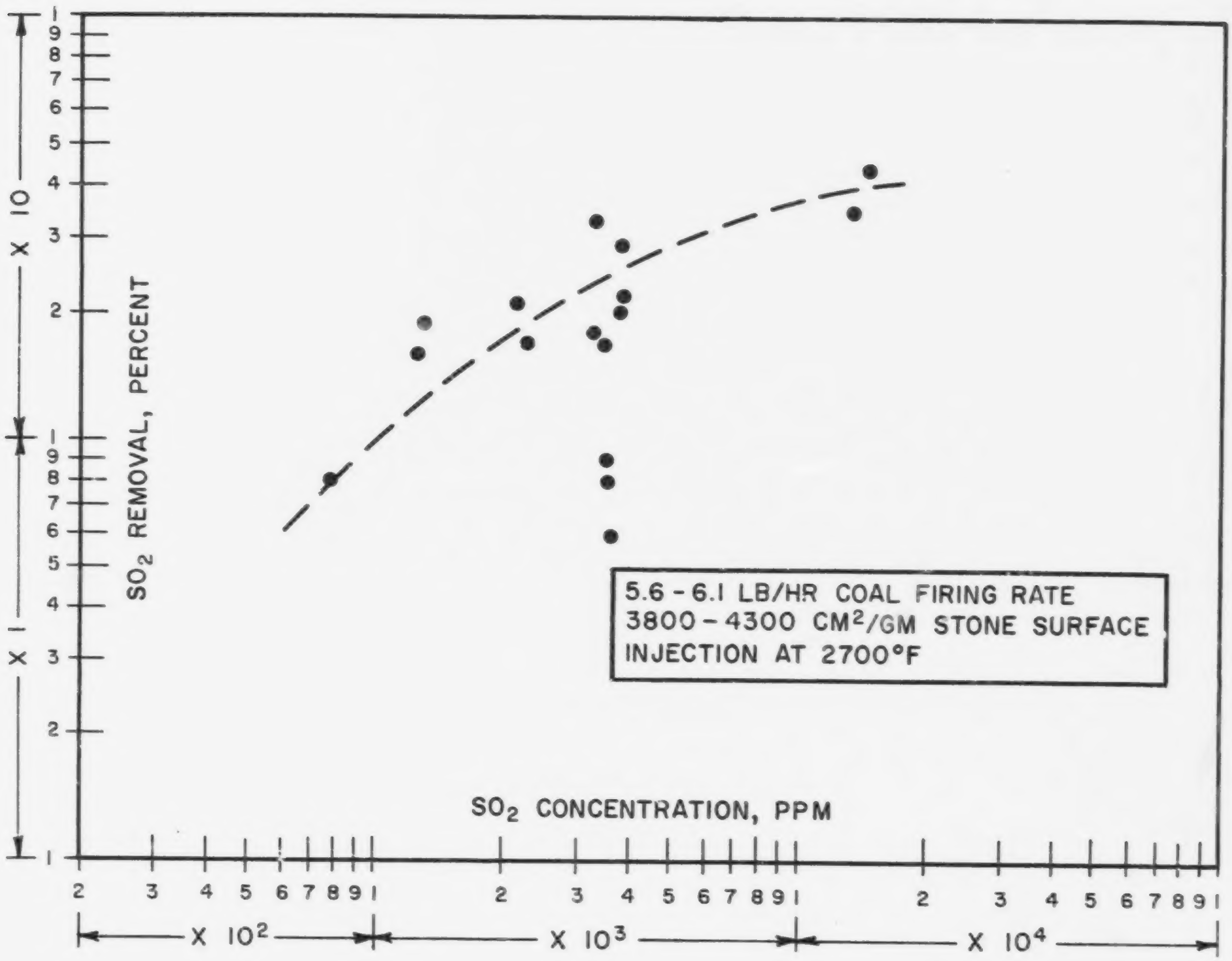

FIGURE 9

EFFECT OF RESIDENCE TIME ON CaO UTILIZATION

LIMESTONE >87% CaO

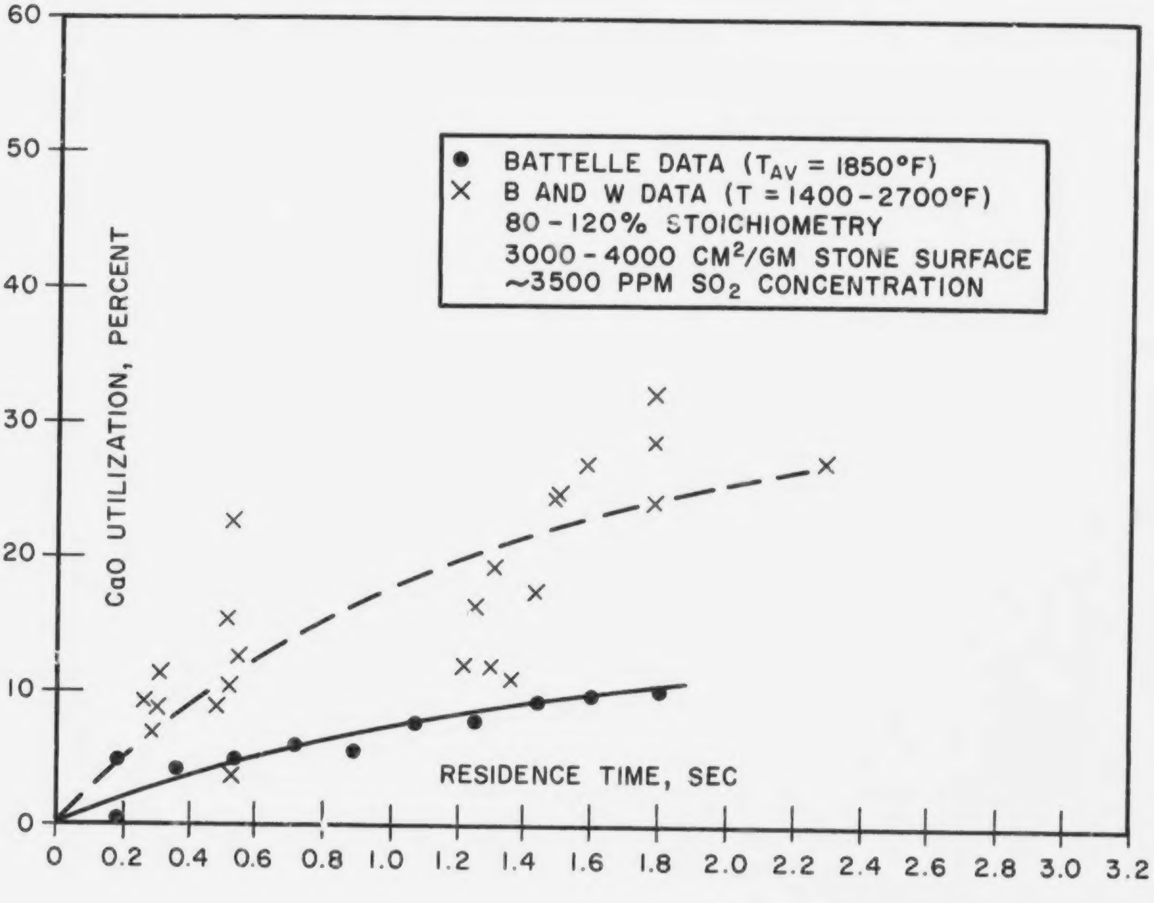

profile ranging from 2700°F down to approximately 1400°F.

(2) The B & W data are extracted from runs utilizing limestones from several sources; the Battelle studies utilized limestone No. 2061 (Fredonia Valley White) exclusively.

b. Data with Dolomites

B & W data for runs with dolomite injection show slightly less scatter than those runs with limestone injection, although an appreciable amount of data scatter persists. As with limestones, dolomite surface also exhibited no apparent correlation with SO_2 removal.

Stoichiometry of the dolomitic runs* (injection at port A) correlated fairly linearly with SO_2 removal at coal rates of 4.5 to 6.7 lb/hr and for raw stone external surfaces ranging from 2200 to 2900 cm^2/gm. Figure 10 illustrates this relationship which exhibits approximately the same slope as the corresponding plot for limestones. A similar graph for data at higher coal firing rates was impossible because of insufficient data over an appreciable range of stoichiometry. Another plot was made, however, for higher coal rate runs in which dolomite was injected into the reaction system at port 1 (Figure 11). This plot indicates increased SO_2 removal with increased stoichiometry, although any definite correlation is excluded due to the limited stoichiometric range of the data available. Figure 12 illustrates the effect of stoichiometry on SO_2 removal for runs in which

---

*Stoichiometry and utilization in the B & W dolomite runs were calculated on the basis of CaO+MgO as reactive species.

FIGURE 10

EFFECT OF STOICHIOMETRY ON SO_2 REMOVAL

DOLOMITES — B AND W DATA

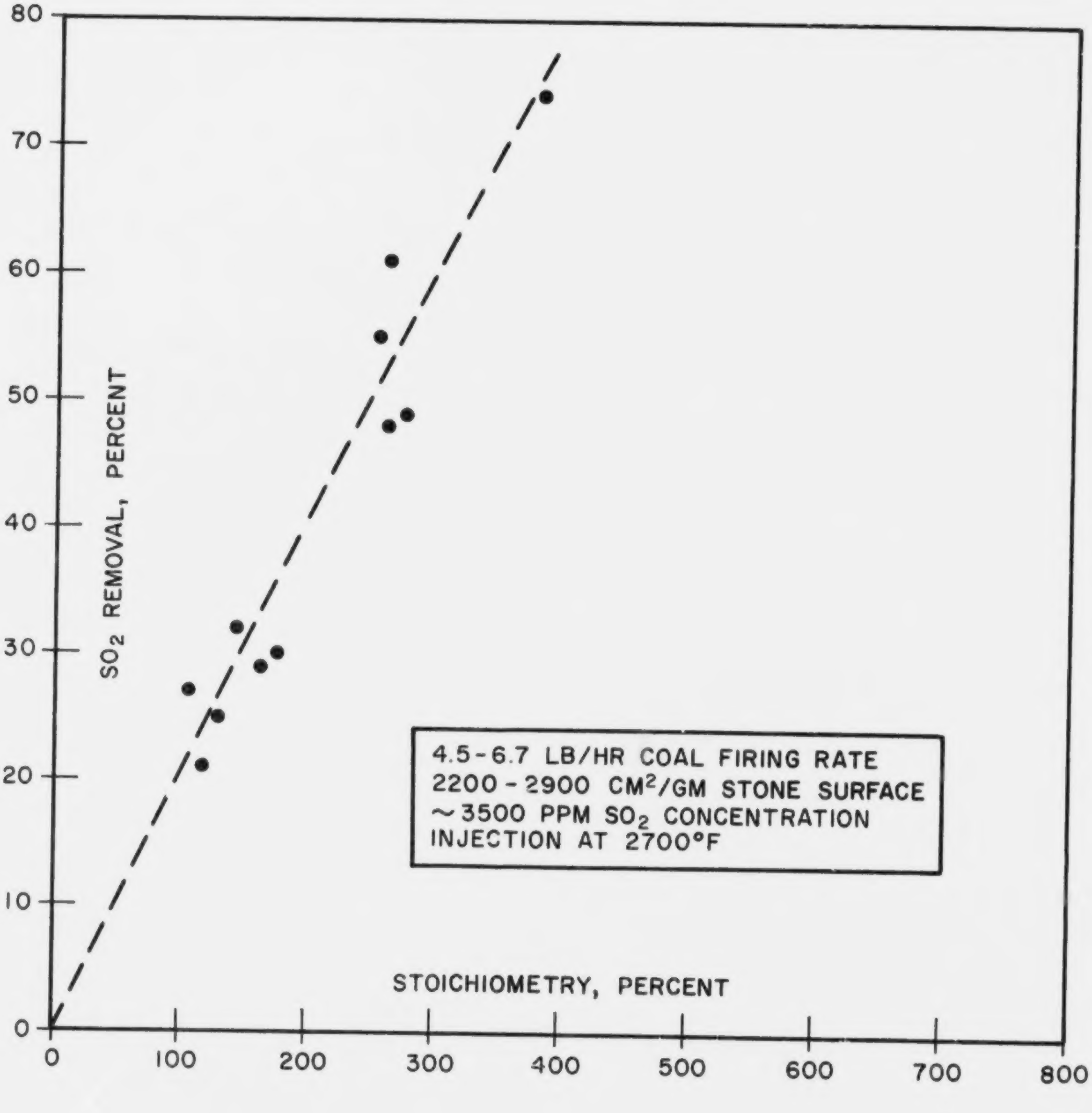

FIGURE 11

EFFECT OF STOICHIOMETRY ON SO_2 REMOVAL

DOLOMITES — B AND W DATA

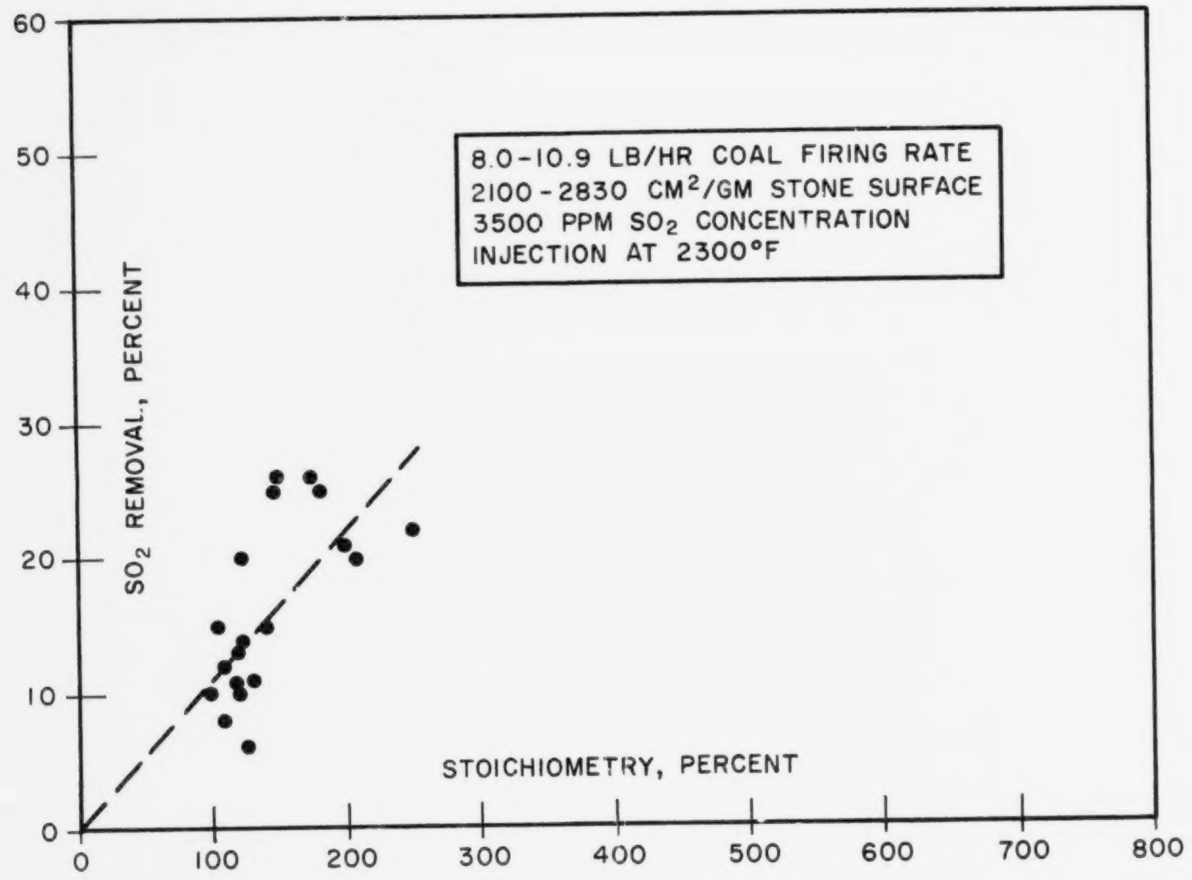

FIGURE 12

EFFECT OF STOICHIOMETRY ON SO_2 REMOVAL

DOLOMITES – B AND W DATA

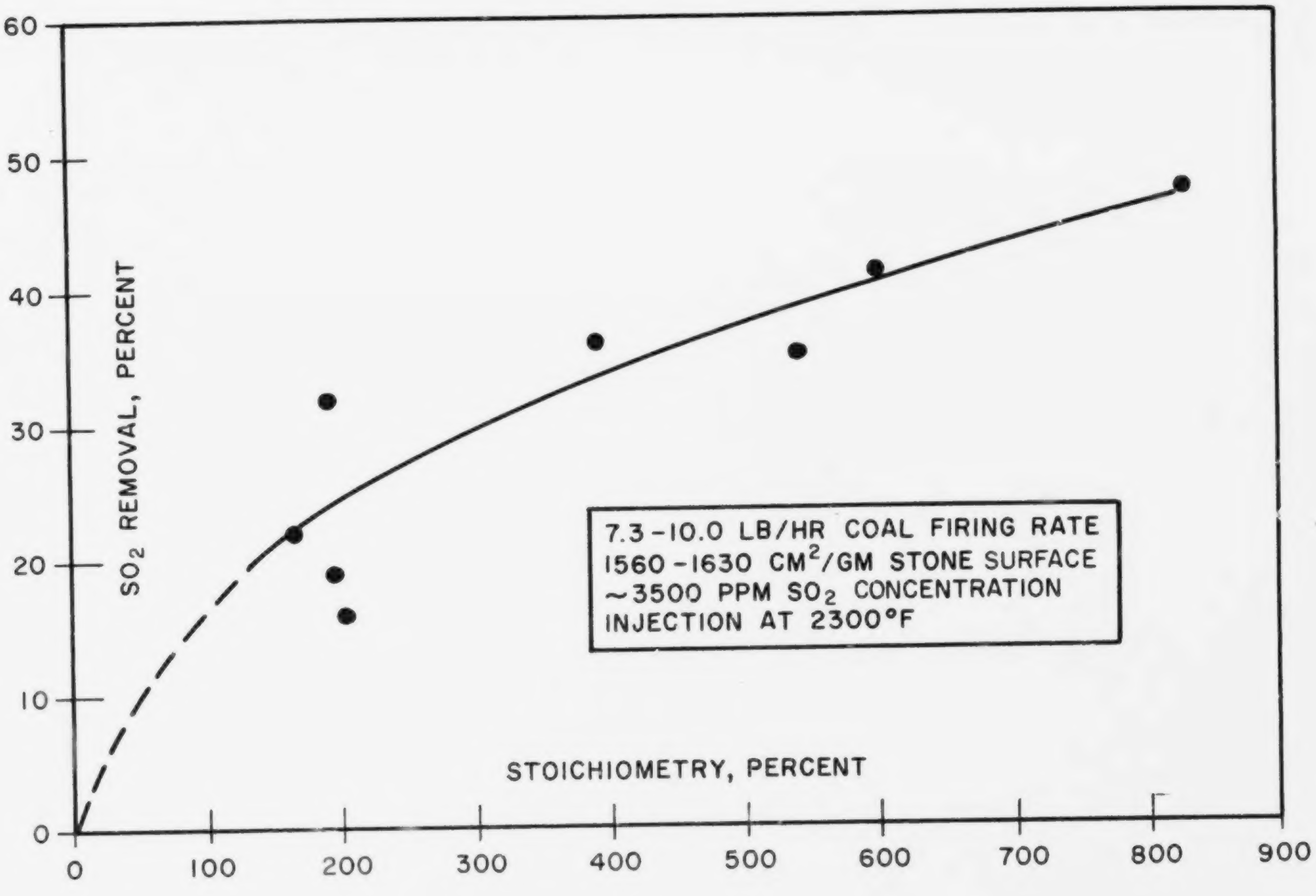

the coal rate varied between 7.3 and 10.0 lb/hr, for specific surfaces of approximately 1600 cm^2/gm, and for injection at port 1. The effect of stoichiometry on SO_2 removal in this case is much smaller than that shown on Figure 10. The difference between the two curves results from a combination of: (1) a residence time effect resulting from varying coal firing rates, (2) a combined residence time and temperature effect stemming from stone injection at two different ports, and (3) an extent-of-reaction effect arising from the difference in total surface available.

It was assumed that B & W reported their data on the basis that both CaO and MgO are equally reactive. Plots of (CaO + MgO) utilization at low (80%-120%) and high (>120%) stoichiometries are illustrated in Figures 13 and 14, respectively. These graphs, although exhibiting wide data scatter, show approximately the same trend as the corresponding plot for limestone (Figure 9). It is also significant to note from Figures 13 and 14 that a stoichiometric rate in the range of 80 percent and greater has little or no effect on (CaO + MgO) utilization for any specified residence time.

In general, the B & W data tend to be less consistent than the Battelle data for a specified set of conditions, although the B & W data do, in fact, tend to indicate higher stone utilizations.

FIGURE 13

EFFECT OF RESIDENCE TIME ON CaO UTILIZATION

DOLOMITES — B AND W DATA

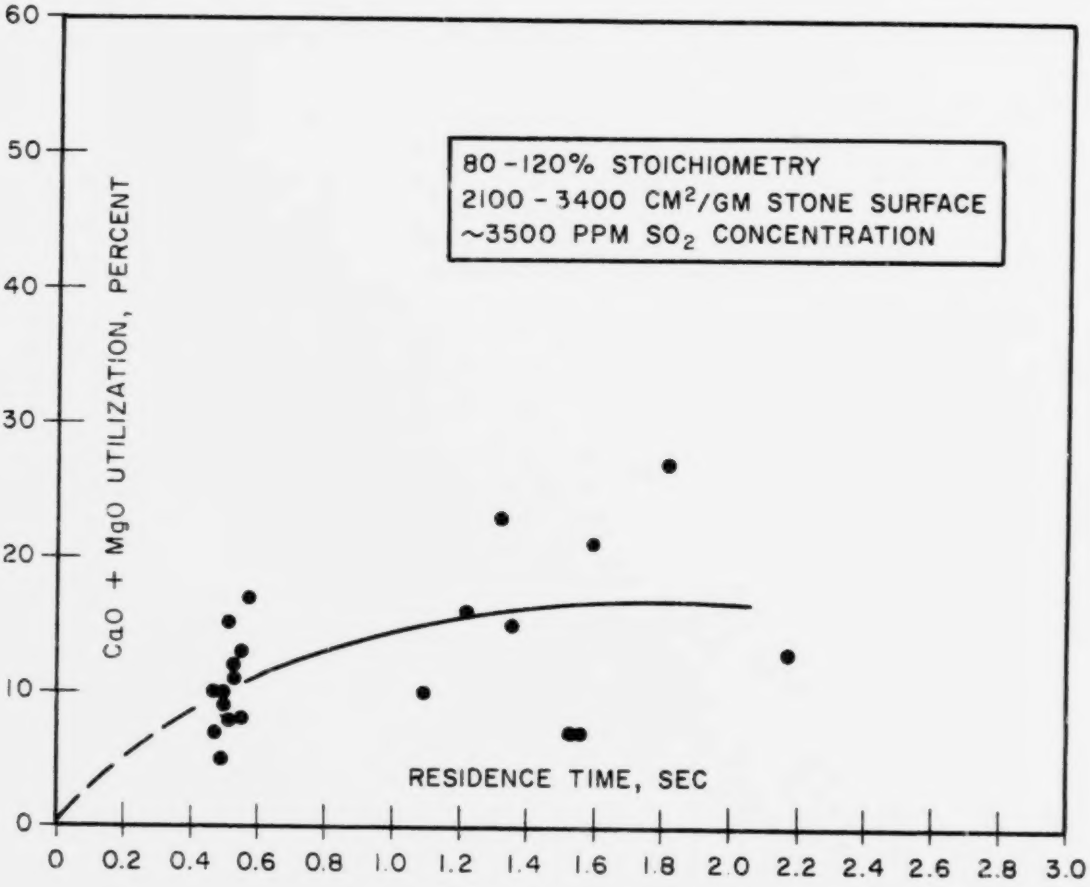

FIGURE 14

EFFECT OF RESIDENCE TIME ON CaO UTILIZATION

DOLOMITES — B AND W DATA

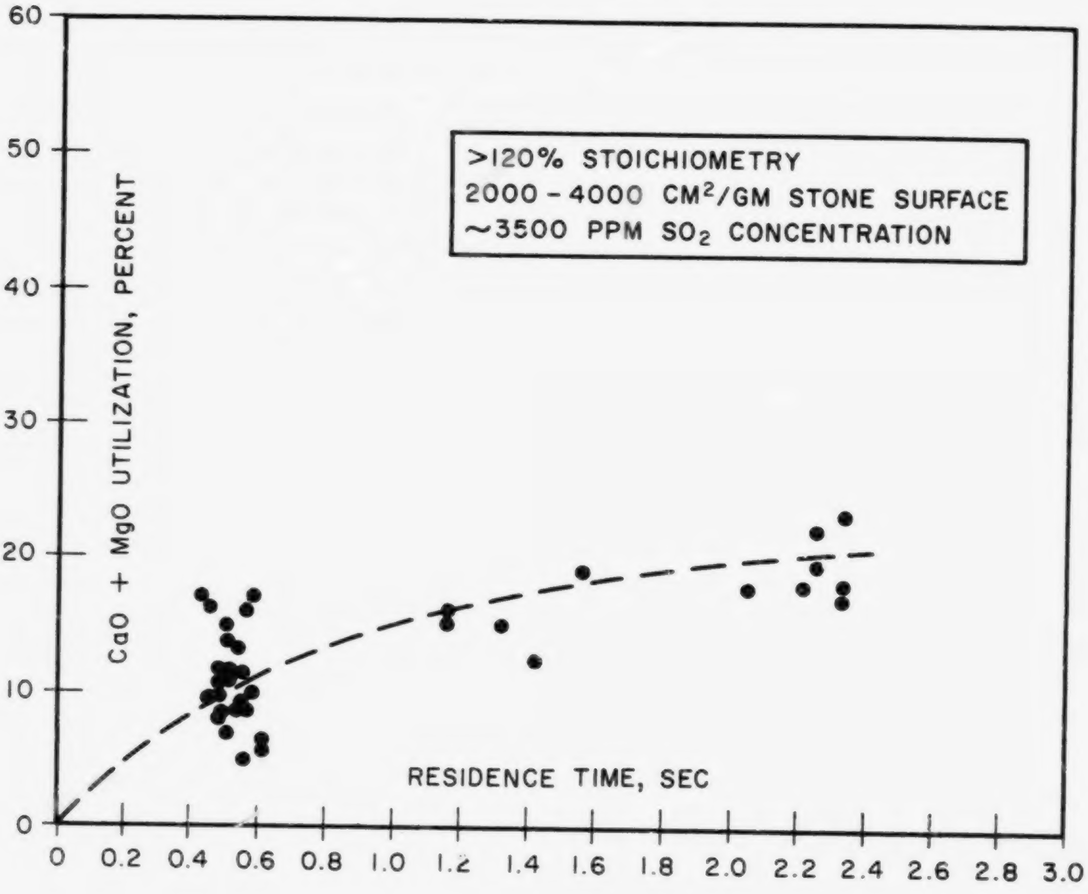

3. Peabody Coal Studies

a. Description of Reactor and Conditions of Operation

The reactor used by Peabody Coal consisted of a pilot-scale coke furnace with a moving chain grate through which primary combustion air passed normally to the coal. Secondary air was also added directly to the flame area above the fire bed. The resulting flue gas then passed through a rectangular refractory duct followed by a cylindrical duct, after which it was quenched with water and bypassed to the atmosphere. The gas was continuously monitored through sampling points prior to the spray cooling section. In order to make possible a sulfur material balance around the reactor, Peabody also sampled the particulate matter prior to the water quench. Since the furnace was not equipped with a standard ash discharge, the ash was sampled before it was dumped from the moving grate.

Temperature was monitored at various places throughout the unit, and temperature profiles for various feed rates were determined and are presented in the Peabody Final Report(3). The injection ports were located vertically in the rectangular section above the flame with additional high temperature (2400° to 2500°F) injection ports toward the front. Peabody defined their residence time calculation basis as beginning at the point of injection and terminating at the water quench point (not less than 1200°F), assuming that the particles travel at combustion gas velocity. Although six different injection materials were tested, the data for Aragonite Stone No. 1683, is emphasized here since its composition was considered to be closest to that of the stones utilized in the other flow reactor studies. It should be noted that two other stones (1359 and 1684) with similar compositions were tested and gave essentially the same results as did No. 1683.

b. Test Results

Figure 15 shows graphically the correlation between SO_2 removal and stoichiometry for three different particle sizes of Limestone No. 1683--the as-received sample size which contained approximately 20 percent -100 mesh material, a-140+200 mesh sample and a -200 mesh sample. The data are scattered, but a straight line was approximated through each set of points. The as-received sample gives a correlation in good agreement with that obtained from the B & W data for limestones and dolomites which were ground to pass 100 percent through a 60 mesh screen. From Figure 15, there appears to be very little difference between the sets of data representing the -140+200 and the -200 mesh samples, and they appear to exhibit a twofold improvement over the as-received sample with respect to SO_2 removal.

In Figure 16, the CaO utilization of Peabody's Limestone No. 1683 (-140+200 mesh and -200 mesh samples) is plotted against residence time of the gas in the reactor. Although the points do not show any clear-cut relation within themselves, they do indicate much higher utilizations than do the data points of Battelle and B & W which appear on the same plot. One possible explanation for this discrepancy lies in the fact that the Peabody test runs used very high excess oxygen levels

FIGURE 15

EFFECT OF STOICHIOMETRY ON SO_2 REMOVAL

PEABODY DATA — LIMESTONE 1683

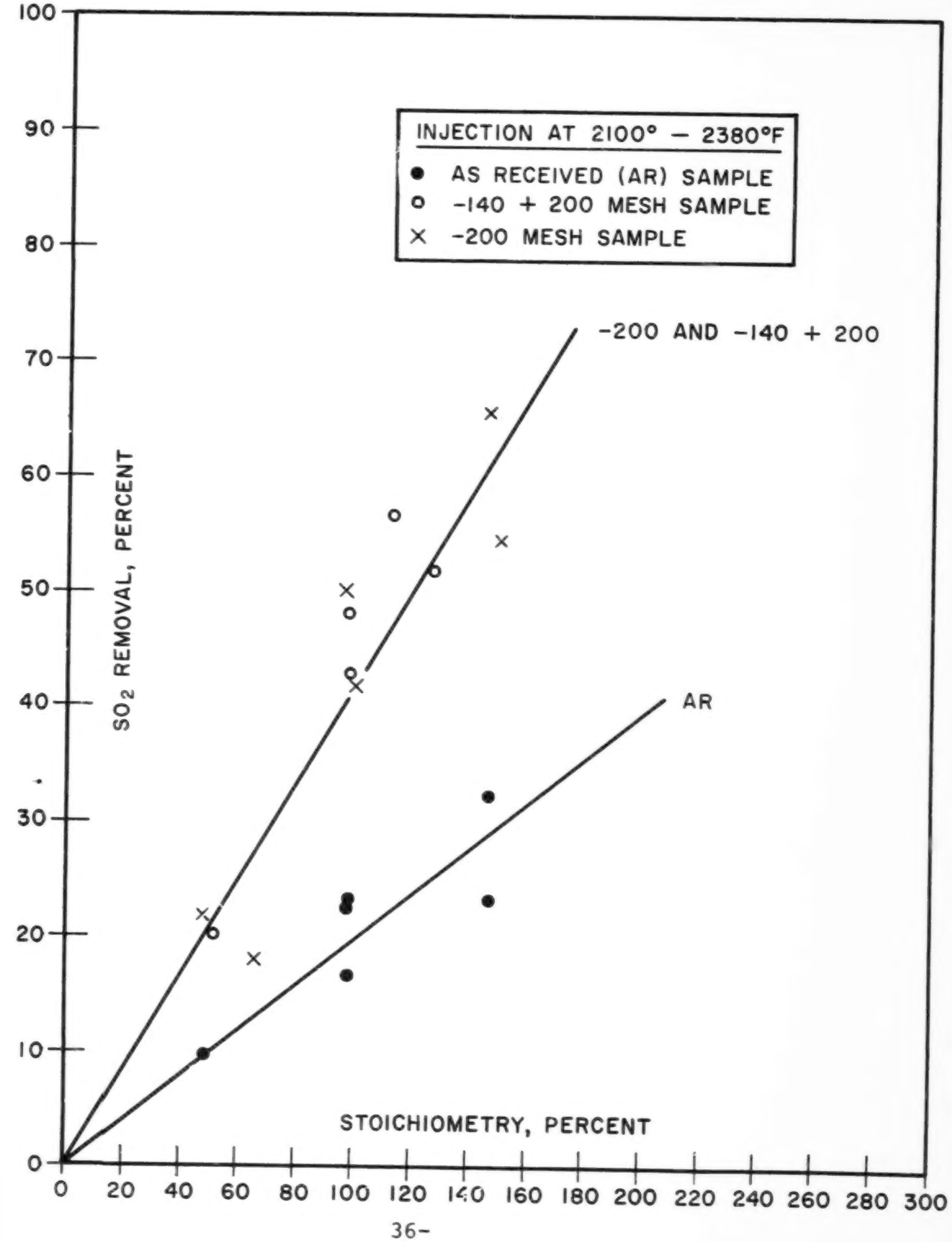

FIGURE 16

EFFECT OF RESIDENCE TIME ON CaO UTILIZATION

LIMESTONE > 87% CaO

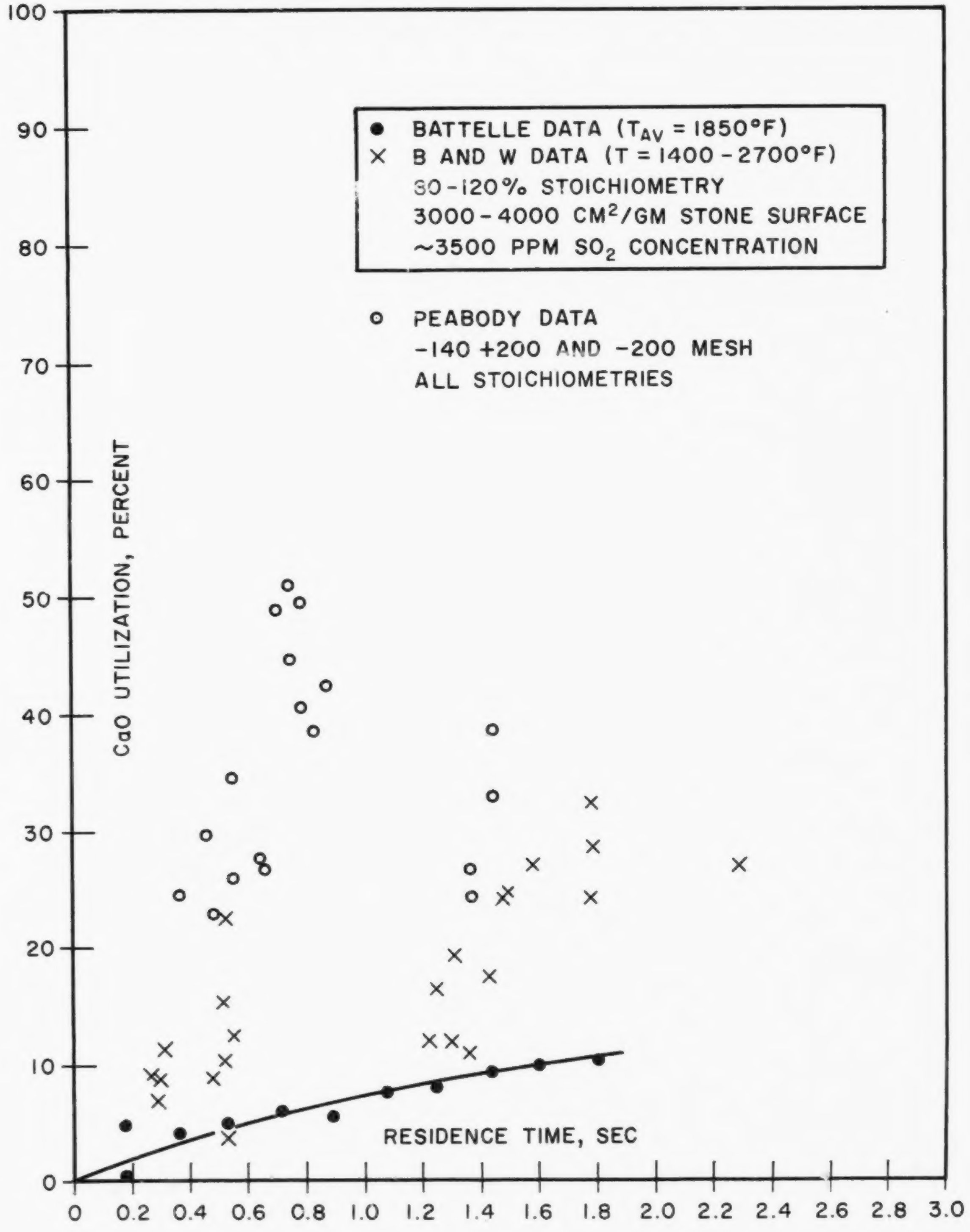

ranging as high as 130 percent. Although there is no consistent evidence within the data to support this conclusion, it is considered a possible explanation for the high CaO utilizations observed. That is, based on diffusion controlling, higher excess oxygen levels would give higher utilizations by increasing the rate of diffusion and subsequent reaction for the same residence time. Note that most investigators have found that SO_2 absorption increases with increasing oxygen concentration. It should be noted also that good sulfur balances generally were not obtained; for example, the average of 5 test runs for stone 1683 is 70% accountability (after correction for fly ash dilution), 83.6% accountability for 1359 (6 points), and 79.5% accountability for 1684 (5 points). This may account for some of the high CaO utilizations reported.

4. Shawnee Plant Data

Results from the first 35 tests run on the full-scale boiler at different injection locations, injection velocities and injection angles were rather scattered (see Table 1). Limestone utilizations for SO_2 gas concentrations of 3000 ppm lie in the range of some of the pilot studies; e.g., at a residence time of approximately 1.5 seconds, CaO utilization ranged from about 7 to 18 percent. However, the particle size range reported for the Limestone No. 2061 used at Shawnee (50% less than 16 microns) was considerably smaller than that employed in the pilot studies (50-90 microns average particle). According to previous correlations of stone utilization with particle size, the Shawnee data should indicate much higher utilizations for its smaller particle size. The shrinking core model developed by M. W. Kellogg predicts CaO utilizations for 16 micron particles of Limestone No. 2061 to be more than threefold the actual values reported.

This apparent anomaly could possibly be attributed to the fact that, if indeed the actual additive particle size range is as small as that reported, there may be an appreciable amount of particle dead-burning occurring since injection temperatures at the coolest injection location (upper rear) exceed 2300°F. Although the shrinking core model has not been validated for particle sizes smaller than 50 microns, it is felt that the discrepancy obtained with the Shawnee data is far too great for considering the model's inadequacies as the explanation.

TABLE I

DRY LIMESTONE PROJECT
PHASE I TEST RESULTS
SHAWNEE STEAM PLANT

Test No.	Injection Location	Stoich.	Coal % S	Injection Velocity (fps)	Load	Excess Air E(%)*	Excess Air W(%)+	Injection Angle	Avg. Part Size Index	Initial SO₂ Level-ppm E*	Initial SO₂ Level-ppm W+	% SO₂ Removal E*	% SO₂ Removal W+	Limestone Utilization E*	Limestone Utilization W+
1	Lower Rear	1.86	2.4	130	140	26.5	24.3	0	4.0	1840	1840	15.1	10.8	11.3	11.7
2	Upper Rear	1.55	2.6	132	140	35.5	33.3	0	4.0	1600	1640	23.0	20.1	11.4	15.1
3	Upper Rear	1.84	2.2	59	143	27.3	20.0	0	4.5	1400	1500	15.2	7.3	6.8	7.7
4	Upper Rear	3.10	1.6	127	144	25.0	20.0	0	4.4	1190	1190	14.9	14.9	9.4	10.1
5	Upper Rear	3.68	1.4	67	142	18.0	16.7	0	4.2	1240	1240		14.7	7.2	6.3
6	Lower Rear	2.11	1.8	68	142	21.7	23.9	0	4.2	1480	1540	11.5	10.4	6.2	6.6
7	Lower Rear	2.30	2.0	130	140	18.3	19.2	0	4.6	2040	2120	11.2	9.4	5.2	6.5
8	Lower Rear	2.43	2.1	68	140	23.5	20.0	0	4.5	1900	1840	12.0	10.9	7.3	5.7
9	Upper Rear	1.47	2.5	940	140	14.1	18.0	0	4.7	2240	2160	13.1	14.1	10.4	9.0
10R2	Upper Rear	1.33	3.8	940	139	35.5	32.9	0	5.0	2400	2480	13.1	11.7	9.4	10.0
11	Front	1.53	3.3	195	139	29.6	31.3	0	5.0	2400	2440	4.7	11.0	7.9	8.6
12R3	Front	1.11	3.6	198	139	37.7	35.0	0	5.0	2360	2400	6.1	12.4	15.1	13.9
13	Front	1.76	2.2	101	142	37.7	37.7	0	4.7	1600	1600	14.2	12.9	7.1	9.1
14	Front	1.46	3.3	192	144	37.7	37.7	0	4.6	1800	1800	16.7	16.7	5.9	7.2
15	Upper Rear	1.75	2.2	945	142	40.0	33.3	0	4.8	1600	1520	27.4	26.7	9.9	12.8
16	Upper Rear	1.50	3.2	940	142	29.6	31.3	0	4.7	2680	2680	15.3	13.7	20.1	16.5
17	Upper Rear	1.01	3.5	131	142	29.6	31.3	+45	4.8	2520	2400	8.1	16.0	14.5	13.0
18	Upper Rear	1.77	2.4	131	141	29.6	37.3	+45	4.7	2680	2480	11.2	17.4	11.9	13.7
19	Upper Rear	1.16	3.0	132	142	38.2	39.1	-45	4.7	2200	2200	13.3	11.9	11.1	12.5
20	Upper Rear	1.69	3.0	132	142	38.2	39.1	-45	4.7	2400	2160	14.3	14.2	9.0	9.0
21	Upper Rear	0.87	2.9	134	138	16.0	16.6	-45	5.1	2200	2080	8.2	6.6	7.2	10.1
22	Upper Rear	1.76	1.7	131	140	25.0	15.4	0	4.8	1600	1680	17.2	15.3	11.8	11.1
23	Upper Rear	1.07	3.7	68	140	33.8	28.8	0	4.4	2720	2760	9.4	5.8	11.0	12.5
24	Upper Rear	1.70	3.2	67	139	32.9	39.1	-45	4.6	2480	2480	6.5	4.6	5.6	7.6
25	Upper Rear	1.29	4.0	68	116	22.1	23.5	0	5.2	3000	2920	8.7	8.9	6.7	5.1
26	Upper Rear	1.29	4.2	131	118	30.4	30.4	-45	4.8	3200	3200	4.4	5.7	7.9	8.7
27	Upper Rear	1.10	2.3	69	120	11.9	11.0	-45	5.7	1960	2000	8.6	11.5	10.2	11.3
28	Upper Rear	1.13	2.5	135	117	26.5	28.2	0	5.7	1800	1900	11.1	11.9	12.4	13.8
6A	Lower Rear	1.19	2.6	69	137	22.8	23.5	0	4.4	2400	2360	6.8	4.3	9.5	8.6
7A	Lower Rear	1.72	2.3	132	139	17.3	21.6	0	4.8	2080	1960	11.2	10.9	6.9	6.1
8A	Lower Rear	2.01	2.4	68	140	22.1	23.5	0	4.5	2080	2000	11.2	10.8	6.5	7.4
2A	Upper Rear	1.11	2.1	133	138	35.5	32.1	0	5.1	1620	1520	11.3	17.0	10.3	12.2
4A	Upper Rear	1.39	1.9	132	139	27.3	20.7	0	4.3	1760	1660	14.5	21.7	6.9	8.0
29	Upper Rear	0.86	1.7	136	78	27.0	28.0	0	5.0	1560	1440	13.0	14.5	12.3	17.0
1A	Lower Rear	1.44	2.7	133	138	25.4	29.2	0	5.1	2440	2480	11.0	8.6	7.4	6.1

*I=East Half of boiler
+W=West Half of boiler

Another parameter which could have an effect on the CaO utilization in the full scale boiler is limestone distribution within the boiler. The model makes no allowance for nonuniform distribution of either limestone or SO_2 in the flue gas; that is, it is assumed that both SO_2 and CaO are distributed uniformly over the boiler cross sectional area. In actual practice, however, the Shawnee tests have shown nonuniform distributions are obtained for both SO_2 and limestone. Thus, even if completely uniform distribution of limestone in the boiler flue gas is obtained, uniform distribution with respect to SO_2 will not be realized owing to the variation in SO_2 concentration from point to point within a given plane. The effect on CaO utilization of this nonuniformity in SO_2 and CaO distribution is difficult to determine but possibly could account for some of the discrepancy between the model prediction and actual data. Hopefully, the studies in progress as of this writing utilizing lower injection temperatures and improved limestone distribution will yield more optimistic results.

B. Bench Scale Sulfation Data

1. OAP Research Studies

The in-house OAP Research studies investigated the SO_2 sorption characteristics of ten diverse types of limestones. In these studies, differential reactor techniques were used to measure the rate of reaction of sulfur dioxide with ten species of naturally occurring limestones after calcination at standardized conditions. The rates were measured as a function of particle size, SO_2 concentration, CaO conversion and temperature, and then correlated to these variables and the physical properties of the stones.

The calcines used in these studies were prepared by a 2-hour kiln calcination at 1796°F. The calcined samples were then crushed and screened into three particle size ranges, i.e., 12/16 mesh, 42/65 mesh and 150/170 mesh. The samples were then placed in the differential reactor where they were exposed to a flue gas containing about 3000 ppm SO_2. The sulfation tests were undertaken at reaction temperatures of 1202°F, 1400°F, 1598°F and 1796°F.

While tabular experimental data for the particle loading versus time are not presented, the report(4) does contain a series of plots of loading versus time for the conditions studied. Further data presented in this report include the following properties: pore volume, mean pore diameter and B.E.T. surface area, by type and particle size, as well as the raw stone composition and ignition loss-by stone type. Using these data, the OAP

Research group developed a sorption rate model which incorporates empirical constants to relate the physical properties and system parameters to the sorption rate. These empirical constants are tabulated in the OAP published report by stone size and type(4).

However, because of the nature of the experimental procedures used, some of the conclusions and results indicated in the OAP report are open to question. There are two primary areas which have caused such speculation to arise:

(1) the calcination technique
(2) the range of residence times studied

One of the primary conclusions drawn from the experimental data was that the rate of reaction was linearly related to the B.E.T. surface area of the calcine. However, there is a significant time-temperature relationship to the stone surface area. While this effect will be discussed in more detail in a later section of this report (Section IV, C.2., D.2.,3; E.3;F.2.b), it is important to note that the flash calcination which would be experienced in a commercial system could result in calcines with surface areas in the range of one to two orders of magnitude higher than measured in the OAP bench scale tests. Thus, the surface area effects seen in this study might not be comparable to those which may occur in a commercial boiler system.

The second source of possible difficulty is the residence time range used in the OAP studies. The range investigated was from 5 to 140 seconds, whereas commercial pulverized coal boilers would offer a maximum residence time in the order of 2 to 4 seconds. Therefore, the mechanisms of sorption which are represented by the empirical model and data of the bench studies may not be those which come into play in a commercial system. These comments are intended to point out some of the inherent limitations involved in this type of bench scale work, and to caution subsequent investigators as to possible difficulties which may be encountered in trying to adapt the resulting data to their particular needs.

2. TVA Studies

The Fundamental Research Branch of TVA has performed numerous sorption studies in an attempt to relate the physical properties of various stones to their sorption characteristics. Most of these sulfation tests utilized calcines which were prepared by long duration calcination, as were the stones in the OAP studies.

One of the most significant finds of the TVA experimentation was the relationship of pore volume or surface area to the rate of SO_2 removal. By comparing the sulfation data of a calcined sample to that of a sample which had been calcined, hydrated, and dehydrated, the results in Figure 17 were obtained(6). The curves in Figure 17 reflect a significantly higher degree of sorption for the hydrated sample than for the anhydrous one. At 25 minutes run duration, the capacity of the former sample was 40% greater than that of the latter. Figure 18 demonstrates that the cumulative pore volume of hydrated material is 40% greater than the "calcined only" sample, which is in line with the difference in capacity. Furthermore, the rapid absorption of SO_2 by the hydrated sample in the first 5 minutes of the absorption test, Figure 17, may be explained by the difference in the distributions of pores in the two samples as shown in Figure 18. Forty percent of the pores in the hydrated sample have diameters greater than 1.75 microns, whereas the calcine has only 18% pores in this range. The larger pores should be more accessible to the SO_2, and samples with high percentages of large pores should react faster if other conditions are the same. Obviously a trade-off between large pores and greater capacity and small pores and greater rates is necessary to optimize for a specific application. When reaction times are very short, as when lime is injected in a combustion gas stream, reaction rate is probably most important.

FIGURE 17

SORPTION OF SO_2 FROM SIMULATED STACK GAS BY CALCINE OF -24 +28 MESH COLBERT LIMESTONE

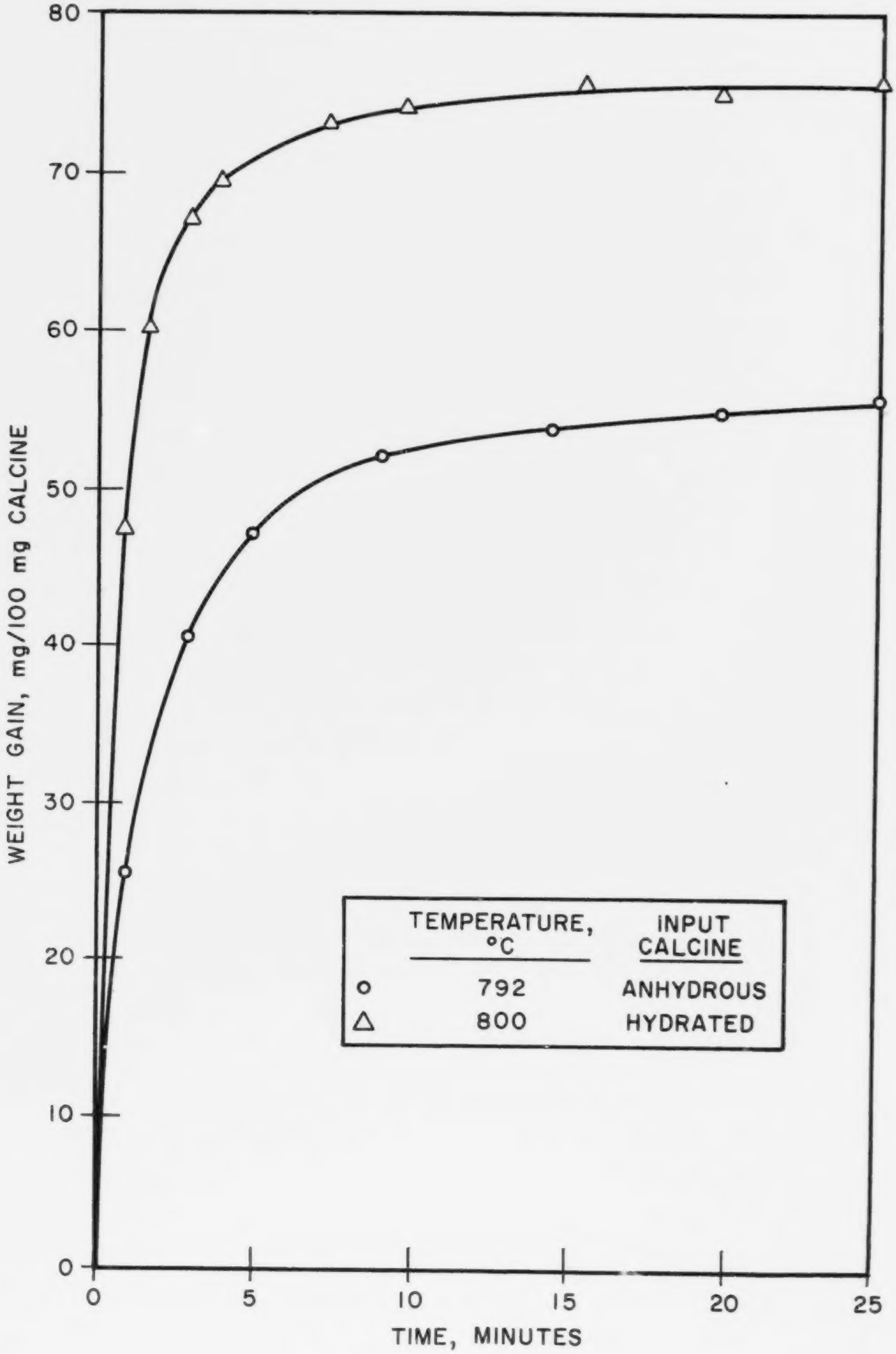

FIGURE 18

PORE VOLUMES OF COLBERT LIMESTONE, -24 +28 MESH

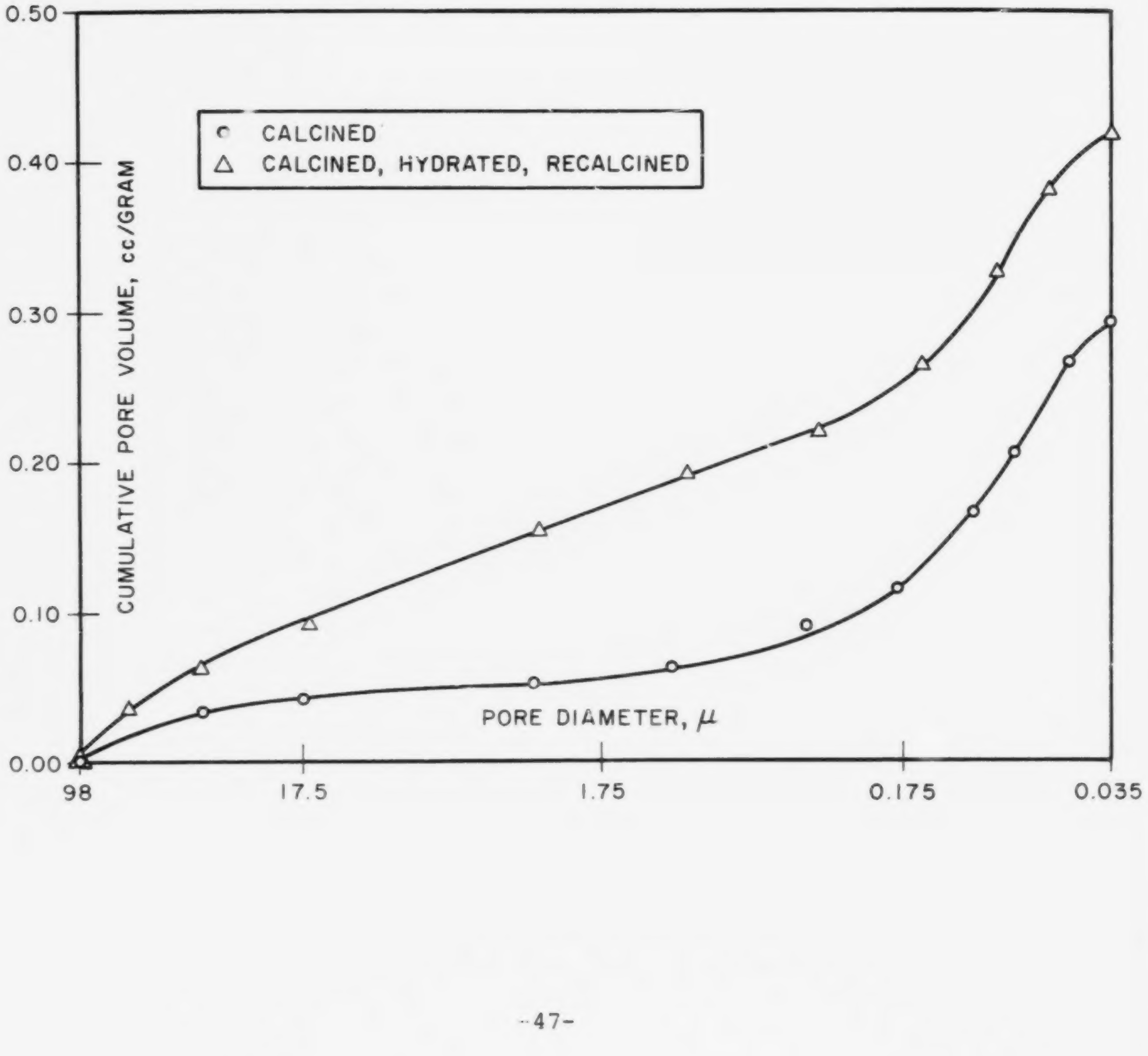

To investigate this possibility, TVA recalculated the total available surface area by the method of Rootare and Prenzlow(5). As shown in Table 2, the differences between surface areas for the calcined and hydrated samples exist only in the larger pores. The larger surface area in the large pores of the hydrated sample could account for the more rapid initial absorption of SO_2 by this sample in the test shown in Figure 17. The ratio of the surface areas of the two samples at 0.2 micron pores or larger is the same as the ratio of weights of SO_2 absorbed in 25 minutes. This suggests that although small pores may contain a large fraction of the total surface area, they are not significant in the total absorption of SO_2.

In an attempt to relate the particle size of a calcine to its sorption rate, the data in Figure 19 were obtained and plotted on a log-log basis. It is evident that there are two distinct reaction stages with different slopes in this relationship. The first stage consists of parallel lines of slope approximately unity; the curves for the smaller particles lie above those of the larger ones, that is, the intercept at $\underline{t} = 1$ ($\log \underline{t} = 0$) is inversely related to the particle size with the exception of the minus 325-mesh samples. An explanation of this discrepancy might be that there has been some aggregation of the very fine particles in this size range, as suggested by others.

The second stage of the reaction starts at 3 to 5 minutes under these conditions, and the slopes of the lines are inversely related to the particle size of the calcine. The intersection of the two stages, found by extrapolating the two straight portions of the curves,

TABLE 2

SURFACE AREAS OF CALCINED AND HYDRATED COLBERT COUNTY LIMESTONE CALCUATED FROM PORE VOLUMES

Pore Diameter, microns	Cumulative Surface Area, m^2/gm	
	Hydrated	Calcined
17.5	0.008	0.003
5.0	0.03	0.007
1.0	0.14	0.04
0.5	0.26	0.14
0.2	0.75	0.53
0.1	2.5	2.4
0.05	7.6	7.6
0.035	10.0	10.6

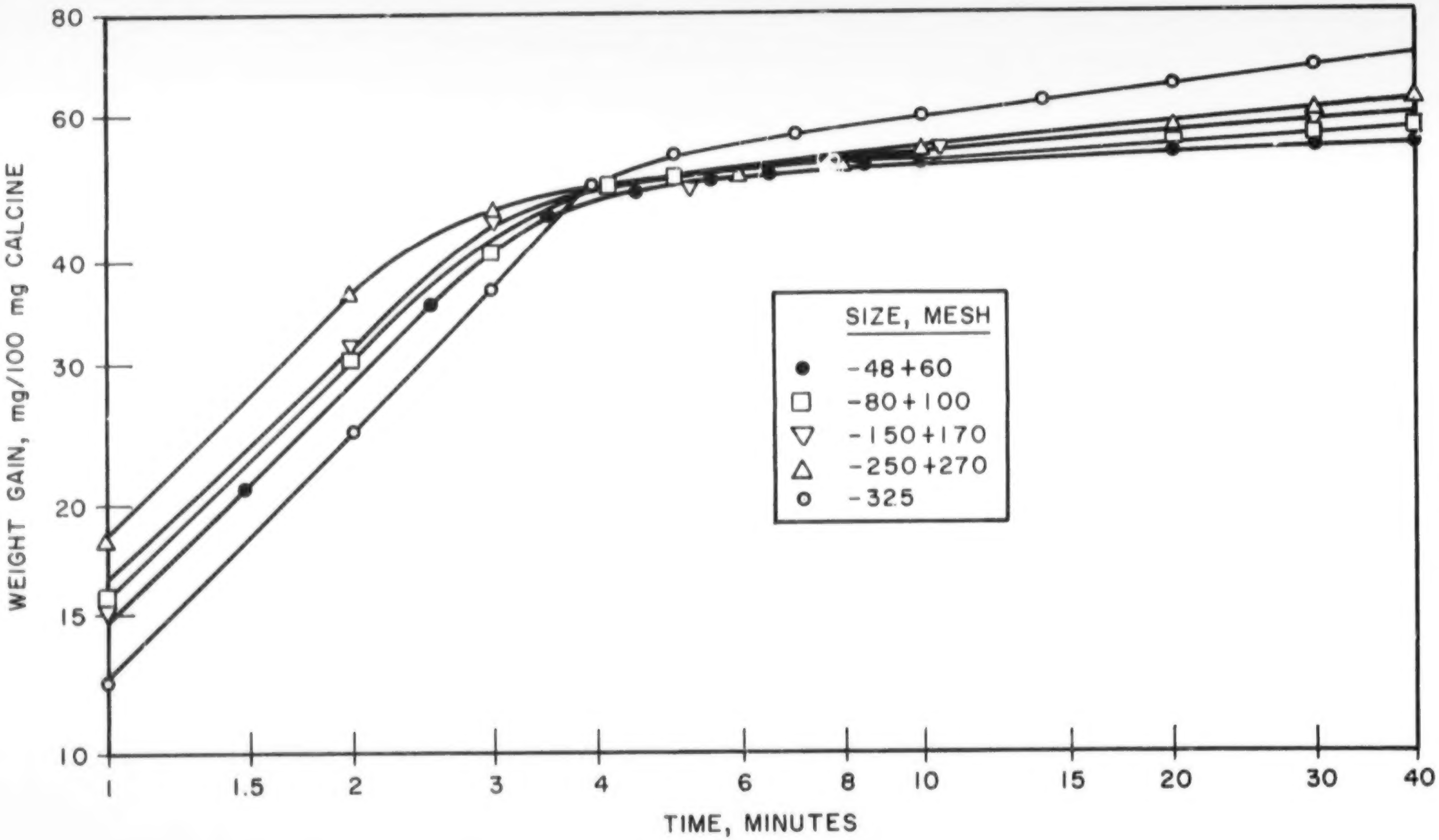

FIGURE 19

EFFECT OF PARTICLE SIZE

ON

THE REACTION OF CALCINED LIMESTONE WITH SO_2 AND O_2

was found to be at about the same value for all particle sizes in weight gain per unit weight of calcine, 48 ± 2 mg/100 mg calcine. This indicates that the proportion of the reaction during the first stage is independent of the particle size of the calcine, and that about 40% of the CaO reacts during the first stage. This would also indicate that in the injection of limestone into a boiler, a maximum of 40% utilization of the CaO can be expected by the first reaction mechanism, and 250% of the stoichiometric amount of limestone would be required to obtain complete removal of SO_2 from the flue gas if the first-stage mechanism can be carried to completion in the boiler. The second stage is so much slower than the first stage that the retention times in the boiler practically eliminate this diffusion-through-product mechanism from consideration. The significance of these results is that the loading of SO_2 on the calcine is insignificant for the first-stage reaction rate as long as there is abundant surface for reaction.

To test the effect of SO_2 gas concentration, the previous experimentation was re-run, this time varying the SO_2 concentration in the flue gas. The results, as shown on Figure 20, are similar to those obtained for the different particle size runs in that two distinct sorption regions are evident, and the intercept of the two straight portions was again about 48 mg SO_3/100 mg calcine or ∼40% utilization of the CaO in the first stage. In other testing, TVA found that O_2 had little effect upon sorption in the primary reaction zone, and that H_2O did not affect the soprtion or calcination kinetics of limestone.

To test the effects of calcination time and temperature, an experiment was performed in which the limestone was rapidly calcined and transferred to a TGA

FIGURE 20

EFFECT OF SO_2 AND O_2 ON REACTION VELOCITY WITH -24 +28 MESH COLBERT LIMESTONE

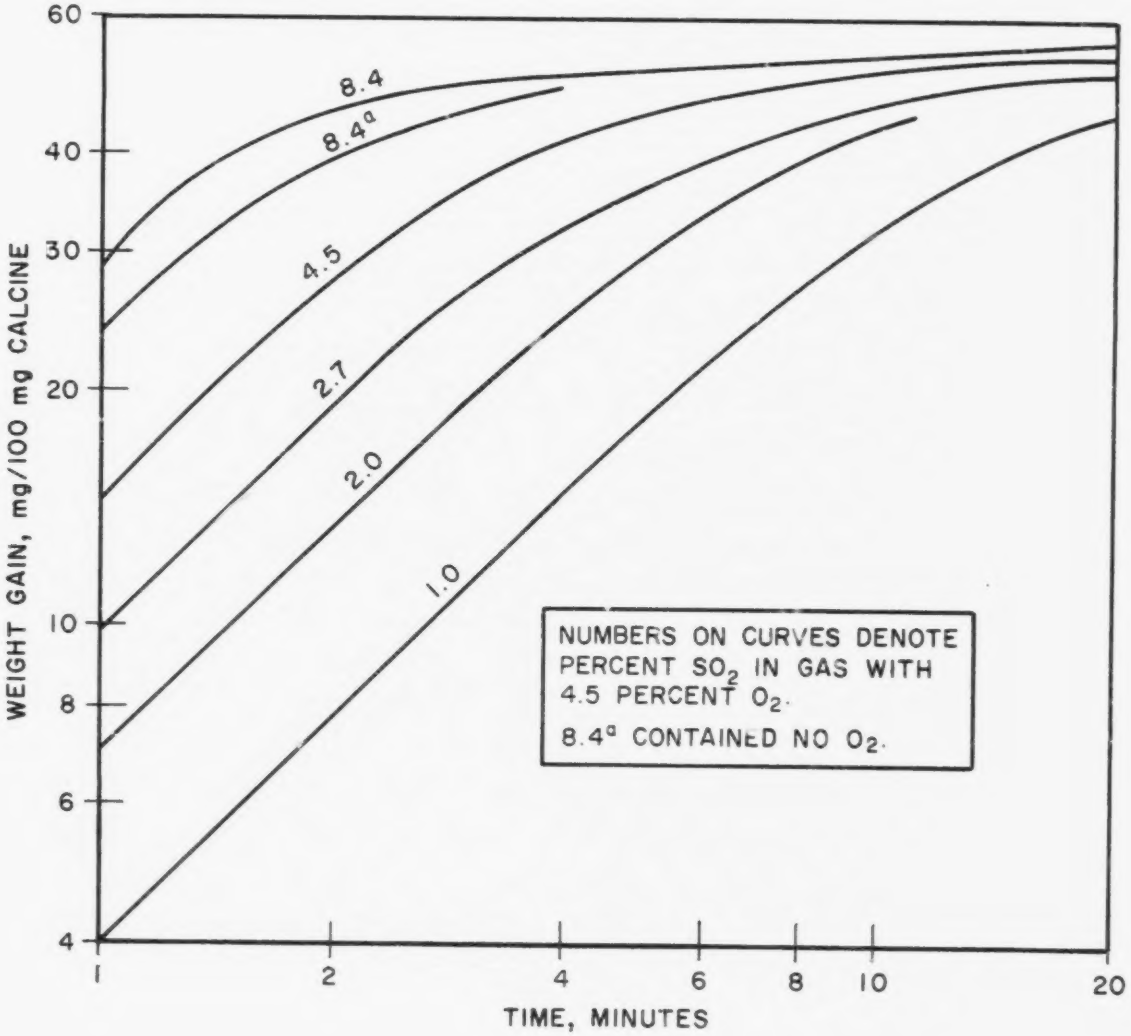

(thermogravimetric analyzer) apparatus for sorption testing in a typical flue gas mixture. As shown in Figure 21, the reactivity of the calcine decreased very rapidly as the calcination temperature was raised, and this loss in reactivity also increased as the time of calcination was lengthened. Based upon these results, it was estimated that the percent loss in reactivity was related to the one-half power of the calcination time and the reciprocal of the absolute temperature by the formula:

$$\text{Loss of reactivity} \quad (\%) = \frac{(445 - 5.7 \times 10^5)}{T} \, t^{1/2}$$

The conclusions drawn by TVA regarding the sorption of SO_2 by limestone calcines may be summarized as follows:

(a) The sulfation reaction is influenced greatly by the conditions of calcination as well as the type of stone and the degree of grinding prior to calcination.

(b) Sulfation of CaO takes place in two stages: reaction of sulfur dioxide with oxygen on the surface of the lime, followed by diffusion of the reactants through the resultant $CaSO_4$ shell into the unreacted lime core.

(c) Pores in the calcine smaller than 0.1 micron do not admit sulfur dioxide rapidly enough to have a significant effect upon sorption at short residence times.

(d) From bench scale testing, there appear to be many interactions between parameters. These effects may be related to the scale of experimentation and it is likely that definitive information will only be obtained under actual conditions simulating the boiler injection process.

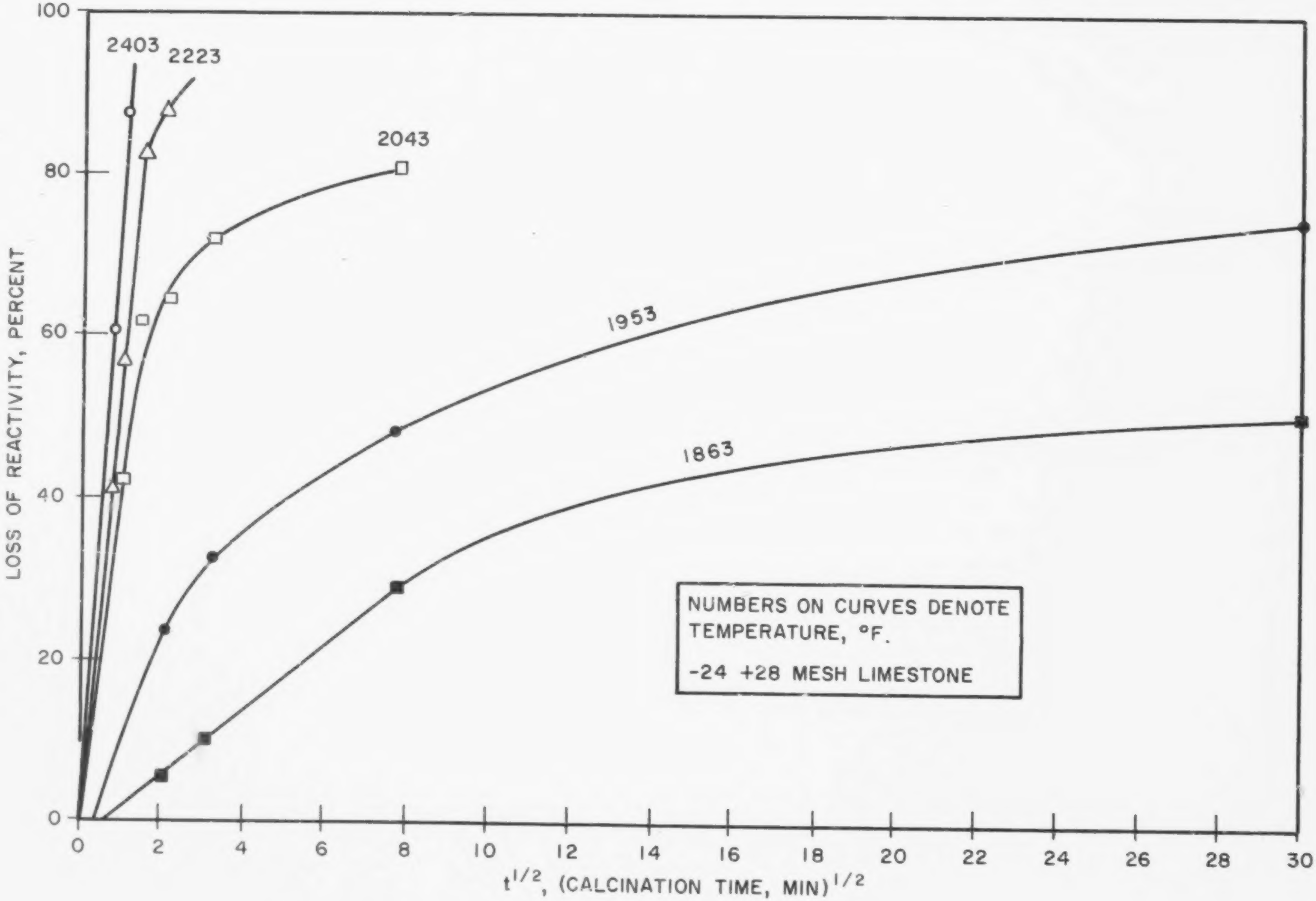

FIGURE 21

EFFECT OF CALCINATION CONDITIONS ON REACTIVITY OF CALCINE

C. Evaluation of Process Models

1. Kellogg Shrinking Core Model (sulfation reaction)

a. Theory and Development

The shrinking core model was developed by Kellogg with assistance from consultant Dr. R. L. Pigford (Univ. California)*. This model considers a single CaO particle of radius, R_s, which consists of tiny nonporous micropellets of radius, R_s, the void spaces between these micropellets being the pores of the larger particles. SO_2 in the gas phase diffuses through these pores to the surface of the micropellets where reaction with SO_2 occurs. As reaction proceeds, a shell of reaction product uniformly accumulates around the surface of the CaO spherical micropellets. Further reaction occurs only after gas diffuses through pore structure of the particle and then through the reaction product layer around the micropellets to their inner core of fresh unreacted CaO which gradually shrinks in size until ideally only a pellet of reaction product remains.

The model is therefore valid under the assumption that chemical reaction is rapid relative to the diffusional process in the form of (1) bulk gas diffusion, (2) pore or Knudsen diffusion, and (3) diffusion of the gas through the cracks and pores of the reaction product. The following expression describes the relationship between the rate of diffusion of SO_2 through the reaction product and the radial velocity of the reaction surface:

---

* See Appendix C for details of model development.

$$K \left(\frac{CH-O}{r-X}\right) 4\pi \, rX = -\frac{d}{dt} \left(\rho s \frac{4}{3} \pi X^3\right) \qquad \text{Eq. (1)}$$

where

K = diffusion coefficient representing transfer of gas through the solid reaction product, cm^2/sec

C = SO_2 gas concentration, gm-moles/cc

H = A Henry's law coefficient representing equilibrium between the SO_2 and the solid reaction product

*r = micropellet radius, cm

X = radius of CaO core of micropellet, cm

rX = square of the geometric mean radius of the spherical shell of reaction product, cm^2

ρs = molal density of reaction product, lb mols/cc

t = time, sec

Diffusion through the pores of the large particles is given by

$$\frac{D}{\tau R^2} \cdot \frac{\delta}{\delta R} \left(R^2 \frac{\delta C}{\delta R}\right) = \frac{\delta C}{\delta t} + \frac{S_V}{\gamma} \left(\begin{matrix}\text{Rate of reaction} \\ \text{per unit area}\end{matrix}\right) \qquad \text{Eq. (2)}$$

where

D = diffusion coefficient depicting bulk gas phase and/or pore (Knudsen) diffusion, cm^2/sec

τ = particle tortuosity

R = radial position in the larger particle, cm

*S_v = total calcined particle surface to volume ratio, cm^2/cc

* γ = porosity of the calcined particle, cc/cc

* These parameters were assumed to remain constant during the sulfation reaction.

The first term on the right-hand side of equation (2) accounts for accumulation of gas in the pores and is considered negligible. By appropriate mathematical manipulation of equations (1) and (2), the following relationship results:

$$\frac{D}{\gamma} \cdot \frac{1}{R^2} \cdot \frac{\delta}{\delta R}\left(R^2 \frac{\delta C}{\delta R}\right) = \frac{\alpha C}{\sqrt{\int_0^t C dt}} \qquad \text{Eq. (3)}$$

where

$$\alpha = \frac{S_v}{\gamma}\sqrt{\frac{KH \ \rho s}{2}}$$

For simplification purposes, a set of dimensionless variables is introduced at this point:

$$c = C/C_i \ ; \quad \xi = R/R_s \ ; \quad \theta = \frac{D^2 C_i}{\alpha^2 \gamma^2 R_s{}^4} t$$

where

C_i = SO_2 gas concentration at the surface of the large particle, gm-moles/cc

R_s = radius of the large particle, cm

In dimensionless terms, equation (3) now becomes

$$\frac{1}{\xi^2} \cdot \frac{\delta}{\delta \xi}\left(\frac{\xi \delta c}{\delta \xi}\right) = \frac{c}{\sqrt{\int_0^\theta c \, d\theta}} \qquad \text{Eq. (4)}$$

with the following boundary limitations:

$$c(\xi, 0) = 0 \ ; \ c(1, \theta) = 1 \ ; \ \frac{\delta c}{\delta \xi}(0, \theta) = 0$$

Equation (4) is a nonlinear, partial differential equation and must be solved by a finite differencing technique. The solution will be of the form

$$c = F(\xi, \theta) \qquad \text{Eq. (5)}$$

It is noted that the solution indicated by equation (5) contains no parameters, i.e., the dimensionless concentration, c, is a function of dimensionless position (ξ) and time (θ) only. There will consequently be a unique solution to equation (5) for all values of the system parameters (R_s, C_i, D, etc.).

The rate of passage of SO_2 into the large particle is obtained from

$$N \text{ (gm-moles/sec)} = \frac{D\gamma}{\tau}(4\pi R_s^2)\left.\frac{\delta c}{\delta R}\right|_{R=R_s} \qquad \text{Eq. (6)}$$

or, in terms of dimensionless variables,

$$N = \frac{D\gamma C_i}{\tau R_s}(4\pi R_s^2)\left.\frac{\delta c}{\delta \xi}\right|_{\xi=1} \qquad \text{Eq. (7)}$$

A dimensionless instantaneous rate of SO_2 consumption may now be defined as

$$G(\theta) = \frac{N}{\left(\frac{D\gamma C_i}{\tau R_s}\right)(4\pi R_s^2)} = \left.\frac{\delta F}{\delta \xi}\right|_{\xi=1} \qquad \text{Eq. (8)}$$

Similarly, a dimensionless variable $Q(\theta)$ representing the total cumulative take-up of SO_2 is

$$Q(\theta) = \int_0^{\theta} G(\theta)\, d\theta \qquad \text{Eq. (9)}$$

A computer program has been developed to solve equation (4), by a finite differencing technique, on the IBM 1130 computer. The one and only solution to equation (4) is exhibited in Figure 22 and is of the form

$$G(\theta) = k'\theta^{-0.25} \qquad \text{Eq. (10)}$$

In terms of the dimensionless total SO_2 consumption, $Q(\theta)$, the solution which is shown in Figure 23 is

$$Q(\theta) = k\theta^{0.75} \qquad \text{Eq. (11)}$$

where

k = a constant

Returning for the moment to dimensional terms, the total cumulative take-up of SO_2 in gm-moles is

$$q(t) = \int_0^t N\,dt \qquad \text{Eq. (12)}$$

Converting the right-hand side of equation (12) to include the dimensionless variables, and utilizing equation (9), the expression for the total gm-moles of SO_2 consumed per particle becomes

$$q(t) = \frac{2\pi R_g^5\ S_v^2\ \tau K\ H\ \rho_s}{\gamma D}\ Q(\theta) \qquad \text{Eq. (13)}$$

By application of the definition of dimensionless time, θ, along with equations (11) and (13), the total SO_2 consumed by one limestone particle is determined. The overall CaO utilization is then computed from

$$\text{CaO utilization} = \frac{q(t)}{4/3\,\pi R_s^3\,(1-\gamma)\,\rho_c}$$

where

ρ_c = molal density of CaO, gm-moles/cc

It is worthy of mention that the unique model solution of equation (10) is an approximate one applicable to dimensionless times approaching zero. There does exist, however, an exact solution which mathematically is the same as that in the case of the poisoning of a catalyst pellet. Although the exact solution is being attempted, it is felt that since the dimensionless times are very small as indicated in Figures 22 and 23, the result will not exhibit any appreciable discrepancy from the existing solution.

The model, as it is presented here, is an extrapolation of the behavior of one limestone particle. Its applicability to the performance of a commercial boiler may in fact be limited by the inherent model assumption that no horizontal or vertical SO_2 concentration gradients exist within the reactor, or, in other words, the Ca/S stoichiometry is constant throughout. Whether or not the shrinking core model will accurately predict large-scale boiler performance will therefore depend on the degree of homogeneity of the atmosphere within the boiler.

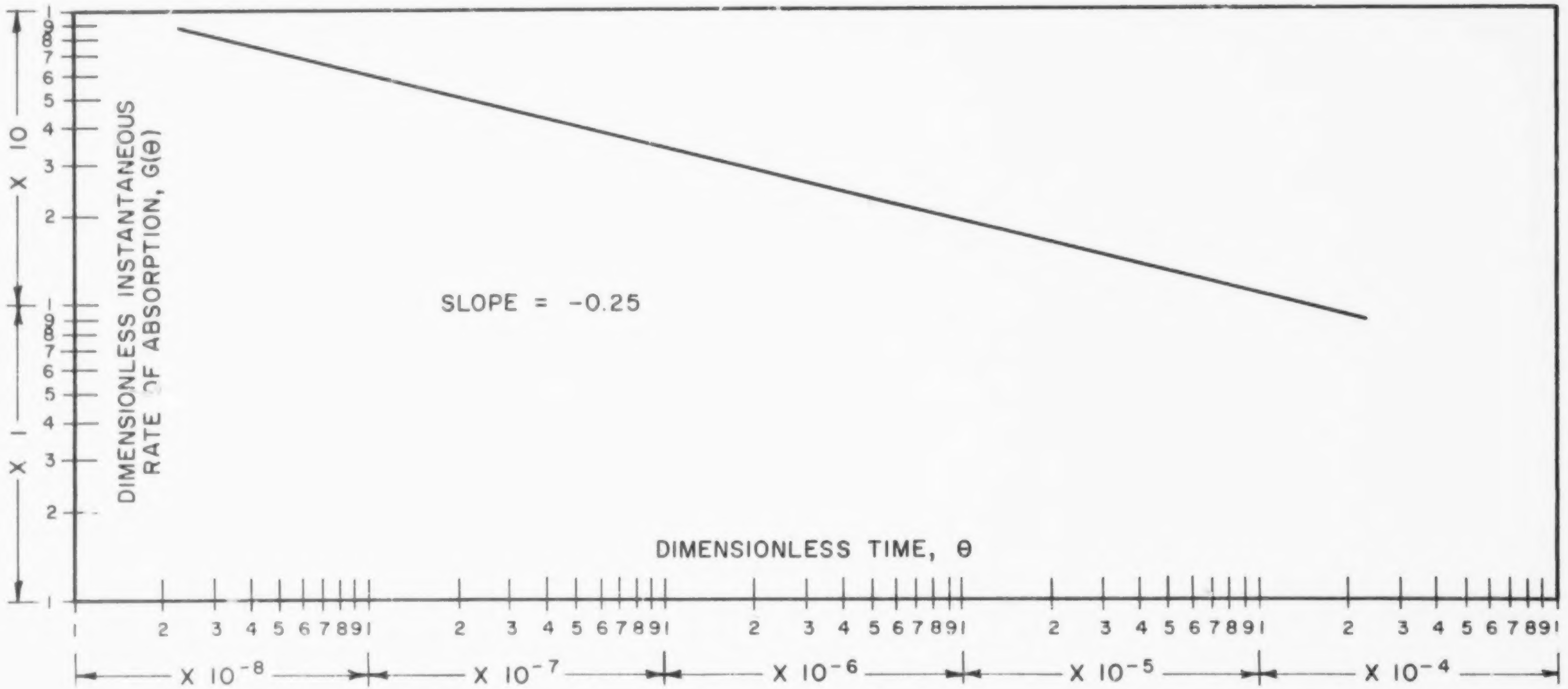

FIGURE 22

MODEL SOLUTION

FOR

DIMENSIONLESS ABSORPTION RATE

FIGURE 23

MODEL SOLUTION
FOR
DIMENSIONLESS CUMULATIVE SO_2 PICKUP

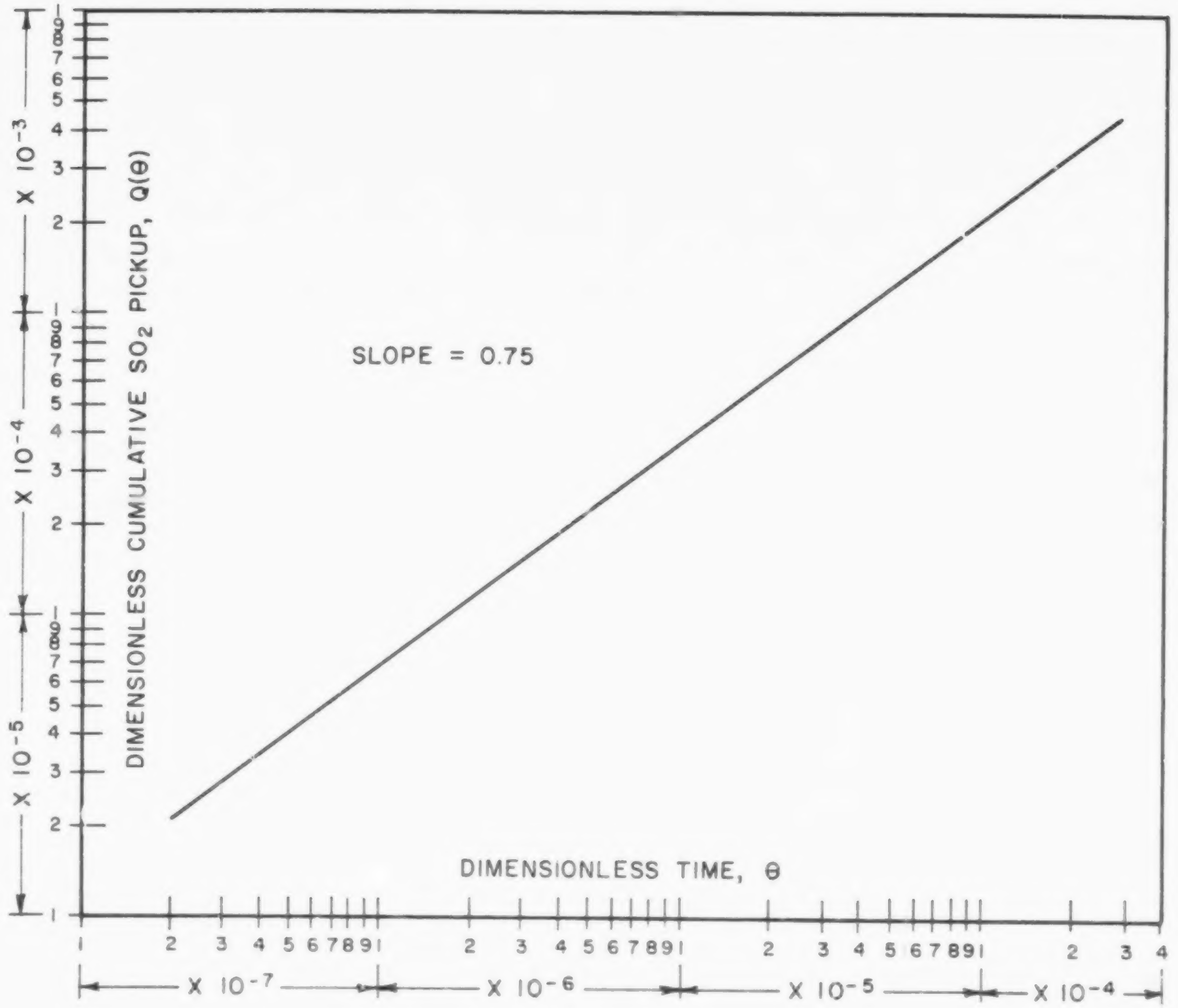

b. Model Parameters and Constants

The gas-phase diffusivity, D, is included in the model as a function of both Knudsen diffusion which involves a square-root dependency on temperature and bulk gas diffusion which depends on temperature to the three-halves power. The former accounts for collision of the gas molecules with the pore walls while the latter deals with diffusion of SO_2 through the gas. The two diffusivities are combined, according to Satterfield and Sherwood(7), in the following manner resulting in an overall effective diffusivity, D_{eff}, which describes gas transfer in the pores of the particle:

$$\frac{1}{D_{eff}} = \frac{1}{D_{bulk}} + \frac{1}{D_{Knudsen}}$$

The individual diffusivities are incorporated into the model program as follows:

$$D_{bulk} = 6.75 \times 10^{-7} \frac{\gamma T^{1.5}}{\tau}$$

and

$$D_{Knudsen} = \frac{14,460 \gamma^2}{\tau S_v} \sqrt{\frac{T}{M}}$$

where

T = gas temperature, °R
M = molecular weight of gas

The SO_2 gas concentration, C_i, at the particle surface was converted to mole fraction by

$$Y_{SO_2} = \frac{Pg\ C_i}{R\ T}$$

where

Pg = gas pressure, atm
Y_{SO_2} = SO_2 mole fraction in the gas at the surface of the particle
R = gas constant in consistent units
T = temperature, ^{o}R

The existing model assumes the SO_2 concentration at the surface of the particle to be constant and an isothermal reactor. The user of the model computer program has the option of maintaining the above temperature constant, thereby simulating an isothermal reactor, or of including temperature as a linear function of time.

For convenience, the diffusivity, K, representing gas transfer through the solid reaction product, and the Henry's Law constant, H, depicting any equilibrium between the SO_2 and the solid reaction product were consolidated into a single constant, k.

(1) Effect of Initial SO_2 Concentration

Data from the Battelle dispersed-phase reactor runs with varying SO_2 concentrations appear in their final report(1). By varying the previously discussed constant k, the model was fit to some of the better Battelle runs (See Figures 26-29). Subsequently, a graph of k versus initial SO_2 mol fraction was plotted (Figure 24), yielding a straight line on log-log paper. The constant k was then incorporated into the computer program as the following function of initial SO_2 concentration:

$$k = e^{(-19.56-1.15 \ln Y_{SO_2})}$$

The above equation suggests that diffusion of gas into the solid reaction product is SO_2 concentration dependent. A feasible explanation for this phenomenon may be the following: If SO_2 is adsorbed strongly onto the surface of the reaction product, then until this surface becomes saturated with SO_2, the diffusivity will appear to decrease with increasing SO_2 concentration, owing to increased adsorption at greater concentrations. It should be emphasized that the above explanation is offered solely as a possibility.

After the constant, k, was programmed as a function of SO_2 concentration, model predictions for the behavior of 74 and 105 micron particles were made at various SO_2 concentrations. The predictions for the 74 micron particles appear in Figure 25 and are based on the following stone and system

FIGURE 24

THE DEPENDENCY OF THE SHRINKING CORE MODEL CONSTANT K ON SO_2 CONCENTRATION

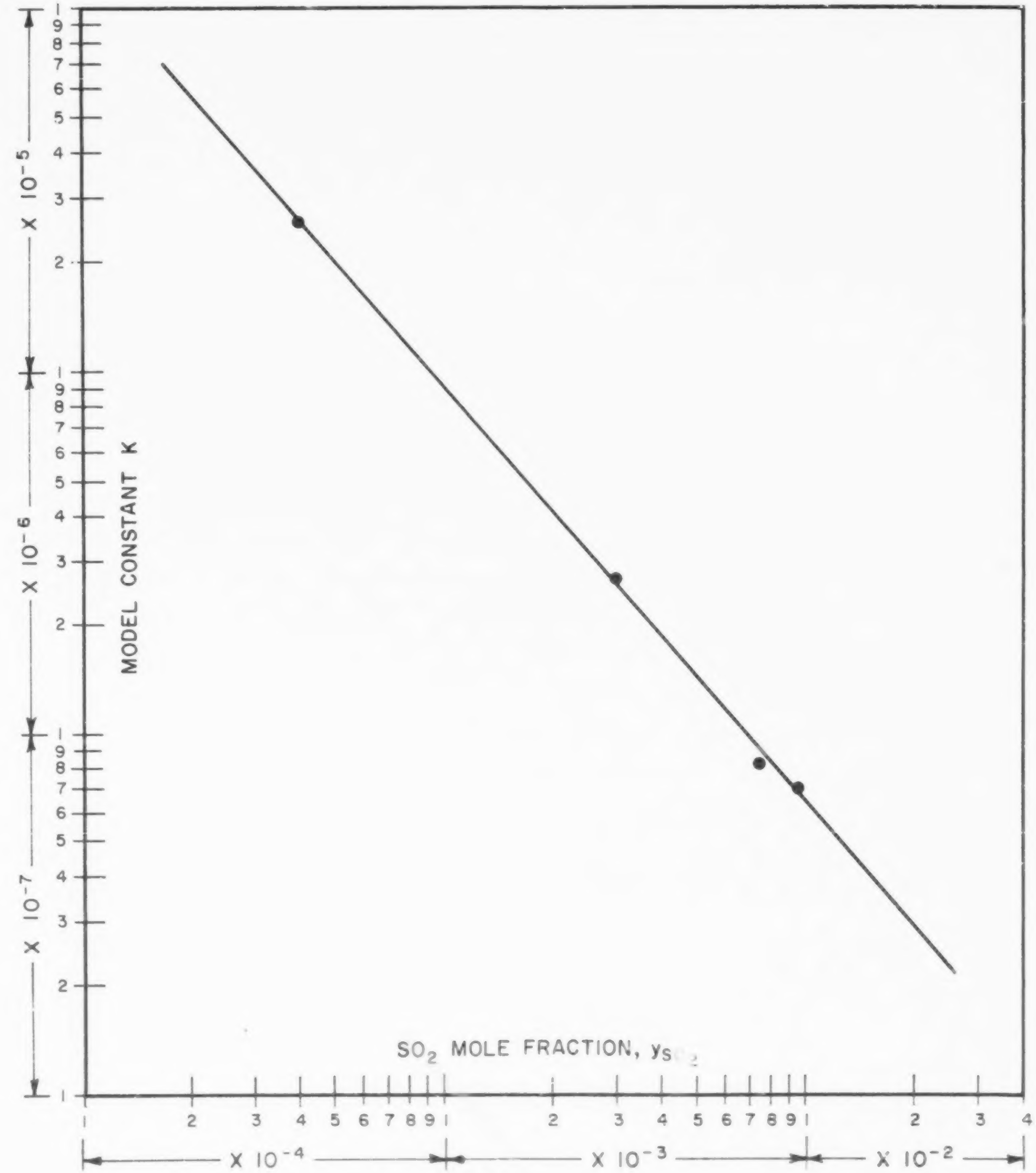

FIGURE 25
SHRINKING CORE MODEL PREDICTIONS
FOR
LIMESTONE 2061

74 MICRON PARTICLES

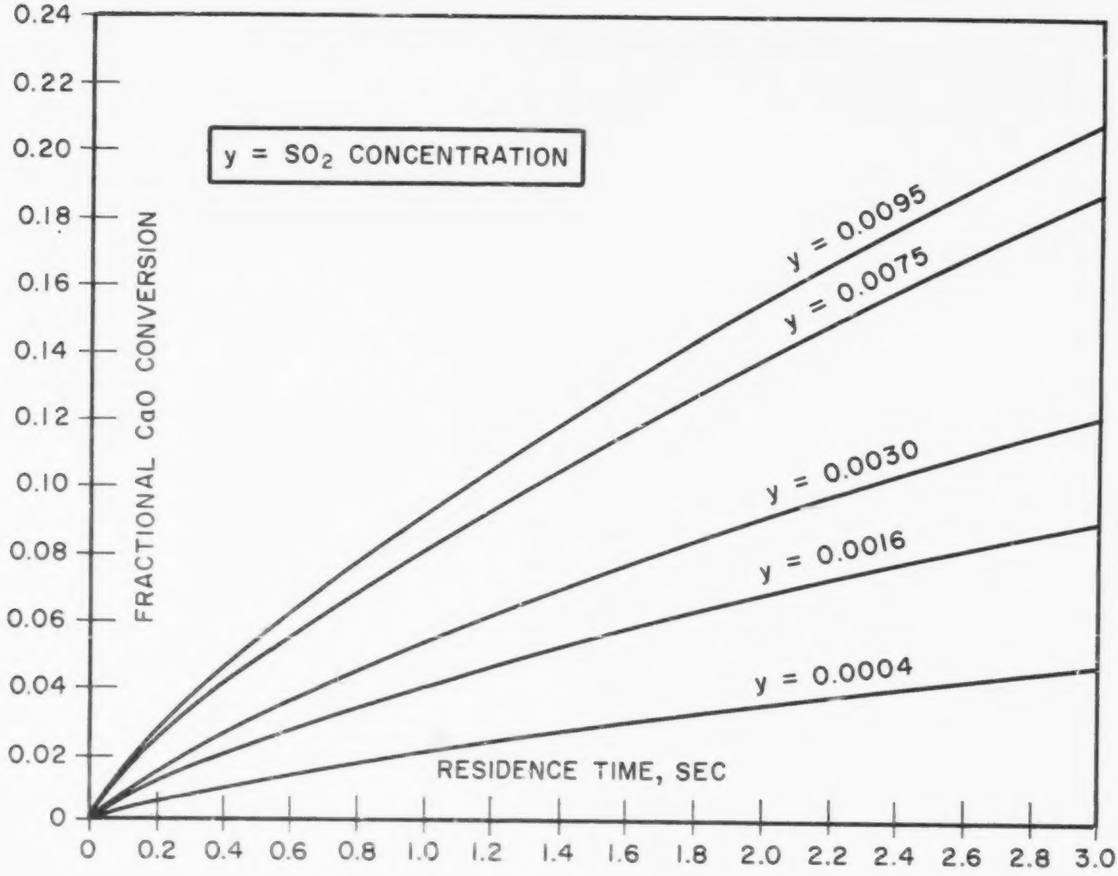

properties:

Gas pressure, Pg = 1 atm
CaO molal density, ρc = 0.0484 gm-mole/cc
Particle porosity, γ = 0.45 cc/cc
Particle tortuosity, τ = 3.0
$CaSO_4$ molal density, ρs = 0.0218 gm-mole/cc
Particle radius, R_s = 0.0037 cm
Temperature, T = 1850°F
Particle surface/volume, S_v = 635,000 cm^2/cc

The above properties were utilized in all of the model predictions except where otherwise noted. Figures 26 through 29 illustrates the fit of the resulting model predictions to the Battelle data for SO_2 mole fractions of 0.0004, 0.0030, 0.0075, and 0.0095. Note that in Figures 26-29 two curves are shown for each SO_2 concentration that is compared to actual data, corresponding to the upper and lower limit of the particle size. Battelle used their test work, viz, 105 and 74 microns respectively (-140+200-mesh). The limits are shown for two reasons: 1) to illustrate the effect of particle size on the model predictions, and 2) because the particle size distribution for the Battelle test material was not available and therefore the average particle size was not known. The arithmetic average (i.e., 90 microns) would apply only if the particles had a linear distribution between the two sizes. It is obvious that the fit is quite good for this particular set of data.

An isothermal reaction system was assumed in all of the predictions. From Figure 30 one sees the validity of this particular assumption. The non-isothermal prediction, assuming a linear temperature profile with time. does not deviate appreciably from the isothermal case up to residence times of approximately 1.5 seconds. Commercial boilers would not involve residence times much greater than this value.

FIGURE 26

SHRINKING CORE MODEL PREDICTIONS

MODEL...... 74μ PARTICLES
BATTELLE DATA..... 74 - 105μ PARTICLES

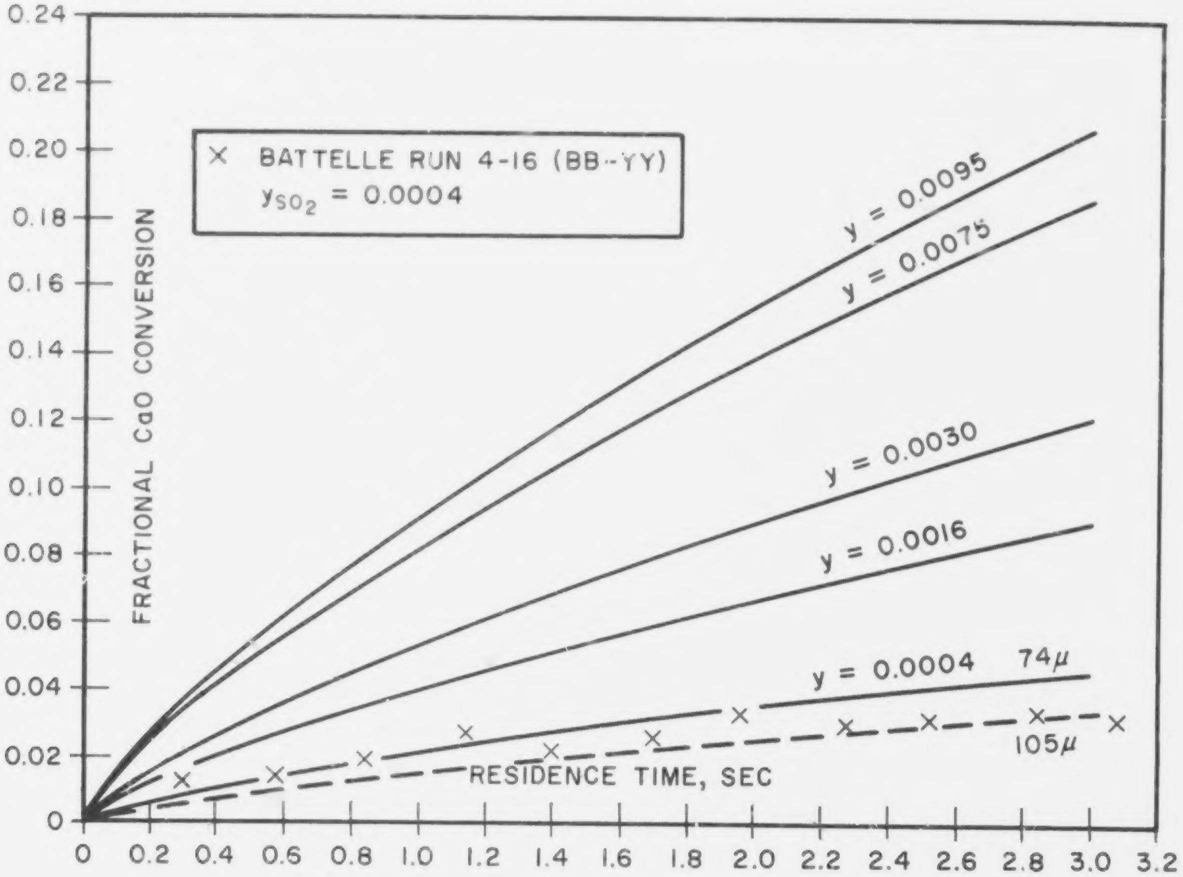

FIGURE 27

SHRINKING CORE MODEL PREDICTIONS

MODEL...... 74μ PARTICLES
BATTELLE DATA.... 74 - 105μ PARTICLES

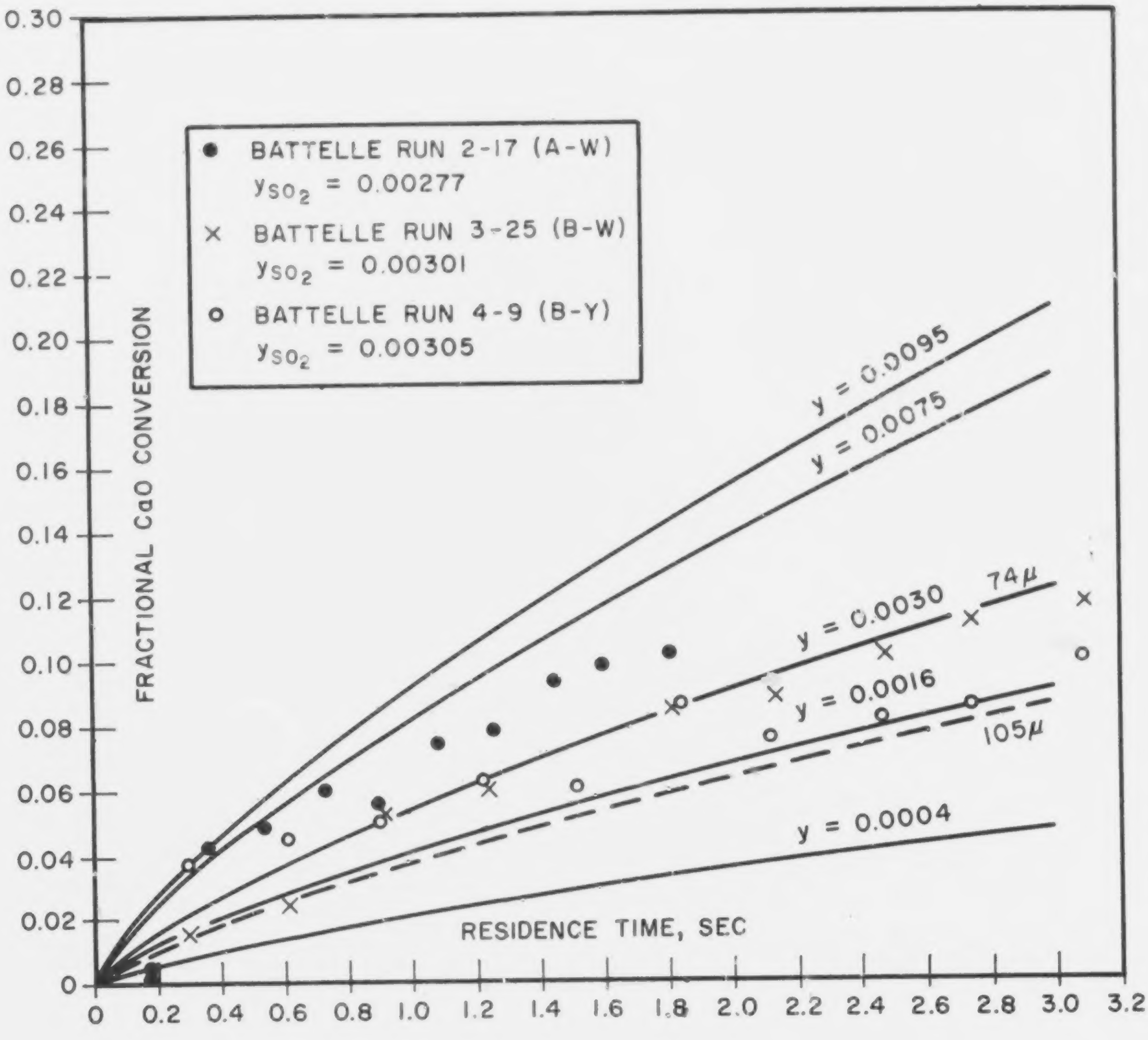

FIGURE 28

SHRINKING CORE MODEL PREDICTIONS

MODEL....... 74μ PARTICLES
BATTELLE DATA.... 74 - 105μ PARTICLES

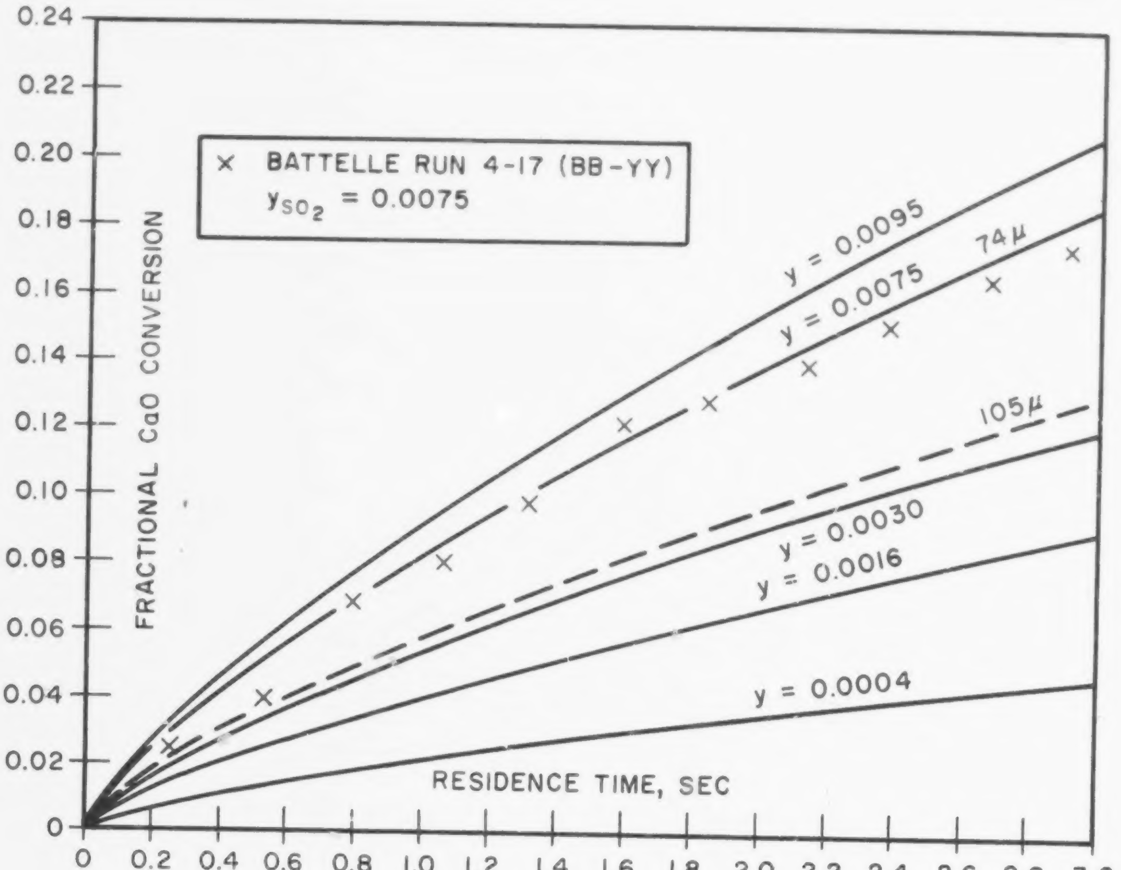

FIGURE 29

SHRINKING CORE MODEL PREDICTIONS

MODEL..... 74 μ PARTICLES
BATTELLE DATA.... 74 – 105μ PARTICLES

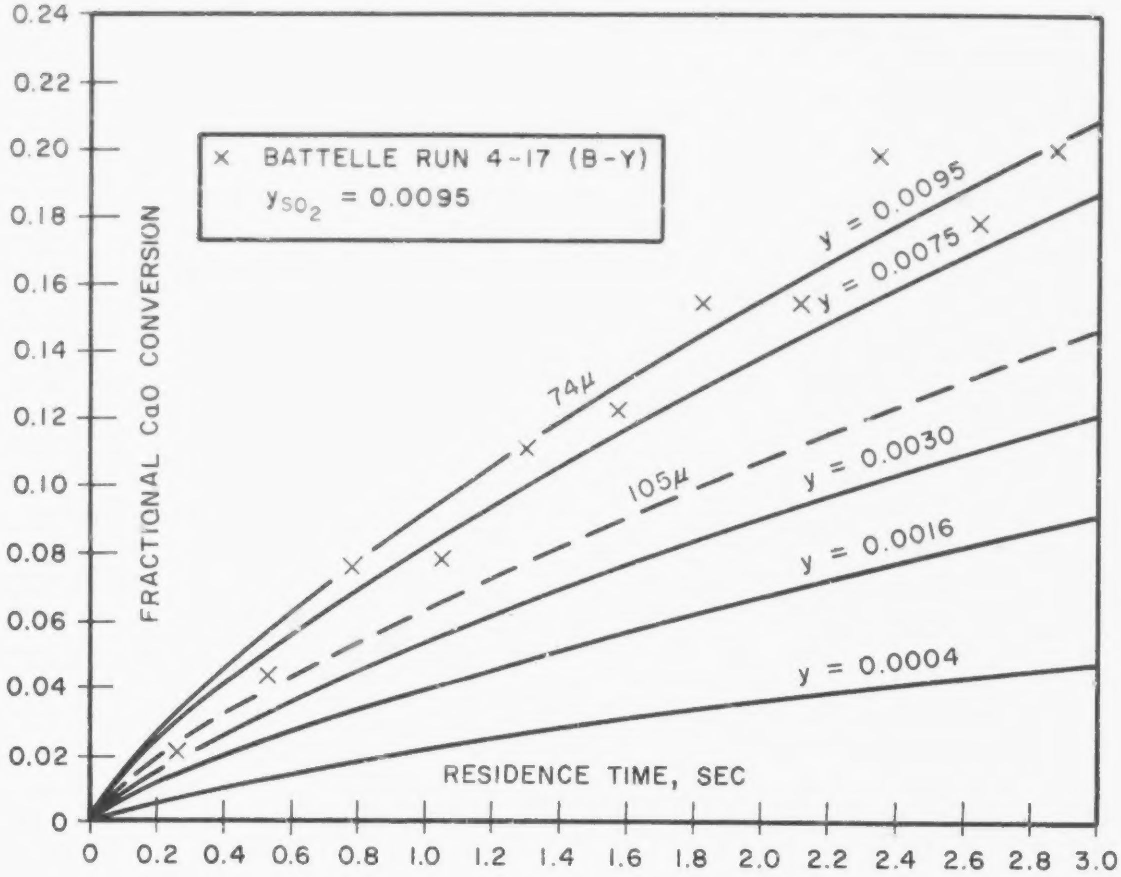

FIGURE 30

EFFECT OF TEMPERATURE PROFILE ON THE SHRINKING CORE MODEL PREDICTION

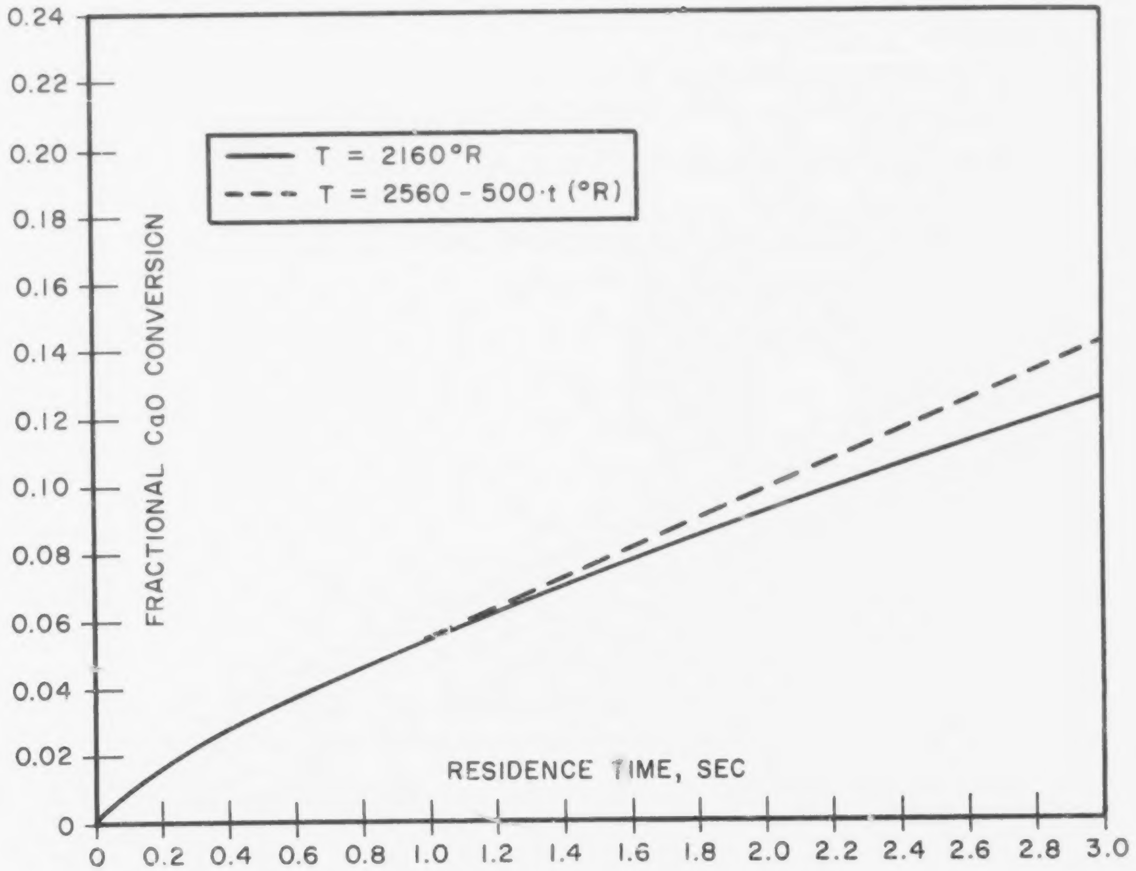

(2) Effect of Temperature

Over the particular temperature range of interest in the Battelle reactor (1400°F-2300°F), the model is essentially independent of temperature. This implies that the following two temperature functions in the model are counteractive: (1) the temperature effect on the gas-phase diffusivity and (2) the temperature effect on the initial SO_2 mole fraction. A check of the Battelle data plots discussed earlier supports the above observation in that the actual dispersed-phase reactor data also did not exhibit any apparent temperature effect other than the low conversions at high temperatures which is evidently a result of deadburning.

(3) Effect of Limestone Surface Area

The limestone surface area is included in the model with the factor S_v which represents the total surface area of a particle per unit volume. Figure 31 illustrates the predicted effect of changing this surface area factor. Surface to volume ratios were varied from 286,000 cm^2/cc to 858,000 cm^2/cc, corresponding to a B.E.T. surface area range of approximately 20 m^2/gm to 60 m^2/gm. CaO utilization varies with the square root of the surface to volume ratio, S_v, in the model. Therefore, as the surface area is increased, its effect on utilization becomes less significant.

(4) Effect of Particle Size

Model predictions for 50 micron particles and four different inlet gas SO_2 mole fractions are given in Figure 32. A comparison of this plot with the predictions illustrated in Figure 25 for 74 micron particles demonstrates the predicted particle size effect for a spec-

FIGURE 31

EFFECT OF TOTAL PARTICLE SURFACE
ON
THE SHRINKING CORE MODEL PREDICTION

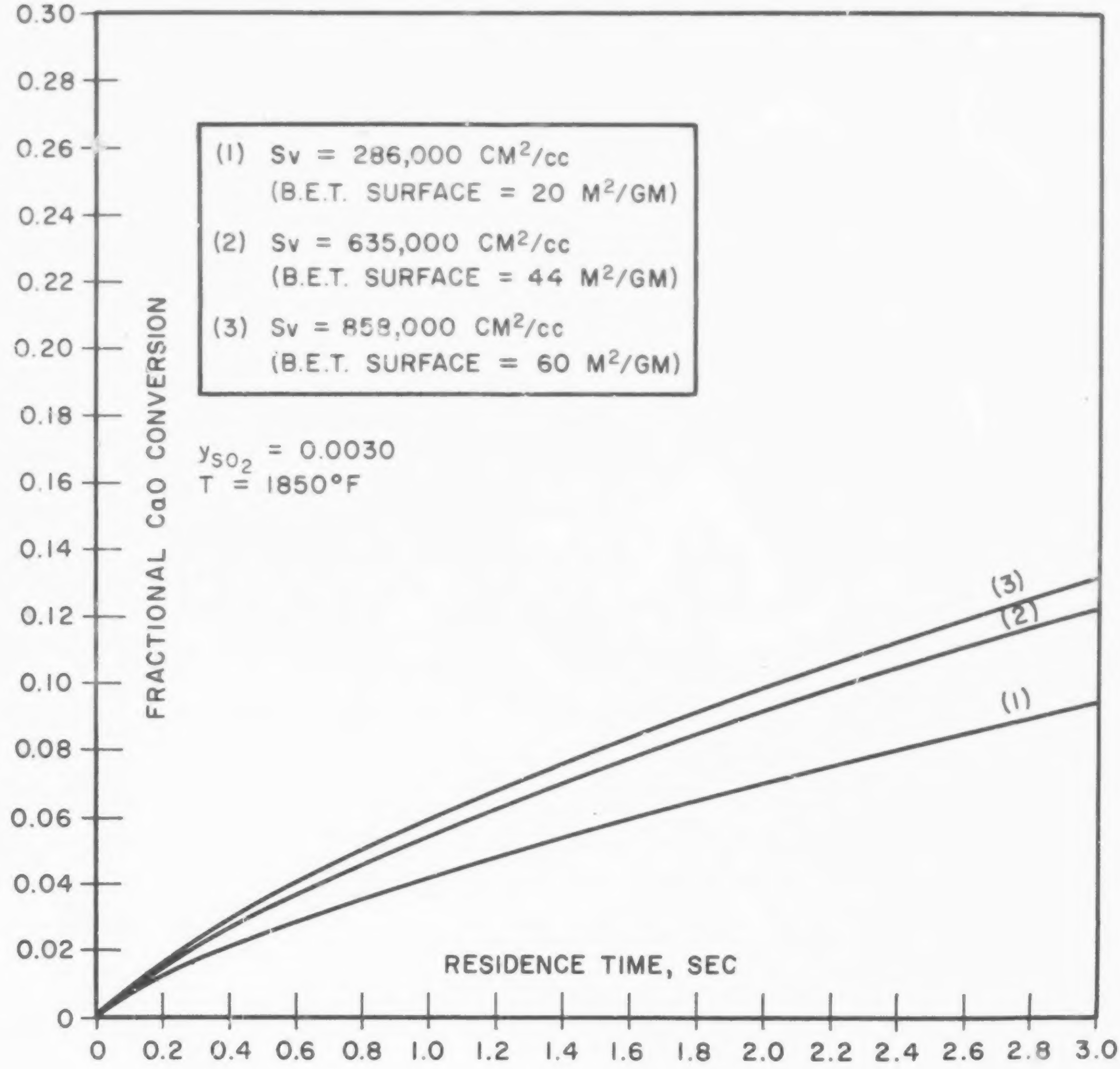

FIGURE 32

SHRINKING CORE MODEL PREDICTIONS
FOR
LIMESTONE 2061

50 MICRON PARTICLES

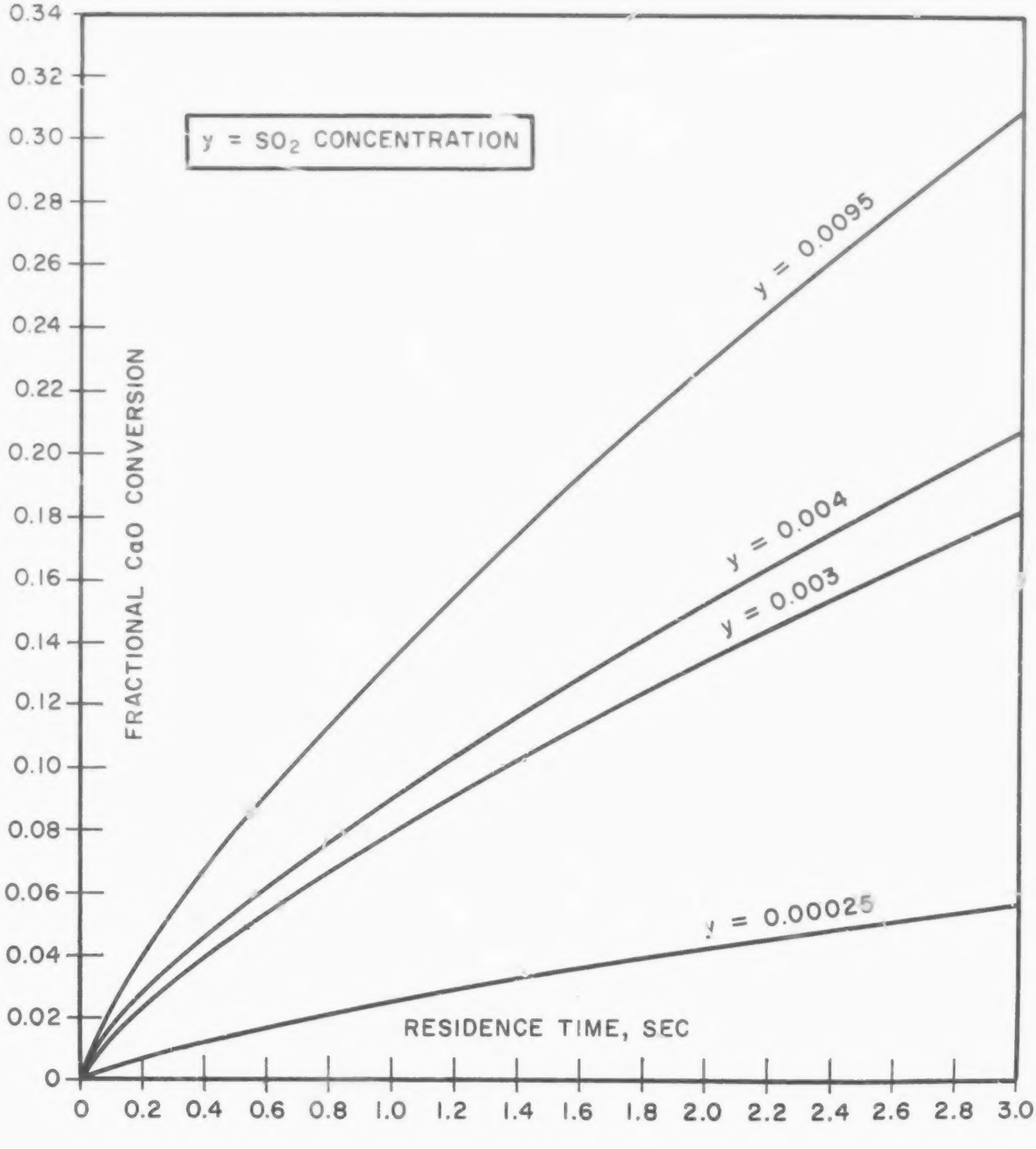

ific SO_2 concentration. To further illustrate the effect of particle size, Figure 32-A shows the model predictions of CaO utilization for a gas concentration of 0.3% SO_2, a temperature of 1850°F, and residence times of 0.5, 1.0 and 1.5 seconds. One can see, therefore, that CaO utilization varies inversely with the first power of particle radius according to the existing model. Figures 33 through 35 compare the predictions for 50 micron particles with the recent Battelle data for inlet SO_2 mole fractions of 0.0025, 0.00398, and 0.0099 for particles in the size range of 44-53 microns. It is obvious that the existing shrinking core model is also valid with respect to the most recent Battelle data.

(5) Comparisons With Other Data

In order to accurately test the validity of the model with any particular set of data, complete physical properties of the calcined limestone must have been determined, i. e., density, porosity, tortuosity, and B.E.T. surface area. In the recent Battelle study which utilized limestone 2061 (Fredonia Valley White) exclusively, all except tortuosity had been determined. For the purposes of this study an assumed average tortuosity of 3.0 was found satisfactory. Other existing data, however, such as that of B & W, Ishihara, and Peabody do not include complete physical properties of limestone calcines as a function of time and temperature in their respective studies, thus making an accurate test of the model an impossiblity. An attempt was made to approximate stone properties by comparison with the corresponding properties of limestone 2061, but the results proved to be incongruous. Still another attempt, this time to compare the OAP bench scale extended residence time data with the model, met with little success

FIGURE 32-A

SHRINKING CORE MODEL PREDICTIONS FOR LIMESTONE 2061

EFFECT OF PARTICLE SIZE

GAS CONCENTRATION 0.3%
TEMPERATURE 1850°F

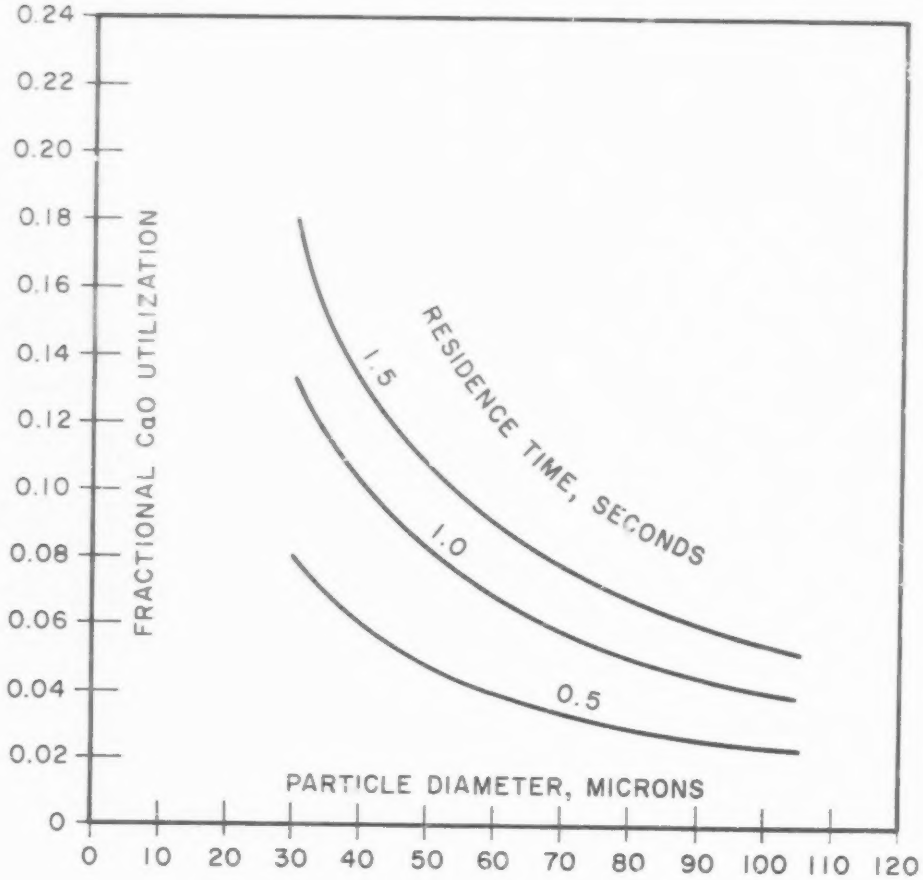

FIGURE 33

SHRINKING CORE MODEL PREDICTIONS

MODEL...... 50μ PARTICLES
BATTELLE DATA.... 44 - 53μ PARTICLES

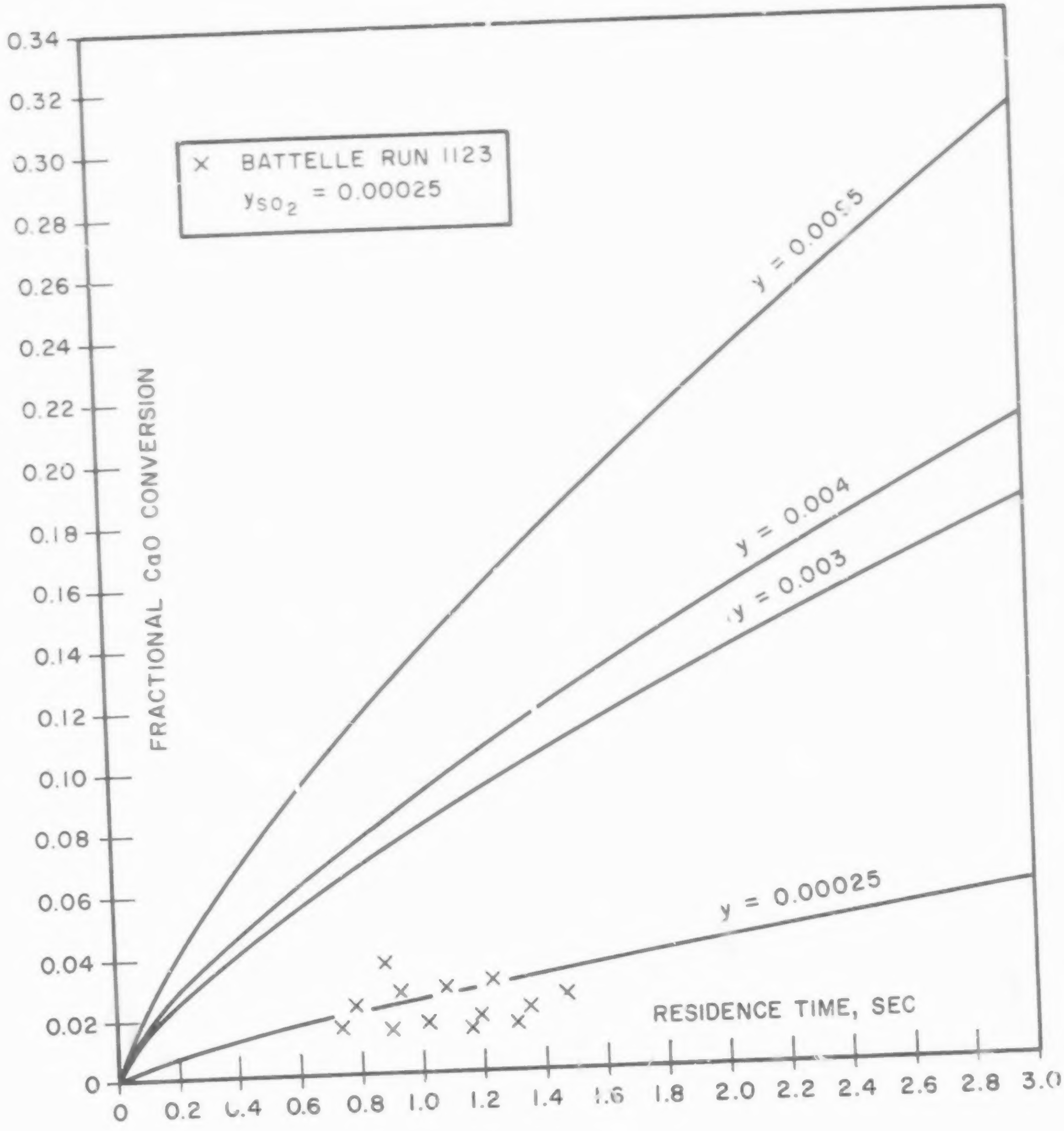

FIGURE 34

SHRINKING CORE MODEL PREDICTIONS

MODEL..... 50μ PARTICLES
BATTELLE DATA.... 44 - 53μ PARTICLES

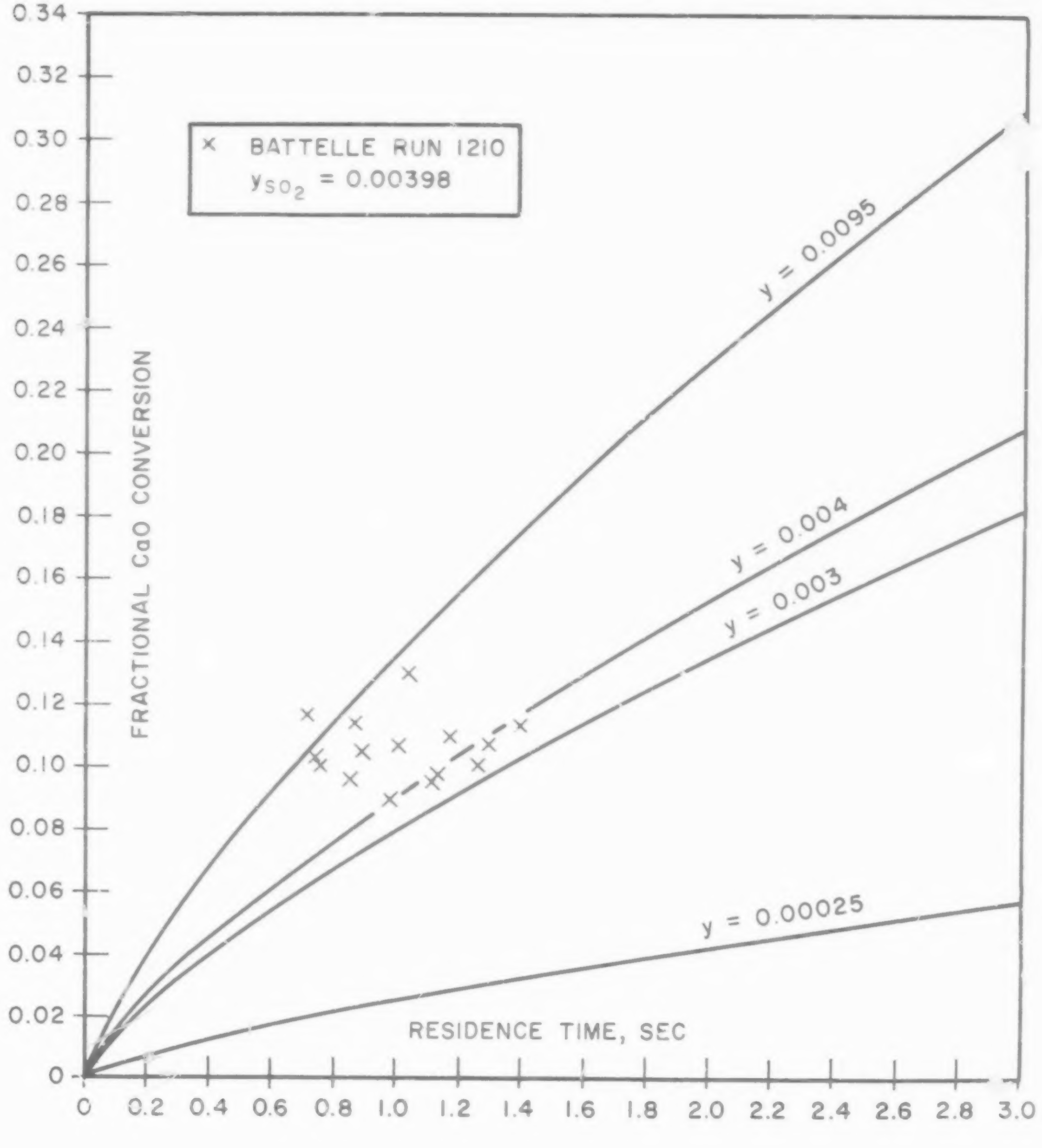

FIGURE 35

SHRINKING CORE MODEL PREDICTIONS

MODEL.... 50μ PARTICLES
BATTELLE DATA.... 44 - 53μ PARTICLES

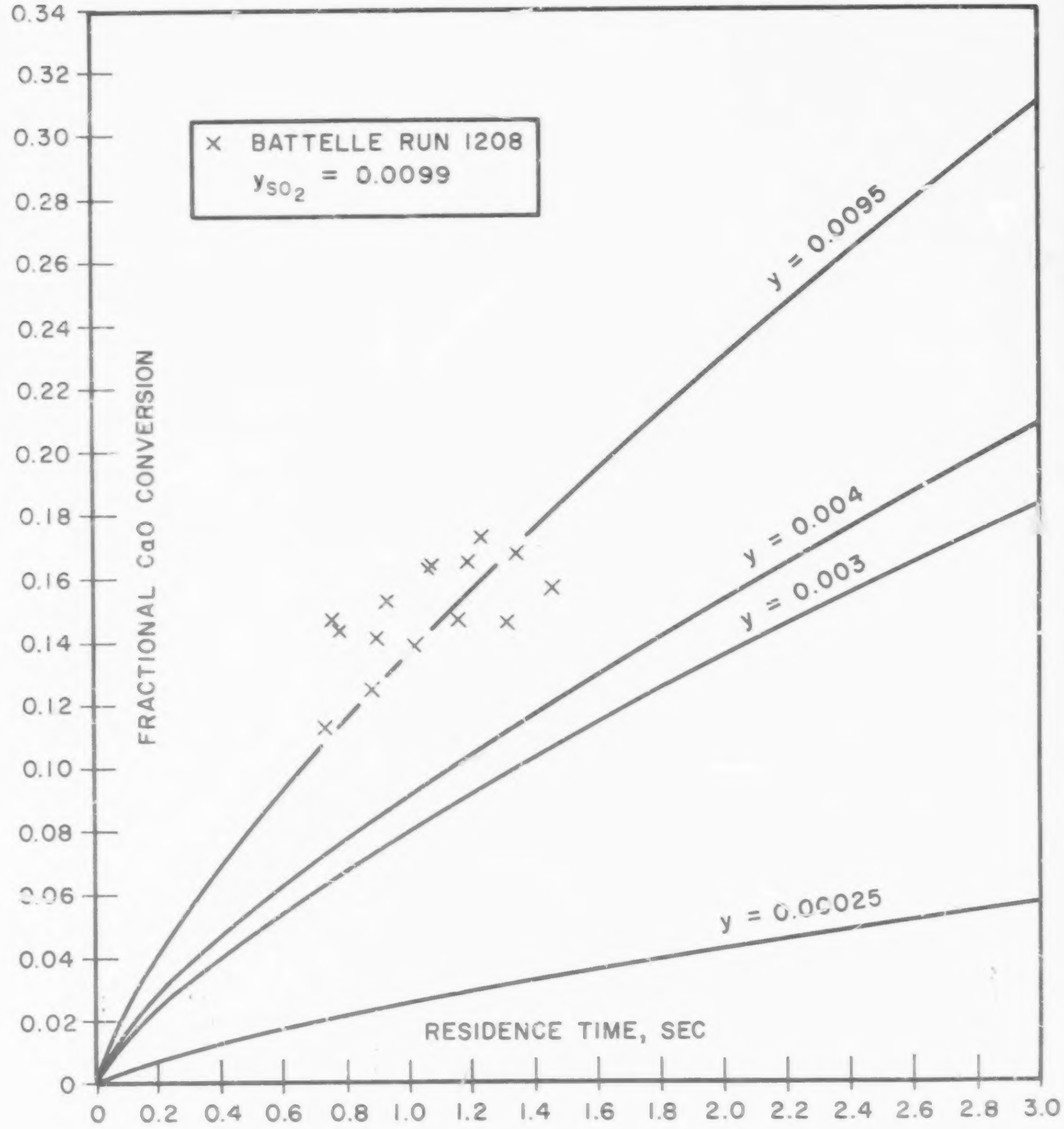

and indicated that this particular model is not valid at these extremely high residence times.

Data which are currently being obtained from TVA power plant at Shawnee should be helpful in validating the proposed Kellogg shrinking core model. All other available data, however, are apparently incomplete with respect to the model requirements.

2. OAP Model

a. General Model Development

In June of 1970, R. H. Borgwardt of OAP presented a paper entitled, "Isothermal Reactivity of Selected Calcined Limestones with SO_2", at the International Dry Limestone Injection Process Symposium$^{(4)}$. In this paper, a sorption model for a limestone removal scheme for SO_2 was developed and the system parameters required by the model for various limestone types were evaluated.

In evaluating the procedure used in the development of the model, two inconsistencies were encountered: (1) the rate of reaction, as expressed in equation (3) of the report, is only a partial representation of the reaction rate, not the total rate; and (2) the Sg (B.E.T. surface area) term was omitted from the final equation (equation (4) of the report). This term is required to satisfy the model development from both a theoretical and dimensional viewpoint. After consultation with Mr. Borgwardt (OAP), it was agreed that these changes should be incorporated in the development of the model.

The equation representing the dry limestone sorption of SO_2 is:

$$\frac{1}{W} \cdot \frac{dn^1}{dt} = A_o \, e^{-Bn^{1/W}} \, e^{-E/RT} C_{SO_2} \, \eta \, S_g$$

where

A_o = frequency factor, cm/sec

C_{SO_2} = gas phase concentration of sulfur dioxide, gm mols/cc

E = activation energy, cal/gm mol

R = gas constant, 1.987 cal/gm mol ^{o}K

S_g = B.E.T. surface area of the calcine, cm^2/gm

T = temperature, ^{o}K

W = weight of the calcine sample, gm

dn^1/dt = rate of change of SO_3 on the solid, gm mols/sec

e = base of the Napierian logarithm, dimensionless

n^1 = sulfate in solid as SO_3, gm mols

t = time, sec

B = empirical correlation coefficient, gm/gm mol

η = effectiveness factor, ratio of the reaction rate to the rate that would be obtained if the entire volume of the particle participated equally in the reaction, dimensionless

Additionally, it was agreed by Mr. Borgwardt that the most useful form of this equation would be the integrated form in which particle loading could be represented as a function of time and the various system parameters. Since the data upon which the OAP model is based were obtained in a differential reactor, the gas concentration and reaction temperature are essentially constant. The rate equation was integrated with these constraints to give the following form:

$$\frac{1}{A_o}\,B \quad e^{BL} = e^{-E/RT} S_g c_{SO_2} \eta \, t + K$$

where

K = constant of integration

L = sulfate loading on the solid as SO_3, with respect to the original weight of calcine sample, gm mols/gm

(THIS PAGE INTENTIONALLY BLANK)

If the loading at time zero is assumed to be negligible, the constant of integration can be evaluated. Substituting this boundary condition, the constant becomes:

$$K = \frac{1}{B}$$

Substituting for K and rearranging the equation in terms of L, the following equation is obtained:

$$L = \frac{1}{B} \ln \left[e^{-E/RT} S_g C_{SO_2} \eta B A_o t + 1.0 \right]$$

The system parameters and empirical constants which are required to satisfy the model are given in Table 3. Initial evaluation of the model consisted of comparing the OAP bench scale loading versus time data to the loading values predicted by the model upon substitution of the appropriate constants. The results of the comparison indicated that the model predictions agreed fairly well with the graphical loading data presented by Mr. Borgwardt. A typical comparison of predicted versus experimental SO_3 loading data is given in Table 4. While the correlation is good, there is a noticeable trend for the model to predict lower than the actual loadings. For the 52 data points in Table 4, an average percent deviation of -17.97 is obtained. Upon further inspection of Table 4, it was noted that these deviations appeared to increase in a negative direction as the time variable increased; while this trend is not evident in the data at 980°C, the data sets for operation at 870°C, 760°C and 650°C all display the trend. Therefore, it was assumed that the increasing negative differences between the actual and calculated values were caused by the empirical

Preceding page blank

TABLE 3

APCO MODEL SYSTEM PARAMETERS FOR DIFFERENT STONES

Part. Size Mesh	Act. Energy Cal/Gm Mol	Freq. Factor (A_o) Cm/Sec	Correl. Factor (B) Gm/Gm Mol	B.E.T. Surface Sq. M/Gm	Effect. Factor Dimensionless	Init. CaO Percent	Calcining Wt. Loss Percent
Stone Type - Calcite, Variety Iceland Spar, Transparent, Colorless, Optically Near Perfect							
12/16	9500	8.50	2540	9.80	0.00	53.50	43.39
42/65	9500	8.50	3040	9.90	0.21	53.50	43.39
150/170	9500	8.50	1340	10.20	1.00	53.50	43.39
Stone Type - Calcite, Very Coarse Spar, Translucent, Milky in Color, Crystalline Imperfections							
12/16	26500	31800.00	1230	0.83	0.17	55.50	43.15
42/65	26500	31800.00	1050	0.70	0.85	55.50	43.15
150/170	26500	31800.00	775	0.70	1.00	55.50	43.15
Stone Type - Calcite Limestone, Coarse Unequal Granular and Porous, Few Fine Grained, Gray							
12/16	15500	119.00	662	1.50	0.62	53.40	43.67
42/65	15500	119.00	383	1.60	0.79	53.40	43.67
150/170	15500	119.00	277	1.80	1.00	53.40	43.67
Stone Type - Calcitic Limestone, Very Fine Equal Granular and Dense, Light Brownish Gray							
12/16	12500	31.20	1250	1.90	0.47	54.80	43.15
42/65	12500	31.20	480	2.10	0.74	54.80	43.15
150/170	12500	31.20	289	2.40	1.00	54.80	43.15
Stone Type - High Purity Dolomite, Medium Grained Granular and Porous, Gray Reef Type							
12/16	19500	484.00	1790	3.60	0.32	30.30	47.24
42/65	19500	484.00	393	3.40	0.49	30.30	47.24
150/170	19500	484.00	303	3.90	1.00	30.30	47.24
Stone Type - 81 Percent Dolomite, With Clay & Quartz, Medium Grain, Granular, Microporous, Non-Reef Type							
12/16	9200	2.78	458	3.60	0.27	26.50	40.46
42/65	9200	2.78	300	3.90	0.63	26.50	40.46
150/170	9200	2.78	192	4.10	1.00	26.50	40.46
Stone Type - Aragonite Sand, Traces of Mg Calcite, Banded Structure of Fibrous Aragonite							
42/65	14400	43.70	2	0.65	1.00	55.20	43.33
150/170	14400	43.70	2	0.79	1.00	55.20	43.33

TABLE 4

A COMPARISON OF THE APCO MODEL TO THE BENCH SCALE DATA FOR A HIGH PURITY DOLOMITE, MEDIUM GRAINED GRANULAR AND POROUS, GRAY REEF TYPE

Part. Size Mesh	Act. Energy Cal/GmMol	Freq. Factor(A_o) Cm/Sec	Correl. Factor(B) Gm/GmMol	B.E. T. Surface Sq. M/Gm	Effect. Factor Dimensionless	Init. CaO Percent	Calcining Wt. Loss Percent
150/170	19500	484.00	303	3.9	1.00	30.30	47.24

Temperature °C	Time Sec.	Actual Loading GmMols SO_3/Gm	Calculated Loading GmMols SO_3/Gm	Deviation GmMols SO_3/Gm	Percent Deviation Percent
980	5	0.1082E-02	0.9437E-03	0.1387E-03	12.81
980	10	0.1457E-02	0.1676E-02	-0.2196E-03	-15.07
980	20	0.2373E-02	0.2783E-02	-0.4102E-03	-17.23
980	30	0.3580E-02	0.3610E-02	-0.3014E-04	-0.84
980	40	0.4121E-02	0.4271E-02	-0.1498E-03	-3.63
980	50	0.4517E-02	0.4821E-02	-0.3046E-03	-6.74
980	60	0.4621E-02	0.5293E-02	-0.6721E-03	-14.54
980	70	0.5349E-02	0.5706E-02	-0.3561E-03	-6.65
980	80	0.5870E-02	0.6072E-02	-0.2023E-03	-3.44
980	90	0.5995E-02	0.6402E-02	-0.4074E-03	-6.79
980	100	0.6702E-02	0.6702E-02	0.3883E-06	0.00
980	120	0.6911E-02	0.7231E-02	-0.3201E-03	-4.63
870	10	0.8951E-03	0.9697E-03	-0.7462E-04	-8.33
870	10	0.9159E-03	0.9697E-03	-0.5380E-04	-5.87
870	20	0.1373E-02	0.1718E-02	-0.3444E-03	-25.06
870	20	0.1519E-02	0.1718E-02	-0.1936E-03	-13.07
870	30	0.1727E-02	0.2328E-02	-0.6002E-03	-34.74
870	30	0.1935E-02	0.2328E-02	-0.3921E-03	-20.25
870	40	0.2123E-02	0.2842E-02	-0.7192E-03	-33.87
870	40	0.2248E-02	0.2842E-02	-0.5943E-03	-26.43
870	50	0.2498E-02	0.3287E-02	-0.7895E-03	-31.60
870	50	0.2581E-02	0.3287E-02	-0.7062E-03	-27.36
870	60	0.2622E-02	0.3679E-02	-0.1056E-02	-40.28
870	60	0.2789E-02	0.3679E-02	-0.8901E-03	-31.91
870	70	0.2955E-02	0.4030E-02	-0.1074E-02	-36.33
870	70	0.2789E-02	0.4030E-02	-0.1240E-02	-44.47
870	80	0.2789E-02	0.4346E-02	-0.1557E-02	-55.82
870	80	0.2747E-02	0.4346E-02	-0.1598E-02	-58.19
870	90	0.3122E-02	0.4635E-02	-0.1513E-02	-48.46
870	90	0.3164E-02	0.4635E-02	-0.1471E-02	-46.50
870	100	0.3372E-02	0.4901E-02	-0.1529E-02	-45.34
870	100	0.3413E-02	0.4901E-02	-0.1487E-02	-43.57
870	110	0.3788E-02	0.5147E-02	-0.1358E-02	-35.86
870	110	0.4080E-02	0.5147E-02	-0.1067E-02	-26.15
870	120	0.3747E-02	0.5376E-02	-0.1629E-02	-43.47
870	120	0.3788E-02	0.5376E-02	-0.1537E-02	-41.90

TABLE 4 (Cont'd)

Temperature °C	Time Sec.	Actual Loading GmMols SO_3/Gm	Calculated Loading GmMols SO_3/Gm	Deviation GmMols SO_3/Gm	Percent Deviation Percent
760	10	0.7494E-03	0.4654E-03	0.2839E-03	37.88
760	20	0.1290E-02	0.8733E-03	0.4172E-03	32.33
760	30	0.1623E-02	0.1236E-02	0.3873E-03	23.85
760	50	0.1998E-02	0.1860E-02	0.1376E-03	6.83
760	80	0.2539E-02	0.2619E-02	-0.8017E-04	-3.15
760	90	0.2706E-02	0.2838E-02	-0.1322E-03	-.488
760	100	0.2872E-02	0.3043E-02	-0.1707E-03	-5.94
760	110	0.2955E-02	0.3236E-02	-0.2805E-03	-9.49
760	130	0.3247E-02	0.3591E-02	-0.3442E-03	-10.60
650	20	0.4787E-03	0.3422E-03	0.1364E-03	28.50
650	40	0.7077E-03	0.6523E-03	0.5537E-04	7.82
650	60	0.9783E-03	0.9358E-03	0.4253E-04	4.34
650	80	0.1020E-02	0.1196E-02	-0.1768E-03	-17.33
650	100	0.1061E-02	0.1438E-02	-0.3770E-03	-35.52
650	120	0.1165E-02	0.1664E-02	-0.4983E-03	-42.75
650	140	0.1207E-02	0.1375E-02	-0.6676E-03	-55.30

Average Absolute Percent Deviation = 88.85

Standard Deviation of Actual Loading = 0.1544E-02

Standard Error of Estimate = 0.4933E-02

Coefficient of Correlation = Imaginary

evaluation of the constants. If, for example, the value for the correlation coefficient, B, is raised from 303 to 450, the statistical coeffecient of correlation, r, would be raised from 0.86 to 0.94 while the average percent deviation would be lowered from -17.97 to -1.52 percent. For a truly definitive evaluation of the proposed model in terms of the OAP data, the constants would have to be redetermined to reflect the inclusion of the B. E. T. surface effect.

Before proceeding to re-evaluate the empirical model constants, it was decided to check the OAP model predictions against the short residence time Battelle test data to see if the same trend was indicated. Figure 36 presents the fractional conversion of the Battelle limestone, No. 2061, versus time for two runs at fairly similar conditions. The third plot represents the fractional conversion predicted by the OAP model for a stone type of similar composition which was given in the Borgwardt report. The plotted results indicate an order of magnitude difference in the calcine conversion when the model is compared to the Battelle data. The major difference between the two results has been postulated to be caused by the method and extent of calcination. The data taken by OAP were obtained in a differential balance reactor using pre-calcined stone. The Battelle data are based upon in situ calcination of the finely ground stone in the furnace. In the former case the raw stone was calcined in a small rotary kiln for two hours at 980°C (1796°F). The calcine was then crushed and screened before charging to the reactor. In the latter testing the raw stone was crushed, screened, and injected into the reactor where both calcination and reaction occurred.

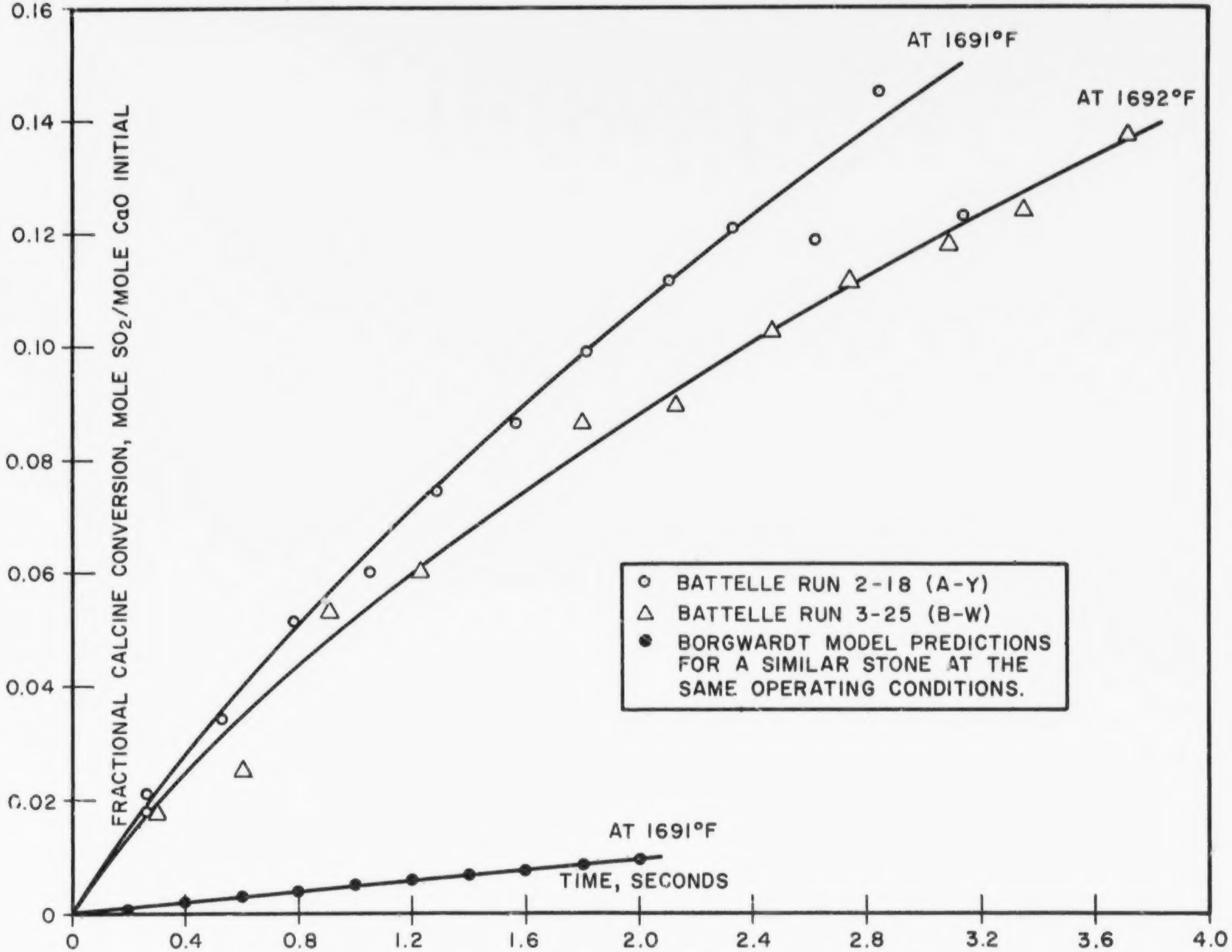

FIGURE 36

FRACTIONAL CALCINE CONVERSION VS TIME

One of the basic premises of the OAP model is that reaction rate increases linearly with surface area for a particular stone. Therefore, it is important to determine what effect the variation in these testing procedures would have upon the surface area of the reactor charge. In Boynton's book (8), "Chemistry and Technology of Lime and Limestone", on page 148, a plot is given of the time-temperature relationship to stone surface area, which is based upon the data of Staley and Greenfield(9). While these data were obtained on fairly large diameter stone, they do indicate a significant lessening of the B.E.T. surface area with increasing calcination time. The minimum time of calcination used in this study was 1 hour, however, while the residence time of a limestone particle in a furnace would be in the order of 1 to 2 seconds.

While it is known that the surface area of calcines is extremely time-temperature dependent, there are no known studies which investigate this effect for systems similar to those which would be encountered in a commercial boiler. However, a series of bench scale experiments performed by researchers at TVA has shown that the sorption characteristics of a typical limestone are severely diminished with increasing time and temperature. Based upon the results obtained in this study, the curves shown in Figure 37 were developed. The curves developed represent extrapolations of the TVA bench scale data to the residence times of interest in a commercial system. Since there appears to be a direct relationship between sorption rate and surface area, and since independent research has verified the time-temperature dependency of both these parameters, and a significant time interval

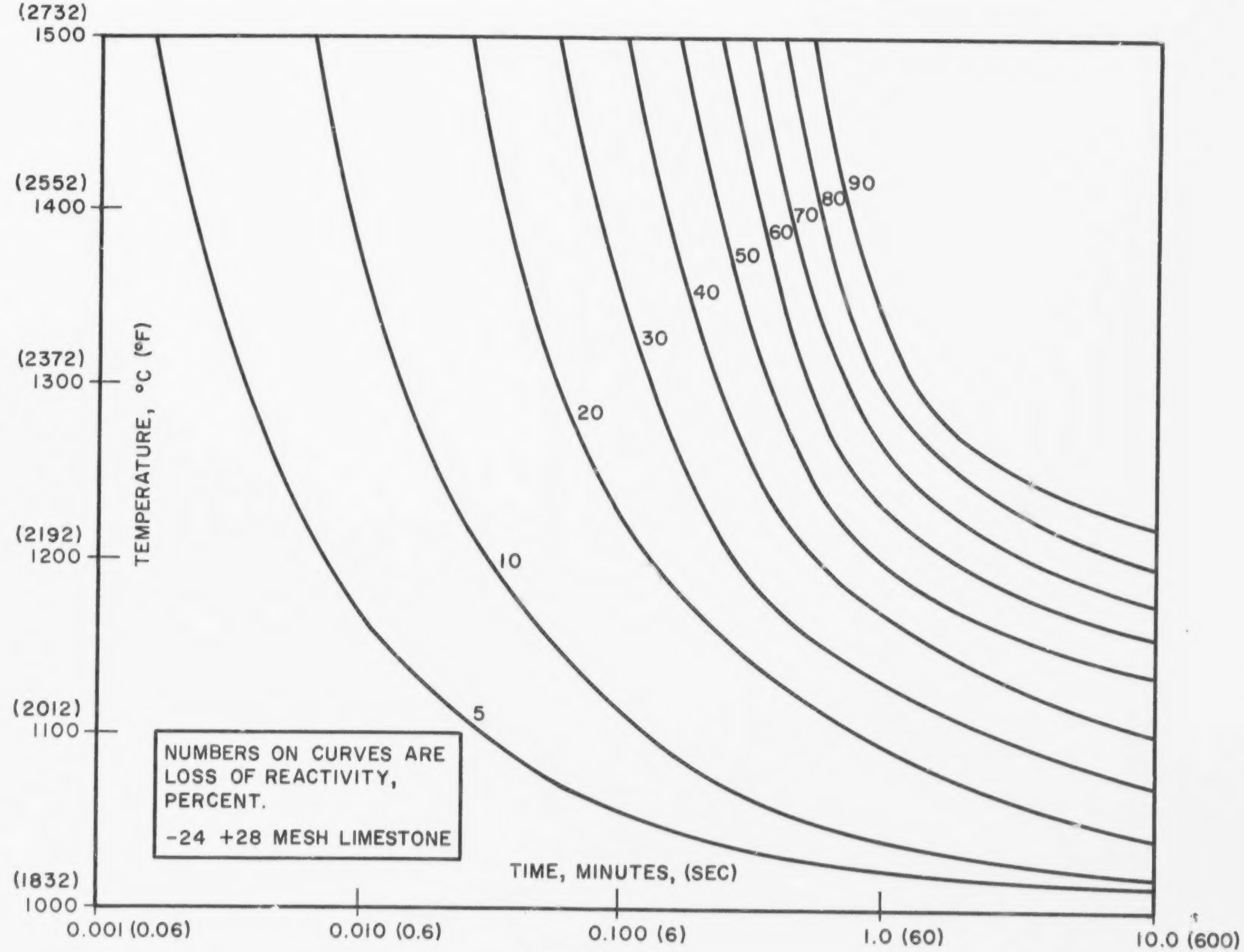

FIGURE 37

EFFECT OF TIME AND TEMPERATURE OF CALCINATION ON REACTIVITY OF CALCINES passes before analysis, the surface areas measured may not be the same as those which would be observed on an in situ measurement (if one were possible). Because of this time dependency, it may be required that samples for surface area measurements be rapidly quenched after exposure to insure a representative sample. Although a rapid quench might also alter the measured stone properties, it is felt that such a procedure would yield the most applicable measurement of the actual, in situ calcine surface area.

Because of the time-temperature relationship upon surface area caused by the calcination method employed and its intrinsic effect upon the empirical constants required in the OAP model, the proposed re-evaluation of these constants to satisfy the adjusted model as a predictor of the OAP bench scale data was abandoned. For subsequent evaluation of this model, it was decided to investigate only those systems which would provide for in situ calcination and residence times comparable to those which would be experienced in a commercial boiler operation. Similarly, a unique set of constants would be calculated for each set of experimental data, and then be compared for consistency with constants derived from other sets of data.

b. Evaluation of Model Constants

Since the model developed by OAP Research was based upon an essentially isothermal test system with constant SO_2 gas concentration, the form of the model was varied to handle the non-isothermal, varying SO_2 concentration systems investigated in the flow reactors of B & W and Battelle. The model may be defined as follows:

$$\frac{\delta L}{\delta t} = A_o . e^{\frac{-E}{RT}} e^{-BL} . \eta . S_g . C_{SO_2}$$

where L is defined as the loading of SO_2 on the sorbent in gm mol SO_2/gm CaO. This term, L, replaces the earlier term, n^1/W, which was Mr. Borgwardt's expression for loading. The equation as written is a function of five variables: t, L, T, C_{SO_2} and Sg, and four system constants A_o, B, η, and R. In the following discussion the equation will be simplified, integrated and analyzed as a potential design model.

The first variable to be considered is Sg, the B. E. T. surface area. While numerous studies have been made to measure the surface areas of calcines and uncalcined stones, no techniques are available to measure the surface of in situ stone. Results based on surface area data which are obtained from the product or reactant material can be misleading owing to the severe thermal shock calcination undergone by the raw limestone upon injection into a furnace. This rapid calcination, coupled with the time and temperature dependent structural relaxation which is undergone by the stone after calcination, make it virtually impossible to measure the actual stone surface area as it exists in the reactor. Furthermore, since the residence time within the furnace is relatively short, say 3 seconds maximum, it will be assumed that the in situ surface area of a particular stone will be a constant.

The second variable to be considered is C_{SO_2}, the gas phase concentration of SO_2. First, eliminate C_{SO_2} by replacing it with an equivalent term, $Y_{SO_2} \cdot \rho Gas$ where Y_{SO_2} is the mole fraction of SO_2 in the gas and ρGas is the molar gas density. The latter term is a function of temperature only since the pressure effects in the system are negligible; thus, ρGas is equal to P/RT where P is the absolute pressure in atmospheres and R is the gas constant. The Y_{SO_2} term can be related to the loading, L, through the system stoichiometry by the relationship:

$$Y_{SO_2} = Yo_{SO_2} \quad (1-S \cdot MW \cdot L)$$

where Yo_{SO_2} is the initial mol fraction of SO_2, MW is the molecular weight of CaO (56.08 gm/gm mol) and S. is the stoichimoetry of the system as gm mol CaO fed/gm mol SO_2 fed.

The third variable to be considered is T, the reaction temperature. By measuring the temperature profile in the reactor, and establishing the gas velocity in the reactor as a function of T and reactor geometry, the temperature versus time profile of the flue gas can be established. Therefore, T = F(t) for a particular reactor. For the purpose of the following calculation, a linear profile will be used for simplicity; however, any relationship which satisfied T may be employed without affecting the form of the solution. After elimination of the variables T, C_{SO_2} and Sg, the rate expression may be rewritten as:

$$\frac{dL}{dt} = \frac{\underline{Y}o_{SO_2} \cdot P \cdot Sg \cdot \underline{A}_o \cdot \eta}{R} \quad \frac{(1-MW \cdot S \cdot L)}{(T_o-mt)} \cdot e^{-BL} \cdot e^{-E/R(T_o-mt)}$$

Collecting like terms on either side of the equation and integrating both sides, the following loading versus time relationship is obtained:

$$-\frac{1}{MW\cdot S}\left[\left(e^{B/MW\cdot S}+1\right)\cdot \ln(1-MW\cdot S\cdot L)+\sum_{1}^{\infty}\left(\frac{B\cdot MW\cdot S\cdot L-B}{MW\cdot S}\right)^{N}\cdot\frac{1}{N\cdot N!}-\sum_{1}^{\infty}\left(\frac{-B}{MW\cdot S}\right)^{N}\cdot\frac{1}{N\cdot N!}\right]=\frac{Y_{oSO_2}\cdot P\cdot S_g\cdot A_o\cdot \eta}{R}\cdot f(t)$$

where

$$f(t)=\frac{1}{m}\left[\ln\left(\frac{T_o}{T_o-mt}\right)+\sum_{1}^{\infty}\left(\frac{-E}{R(T_o-mt)}\right)^{N}\frac{1}{N\cdot N!}-\sum_{1}^{\infty}\left(\frac{-E}{RT_o}\right)^{N}\frac{1}{N\cdot N!}\right]$$

The arbitrary system constants S_g, A_o and η cannot be isolated in this form of the equation and therefore can be combined to give a single constant K. Thus, the system is defined in terms of two variables t and L, three arbitrary system constants B, E and K, three boundary conditions Y_{oSO_2}, T_o and S, and the true constants P, R and MW. It should be noted that a series expansion form will result for the time variable if any polynomial functional relationship is used to relate T to t. Use of a model in this form is extremely difficult since the dependent variable L is given in an implicit form rather than the normally found explicit one. Therefore, if suitable system constants can be obtained, the value for the loading at a particular time would have to be determined by a trial and error procedure.

Before proceeding with an evaluation of the model, the constants E, K and B must be determined. In this regard, the following published discussion is applicable: "There are two procedures for analyzing experimental kinetic data, the integral and the differential method . . . There are specific advantages and disadvantages to each of these methods. The integral method is easy to use and is recommended when testing specific mechanisms, when fitting relatively simple mechanisms, or when the data are so scattered that we cannot reliably find the derivatives needed in the differential method. The differential method may be more useful in more complicated situations but requires more accurate or larger amounts of data"(10).

Ideally, therefore, the system constants could be evaluated from the rate expression, which implies the differential method. However, the experimental procedure and the significant scatter exhibited by the data virtually preclude this type of analysis. While the integrated form is more difficult to handle from a calculational viewpoint, the results will be significantly more reliable when applied to a design equation. It may be argued from a mechanistic point of view, that the loading relationship e^{-BL} is not correct, but rather is a simplification of the effect of a series of kinetic resistances. However, since we are interested in a design equation, the empirical relationship should be sufficient for the purposes of this study. Furthermore, a simplification of this type will avoid the arduous solution techniques required by the mechanistic series resistance equations which are also under consideration.

Two sets of data were investigated in an attempt to develop constants which would satisfy the OAP model. The first data set evaluated was that of Babcock and Wilcox(2). In these data, the sorption of SO_2 by various stone types was investigated for system parameters of residence time, loading, stoichiometry and temperature. However, because of the nature of the system, only two effective inlet temperatures were studies. This factor, coupled with the rather large degree of scatter exhibited by the B & W data, precluded any attempts to correlate constants for the OAP sulfation model.

The second data set to be evaluated was that of Battelle(1). The reported CaO utilization data plus additive injection rate data received from R. W. Coutant of Battelle on March 12, 1971, were compiled and grouped for analysis. However, one important data criterion was missing, namely, the gas temperature at the stone injection point. However, the data did provide the mean reactor temperature and a gas temperature profile versus reactor length. Using this information, the reported Reynold's number, and the assumption of an equal residence time profile around the center of the reactor, a temperature profile versus residence time was obtained. The following equation represents the derived temperature profile:

$$T = T_M \exp(-3.779\text{x}10^{-5} \cdot Re \cdot t_1)$$

where T_M is the reactor midpoint temperature, Re is the Reynold's number calculated at the reactor midpoint temperature, and t_1 is the modified residence time dictated by the half-range formula such that t_1 varies from $-\Delta t/2$ to $+\Delta t/2$ where Δt is the reported residence time.

Since for this system, the relationship of T to t is by an exponential rather than a polynomial expression, an explicit relationship can be developed for the time function in the integrated OAP model. This time function may be defined as follows:

$$f(t) = \frac{-52579}{E \cdot Re} \left[\exp\left(-E * EXP\left(.3779 x 10^{-5} * Re * \Delta t/2\right) / RT_M\right) - \exp\left(-E * \exp\left(-3.779 x 10^{-5} * Re * \Delta t/2\right) / RT_M \right] \right.$$

Upon substitution into the OAP model the relationship becomes:

$$- \frac{1}{MW \cdot S} \left[g(B,L) + g_1(B) \right] = K \; f(E, \Delta t)$$

The constants B and K were evaluated by performing a non-linear regression analysis using an assumed value for E based on experimental values as follows:

Source	E, kcal/mol
• TVA, 1/68 monthly report	16.7
• Borgwardt, Table 1, Paducah* paper, 9.2→26.5, 9 stone average	14.0
• Ishihara, Paducah*paper, 14 runs, range 18→50, average	28.0
• Battelle, Paducah*paper	22.0
• Ishida & Wen, Paducah*paper	17.5
Average	19.6
Range	14 - 28

The results of the regression analyses are given in Table 5. The high correlation coefficients indicate that the model is internally consistent with the results from each individual Battelle test run, with the exception of Run 4-9. However, when an attempt was made to develop a unique set of

---

* Fourth International Symposium on Dry Limestone Injection Process, Paducah, Kentucky, June 22-26 (1970).

TABLE 5

VALUES OF APCO MODEL CONSTANTS OBTAINED BY NON-LINEAR REGRESSION ANALYSIS USING THE BATTELLE DATA

Battelle Run No.	Feed Stoichiometry (gm CaO/gm mol SO_2)	Activation Energy (cal/gm mol)	SO_2 Concentration ppm	B	K	Correlation Coefficient
2-17	7.493	20,000	2770	2.959	2.738×10^{6}	0.841
3-25	10.335	20,000	3010	1.769	2.201×10^{6}	0.941
4-9	10.318	20,000	3050	1.881	1.777×10^{6}	0.381
4-16	7.382	20,000	3000	2.139	2.745×10^{6}	0.944
4-17(A)	1.887	20,000	9540	18.634	1.174×10^{10}	0.946
4-17(AA)	2.392	20,000	7480	23.645	1.370×10^{10}	0.932
2-17	7.493	15,000	2770	2.618	3.858×10^{5}	0.848
3-25	10.335	15,000	3010	1.109	2.762×10^{5}	0.957
4-9	10.318	15,000	3050	1.488	2.183×10^{5}	0.523
4-16	7.382	15,000	3000	2.076	3.560×10^{5}	0.956
4-17(A)	1.887	15,000	9540	22.328	1.048×10^{10}	0.959
4-17(AA)	2.392	15,000	7480	24.613	2.598×10^{9}	0.949
2-17 thru 4-16	varies	20,000	~3000	1.778	2.172×10^{6}	0.774
2-17 thru 4-16	varies	15,000	~3000	1.683	2.620×10^{5}	0.770

constants to satisfy the total body of the Battelle data, no significant correlation could be obtained. A second attempt was made to correlate the grouped data by regressing the Battelle runs tabulated which were made at approximately 3000 ppm SO_2. This attempt succeeded and provided a fairly high correlation coefficient of 0.77.

Since the constants developed by regression analysis are not true constants, but apparently are dependent upon the system stoichiometry, it must be concluded that either the model must be modified in some way, or that the constants derived at the different stoichiometry levels are related to differences in stone properties or experimental operating conditions. The latter possibility could reflect an abnormal experimental stone size distribution, unusual reactor temperature profile, or other system variations which are not evident from the reported data. On the other hand, if these data do give a complete representation of the system, then the proposed OAP Research model as it is presently constituted must be modified to satisfy the data presented by Battelle.

This modeling modification may be required to satisfy potential reaction mechanism differences between the bench scale data, upon which the model was developed, and the pilot plant data upon which the model was tested. As was discussed in an earlier section of this report, such differences are possible due to the calcination techniques, as well as the different residence time ranges used by OAP and Battelle. When further data for flow reactors or simulated commercial systems become available, they should be tested against the constants developed for the Battelle data to determine concretely the applicability of the OAP model. However, until such time as any future data confirm or reject the present form of the proposed model, it remains as one of the more desirable of the proposed sulfation models because of its relative simplicity and adaptability to a commercial system.

3. Wen Model

The rate of sorption of SO_2 by an agglomerated single sphere of calcium oxide powder has been investigated by Dr. C. Y. Wen of the University of West Virginia. Based upon this investigation and the investigations of OAP, TVA and Battelle, Dr. Wen has proposed that the kinetics of limestone sorption can be represented by a series resistance type model in which one or a combination of resistances represents the rate controlling mechanism. The "zone-reaction" model which Dr. Wen proposes defines the relationship between the chemical reaction rate of each grain contained in the solid particle, the diffusion rate and the overall reaction rate. A general development for this type of model has been presented by Ishida and Wen in several published articles(11,12). However, a specific design model proposed for the non-isothermal $CaO-SO_2$ reaction system and pertinent rate constants have not been made available to Kellogg at the time of this evaluation.

In the initial analysis of the model's applicability to the dry limestone process, the reaction rates per unit concentration of SO_2 were plotted versus temperature, as shown in Figure 38. Table 6 is provided as a key to the data used in Wen's studies. In the low temperature regions, the rate is shown to be less sensitive to particle size than in the high temperature region. This plot demonstrates that diffusion resistances are controlling the reaction at high temperatures, while in the lower temperature region, the system is chemical reaction rate controlled. Furthermore, the effect of particle size is demonstrated by the increase of diffusion resistance with increasing particle size at a given temperature.

FIGURE 38

REACTION RATE VS TEMPERATURE

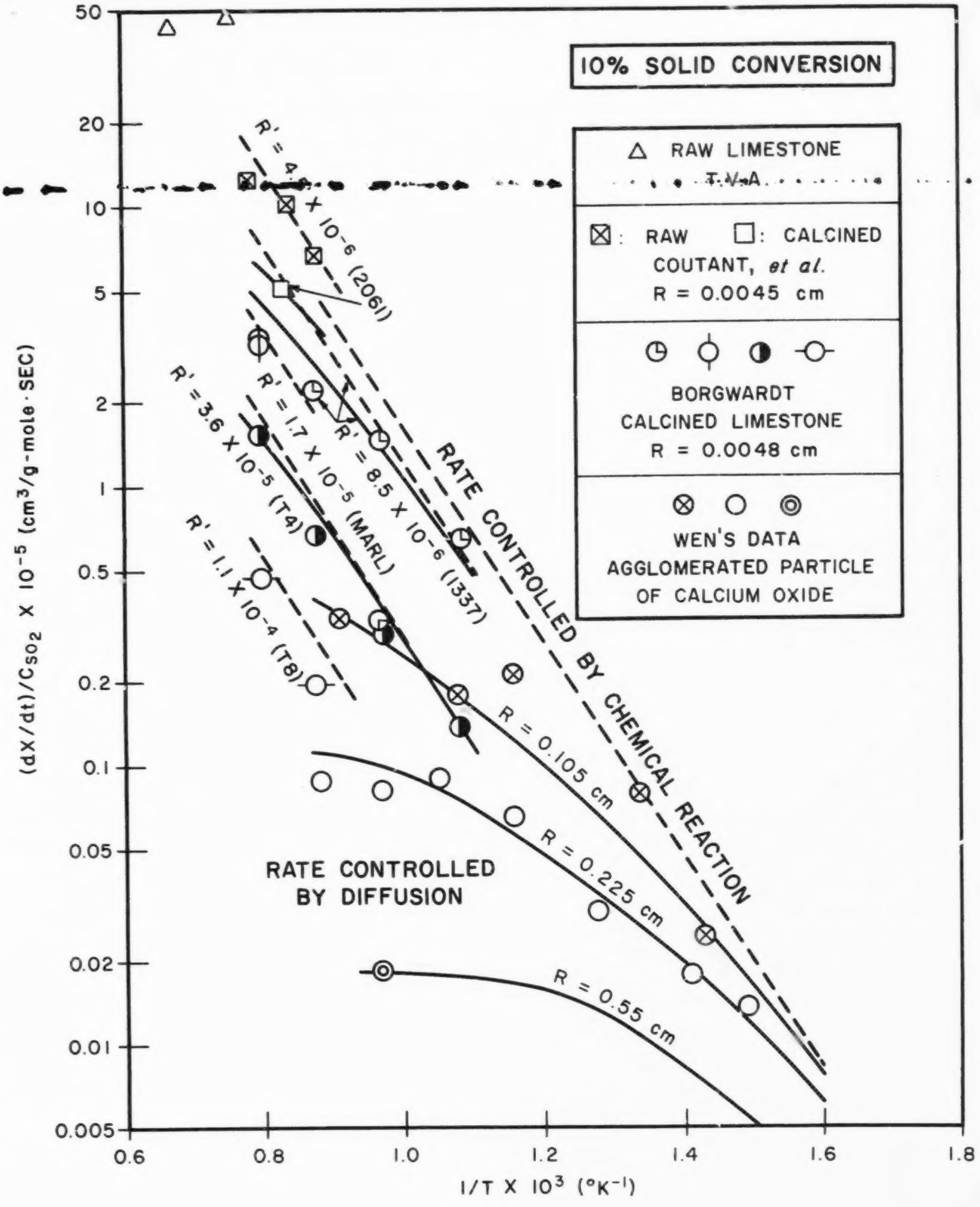

TABLE 6

DATA KEY FOR WEN'S MODELING STUDIES

Key	Stone*	Investigator	Type	CaO (Wt. % in Calcine)
◷	C	Borgwardt	1337	55
◶	C		1351	54
◵	C		1343	94
◴	C		1360	81
◓	C	Borgwardt	T2	98
◒	C		T3	95
◑	C		T4	96
◐	C		T5	58
-○-	C		T8	97
⌽	C		Marl	88
□	C	Coutant, et al	2061	90
⊠	R		2061	90
△	R	T.V.A.		
○	C	Wen	Agglomerated CaO	100
○	C			
◎	C			

---

* C denotes calcined stone; R denotes raw stone

Figure 39 was developed to demonstrate the effect of diffusion upon reaction rate. This plot illustrates the effect of diffusion upon the overall reaction rate at different calcine conversions for the forms of the model which represent volumetric and grain reaction. At initiation, where solid conversion (X) equals zero, both models give the same curve, and the effect of diffusion on overall rate is small for small values of ϕ_V. (ϕ_V is a Thiele modulus based upon the effective diffusivity.) For the curves shown on Figure 39, the effective diffusivity, D_{eA}, was assumed constant. If D_{eA} changes, the rate representation would also change, but since no data are available to investigate this variable, it was decided to compare the various experimental results at low conversions to minimize any diffusional effects.

This comparison is shown in Figure 40, where the upper curve represents the data of Wen while the lower curve reflects the OAP bench scale data. If the rate is extrapolated toward zero particle radius, as represented by the horizontal dashed lines, the reaction rate constant for the chemical reaction controlling region may be obtained. Since SO_2 concentration is constant in this region, the value of k's/R' may be calculated from the rate data, where k's is the reaction rate constant based on the surface area in the grain, and R' is the radius of the spherical grain. Using this ratio, and the function defined for the Thiele modulus(11), an effective diffusivity may be obtained. Furthermore, by plotting this ratio versus the grain radius using sulfation data of many investigators (Figure 41), Wen concludes that the rate constant (k's) is practically independent of particle size and is a function of temperature only. The

FIGURE 39

DIFFUSION EFFECT UPON REACTION RATE

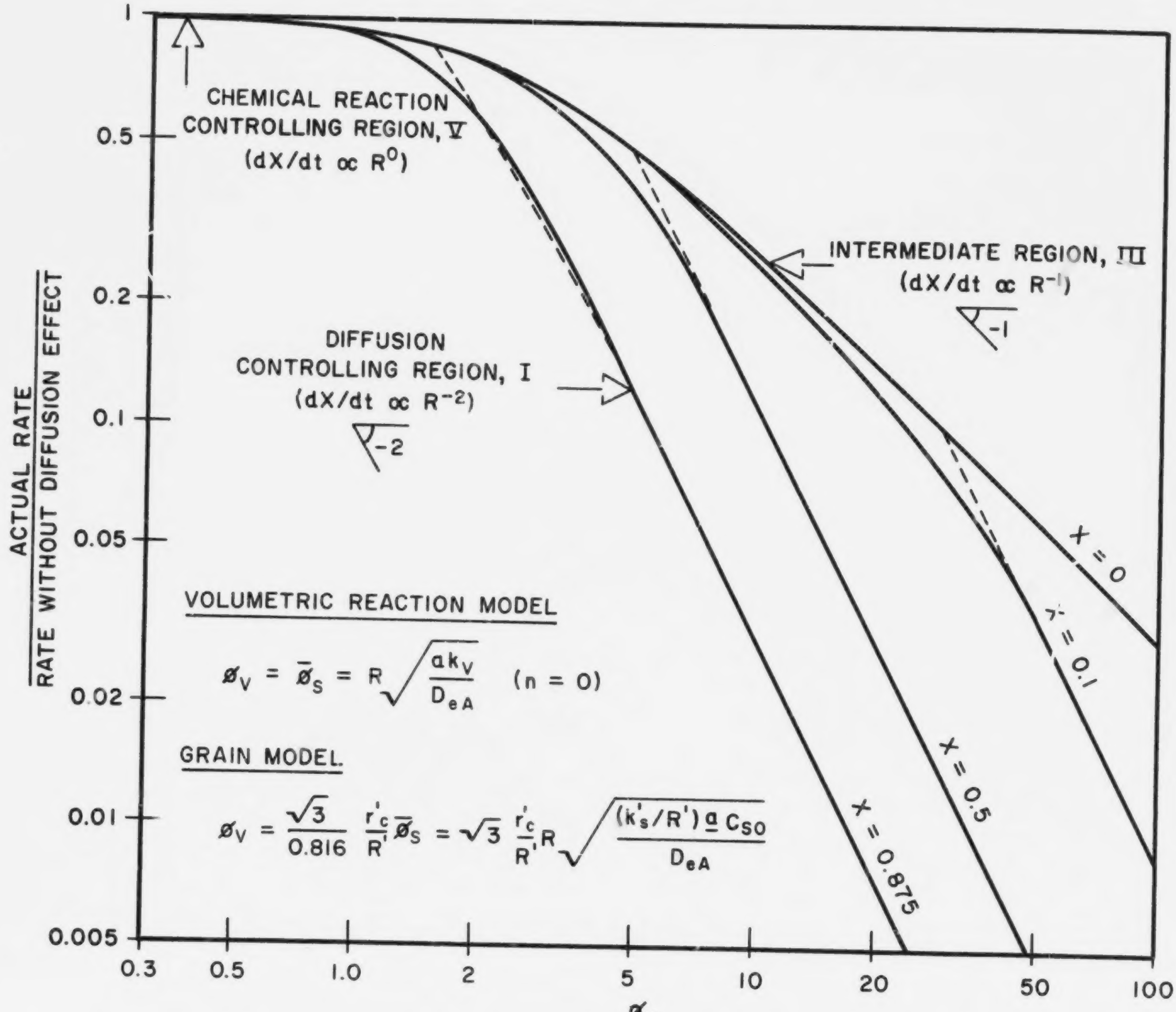

FIGURE 40

REACTION RATE VS PARTICLE SIZE

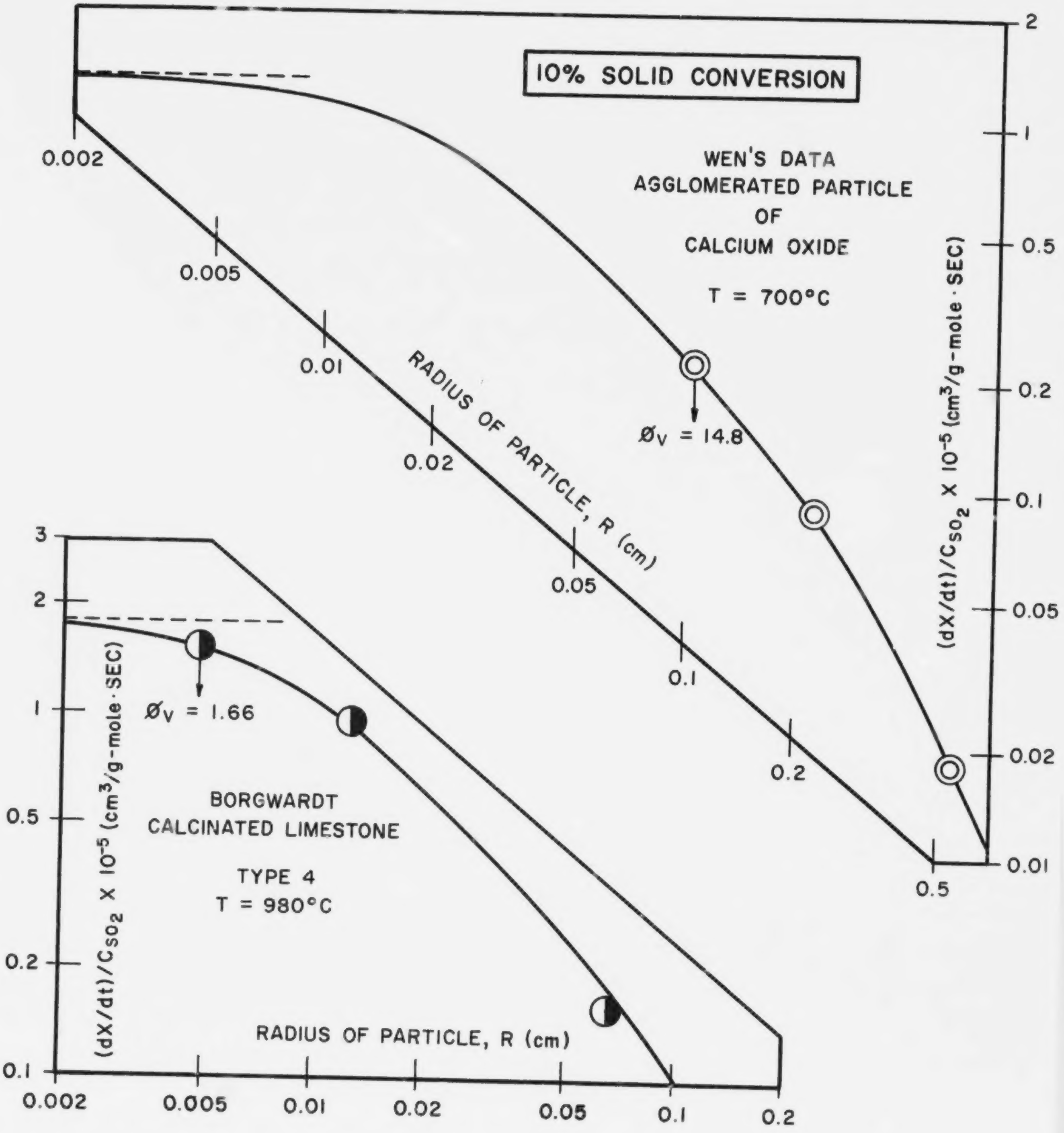

FIGURE 41

REACTION RATE CONSTANT VS GRAIN RADIUS

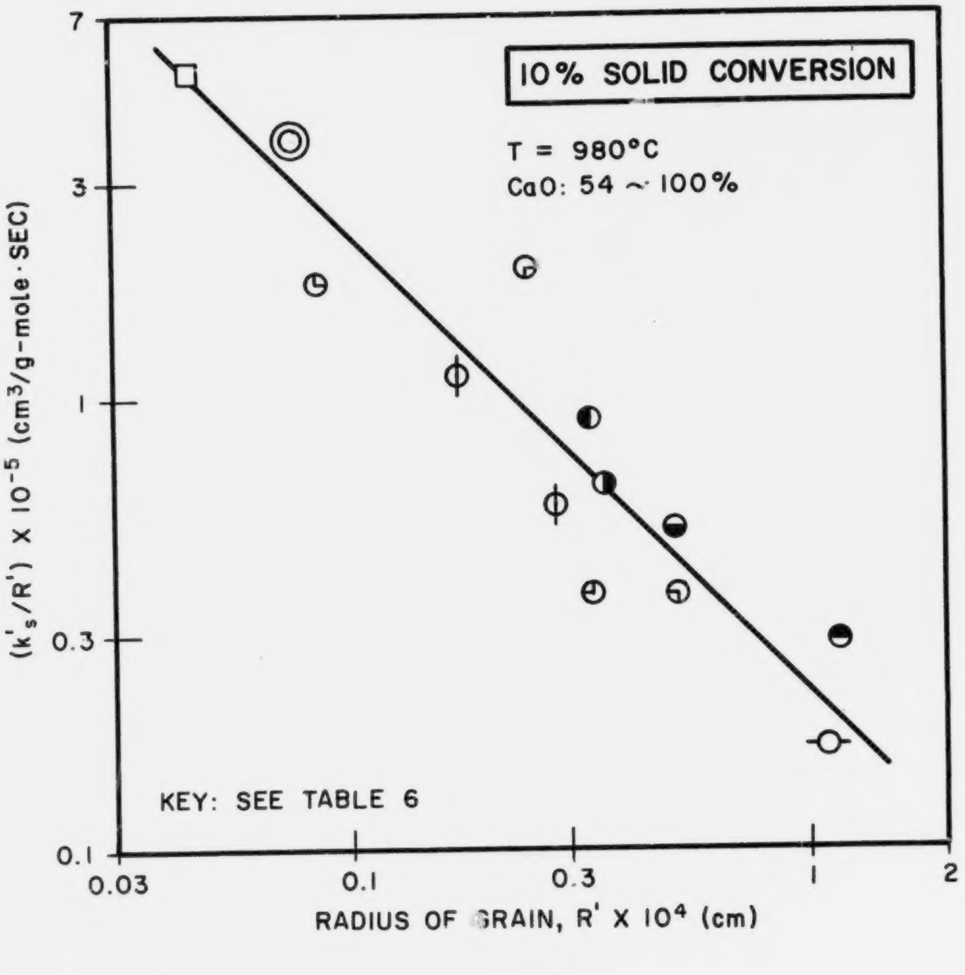

same conclusion is demonstrated on Figure 42 by a standard Arrhenius approach, i.e., a plot of reaction rate constant versus reciprocal absolute temperature.

As of this writing, the reaction modeling by Dr. Wen is continuing. The grain reaction model which he proposes appears to answer many of the questions which arose over the order of magnitude deviations in reaction rate data of OAP and Battelle. Present efforts by Dr. Wen involve the modeling of the calcination of the raw limestone, and integration of the calcination reaction and sulfation reaction models into a single non-isothermal model to simulate the design conditions which would exist in a commercial boiler system.

FIGURE 42

ARRHENIUS PLOT

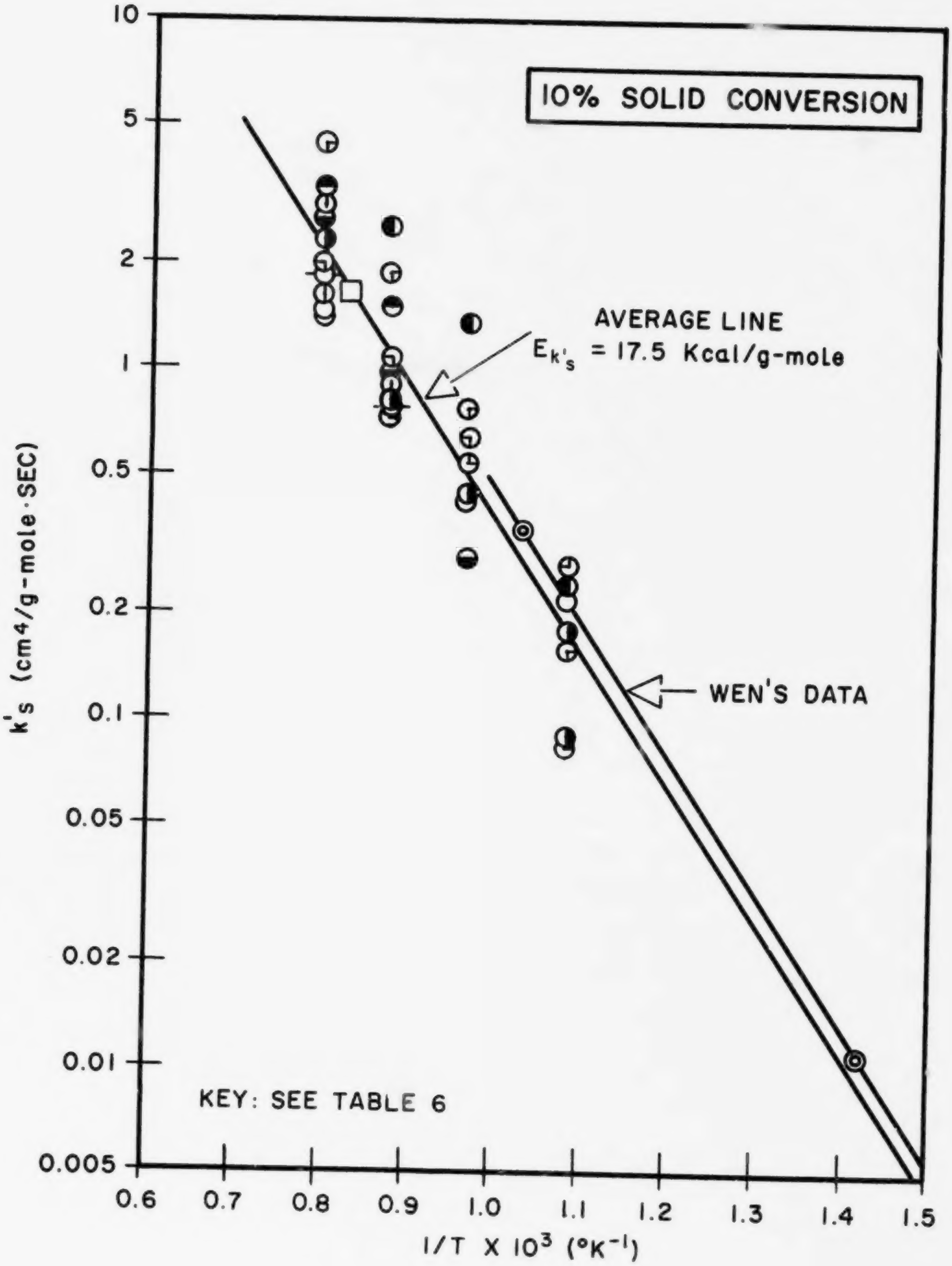

4. M.I.T. Model

The proposed MIT model represents a solution of a series resistance type approach to the sorption of SO_2 by calcines. A report published by Dr. J. B. Howard and co-workers at MIT(13) presents a discussion of the development and testing of this model. The model includes the following steps: mass transfer from the ambient gas to the particle, diffusion and reaction within the pores of the particle, and solid diffusion within the calcium oxide grains. To represent the internal structure of the calcine particle, a simple geometric model was developed.

In order to evaluate the accuracy of the proposed MIT model, the model's constants had to be evaluated. This was accomplished in studies at MIT by the simultaneous solution of the partial differential equation representing the previously discussed series resistances. The solution method presented in the MIT report employs a finite difference technique and requires a computer solution. In this manner, the model calculated values for the pore diffusion coefficient, reaction rate constant, solid diffusional coefficient and the effective structural properties of the calcine. The data used in the development of the model constants are those which were published by Mr. Borgwardt of OAP(14). Using the OAP bench scale data, the constants shown in Table 7 were developed to represent the sorption characteristics of "Calcine 9", a calcitic dolomite (70% dolomite, 18% calcite). These particular constants are the only ones presented in support of the model by the MIT report.

In an attempt to verify the development of the MIT model constants, and to obtain constants for the

TABLE 7

THE EFFECT OF TEMPERATURE ON REACTION PARAMETERS AND EFFECTIVE STRUCTURAL PROPERTIES OF CALCINE 9

Temperature, ^{o}F	1796	1598	1400	1202
Pore Diffusion Coefficient, cm^2/sec	0.23	0.21	0.20	0.18
Reaction Rate Constant, cm/sec	27.5	5.5	0.78	0.067
Solid Diffusion Coefficient, $cm^2/sec \times 10^{10}$	1.12	1.00	0.87	0.073
Effective Surface Area per Unit Volume, $cm^{-1} \times 10^{-6}$	0.235	0.765	6.52	199
Effective CaO Grain Radius, cm	0.7	0.5	0.1	0.02

other calcines studied by OAP, the MIT modeling procedure was adapted to the Kellogg Laboratory IBM-1130 computer. However, considerable difficulty was encountered in this endeavor due to the size of the program's calculational matrix. The original MIT modeling program was developed for use on an IBM 360-65 machine and utilizes some 88,000 programming words. The Kellogg machine has only 5,500 words available for use, thus necessitating a decrease in the time and space steps required by the iterative solution. One further problem arose in attempting to simulate the MIT program on the smaller machine, viz., a loss of calculational precision. The IBM-360 uses 12 significant figures to represent a number, whereas the 1130 computer uses only 6. In the finite difference calculational technique, the determining factor for a solution is the representation of the slope of a function by the difference between two adjacent values. Because of the two computing limitations encountered, a suitable representation of the MIT model could not be made on the Kellogg Laboratory computer.

Since the MIT model constants presented in their final report were for only one of the 11 calcines studied by OAP, and since the bench scale experimental data may not sufficiently describe the mechanisms encountered in a commercial boiler system, no judgments as to the accuracy of the proposed MIT model can be made at this time. The Kellogg effort to study the MIT method of analysis for other sets of experimental data has been limited by the lack of sufficient computer size. Since other experimental models using the series resistance technique are being investigated, further work on the MIT modeling procedure has been discontinued. Should the other proposed models prove insufficient in their description of the process system, further system analysis may be required using the more complex MIT modeling.

D. Calcination Studies

1. Particle Heat-up Calculations

Particle heat-up time was estimated by making a heat transfer calculation on a single calcine particle. This calculation consisted of an isothermal heat balance around the particle, i.e., it was assumed that no temperature gradient exists throughout the particle itself. The following heat balance was used:

$$\text{Accumulation} = \text{input} - \text{output} + \text{generation}$$

The differential accumulation term for a spherical particle of diameter D_p is

$$\text{Accumulation} = \left(\frac{\pi D_p^3}{6}\right) \rho_p \, c_p \left(\frac{d\,T_p}{d\,\theta}\right)$$

where

ρ_p = particle density, lb/ft^3
c_p = solid specific heat, Btu/lb, ^oF
T_p = particle temperature, ^oF
θ = time, hr

Heat input to the particle occurs by convection and is given as follows:

$$q_c = h_c(\pi D_p^2)(T_g - T_p)$$

where

q_c = convective heat, Btu/hr
h_c = convective heat transfer coefficient, Btu/hr, ft^2, ^oF
T_g = gas temperature, ^oF

The output term in the heat balance equation is represented by radiation heat loss terms. In the system considered, there are two radiation terms--(1) radiation between the particle and the steam-jacketed boiler wall, and (2) radiation between the particle and the furnace flame. The two radiation terms are additive, and are thus lumped into one radiation heat loss term as follows:

$$q_r = h_{rw}(\pi D_p^2)(T_p - T_w) + h_{rf}(\pi D_p^2)(T_p - T_f)$$

where

q_r = radiation heat, Btu/hr
h_{rw} = wall radiation heat transfer coefficient, Btu/hr, ft^2, ^{o}F
h_{rf} = flame radiation heat transfer coefficient, Btu/hr, ft^2, ^{o}F
T_w = wall temperature, ^{o}F
T_f = flame temperature, ^{o}F

The generation term in the heat balance equation represents the heats of reaction and is assumed to be zero. The basis for this assumption lies in the fact that the decomposition of the carbonate is endothermic while the reaction of SO_2 with CaO is exothermic. Thus the heats of reaction tend to cancel each other.

With the above assumptions, the heat balance equation for a single particle becomes

$$\frac{d\,T_p}{d\,\theta} = \left(\frac{6}{\rho_p c_p D_p^2}\right)\left[Nu\ k_g(T_g - T_p) - h_{rw}D_p(T_p - T_w) - h_{rf}D_p(T_p - T_f)\right]$$

where

k_g = thermal conductivity of the gas (assumed to be pure N_2), Btu/hr, ft^2, °F/ft

Nu = Nusselt number

Other terms as previously defined

The above equation was programmed on the Kellogg IBM 1130 computer. The variation of the gas temperature, Tg, was assumed to be linear with respect to time, the relationship of which was obtained from the Battelle project report of June 30, 1966(15). The following conditions were used in obtaining a solution to the differential heat balance equation:

1. Particle injection temperature = 150°F
2. Gas temperature at the injection point = 2400°F
3. Wall temperature was assumed constant at 700°F
4. Flame temperature was assumed constant at 3000°F
5. k_g and C_p were programmed as functions of T_g and T_p, respectively
6. h_{rw} and h_{rf} were programmed as functions of T_p
7. ρp was assumed constant at 102.9 lb/ft^3 (porosity = 0.45 cc/cc)

Figure 43 illustrates the Kellogg computer solution graphically showing particle temperature as a function of time for particle diameters of 44, 74 and 100 microns. As would be expected, the heat-up time increases with increasing particle size, e.g., the heat-up time for 44 micron limestone particles is approximately one-third that for 100 micron particles. The effect of the Nusselt number on heat transfer has also been determined, and it also is shown on Figure 43 that increasing the Nusselt number by a factor of ten (from 0.2 to 2.0) approximately halves the particle heat-up time. Even for 100 micron particles, however, the heat-up time of 0.07 seconds is small compared to the actual total residence time of approximately one to two seconds available in a boiler. It is, therefore, reasonable to assume that particle heat-up time is not a limiting factor in the overall limestone sulfaction reaction.

FIGURE 43

PARTICLE HEAT-UP TIME FOR LIMESTONE

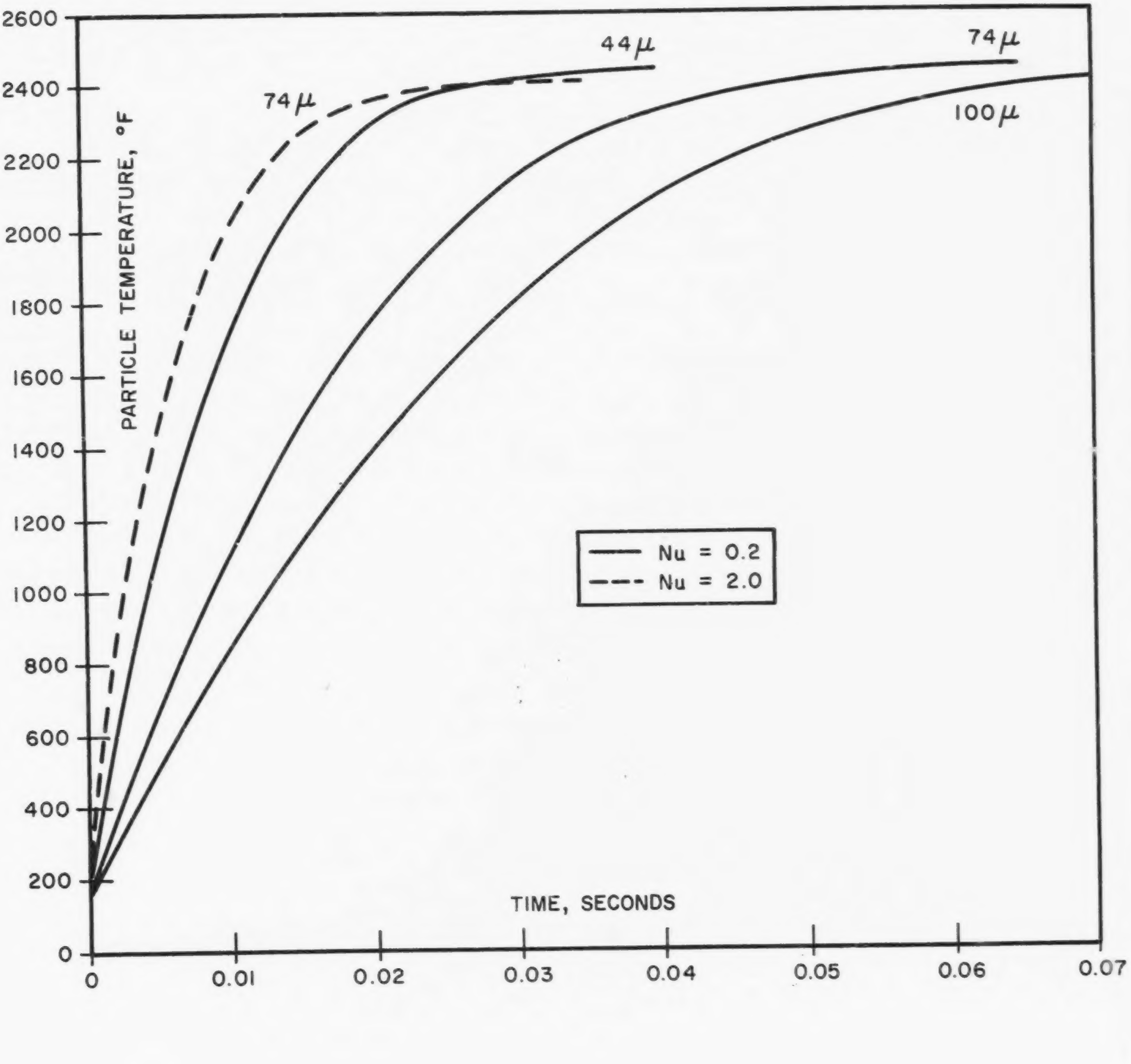

2. Deadburning Studies

Studies aimed at evaluating the degree of deadburning of limestones and dolomites were published by Dr. Drehmel of OAP(16). It previously had been noted that as limestones are calcined for longer times and at higher temperatures, they lose reactivity and experience a shrinkage in volume along with a loss of surface area and porosity. In this study, Limestones No. 2061 and No. 2062, and Dolomite No. 2069 were calcined in a rotary kiln for two hours at temperatures of 1700, 2000, 2300, 2600 and 3200°F. The resultant calcined samples were subsequently analyzed for B.E.T. surface area, density, porosity, distribution of pore volume, and median pore size. Along with physical property measurements, the following chemical reactivity experiments were conducted on the calcines:

1. Absorption of sulfur dioxide from flue gas
2. Absorption of sulfur dioxide from pure SO_2
3. Absorption of carbon dioxide
4. Absorption of steam
5. Modified coarse-grain acid titration
6. Hydration-weight gain

Table 8 is a typical example of the results obtained in OAP's published study. As expected, density increased with increasing calcination temperature, while B.E.T. surface area, pore volume, and chemical reactivity each decreased. It can be noted from Table 8 that except for CO_2 absorption, all of the physical properties tested

TABLE 8

PROPERTIES OF LIMESTONE NUMBER 2061
SET I, 70/140 MESH PARTICLE SIZE RANGE

	Calcine Temperature, °F				
	1700	2000	2300	2600	3200
Flue Gas Absorption 1800°F, 2 min, mg/30 mg	8.6	5.9	2.5	1.6	1.0
Pure SO_2 Absorption* 1800°F, 30 min, % gain	66.0	40.7	21.9	10.4	8.0
Pure CO_2 Absorption* 1400°F, 60 min, % gain	37.4	8.7	5.8	2.6	1.7
Steam Absorption 500°C, 5 min, % gain	29.7	22.5	12.5	10.8	7.2
B.E.T. Surface Area m^2/g	3.1	1.6	1.0	0.8	0.3
Total Pore Volume cc/g	0.61	0.51	0.33	0.25	0.33
Small Pore Volume cc/g	0.28	0.14	0.09	0.04	0.04
Density by Mercury Intrusion, g/cc	2.82	2.44	3.23	3.34	3.30

---

*Note: Listed values for 140/200 mesh

plus the reactivities change in approximately the same manner between successive calcination temperatures. CO_2 absorption drops sharply at 2000°F, and this behavior has been attributed to the shrinking, melting, and fusing of the crystals, thus obstructing carbon dioxide penetration into the lime(17).

The following conclusions regarding parameter effects on limestone reactivity were drawn from this particular study:

1. CO_2 absorption was nearly independent of particle size, but SO_2 absorption was slightly lower for the largest particle size ranges.
2. CO_2 absorption was affected drastically by calcination temperature, but SO_2 absorption was not.
3. Both CO_2 and SO_2 absorption were independent of gas flow and weakly dependent on reaction time.

A statistical analysis by Dr. Drehmel supported the fact that the loss in surface area and pore volume at higher calcination temperatures accounted for the loss in reactivity. No explicit conclusion concerning an optimum temperature of limestone injection is obvious from this study. From Table 8, however, it appears that the best calcination temperature lies somewhere between 1700°F and 2000°F. In order to allow sufficient time for sulfation to occur, the overall optimum injection temperature would probably be closer to 2000°F.

3. Battelle Calcination Data

The calcination results discussed in this section are obtained from the data presented in the Battelle final project report(1). Figure 44 is a plot of the Battelle data for Limestone No. 2061, and shows the percentage calcination as a function of gas residence time over the temperature range 1604°F to 2068°F. Curves A, C and D represent calcination data for -140+200 mesh particles (74-105μ). Curve B illustrates the data for -270+325 mesh particles (44-53μ) calcined at a gas temperature of 1770°F. Battelle originally reported data for the -140+200 mesh particles at a temperature of 1770°F; however, in their final report they stated that this particular set of data is unreliable. Hence, while there is no direct effect of particle size derivable from the data, interpolation of the above curves would indicate a very minor effect.

The initial rate of calcination evidenced from the initial slope of the above curves, increases with increasing gas temperature as expected. The extent of calcination at a reactor residence time of two seconds ranges from about 70% to about 90% in the temperature range of 1600-2068°F. It should also be noted that the curves extrapolate to a residence time of approximately 0.1 second at zero conversion of the stone. This value is in good agreement with a particle heat-up time of 0.07 seconds which was estimated from heat transfer calculations.

Some recent Battelle experimental studies presented in their monthly project reports to OAP (Sept. 1970 to Nov. 1970) also were reviewed. The results of

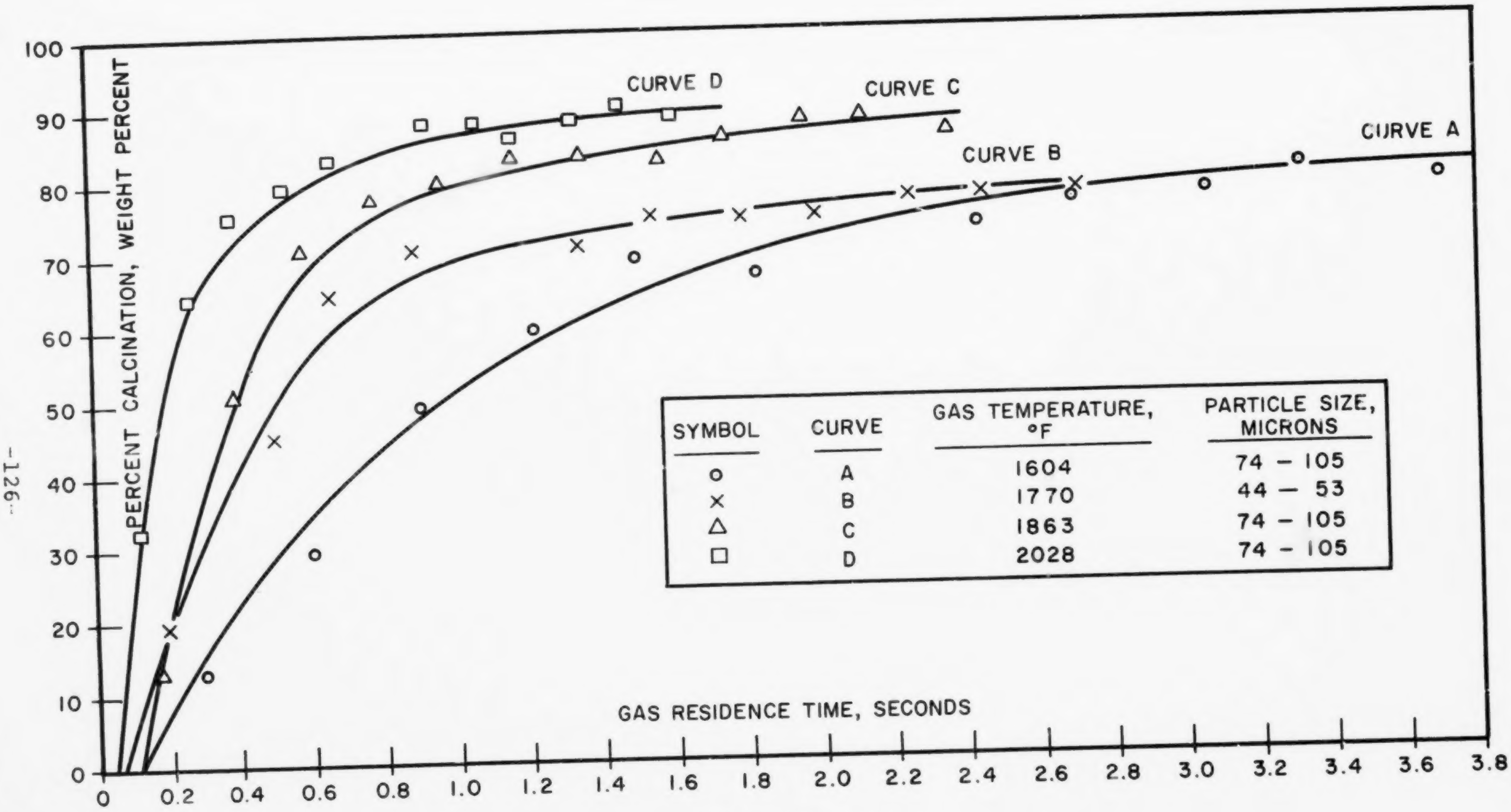

FIGURE 44

BATTELLE CALCINATION DATA

LIMESTONE NO 2061

calcination tests carried out with -270+325 mesh (44-53M) Limestone No. 2061 are summarized in Table 9. The flow reactor inlet and outlet gas temperatures are listed along with the average gas residence time. The measured extent of calcination cannot be compared directly with the earlier plot of data (Figure 44), because of the different particle size and non-isothermal reactor profiles. The most significant aspect of the recent Battelle work is that B.E.T. surface area determinations have been made on stones calcined under short residence time conditions. The surface area values tabulated generally range from 20 to 60 m^2/gm CaO. This range is significantly higher than the values of 1 to 10 m^2/gm CaO reported by OAP(4) and TVA(18) from bench scale tests involving longer calcination times, i.e., 1 to 120 minutes, which illustrates the potential problem of decreased intraparticle surface area and loss of reactivity due to deadburning. The data of Table 9 do not exhibit any obvious correlation with residence time; however, there does appear to be a loss of surface area at high injection temperatures (>2000°F) coupled with the higher residence times.

The results of additional limestone calcination measurements from the recent Battelle monthly reports for simultaneous calcination-sulfation tests in their dispersed-phase reactor are shown in Table 10. The most interesting observation from the data is the fact that the percentage calcination at low residence times with in situ sulfation of the calcine is much greater than indicated by Figure 44. For example, 58-65% calcination is indicated for a 1900-2000°F injection temperature and 0.2 second gas residence time, whereas the above cited plot would predict about

TABLE 9

BATTELLE CALCINATION DATA (NO SO_2 PRESENT)
LIMESTONE NO. 2061
PARTICLE SIZE: -270+325 MESH (44-53μ)

Gas Temperature Injection (°F)	Gas Temperature Collection (°F)	Residence Time (seconds)	Percentage Calcination (wt. %)	Surface Area (m^2/gm CaO)
1830	1440	1.82	73.0	61.3
1830	1765	0.23	19.0	44.2
1849	1782	0.18	45.0	42.9
1920	1500	1.35	78.0	36.6
1996	1920	0.17	28.0	67.8
2156	2073	0.16	45.0	66.7
2224	1440	2.86	86.0	21.3
2224	1765	1.27	83.0	21.3
2243	2156	0.15	40.0	52.9
2243	1500	1.99	85.0	7.6

TABLE 10

BATTELLE CALCINATION DATA (IN SITU SULFATION)
LIMESTONE NO. 2061
PARTICLE SIZE: -270+325 MESH (44-53 μ)

Gas Temperature Injection (°F)	Gas Temperature Collection (°F)	Residence Time (seconds)	Percentage Calcination (wt. %)
1908	1842	0.17	58.0
1974	1567	1.28	88.0
2046	1974	0.16	65.0
2197	2120	0.15	71.0
2277	2197	0.15	72.0
2277	1567	1.90	95.0

30-40%. One possible explanation for the increased calcination rate in the presence of SO_2 is offered by Ishida and Wen (Univeristy of West Virginia) who postulate that it is caused by the exothermic heat of sulfate formation. It appears that this question does merit further study.

Effect of injection temperature on surface area of the calcines is illustrated in Table 11 taken from a recent Battelle project report. Battelle has taken three different limestones and injected them into a pilot reactor at three different temperatures while maintaining the gas residence time approximately constant. Inspection of Table 11 reveals that with respect to surface area, the optimum injection temperature appears to be approximately 2000°F. This result is consistent with other studies discussed in this section of the report. It should also be noted that different stones (IGS-4 and No. 1336) yield similar surface areas at the optimum injection temperature whereas significant difference exist at other injection temperatures. In all cases shown in Table 11 marl has much less area than the other stones, possibly indicating that it dead burns easier than the other stones.

TABLE 11

EFFECT OF INJECTION TEMPERATURE ON SURFACE AREA

Run	Stone Type(a)	Temperature		Residence Time (seconds)	Percentage Calcination	Area m^2/gm(b)
		Injection	Collection			
317-A	Mich. Marl	2155	1785	1.17	66	7.5
317-B	IGS-4	2155	1785	1.17	80	16.3
317-C	No. 1336	2155	1785	1.17	83	23.7
318-A	Mich. Marl	2006	1712	1.03	52	13.6
318-B	IGS-4	2006	1712	1.03	72	24.8
318-C	No. 1336	2006	1712	1.03	71	26.4
318-D	Mich. Marl	2263	1828	1.14	74	5.9
318-E	IGS-4	2263	1828	1.14	81	8.2
318-F	No. 1336	2263	1828	1.14	84	14.1

(a) -140+200 mesh

(b) area per gram of sample

4. T.V.A. Calcination Data

Extensive bench scale experimental studies of limestone calcination rates have been carried out by the TVA Fundamental Research Branch. The work entailed fixed bed studies of limestone calcination at long residence times (1 to 30 minutes) in an inert gas atmosphere. The TVA final correlation of the calcination reaction rate is presented in their October 1969 monthly project report to OAP. The correlation equation was used to calculate Table 12, which gives the time required for 75% calcination for different particle sizes and gas temperatures. An assumed activation energy of 30 kcal/gm mole is incorporated into these calculations. The results do indicate that for an average particle diameter less than 100 microns, and a gas temperature of 1900°F or greater, the time required for 75% calcination will be under 0.20 seconds. The TVA correlation yields a higher predicted percentage calcination at low residence times than the plot of the Battelle calcination data. However, the discrepancy may merely reflect a loss of accuracy inherent in extrapolating the TVA bench scale data to much lower residence times (less than 1 second).

The principal conclusion from the analysis of both the Battelle and TVA data is that at least 40% stone calcination can be achieved in 0.2 second residence time in a boiler with a minimum injection temperature of 1900°F. Also, as Battelle(1) point out, the sulfation reaction apparently begins immediately upon injection of the stone into the reactor which, coupled with the increased calcination rates obtained in the presence of SO_2, indicates that the calcination step does not appear to be critical in the overall sulfation process, and detailed

TABLE 12

TVA CALCINATION CORRELATION PREDICTIONS*
ACTIVATION ENERGY 30 kcal/gm mole (Assumed)

Particle Size (microns)	Time Required (Seconds) For 75% Calcination At Indicated Temperature			
	1832°F	2012°F	2019°F	2370°F
57	0.14	0.061	0.029	0.015
99	0.24	0.10	0.049	0.025
161	0.41	0.17	0.081	0.042

---

* TVA Monthly Project Report to OAP (October 1969)

kinetic modeling of the limestone calcination reaction does not appear to be justified at this time. Preliminary surface area measurements from the Battelle flow reactor indicate an optimum additive injection point corresponding to a gas temperature range of 1900°F to 2100°F. The most useful aspect of future experimental studies of limestone calcination would appear to lie in the analysis of parameters that control the particle surface area to pore volume characteristics.

E. Gas-Particle Mass Transfer

1. Kellogg Calculations

A relationship describing the mass transfer of sulfur dioxide can be derived by utilizing the j-factor analogy between heat and mass transfer as follows:

In the case of heat transfer, the j-factor is defined as

$$j_H = \frac{Nu}{Re\ Pr} (Pr)^{2/3}$$

where

Nu = Nusselt Number
Re = Reynolds Number
Pr = Prandtl Number

By a direct analogy to heat transfer, the mass transfer j-factor can be expressed as

$$j_M = \frac{Gz'}{Re\ Pr} (Sc)^{2/3}$$

where

Gz' = Modified Graetz Number

Zenz and Othmer(19) give an expression for the modified Graetz Number for the case of fluid flow around a sphere as

$$Gz' = \frac{\pi D_p\ M_m\ P_m\ K_g\ c_p}{k_g}$$

where

D_p = Particle diameter
K_g = Overall mass transfer coefficient
P_m = Mean pressure of non-transferring gas
M_m = Mean gas molecular weight
c_p = Specific heat of non-transferring gas
k_g = Thermal conductivity of non-transferring gas

An expression for the mass transfer coefficient is obtained by solving the above equation for K_g:

$$K_g = Gz' \left(\frac{k}{c_p}\right)_g \left(\frac{1}{\pi D_p M_m P_m}\right)$$

Equating the j-factor equations then results in an expression for the modified Graetz Number, from which a numerical value may be obtained for use in the above equation to find the mass transfer coefficient:

$$Gz' = Nu \left(\frac{Pr}{Sc}\right)^{2/3}$$

The rate of mass transfer of SO_2 is now expressed as

$$N_t = \int_0^{\theta} (K_g A_t)\, p_{SO_2}\, d\theta$$

$$N_t = \int_0^{\theta} K_g \left(\frac{6 W_p}{\rho_p D_p}\right) p_{SO_2}\, d\theta$$

where

N_t = Rate of SO_2 transferred
A_t = Total external surface area of all particles
P_{SO_2} = Local partial pressure of SO_2 in the gas
θ = time
W_p = Weight rate of solids injection
ρp = particle density of calcine

After substituting the previously derived expression for the mass transfer coefficient, Kg, into the above equation, the final relationship describing the rate of mass transfer of SO_2 is

$$N_t = \int_o^{\theta} Gz' \left(\frac{k}{c_p}\right)_g \left(\frac{1}{M_m P_p}\right) \left(\frac{6\ W_p}{\pi D_p^2 \quad {}_p}\right) P_{SO_2}\, d\theta$$

This equation is the same as that used by Battelle$^{(15)}$ in their mass transfer calculations.

Based on the above relationship, mass transfer calculations were made assuming that the CaO-SO_2 reaction is relatively fast compared with the diffusion of sulfur dioxide through the inert gas. Sulfur dioxide conversion in a typical stack gas (0.3 mole percent SO_2) was calculated as a function of the stoichiometric Ca/S ratio using a typical limestone additive (94% $CaCO_3$, 45% porosity). The active boiler injection zone for the desulfurization reaction was assumed to have an average temperature of 1600°F and to provide a gas residence time of 2.0 seconds. Results of this calculation are presented on Figure 45 for particle sizes of 44 microns (325 mesh), 74 microns (200 mesh) and 100 microns (140 mesh). The calculated conversion increases with Ca/S ratio since more total particle

FIGURE 45

SO_2 CONVERSION VS STOICHIOMETRIC CaO FOR VARIOUS PARTICLE DIAMETERS

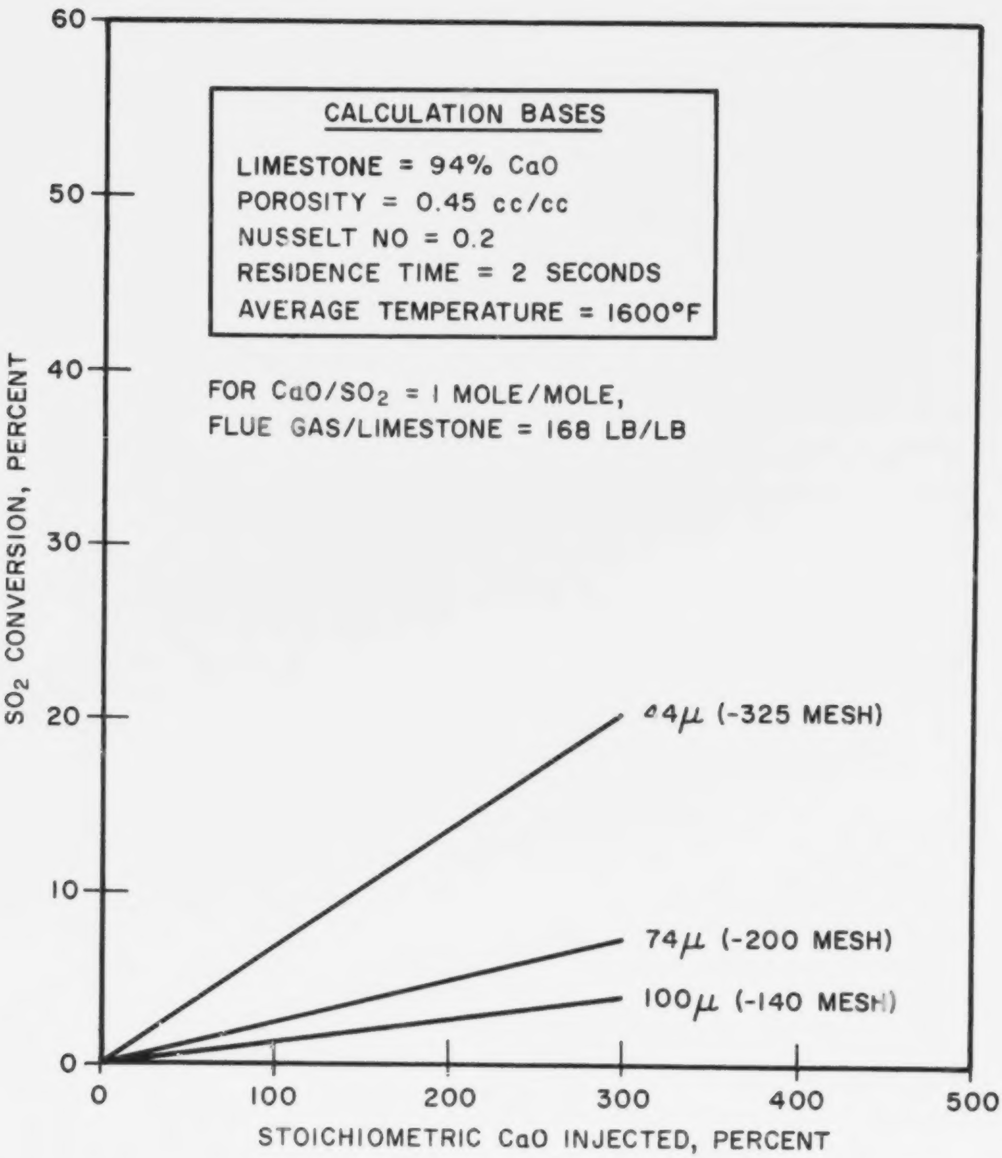

TABLE 13

GAS-PARTICLE MASS TRANSFER CALCULATIONS

Stone	CaO Content (wt. %)	Stone Injection Rate (lb/hr)	Flue Gas Rate (lb/hr)	D_p (μ)	D_p (ftx10^4)	Porosity (cc/cc)	Skeletal Density (lb/ft^3)	Particle Density (lb/ft^3)	Stoich. CaO %	Nu	Average Temp. (^oF)	Residence Time (sec)	SO_2 Conversion (%)
Dolomite	54	115,526	1.08x10^7	74	2.43	0.56	187	82.3	100	0.2	1600	2	5.2
"	54	115,526	1.08x10^7	74	2.43	0.56	187	82.3	100	0.2	900	2	3.5
"	54	115,526	1.08x10^7	74	2.43	0.56	187	82.3	100	0.2	1600&900	4	8.7
"	54	115,526	1.08x10^7	74	2.43	0.56	187	82.3	100	2.0	1600	2	51.9
"	54	115,526	1.08x10^7	74	2.43	0.45	187	102.9	100	0.2	1600	2	4.1
"	54	115,526	1.08x10^7	74	2.43	0.56	212	93.4	100	0.2	1600	2	4.6
"	54	231,052	1.08x10^7	74	2.43	0.56	187	82.3	200	0.2	1600	2	10.4
"	54	346,578	1.08x10^7	74	2.43	0.56	187	82.3	300	0.2	1600	2	15.6
"	54	115,526	1.08x10^7	100	3.28	0.56	187	82.3	100	0.2	1600	2	2.9
"	54	231,052	1.08x10^7	100	3.28	0.56	187	82.3	200	0.2	1600	2	5.8
"	54	346,578	1.08x10^7	100	3.28	0.56	187	82.3	300	0.2	1600	2	8.7
"	54	115,526	1.08x10^7	44	1.44	0.56	187	82.3	100	0.2	1600	2	14.2
"	54	231,052	1.08x10^7	44	1.44	0.56	187	82.3	200	0.2	1600	2	29.4
"	54	346,578	1.08x10^7	44	1.44	0.56	187	82.3	300	0.2	1600	2	44.1
Limestone	94	66,366	1.08x10^7	74	2.43	0.45	187	102.9	100	0.2	1600	2	2.4
"	94	132,732	1.08x10^7	74	2.43	0.45	187	102.9	200	0.2	1600	2	4.8
"	94	199,098	1.08x10^7	74	2.43	0.45	187	102.9	300	0.2	1600	2	7.2
"	94	66,366	1.08x10^7	100	3.28	0.45	187	102.9	100	0.2	1600	2	1.3
"	94	132,732	1.08x10^7	100	3.28	0.45	187	102.9	200	0.2	1600	2	2.6
"	94	199,098	1.08x10^7	100	3.28	0.45	187	102.9	300	0.2	1600	2	3.9
"	94	66,366	1.08x10^7	44	1.44	0.45	187	102.9	100	0.2	1600	2	6.8
"	94	132,732	1.08x10^7	44	1.44	0.45	187	102.9	200	0.2	1600	2	13.6
"	94	199,098	1.08x10^7	44	1.44	0.45	187	102.9	300	0.2	1600	2	20.4

surface is available at higher additive injection rates. However, the results do indicate extremely low potential SO_2 conversions (6% maximum) at practical additive rates (100-250% stoichiometric CaO/SO_2) for a standard 140-200 mesh particle size range. The curves also illustrate the substantial benefit attainable from fine grinding to 325 mesh if mass transfer were the controlling mechanism.

Table 13 illustrates the effect of a few of the parameters on overall SO_2 conversion. The parameters involved include particle porosity, skeletal density, particle density, stoichiometric ratio, particle diameter, and CaO content of the stone. From the equation utilized, overall SO_2 conversion is directly proportional to the stone injection rate and inversely related to both particle density and the square root of particle diameter. It is interesting to note that these mass transfer calculation results differ from those obtained when the shrinking core model is used in that the latter shows utilization varying inversely as the first power of the particle diameter. The calculations shown for the dolomitic stone assume that the MgO content is not reactive with SO_2 under boiler conditions in accordance with the Battelle results(20). The specific dolomite and limestone used for this case are stone types 1351 and 1343, respectively, taken from Borgwardt's published studies(14). A flue gas rate of 5,400 tons/hr and a sulfur dioxide mole fraction of $3x10^{-3}$ were used as assumed in the Battelle mass transfer predictions(15).

A major limitation in the accuracy of the above calculational results exists because of a lack of basic heat transfer data for gas-to-dilute dispersions of solid particles in a small size range (10M-100μ). A good discussion of the problem, including available background information, is presented in the literature(19). The implications of this problem and inherent related calculational uncertainties when applied to The Dry Limestone

Process are presented and discussed below.

A substantial number of experimental studies have been carried out to determine heat and mass transfer to single spherical particles suspended in flowing gas streams. Unfortunately, there are very few analogous investigations which tested very dilute dispersions of particles, i.e., bed voidage greater than 99%. The most pertinent published study appears to be the work of Johnstone, et al(21) on heat transfer to clouds of particles. In this particular investigation, measurements of the temperature rise of particles falling through a stagnant gas (air or CO_2) were made. The particle size range of 326M-545M was evaluated for the test materials, viz. sand, aloxite and carborundum.

The results of the published study are shown in Figure 46 as a plot of the average particle Nusselt Number versus the average particle Reynolds Number. The Johnstone data include Reynolds Numbers ranging from 10 to 100 with a corresponding Nusselt Number range of 1 to 10. The dashed curve shown on the plot represents a somewhat arbitrary extrapolation of the data to a Reynolds Number of 1.0. Also shown on this figure is a generalized correlation for heat transfer to single spherical particles(19), which approaches an asymptotic Nusselt Number of 2.0 at very low Reynolds Numbers. It is apparent that the Johnstone study of heat transfer to dilute dispersions resulted in particle-to-gas convective heat transfer coefficients which are an order of magnitude lower than predicted from the accepted correlation for single spheres. The literature tends to rationalize this discrepancy as the result of interparticle hindrance effects, which appears to be a plausible explanation.

FIGURE 46

HEAT TRANSFER TO CLOUDS OF PARTICLES IN AIR

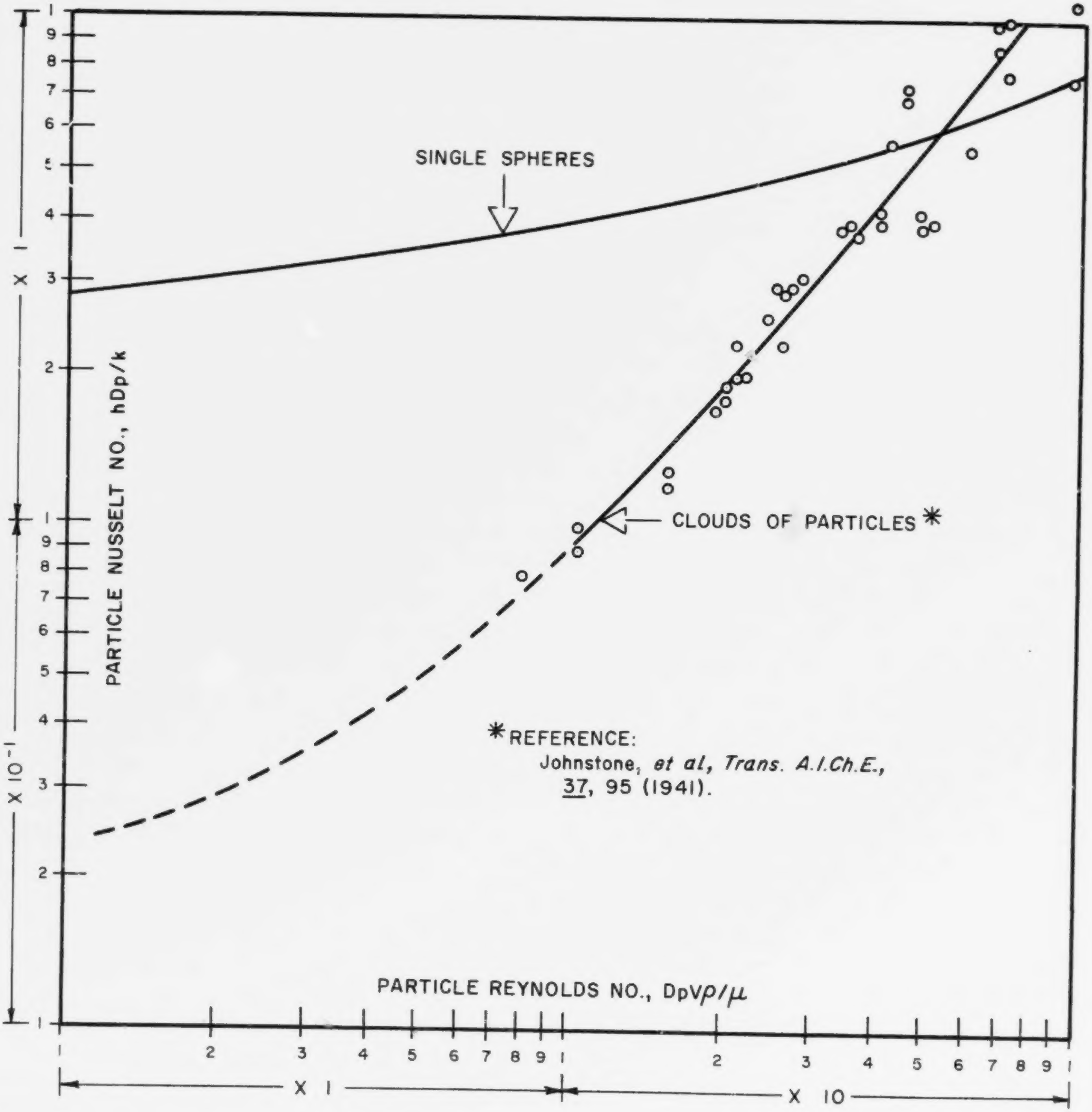

*REFERENCE:
Johnstone, *et al*, *Trans. A.I.Ch.E.*, 37, 95 (1941).

For comparison purposes, Table 14 was prepared showing solids concentrations and particle Reynolds Numbers for the Johnstone data, Battelle reactor data and predictions for the full-size boiler at Ca/S ratios of 1.0 and 2.0. The calculated particle Reynolds Number is based on the slip velocity as calculated from a published equation(22). There are valid questions concerning the accuracy of this slip velocity correlation in a multiple particle system. Nevertheless, the calculated Reynolds Number for the Battelle reactor conditions and commercial boiler will be about unity. It is thus apparent that a major extrapolation of existing data will be required to predict heat transfer coefficients in the Battelle reaction system or the commercial injection system.

Table 14 illustrates an important difference in the comparison between various reactor systems. It is noted that the concentration of particles in the Battelle dispersed-phase reactor (5,700 particles/cu ft) is appreciably lower than in the Johnstone study (476,000 particles/cu ft) or the commercial boiler design (146,000-292,000 particles/cu ft). The low density in the Battelle reactor reflects the fact that a much lower additive injection rate was used (approximately 7-14% stoichiometric Ca/S) than that required in the full scale installation. The Kellogg predictions of mass transfer in the boiler system utilized a low coefficient, corresponding to a Nusselt Number of 0.2, to offset uncertainties in the Johnstone data extrapolation. If the Nusselt Number is influenced by particle density and hindrance effects as postulated earlier, it is possible that transfer coefficients in the Battelle reactor could approach the single particle correlation, and thus be an order of magnitude higher than values predicted for the commercial design. The importance

TABLE 14

COMPARISON OF SOLIDS CONCENTRATION

	A	B	C	D
Particle Diameter, μ	326	90	74	74
Gas Velocity, ft/sec	0	7	62.5	62.5
Slip Velocity, ft/sec*	6.2	1.1	9.3	9.3
Reynolds No. (slip)	3.8	0.2	1.4	1.4
Lb Solids/cu ft	5.04×10^{-2}	8.0×10^{-6}	11.2×10^{-5}	22.4×10^{-5}
Particles/cu ft	476,500	5,740	145,700	291,400

A = Data of Johnstone, et al
B = Battelle data
C = Commercial-scale operation, 100% stoichiometry
D = Commercial-scale operation, 200% stoichiometry

---

* Calculated using the correlation given, for horizontal ducts, by Leva, in Fluidization, McGraw-Hill (1959). Since the terminal falling velocity of small diameter particles is low (e.g., inches per second), it is assumed that the correlation will apply also to vertical travel.

of this question in the calculation of mass transfer limitations in The Dry Limestone Process is explored below.

The basis of the mass transfer predictions is an assumption that the CaO-SO_2 reaction is relatively fast compared with the diffusional processes: that is, the limiting step is taken to be the gas phase mass transfer of SO_2 to the particle surface, and this basis would represent the upper limit of potential SO_2 removal. The gas-to-particle mass transfer coeffecients were obtained directly from the Chilton-Colburn j-factor analogy using the particle heat transfer data discussed above (Figure 46). The following additional calculational bases were used:

limestone composition : 94% $CaCO_3$

calcine porosity : 45%

average particle size : 74M

reactor residence time : 2.25 sec

average temperature : 1900°F

The results of mass transfer calculations are presented on Figure 47 as the percentage SO_2 removal versus the additive injection rate (% stoichiometric). The SO_2 removal will increase proportionally at higher additive rates in this calculation since greater total particle surface area will be available. Two curves are plotted representing the extremes in the range of the predicted mass transfer coefficient, corresponding to particle Nusselt Number values of 2.0 and 0.2. The calculated SO_2 removal will vary directly with the mass transfer coefficient which explains the wide range attainable from the curves plotted. For example, at a stoichiometric injection rate of 2.0 (Ca/S), the maximum possible removal is 60%, and the minimum is 6%.

FIGURE 47

PARTICLE-GAS MASS TRANSFER CALCULATIONS

SO_2 REMOVAL VS ADDITIVE INJECTION RATE

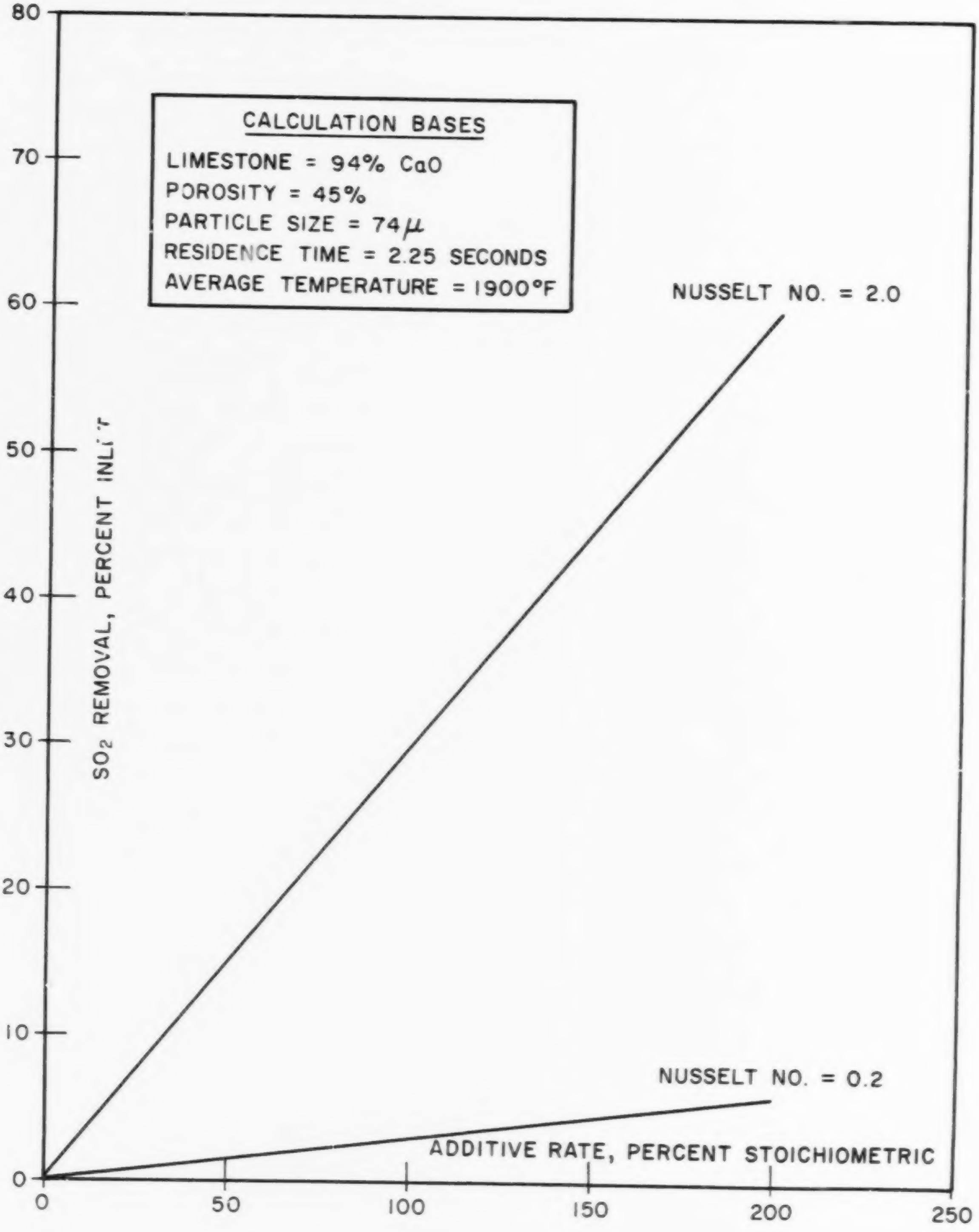

It is possible that for the Battelle dispersed-phase reactors, where the additive rates and resulting particle concentrations are low, relatively high transfer coefficients could be realized. This could imply that heat and mass transfer limitations were unimportant in the Battelle tests, and the results should provide some data on the system kinetics. On the other hand, the transfer coefficients could be much lower in the full scale boiler system because of higher injection rates, which would result in significant mass transfer limitations. The key point is that entirely different mechanisms could be governing the performance of the commercial boiler, and the information developed in the pilot reactor would be of limited utility to the process designer due to an inadequate simulation of the actual reaction system.

2. Comparison with Other Studies

Thomas(23) carried out a study on gas-solid mass transfer for the reaction of SO_2 and limestone in which he compiled mass transfer data from several sources and correlated them on a plot of Sherwood Number versus particle Reynolds Number. For the particular Reynolds Number range calculated in the previous section of this report (0.2 to 3.8) and for a tubular reactor, the Thomas correlation indicates a Sherwood Number of 2.0 which is the expected lower limit in diffusion involving a single particle. This value is also applicable to the Nusselt Number which is the heat transfer equivalent of the Sherwood Number.

In a similar study on fluidized beds, Kato, Kubota and Wen(24) show that for a particle Reynolds Number of approximately 1.0, the Sherwood Number lies in the range of 0.1 to 0.5, depending on the particular study and the particle size utilized. This study and that of Thomas, therefore, continue to support the prior conclusion that the appropriate value of the Nusselt Number (for heat transfer) or the Sherwood Number (for mass transfer) lies somewhere between 0.2 and 2.0, with the use of 0.2 yielding the most conservative results.

3. Comparison with Initial SO_2 Reaction Rates

In a recent study by Borgwardt and Harvey(25) a correlation is presented for the initial reaction rates of limestones with their measured B.E.T. surface area. This correlation indicates a linear relationship on a log-log plot, Figure 47-A, from which it is concluded that chemical reaction is the controlling mechanism.

The data shown on Figure 47-A are for a wide range of calcination times, viz., from fractions of seconds up to and including two hours. The shorter times correspond to the dispersed reactor used in the Battelle tests while the longer residence times represent stones calcined in a kiln for the OAP evaluations. Note that flash calcination produces surface areas an order of magnitude higher than obtained by calcining in a kiln for long residence times. However, all of the data correlate well with the OAP B.E.T. surface area - initial rate concept, thus leading to the conclusion that chemical reaction is the controlling mechanism.

The average B.E.T. surface area of the calcined limestones used in the Battelle study is approximately 40 m^2/gm for which Borgwardt's plot indicates an initial reaction rate of 0.002 gm moles SO_2/gm CaO, sec. Assuming this reaction rate applies and is constant over the entire range of sulfate loading, then for a two-second residence time, 100 percent stoichiometry and 100 micron particle, the SO_2 removal is calculated to be 22.4 percent. From the results of the mass transfer calculations presented in Table 13, the SO_2 conversion for the same physical properties, but assuming gas-particle mass transfer to be limiting, is 1.3 percent using the lower limit of the Nusselt Number (0.2). This value is much lower than that obtained when chemical reaction is assumed to control.

FIGURE 47-A

INITIAL REACTION RATE VS B.E.T. SURFACE AREA

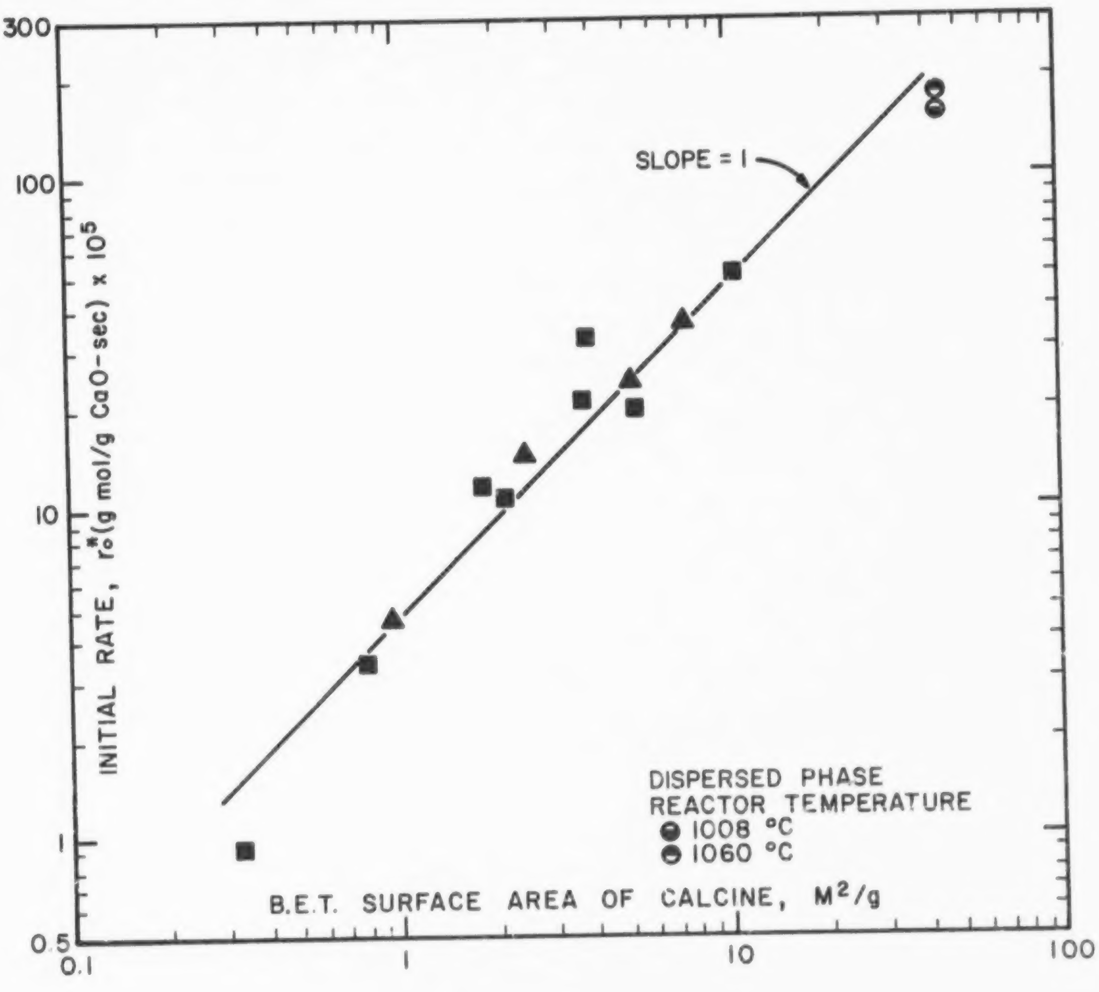

Although the first calculation described above may yield a result which appears higher than the actual value of SO_2 conversion since the initial reaction rate was utilized, it is felt that the size of the decrease in reaction rate over a time interval as small as two seconds would not alter the result significantly. On the other hand, the mass transfer calculation gives a result which tends to be too low, but even if the upper limit of the Nusselt Number (2.0) were utilized, the mass transfer calculation would still yield only 13% SO_2 conversion. Battelle's data in Figure 10(1) for an SO_2 concentration of 0.3%, 74-105 micron particles, and a residence time of two seconds, shows about 118 mg SO_3/g calcine which is equivalent to 9.1% CaO utilization. Thus, for the two extremes of mass transfer calculations cited (Nusselt Numbers of 0.2 and 2), the conversions of 1.3% and 13% range from about 15% to 150% of the actual data reported by Battelle. Since the Nusselt Number is 0.2 as the Reynolds Number approaches 0 (for dilute suspension), and since the Reynolds in this case is about 1, then the mass transfer calculation that applies is closer to 1.3% than 13%. The obvious conclusion therefore is that mass transfer, which indicates much lower SO_2 conversions, should not be totally disregarded as playing a role in the overall controlling mechanism of the SO_2-CaO reaction.

F. Thermochemical and Physical Property Data

1. Thermodynamic Data

In a report entitled "Fundamental Study of Sulfur Fixation by Lime and Magnesia"(15), Battelle has compiled and analyzed the thermodynamic free energy data for the reaction of limestones and dolomites in boiler atomospheres. The free energy data used in the Battelle study are presented in Appendix A of the report, and thermodynamic equilibrium calculations were performed based upon these data. In this manner, the extent to which many of the proposed sulfation and calcination reactions might proceed was determined.

The major reactions investigated were those of CaO and MgO with SO_2 and O_2. For these two systems, at an assumed O_2 level of 2.7 vol. % and a solid activity ratio of unity,the equilibrium partial pressures of SO_2 were calculated versus temperature and are reported in Table 15. The calculated results indicate that SO_2 sorption is only possible below temperatures of ∿2250°F for CaO and ∿1550°F for MgO. However, it must be remembered that these calculations represent the theoretical equilibrium conversions, whereas reaction kinetics will dictate the actual SO_2 concentration within a practical reactor system.

Other conclusions concerning reaction equilibria which have been drawn from the free energy data are:

(1) CaO will tend to recombine with CO_2 to form $CaCO_3$ at temperatures below 1415°F.

(2) $CaCO_3$ can desulfurize flue gas at temperatures below its calcination temperature.

(3) Compared to the formation of $CaSO_4$, producing $CaSO_3$ has no advantages.

TABLE 15

EQUILIBRIUM CONCENTRATION OF SO_2 VERSUS TEMPERATURE FOR THE REACTIONS[a]:

Reaction 1. $CaO + SO_2 + 1/2\ O_2 \rightleftarrows CaSO_4$

Reaction 2. $MgO + SO_2 + 1/2\ O_2 \rightleftarrows MgSO_4$

Temperature (^{o}F)	SO_2 Conc. by Reaction 1 (ppm)	SO_2 Conc. by Reaction 2 (ppm)
1000	1.66×10^{-11}	1.3×10^{-3}
1200	1.09×10^{-7}	1.0
1400	1.01×10^{-4}	1.8×10^{2}
1600	2.34×10^{-2}	1.1×10^{4}
1800	1.95	3.2×10^{5}[b]
2000	7.47×10^{1}	$>10^{6}$[c]
2060	2.12×10^{2}	
2240	2.95×10^{3}	
2420	2.87×10^{4}	
2500	6.30×10^{5}[b]	
3000	$>10^{6}$[c]	

---

[a] Basis 2.7 vol. % O_2 and unit activity of the solids

[b] Insufficient sulfur in the fuel to supply this level of SO_2

[c] Implies an SO_2 concentration greater than 100% is required for equilibrium

(4) SO_2 will tend to react with O_2 in the flue gas at temperatures up to ~1400°F.

(5) Calcium and magnesium sulfates can be reduced by CO at temperatures greater than 800°F.

(6) The iron oxides and calcium silicates present in the ash do not appear significant from a desulfurization point of view.

(7) Na_2CO_3 and alumina (constituents of ash) can react with SO_2 throughout the range of boiler temperatures.

(8) Hydration of lime by steam in the flue gas will not occur.

2. Stone Property Data

a. R. D. Harvey Report(26)

Dr. Harvey of the Illinois State Geological Survey has investigated the physical properties of a cross-section of limestone-bearing materials under an OAP funded contract. The basic petrography of the materials studied is given in Table 16 and the mineralogy is contained in Table 17. Included in the Harvey Report are the chemical composition of the limestone samples and the trace elements contained therein, which are presented in Tables 18 and 19, respecitvely.

Further petrographic analyses are presented in the report to relate the grains, grain size and shape distributions, and pore structure of the samples. The procedures employed involved the use of a scanning electron microscope and a Quantimet (QTM), an image-analyzing computer with a polarizing microscope. Sample resolutions were obtained with this equipment at magnifications of up to 20,000 times, and the results of this investigation are given in Tables 20 and 21.

Similar studies were then performed on samples of the stones which had been calcined by the Process Research Section of OAP. The mineralogical studies do not show significant or consistent differences between the calcine samples for different size fraccions as can be observed from Table 22. In an attempt to correlate the results obtained from Dr. Harvey's study to the SO_2 sorption characteristics measured by OAP, the following conclusions were

TABLE 16

PETROGRAPHIC DESCRIPTION AND SOURCE OF SAMPLES

Sample Type No.	Rock or Mineral Classif.	Distinguishing Characteristics	Color	Relative Grain Size	Grain Shape	Degree of Grain Interlocking	Other Textural Features	Source of Samples
1	Calcite	Iceland spar	Clear	Very coarse	Cleavage rhombs	None	Nearly perfect crystals	Ecjungo, Durango, Mexico
2	Calcite	Abundant crystal defects	Milky	Very coarse	Cleavage rhombs	None	Abundant intracrystalline voids, solid inclusions, and twin lamellae; subgrains present in some specimens	Hillside mine dump, Rosiclare, Illinois
3	Limestone	Coarse-grained, high purity	Gray	Coarse	Anhedral	High	Inequigranular; crinoid and bryozoan fossil fragments; intragranular voids abundant	Columbia Quarry Co. mine, Valmeyer, Illinois
4	Limestone	Fine-grained, high purity	Gray	Fine	Anhedral	High	Equigranular and dense; a few veinlets occur with medium-sized grains of clear calcite	Allied Stone Co. Quarry, Milan, Illinois
5	Dolomite	Reef type, high purity	Gray	Medium	Anhedral	High	Recrystallized granular and microporous; abundant intragranular voids	Midway Stone Quarry, Osborne, Illinois
6	Dolomite	Nonreef type, clayey and silty	Buff	Fine	Anhedral & rhombic	Low	Equigranular and microporous; grains adjacent to pores are rhombic. Clay occurs along bedding planes, iron oxide along dolomite grain boundaries	Abandoned quarry near Bourbonnais, Illinois
7	Magnesite	Fine-grained, high purity	Milky	Fine	Anhedral & rhombic	Low	Equigranular and microporous	Red Mountain Dist., Santa Clara Co., California
8	Aragonite	Oolitic and strontium-bearing	Light buff to milky	Fine	Fibrous & bladed	High	Elliptical and cylindrical remains of marine organisms abundant; very smooth exterior surfaces; most microporous	North Cat Cay, Bahama Islands
9	Dolomite	Limonite- and calcite-bearing	Brown & gray	Fine	Anhedral & rhombic	Low	Equigranular and microporous; rhombic grains along pores; fibrous limonite (?) occurs along dolomite grain boundaries; abundant intragranular voids	Jeffrey Limestone Co. Quarry, Parma, Michigan
10	Dolomite	Strontianite- & calcite-bearing	Buff-gray	Medium	Anhedral	Low	Inequigranular; fibrous strontianite crystallites along pores	Abandoned quarry near Ida, Michigan

TABLE 17

MINERALOGY OF TYPE SAMPLES IN WEIGHT PERCENTAGE

Sample	Major Component (%)	Minor and Trace Components	Insoluble Residue (%)
Type 1	100 calcite	None detected	0.0
Type 2	100 calcite	Traces of soluble salts of Cl and SO_3	0.1
Type 3	91 calcite	8% dolomite and <1% limonite	0.2
Type 4	98 calcite	< 2% quartz	0.9
Type 5	99 dolomite	<1% calcite; approximately 0.3 mol % $FeCO_3$ is present in the dolomite	0.1
Type 6	81 dolomite	9% quartz; 4% calcite; 5% clay; approximately 0.8 mol % $FeCO_3$ is present in the dolomite	14.4
Type 7	99 magnesite	< 0.5% quartz and clay; approximately 0.26 mol % $FeCO_3$ and 4.51 mol % $CaCO_3$ are present in the magnesite	0.1
Type 8	96+ aragonite	Approximately 3% Mg-calcite and <1% clay; approximately 1.38 mol % $SrCO_3$ is present in the aragonite	0.4
Type 9	70 dolomite	18% calcite; 5% quartz, 2% clay; 5% limonite	4.08

TABLE 18

CHEMICAL ANALYSES IN WEIGHT PERCENTAGE

(Analyses by Analytical Chemistry Section of the Illinois State Geological Survey)

Oxides	Sample Type Number									
	1	2 (69-104)	3 (69-103)	4 (69-101)	5 (69-102)	6	7	8	9 (BCR-1701)	10 (IDA)
SiO_2	ND[a]	ND	ND	1.53	0.03	11.8	0.47	0.19	5.88	1.95
TiO_2	ND	ND	ND	ND	ND	0.02	ND	ND	0.15	-
Al_2O_3	ND	0.01	ND	0.01	0.02	1.77	0.08	0.27	0.69	0.23
Fe_2O_3	ND	0.19[c]	0.20[c]	0.31[c]	0.34[c]	0.13	ND	ND	2.82	0.09[c]
Fe	0.13	-	-	-	-	0.41	0.07	0.01	1.75	-
MnO	ND	0.06	0.10	0.09	0.02	0.02	ND	ND	0.21	-
MgO	ND	ND	1.86	0.00	21.40	17.4	44.2	ND	15.33	5.06
CaO	55.3	55.5	53.4	54.8	30.30	26.5	2.93	55.2	30.82	26.31
Na_2O	0.003	0.015	0.015	0.047	0.008	0.040	0.026	0.53	0.16	-
K_2O	0.02	0.02	0.02	0.04	0.03	0.90	0.03	0.03	0.22	trace
P_2O_5	trace[b]	-	-	-	-	0.02	trace	0.01	0.10	trace
CO_2	43.95	43.35	43.75	43.35	47.30	40.27	50.96	42.10	40.68	36.54
SO_3	0.01	0.17	0.20	0.15	0.13	0.03	0.01	0.37	0.42	0.14
SrO	0.014	0.002	0.009	0.019	0.019	0.04	0.01	0.10	0.04	27.23
Cl	ND	0.04	0.03	ND	0.09	trace	ND	0.24	ND	-
Ign.Loss	43.49	43.15	43.67	43.15	47.24	40.46[d]	51.56[e]	43.33	41.85	36.71

[a] ND - not detected: Limits of detection for SiO_2, 0.03; TiO_2 and MnO, 0.01; Al_2O_3, 0.05; Fe_2O_3, 0.01; MgO, 0.10; Cl, 0.02.

[b] Trace of P_2O_5, approximately 0.005%.

[c] Percentage of total iron expressed as Fe_2O_3.

[d] Includes 0.30% H_2O+.

[e] Includes 0.61% H_2O+.

TABLE 19

TRACE ELEMENT ANALYSES OF TYPE CARBONATE ROCKS DETERMINED BY NEUTRON ACTIVATION METHODS

(Analyses by Dr. R.R. Ruch of the Analytical Chemistry Section of the Illinois State Geological Survey)

Type	Element (ppm)							
	Cu	Br	La	Sc	Eu	As	Ga	Cr
1	15	<2	<0.3	0.03	<0.03	2	<1	<2
2	44	<2	3.3	0.35	5.2	<2	<7	<11
3	<7	<3	1.6	0.16	<0.07	2	<2	<5
4	<3	17	<1	0.10	<0.2	a	<6	<2
5	11	<1	1.2	0.23	<0.05	<0.8	<2	<4
6	<25	<5	9.6	1.4	<0.3	<4	<6	35
7	<8	<0.9	<0.2	0.06	<0.1	<0.7	<3	127
8	b	17	<1	0.05	b	a	b	<12
9	25	<1	3.4	1.0	<0.7	<2	<14	<31

---

a Not determined, excessive interference from Br
b Not determined, excessive interference from Na

TABLE 20

RESULTS OF QUANTIMET (QTM) STUDIES OF THE PORE STRUCTURE OF CARBONATE ROCK TYPES*

Type	QTM Pore Volume		QTM Pore Boundary Projection		Frequency of QTM Pore Chord Intercepts Within Micron Intervals					Mean QTM Surf.Area (mm^2/mm^3)
	Mean (%)	S.D.**	Mean Length (mm)	S.D.**	1-8	8-16	16-31	31-63	63	
1	0.19	0.17	0.198	0.12	97.98	1.52	0.51	0	0	30
2	10.43	2.18	9.547	1.59	98.64	1.13	0.21	0.03	0	1610
3	18.42	16.99	4.814	1.99	78.21	12.11	5.32	3.10	1.27	890
4	9.65	3.34	6.615	2.02	95.31	4.37	0.32	0	0	1110
5	24.46	9.22	9.726	2.22	85.03	10.95	3.23	0.53	0.26	1950
6	43.98	6.88	8.005	3.84	57.19	21.64	15.88	4.97	0.32	2160
7	35.66	4.22	18.040	3.73	90.35	8.71	0.93	0.01	0	4220
8	4.69	4.79	2.975	2.68	91.06	6.69	1.95	0.30	0	480
9	24.81	6.06	5.410	1.41	64.62	20.55	11.96	2.74	0.13	1090

---

* Magnification of X1300

** Standard deviation

TABLE 21

GRAIN-SIZE DISTRIBUTION

Size Interval (μ)	Frequency of Grains (%)						
	Type 3	Type 4	Type 5	Type 6	Type 7	Type 8	Type 9
250-4000	0.1	0	0.1	0	0	0	0
125-250	1.7	0	0.5	0	0	0	0.1
63-125	2.4	0.1	1.1	2.1	0	0.1	0.3
32-63	2.3	0	10.4	2.7	0	0.1	1.9
16-32	4.9	0.1	33.8	34.3	0.1	0.5	24.2
8-16	4.8	4.2	33.1	30.8	4.9	1.0	33.7
4-8	12.6	32.8	16.4	27.4	33.2	1.6	25.8
1-4	71.2	62.7	4.7	2.7	61.8	96.7	14.0
Arithmetic mean* (μ)	44	4	81	17	4	3	13
Arithmetic standard deviation* (μ)	136	8	99	15	2	4	23

---

* Statistical methods of Krumbein and Pettijohn (1938, p. 240 for mean and p. 248 for standard deviation).

TABLE 22

DESCRIPTION OF THE CALCINES

Sample Type	Temp. (^{o}F)	Minerals Present	Particle Size* (μ)	Texture	Relative Porosity
1	1700	Lime	0.1 to 0.5**	Granular	Very low
	1800	Lime	1 to 2	Rounded	Moderate
2	1700	Lime and minor calcite	2 to 4	Partly spongy	Low to moderate
	1800	Lime	2 to 5	Spongy	Low
	1900	Lime	2 to 10	Blocky	Low
3	1800	Lime, minor periclase	1 to 2	Spongy, partly rounded	Moderate to high
4	1800	Lime	0.5 to 1	Granular, partly spongy	Low to moderate
5	1800	Lime and periclase	0.2 to 1	Granular-agglomeratic	Moderate
6	1800	Lime, periclase, and quartz	0.2 to 1	Granular-agglomeratic	High
7	1800	Periclase	0.1 to 0.5	Granular	Very low
8	1800	Lime	2 to 10	Spongy, partly blocky	Low to moderate
9	1800	Lime and periclase	0.5 to 2	Granular-agglomeratic	Moderate

---

* Determined from scanning electron micrographs.

** These particles are subgrains of 1 mm grains that are anisotropic and laminated. All other samples are isotropic limes.

drawn:

(1) No correlation is apparent between the SO_2 sorption and the mineralogy of the sample.

(2) Only one significant correlation could be obtained between the chemical composition of the samples and the measured sorption capacity.

(3) Little or no correlation is apparent between the surface areas determined by QTM data and sorption capacity, but a significant correlation was obtained when pore volume data were compared.

A tabulation of SO_2 sorption capacity for various stone types and attempted correlations thereof is presented in Table 23. The logarithm of Na_2O concentration is seen to have a high correlation coefficient (0.84). In this correlation method, the sodium is considered only as an index, not as an element which reacts with SO_2. Dr. Harvey hypothesizes, however, that Na_2O may be promoting a catalytic or fluxing effect to account for the higher reactivity of the calcine.

TABLE 23

SO_2 SORPTION CAPACITY OF TYPE SAMPLES* AND STATISTICAL LINEAR CORRELATION COEFFICIENTS BETWEEN SO_2 SORPTION AND VARIOUS CHEMICAL ELEMENTS AND PETROGRAPHIC PROPERTIES

Sample Type	SO_2 Sorption Capacity** (in gr[illegible])	Chemical Element Or Property	Linear Correlation Coefficient with SO_2 Sorption Capacity***
1	5.[illegible]	SiO_2, Al_2O_3	0.37
2	11.65	MnO	0.30
3	10.73	Fe_2O_3 (total Fe)	0.35
4	6.97	Na_2O (log)	0.84[a]
5	9.03	Cu	0.18
		Br	0.32
6	13.68	La	0.45
		Sc	0.46
7	1.78	As	0.19
		Ga	0.25
8	18.30	Cr	-0.44
		Mean pore volume determined by QTM	0.74[b]
9	14.91	Frequency of 8-16 μ pore chord lengths (QTM)	0.77[b]
10	10.2	Mean grain size (log)	0.51[a]

---

* Test data of R. Borgwardt, Process Research Section, OAP, Cincinnati, Ohio.

** Reaction temperature was 1800°F for all samples except type 1, which was 1700°F.

*** For a confidence level of 95% the critical correlation coefficient is 0.532 for the number of the samples considered in this analysis (D.C. Drehmel, Division of Process Control Engineering, OAP - personal communication).

[a] Excludes data on type 7.

[b] Excludes data on types 7 and 8.

b. G. H. McClellan Report[27]

In this report, Dr. McClellan of TVA examines the differences in limestone physical properties resulting from differences in calcination temperature, and the effect of these properties upon the reactivity of calcines with sulfur dioxide. The procedures used in determining properties include X-ray diffraction analysis, petrographic analysis by means of scanning electron microscopy, and porosity analysis via mercury intrusion techniques.

A comparison of the data obtained by mercury intrusion and electron microscopy for stone surface area is presented in Table 24. The relatively good agreement between the two methods over the range of calcination temperatures studied supports the accuracy of the pore size distribution measurements which were made by the mercury intrusion technique. The data of Table 25 show the effective contribution of pore surface area to the total stone surface area for limestone and Iceland spar calcines. It can be seen that the largest contributor to the stone surface area is the pores of 0.05 to 2.0 micron diameter size range.

The reaction of calcines with SO_2 was then investigated at 1382°F, 1922°F, and 2192°F under two different experimental conditions--calcination for 16 hours and subsequent sulfation, and simultaneous calcination and sulfation. The crystallite size of calcium sulfate grew larger with increasing temperature, and crystallite sizes for the limestone calcines were consistently larger than those for the Iceland spar, as shown in Table 26. Furthermore, the samples calcined and sulfated simultaneously at 1382°F for 15 minutes, were found to have undergone virtually no calcination. However, at the other temperature levels studied, the limestone did undergo sulfation to a larger degree than the Iceland spar.

TABLE 24

CORRELATION OF POROSIMETER AND SCANNING ELECTRON MICROSCOPE MEASUREMENTS

	Porosimeter		Scanning Electron Microscope		
Calcination Temp., °F	Surface Area, m^2/gm	Pore Size, μm[a]	Surface Area, m^2/gm	Pore Size, μm	No. of Pores[b]
Limestone 89					
1382	36.0	0.05	27.4	0.06	482
1562	20.3	0.09	14.6	0.12	514
1742	4.7	0.37	4.2	0.42	471
1832	6.8	0.26	6.7	0.26	502
2012	1.2	1.44	1.4	1.27	188
Iceland Spar					
1382	62.9	0.03	66.5	0.03	477
1562	32.2	0.05	46.4	0.04	470
1742	-	-	46.0	0.04	348
1832	7.0	0.25	10.8	0.16	368
2012	1.1	1.58	0.9	1.92	75

---

[a] Calculated from the relation $A = 6/D \cdot \rho$, where A = surface area, m^2/gm; D = mean diameter, μm, of pores assumed to be spherical; ρ = absolute density, gm/cm^3.

[b] Number of pores measured for calculation of pore size.

TABLE 25

SURFACE AREAS OF CALCINES CALCULATED FROM POROSIMETER MEASUREMENTS

Pore Size, Microns	Surface Area[a]		Surface Area[a]		Surface Area[a]	
	m^2/gm	% of Total	m^2/gm	% of Total	m^2/gm	% of Total
			Limestone 89			
	1382°F Calcine		1562°F Calcine		1742°F Calcine	
17.5	0.12	0.3	0.08	0.04	0.07	1.5
5.0	0.17	0.5	0.12	0.6	0.11	2.4
1.75	0.22	0.6	0.16	0.8	0.19	4.0
1.0	0.36	1.0	0.26	1.3	0.28	5.9
0.5	0.54	1.5	0.43	2.1	1.15	24.5
0.4	0.71	2.0	0.84	4.1	1.87	39.8
0.2	3.72	10.3	8.62	42.4	3.76	80.0
0.1	26.26	72.9	20.17	99.3	4.70	100.0
0.05	35.68	99.0	20.31	100.0	4.70	100.0
0.035	36.03	100.0	20.31	100.0	4.70	100.0
	1832°F Calcine		2012°F Calcine		2192°F Calcine	
17.5	0.04	0.6	0.06	5.2	0.03	5.9
5.0	0.08	1.1	0.09	7.3	0.05	9.7
1.75	0.15	2.2	0.17	13.7	0.09	16.1
1.0	0.32	4.7	0.37	29.2	0.31	57.6
0.5	0.67	9.9	0.82	65.4	0.50	92.3
0.4	0.96	14.1	0.92	73.2	0.54	100.0
0.2	4.88	71.8	1.06	84.5	0.54	100.0
0.1	6.79	100.0	1.12	89.6	0.54	100.0
0.05	6.79	100.0	1.25	100.0	0.54	100.0
0.035	6.79	100.0	1.25	100.0	0.54	100.0
			Iceland Spar			
	1382°F Calcine		1562°F Calcine		1832°F Calcine	
17.5	0.01	0.0	0.01	0.0	0.01	0.1
5.0	0.03	0.0	0.01	0.0	0.01	0.1
1.75	0.09	0.1	0.04	0.1	0.02	0.3
1.0	0.19	0.3	0.06	0.2	0.05	0.7
0.5	0.25	0.4	0.06	0.2	0.05	0.7
0.4	0.28	0.4	0.06	0.2	0.05	0.7
0.2	0.38	0.6	0.06	0.2	0.08	1.2
0.1	0.38	0.6	4.26	13.2	1.02	14.5
0.05	47.38	75.3	29.86	92.7	5.95	84.3
0.035	62.93	100.0	32.20	100.0	7.06	100.0

---

[a] Area contributed by pores of indicated and all larger sizes

TABLE 25 (Cont'd)

SURFACE AREAS OF CALCINES CALCULATED FROM POROSIMETER MEASUREMENTS

Pore Size, Microns	Surface Area[a]		Surface Area[a]		Surface Area[a]	
	m^2/gm	% of Total	m^2/gm	% of Total	m^2/gm	% of Total
			Iceland Spar			
	2012°F Calcine		2192°F Calcine		2372°F Calcine	
17.5	0.00	0.0	0.00	0.1	0.00	2.0
5.0	0.01	0.7	0.01	0.4	0.01	5.0
1.75	0.01	0.7	0.01	0.6	0.02	11.6
1.0	0.03	2.5	0.02	1.0	0.03	15.6
0.5	0.04	3.4	0.02	1.0	0.06	29.1
0.4	0.05	5.0	0.04	1.9	0.10	50.8
0.2	0.08	7.6	1.14	56.6	0.20	100.0
0.1	0.40	37.9	1.89	93.8	0.20	100.0
0.05	0.69	65.2	2.02	100.0	0.20	100.0
0.035	1.06	100.0	2.02	100.0	0.20	100.0

---

[a] Area contributed by pores of indicated and all larger sizes.

TABLE 26

PROPERTIES OF SULFATION PRODUCTS

Sulfation Conditions Temp. °F	Sulfation Conditions Time, Min.	Crystallite Size of $CaSO_4$, Å	Ratio of Areas of $CaCO_3$	Ratio of Areas of CaO	Ratio of Areas of $CaSO_4$
Sulfation of Limestone Calcines					
1382	15	1725	0	1.00	2.20
1922	5	2950	0	1.00	0.35
1922	15	2325	0	1.00	0.42
1922	30	2450	0	1.00	0.68
2192	15	3075	0	1.00	0.13
Sulfation of Iceland Spar Calcines					
1382	15	1350	0	1.00	0.48
1922	5	1600	0	1.00	0.05
1922	15	2050	0	1.00	0.03
1922	30	1950	0	1.00	0.35
2192	15	2275	0	1.00	0.07
Simultaneous Calcination and Sulfation of Limestone					
1382	15	2400	1.00	0.02	0.07
1922	15	2550	1.00	0.03	0.65
2192	15	3150	0	1.00	1.73
Simultaneous Calcination and Sulfation of Iceland Spar					
1382	15	0	1.00	0	0
1922	15	2825	1.00	0.24	0.19
2192	15	1950	0	1.00	0.33

Further examination of the sulfated samples was then performed to determine the growth pattern and distribution of the sulfate grains in the hope of ascertaining the mechanism of the sulfation reaction with calcines. The following conclusions were drawn by Dr. McClellan from this study:

(1) Sulfation of lime occurs in two stages--reaction of the sulfur dioxide and oxygen with the exposed surface of lime, followed by diffusion of the gaseous reactants through the resultant shell of calcium sulfate to the core of unreacted lime. Pores in the calcine smaller than about 0.1 micron do not admit sulfur dioxide rapidly enough to have significant effect on the sulfation reaction at short retention times.

(2) Calcines react best with sulfur dioxide at temperatures below 1922°F, but simultaneous calcination and sulfation, which is required when powdered limestone is injected into power plant furnaces, occurs best at temperatures of 1922°F and above.

It can be inferred from these results that solid-gas reactivity is correlated with pore distribution and surface area. The pores provide the reactant gas with access to the surface area. If diffusion of the gas in small pores is slow, then each stone has some optimum time and temperature of calcination for development of a favorable pore size distribution and surface area that results in a reactive lime. Furthermore, the physical and chemical properties of a calcine are influenced markedly by the crystallite size of the parent limestone. The high thermal stability of Iceland spar reflects its relatively large crystallite size, and its calcines react slowly with sulfur dioxide. In addition to the decomposition of the calcium carbonate, calcination effects a recrystallization of the resultant calcium oxide which is accelerated by rising temperature and which decreases the reactivity of the calcine with sulfur dioxide.

G. Process Effects on Equipment Performance

1. Electrostatic Precipitator Efficiency Studies

a. Summary

The results of the tests performed on TVA Shawnee Steam Plant Unit 10 Precipitator A and Research Cottrell studies, as reported in References 28, 29 and 30 respectively, are summarized in the attached graphs, Figures 48-50. Conclusions which can be drawn from the reported data are as follows:

(1) In 1969 TVA performance tests without additives indicate that the electrostatic precipitator (ESP) was operating at a high efficiency level, along the predicted upper limit curve, about 3 to 5% above the ESP guarantee efficiency value.

(2) The 1970 TVA performance tests without additives indicate that the ESP performance had deteriorated compared to 1969 performance data. The test results are scattered, but in general, indicate a lower ESP collection efficiency. Several of the test points fall 3 to 5% below the minimum predicted ESP operating line or guarantee efficiency curve.

(3) The 1970 performance tests with additives give widely scattered results; however, the majority of test runs showed performance considerably better than had been predicted. The decrease in efficiency due to the introduction of additives was roughly half of the predicted decrease in a majority of the runs. Eighteen of the twenty two ESP tests were run at 94% to 106% of the rated gas flow capacity, and show a collection efficiency varying from 68% to 88%. Four of the tests were run at 76% to 82% of rated capacity, and these runs show a collection efficiency of 87% to 91%.

(4) The tests were run at limestone additive rates varying from 2,600 lb/hr to 20,000 lb/hr. There is no detectable trend in ESP collection efficiency attributable to variations in the additive rate.

(5) EPA has contracted Cottrell Environmental Systems (a Division of Research Cottrell) to conduct additional, more detailed, testing and evaluation of the effects of additives on ESP performance. The study will include evaluation of possible operating modes and other potential solutions to minimize or eliminate the observed effects. In addition, the effects of additives on mechanical collector performance also will be assessed.

b. Discussion of Test Results

(1) Figure 48 - Gas Volume Flow Versus Precipitator Collection Efficiency

Figure 48 includes predicted ESP performance ranges for operation with and without additives (Reference No. 30), and ESP collection efficiencies obtained during performance tests run in 1969 and 1970, both with and without additives (References No. 28 and 29). The pre-installation collection efficiency for this ESP was predicted by Research-Cottrell to be 90-94.6% at rated design capacity without addivites, decreasing to 70.3-74.7% with additives. The initial TVA performance tests carried out during July-August 1969 without additives indicated that the measured ESP collection efficiencies fell along the upper limit of the predicted performance range, which was 3 to 5% above the guarantee curve. Individual test runs deviated only slightly from the predicted performance curve over the entire operating range from 75% to 106% of rated flow capacity.

The performance tests run during June-July 1970 without additives showed a considerable deterioration in the ESP collection efficiency when compared to the

FIGURE 48

GAS VOLUME FLOW VS PRECIPITATOR COLLECTION EFFICIENCY

TVA SHAWNEE STEAM PLANT UNIT 10, PRECIPITATOR A

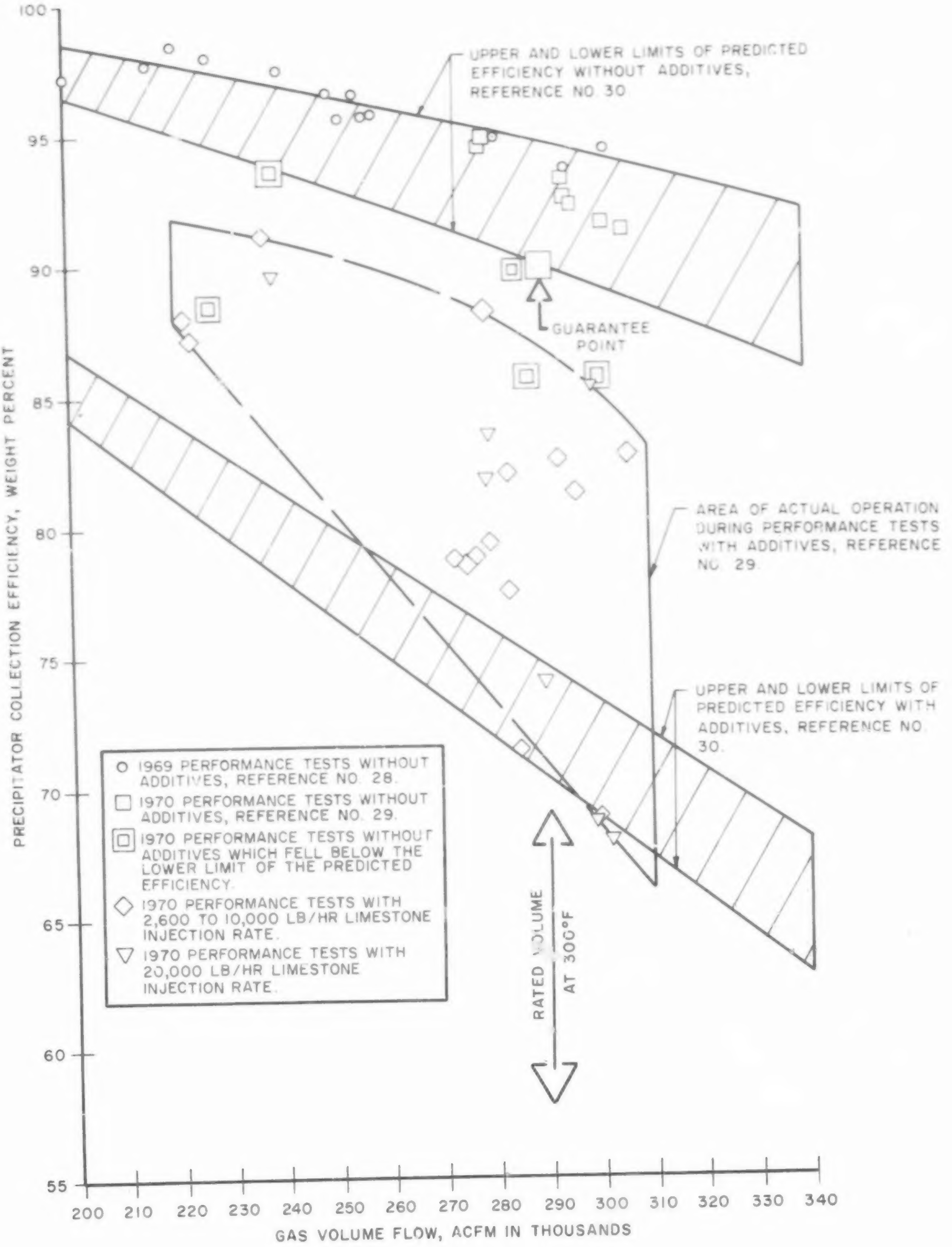

1969 test results. The 1970 test results exhibit considerable scatter, and the collection efficiencies fell below the upper limit of the predicted efficiency range. Several test points fell considerably below the minimum predicted performance curve for no apparent reason. The 1970 tests run with additive amounts varying from 2,600 lb/hr to 20,000 lb/hr showed widely scattered results with no evident pattern attributable to variation in additive rate. Of the twenty two acceptable tests run with additives, eighteen were run in the narrow range of 94-106% of rated flow capacity. These tests showed ESP collection efficiencies varying from 68-88%. The four remaining tests which were run at 76-82% of rated capacity showed collection efficiencies varying from 87-91%.

These test results indicate that the decrease in ESP collection efficiency caused by introducing additives is less when operating below the rated design capacity than it is when operating near the rated capacity. It is possible however, that a greater number of tests run in the lower capacity region would show a wider scatter pattern. The reported collection efficiencies pertain to the ESP only. The TVA Shawnee Unit No. 10 installation consists of a mechanical separator followed by the ESP, consequently overall solids collection efficiencies are higher. No data are available to permit calculation of the mechanical collector efficiency or the overall solids removal efficiency for different loadings.

(2) Figure 49 - Electrostatic Precipitator Collection Efficiency Versus Percent of Rated Capacity

Figure 49 represents a simplification of Figure 48 which is intended to show the extent of the ESP operating region with additives, in relation to the guaranteed performance curve without additives, as a function of rated flow capacity. The curve showing predicted mechanical separator efficiency was derived from Reference No. 30, and corresponds to the specific mechanical separator used in conjunction with Precipitator A on Shawnee Unit 10.

(3) Figure 50 - Ratio $\frac{A_2}{A_1}$ $\frac{\text{Precip. Area with additives}}{\text{Precip. Area without additives}}$ Versus Percent of Rated Capacity

The required collecting electrode surface area (A_2) calculated for use with additives is based on maintaining the same outlet gas solids concentration as would be obtained by the base case electrode area without additives. The required area was calculated from the equation:

$$\eta = 1-\frac{Co}{Ci} = 1- e^{-\frac{A}{V}W}$$

where:

η = collection efficiency - fractional
Co = outlet concentration
Ci = inlet concentration
A = collecting electrode surface area
V = volumetric flow rate
W = effective migration velocity

W was obtained from the test results.

FIGURE 49

ELECTROSTATIC PRECIPITATOR COLLECTION EFFICIENCY
VS
PERCENT OF RATED CAPACITY

TVA SHAWNEE STEAM PLANT UNIT 10, PRECIPITATOR A

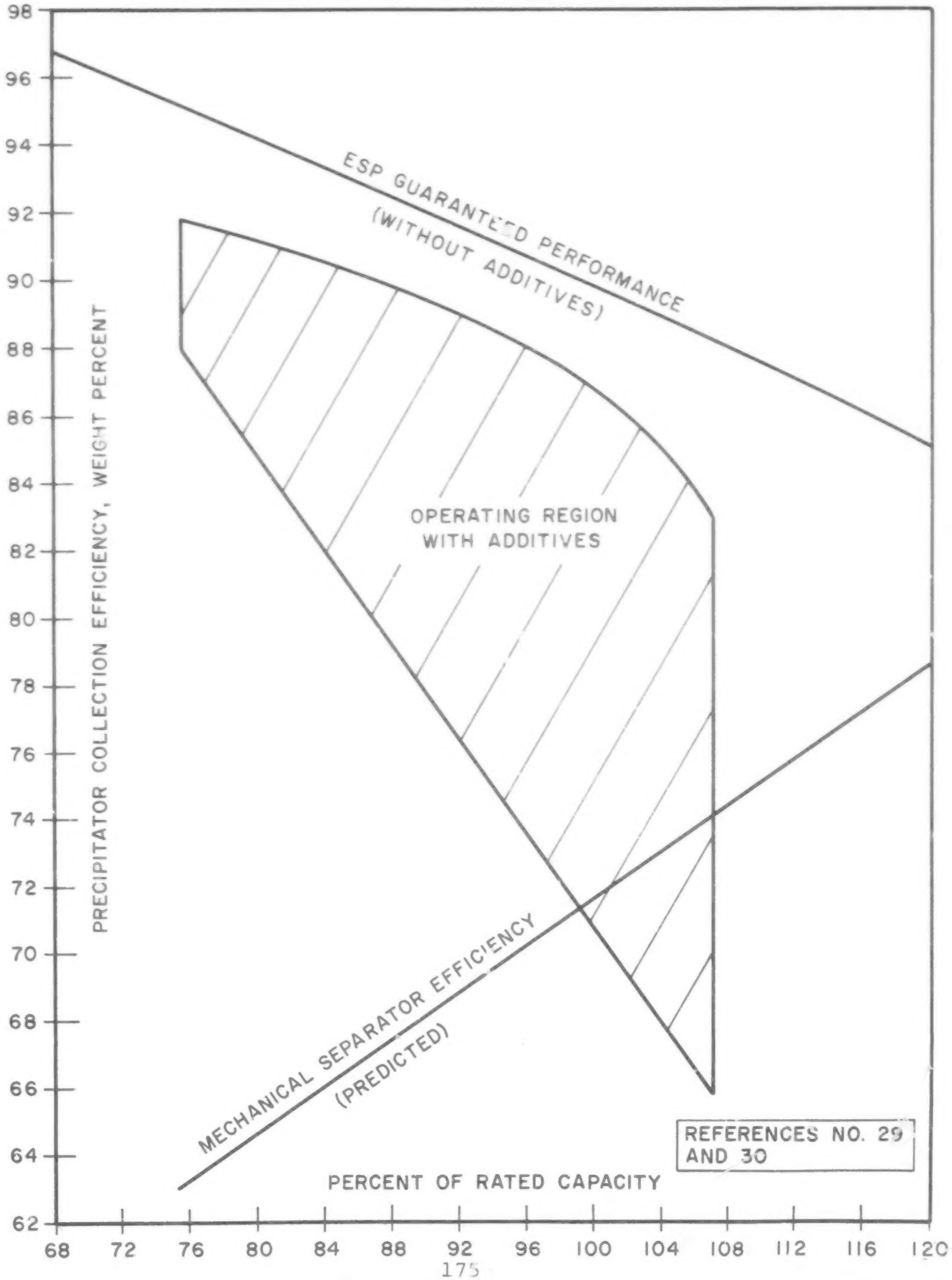

FIGURE 50
RATIO OF ESP AREA WITH ADDITIVES TO ESP AREA WITHOUT ADDITIVES VS PERCENT RATED CAPACITY

TVA SHAWNEE STEAM PLANT UNIT 10, PRECIPITATOR A

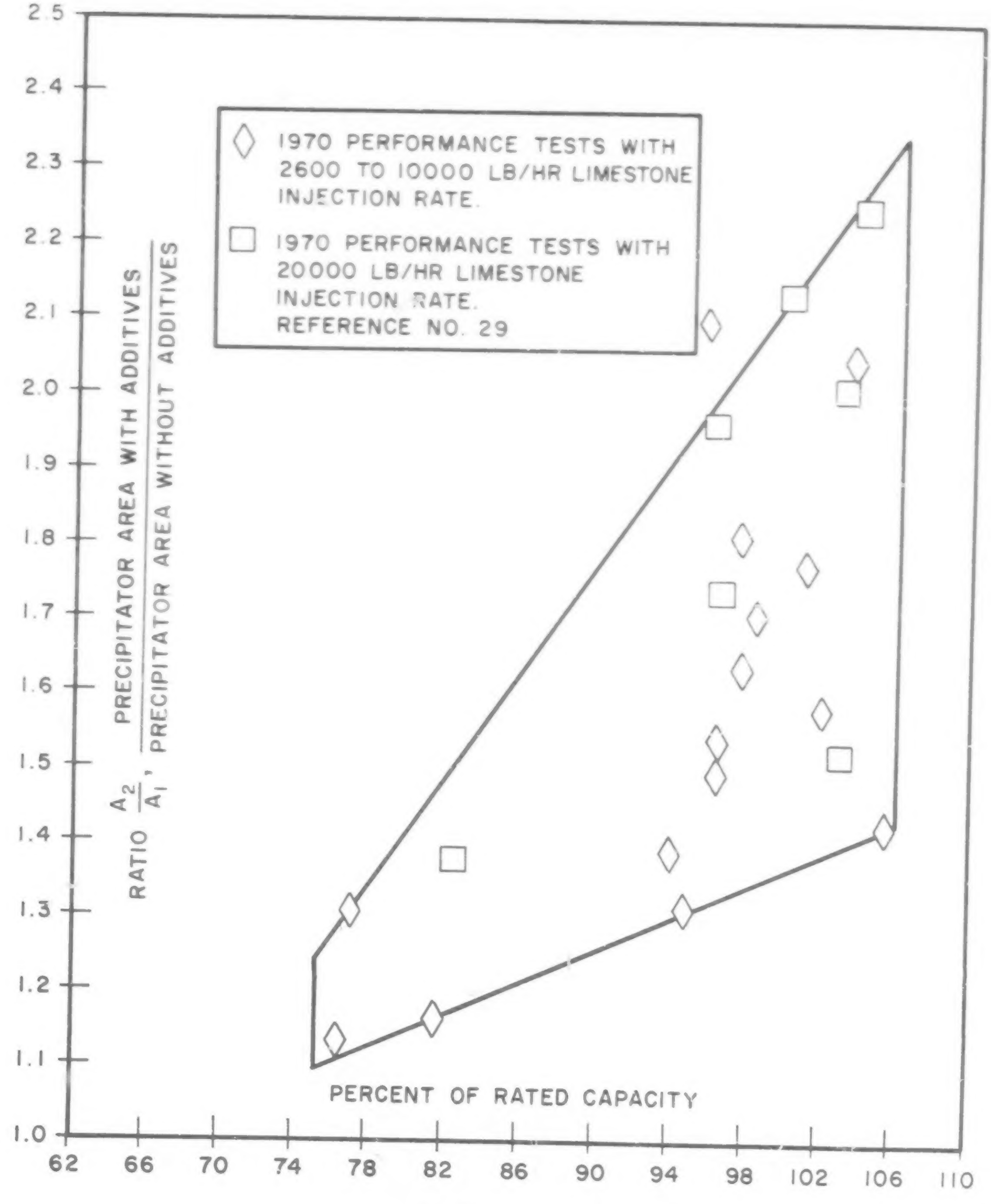

Inlet dust loadings studied ranged from 1.260 to 2.173 grains/standard cubic foot (gr/SCF) for the tests using limestone injection while the range for tests without injection was 1.119 to 1.737 gr/SCF. Concentrations in the effluent gas from the ESP ranged from 0.162 to 0.674 gr/SCF with additives and from 0.0728 to 0.214 gr/SCF without additives.Results are plotted for the 22 test runs with additives calculated on the same basis as the results obtained from the 12 tests run without additives. Individual test points are widely scattered showing the same general configuration as Figure 48. In the operating region of 76-82% of rated capacity, the area ratio (A_2/A_1) is about 1.1 to 1.4, while in the region of 94-106% of rated capacity, the area ratio varies from 1.3 to 2.25. If this difference in collection efficiency is valid for the general case, it may be more economical to design the ESP for a higher rated gas volume capacity and operate at 75% of rated capacity, than to design for and operate at the normal rated capacity.

The results of these tests are applicable only to comparable modern ESP units designed specifically for a high solids collection effeciency, which are maintained and operated with a high degree of efficiency. In comparison, the data reported in Reference No. 30 for the Detroit Edison St. Clair station ESP tests show a collection efficiency with additives of only 55%. This requires an area ratio of 3.15 to maintain the same outlet dust loading as the base case where the ESP test efficiency was 80%. This type of performance is more indicative of existing ESP units which were not originally designed for high collection efficiency.

(4) Effect of Additives on Dust Resistivity

The effect of additives on dust resistivity and consequently on ESP collection efficiency is discussed in Reference No. 30. It was pointed out that all limestone or dolomite additives would result in high dust resistivity values, above the critical range of 10^{10} to 10^{11} ohm-cm. The increased resistivity results in a lower particle migration velocity and a lower electrode collection efficiency. The resistivity values reported in Reference No. 29 show a relatively smaller increase in resistivity from the use of additives than is predicted in Reference No. 30. One composite limestone-fly ash sample indicated a decrease in resistivity for an additive injection rate of 20,000 lb/hr as compared to zero additive. Assuming that the other reported resistivity values are truly representative of limestone-fly ash mixtures, the decrease in ESP collection efficiency would be less than predicted from the use of limestone additive. Figure 48 shows that this was the case for the TVA tests. This reduced sensitivity of the dust particle resistivity is probably due to a conditioning effect caused by the presence of SO_3 or some other chemical in the flue gas.

2. Coal Ash Deposition Studies

a. Summary

The effect of additives on ash deposition on boiler surfaces has been reviewed following the guidelines presented in the B & W Report(2). This review was carried out with the aim of establishing generalized correlations relating the B & W data to both types of ash deposition at various additive to ash ratios. The two types of ash deposition under consideration are: (1) fused-slag deposits which form mainly on the furnace radiant section surfaces; and (2) bonded deposits which form on the convection section heating surfaces. These two types of ash deposits are treated separately since the tendency for such deposits to form is related to different physical characteristics of the coal ash. Fused-slag deposits are related to ash fusion temperature and ash viscosity which are in turn greatly influenced by the ambient atmosphere in the area of the deposit. The atmosphere can be either oxidizing or reducing depending on furnace operating characteristics. Bonded deposits are related to the fly ash sintering strength which is dependent on the ash composition and would therefore be directly influenced by additives.

A review of the published literature relating to ash deposition on boiler surfaces has turned up only one paper (Reference No. 31) which attempts to correlate quantitatively the physical and chemical properties of a coal ash (without additives) with the tendency to form fused-slag deposits and bonded deposits. It developed that the correlations contained in Reference 31 had very limited applicability to the data contained in Reference 2. Consequently, the slagging problem was referred back to B & W to obtain further clarification of their published correlations, and any other information relating to the possibility of correlating the data on slag viscosity contained in Reference 2 with slagging tendency. Results achieved in this effort have been negative, and it must be concluded that the type of generalized correlations which were originally planned are beyond the present state of the art.

It should be noted that Energopomiar (Power Metrology Research Organization, Poland) are investigating the effect of limestone additives on ash deposition on boiler surfaces and,based on results reported in reference 36, concluded that no correlation could be developed relating fouling tendencies to mixture properties. The Energopomiar work comprised the following determinations (taken from reference 36):

1. The effect of the quantity of additive on the laboratory ash fusion.
2. The effect of the quantity of additive on the fly ash fusion.
3. The effect of the quantity of additive on the laboratory ash viscosity in the pyroplastic state.
4. The effect of the quantity of additive on the fly ash viscosity in the pyroplastic state.

Although it was found that additives changed the ash fusion temperatures (raising it in a reducing atmosphere and lowering it in an oxidizing one) no correlations with fouling tendencies were developed. Similar results were obtained for ash viscosity, i.e., additives changed the viscosity, (in some cases increasing it, in others lowering it) but no correlations with fouling tendencies were found. This work is continuing to develop data for possible correlation with fouling tendencies, particularly with respect to coal composition.

Although no correlations have been developed to relate increased ash deposits with additives injected into the boiler, it should be noted that such increased deposits have been observed in the full-scale tests at TVA's unit No. 10, Shawnee Steam Plant, Paducah, Kentucky.[37] In these tests, heavy deposits have been observed in the reheat steam superheater section which comprises a bank of 2-inch diameter tubes spaced on 3-inch centers. Heavy deposits accumulated on these tubes after injection of only 592 tons of limestone resulting in a unit outage to rod out the material. Following the outage, a tube leak caused a forced outage (about four weeks after the first outage) which revealed heavy deposits had accumulated in the same section as before. About 322 tons of limestone had been injected during these four weeks. The deposit was very hard and although steam soot blowing frequency was increased by 25%, it may not be possible to control buildup by these techniques. Coal composition and process and operating variables will be studied during the test program for possible correlation and solution to the problem of deposition.

The present technology can be summed up by quoting a statement from the summary of the B & W Report: "In the study of ash deposition, the results indicate that general statements concerning the effects of additives on furnace wall slagging and tube bank fouling would be misleading". It would be possible for an experienced boiler designer to analyze, at least directionally if not quantitatively, the effects of additive injection on ash deposition utilizing the type of data contained in Reference 2. This analysis, when used in conjunction with other operating and design variables, such as method of firing, furnace and steam generator design, coal ash composition, soot blower effectiveness, deposit conditions and combustion conditions, would enable the designer to modify the furnace to obtain improved performance. The following discussion will review the general significance of the data presented in Reference 2 relating to ash fusion temperatures, slag viscosity characteristics, sintering strength and chemical composition of the ash.

b. Fused-Slag Deposits

Fused-slag deposits form on furnace walls and other areas which are predominantly exposed to radiant heat. This type of deposit is mainly due to molten ash particles carried in the flue gas, but can be caused by selective condensation of ash constituents vaporized during the combustion process. Such selective condensation causes enrichment of certain components on cooler surfaces making it relatively more difficult to predict slagging tendencies. Ash fusion temperatures can sometimes be used as a means of roughly approximating the slagging tendency of a coal ash. When the initial deformation temperature (ASTM-DI857-66T) is above the 2500-2600°F range, the slagging tendency should be very low. If the initial deformation temperature is below the 2000-2100°F range, slagging problems can be expected. Between these temperature limits, the slagging tendency is variable and depends largely on the boiler characteristics and operating conditions. Many coal ashes with similar chemical analyses and ash fusion temperatures have been found to exhibit widely divergent slagging tendencies.

The ash fusion temperature data contained in Reference 2 are presented as plots against the percentage additive for both oxidizing and reducing atmospheres. The following comments on the reported B & W data refer to general distinct trends exhibited by a majority, but not necessarily all of the samples tested. The inclusion of additives in the ash initially causes the ash deformation temperature to decrease to a minimum value corresponding roughly to an ash with an additive content of 20 to 40%. As the additive percentage is increased further, the ash deformation temperature increases fairly rapidly exceeding the 2600°F level at high additive percentages. The minimum initial deformation temperature occurs in the general range of 100-200% stoichiometric CaO/SO_2 ratio. Since this is the most likely operating range for the Dry Limestone Injection Process, most boiler operations will be carried out in the lower ash fusion temperature region, where slagging tendency is determined largely by boiler characteristics and operating conditions, and therefore is less amenable to prediction. The B & W data further show that additive amounts varying from 250-800% of stoichiometric were required to raise ash fusion temperatures above the 2500-2600°F range where slagging would not be expected to occur.

Slag viscosity has been found to be the most reliable criterion for predicting the slagging tendency of a coal ash (Reference 31). The slag viscosity data of Reference 2 are presented in the form of graphs of slag viscosity versus temperature for both oxidizing and reducing atmospheres. As a general statement, large overall plastic ranges (~500 poises to solid slag), and a relatively greater sensitivity of the ash to either oxidizing or reducing conditions, requires special furnace design. There are no available guidelines unfortunately, relating plastic range extent with the degree of slagging tendency. A comparison of the viscosity characteristics of ash samples containing additives, with coal ash samples without additives, shows that the introduction of additives results in a pronounced reduction in the extent of the plastic region for both oxidizing and reducing atmospheres. This indicates directionally, a potentially smaller zone wherein slagging would be expected to occur, and consequently a reduced need for special furnace design considerations.

A slagging index (R_S) can be used to predict slagging tendency in the absence of other data. This type of correlation was developed(31) for bituminous coals without additives, which normally have a Base/Acid ratio less than 1.0. The correlation is convenient to use since it requires only a knowledge of the chemical composition of the coal ash. However, it gives completely erroneous results when applied to a coal ash-limestone additive mixture which generally will have a Base/Acid ratio greater than 1.0.

c. Bonded Deposits

The tendency of an ash obtained from bituminous type coals to form hard bonded deposits on the convection tube banks of boilers has been related to the sintering strength of the ash by means of a standard test(32). A correlation applicable to bituminous coals without additives relating sintering strength, ash fouling index (R_F) and chemical composition has been empirically developed (Reference 31, Figure 5). The fouling index and sintering strength are then related to fouling category as follows:

Fouling Category	Fouling Index, R_F	Sintering Strength, psi
Low	<0.2	<1000
Medium	0.2-0.5	1000-5000
High	0.5-1.0	5000-17000
Severe	>1.0	>17000

Reference 2 presents sintering strength data* for six coal samples without additives and 13 coal samples with additives. The sintering strengths of 11 samples were very substantially reduced by the additives, and for 2 samples which had very low initial sintering strengths, were increased by the additives. The indication is strong that additives will have a tendency to lower ash sintering strength thereby reducing the tendency to form bonded deposits. However, due to the limited sampling and the unexplained exceptions, this conclusion may not be valid for every case.

---

*Based on pilot plant tests.

Fouling categories calculated using the ash chemical composition were in fair agreement with the categories obtained from sintering strength data for the six coal samples without additives. However, for the 13 samples with additives, there appears to be no correlation between the two methods. For 12 of the samples, the calculated fouling index is much higher, indicating an increased fouling tendency due to the introduction of additives. This is true even for those samples where the Base/Acid ratio with additives is substantially below 1.0. Since the calculated trends obtained from the fouling index are in contradiction to the results obtained from sintering strength test data, it is concluded that the correlation relating fouling index and chemical composition is not applicable to coal ash in the presence of limestone additives.

3. Water Quality Control Studies

In a typical coal-fired thermal power plant, water is used to sluice collected fly ash to a disposal area, and after the solids have settled from it, is discharged to a watercourse. Consequently, any water soluble compounds in the fly ash will be dissolved in the sluice water and discharged into the watercourse. Alternatively, if a dry solids handling system were used, the soluble compounds eventually would be leached out of the fly ash disposal pile by rain water. In either case a potential water pollution problem exists. Only the wet disposal system is considered here.

The quantity of water discharged from the ash sluice system of coal-fired power plants is a function of the type of fuel-feed system, the ash content of the coal, the type and efficiency of the ash-collection system, the type of pumping system, and the quantity of coal burned. The following data are typical of pulverized fuel type plants (these and other data shown in this report are taken from a paper presented by J.S. Morris, TVA(33)):

Ash Collector System	System Efficiency	Percent Ash In Coal	Average Flow Gals/Ton Coal
Mechanical	60-68	11-14	1600 ± ~25%
Electrostatic Precip.	90-98	11-14	1900 "
Mechanical-Electrostatic	96-98	11-14	2000 "

The above data represent typical power plant conditions and do not include the effects of adding on a process for controlling SO_2. Installing a system such as the limestone injection process, either wet or dry, will appreciably increase the quantities of water and of solid wastes discharged. In the dry process, the fly ash, reaction products, and unreacted lime are removed via the ash sluice system.

Additional water is required since the total quantity of solids to be removed is increased by limestone injection. Figure 51 shows the theoretical increase in ash pond flow and solid waste produced as a function of stoichiometric limestone injected into the boiler. Calculations have been made based on preliminary test data from TVA's Shawnee plant (1.7 stoichiometric = 0.16 lb limestone/lb coal) and the results indicate an 82% increase in the quantity of fly ash-limestone requiring disposal.

The sluice water from a power plant normally is discharged to a receiving stream after the solids have been removed by settling. The generally large receiving streams usually provide ample dilution to reduce the various water quality parameters to acceptable limits (beyond a short mixing zone) even though the ash pond discharge often exceeds the standards. Table 27 lists water quality analyses from typical steam plant ash pond discharges. (The present recommended limit for sulfate in drinking water is 250 ppm but recent proposals have included reduction to 150 ppm. The present limit on total dissolved solids is 500 ppm.) The concentration in sluice water of a few selected parameters is shown in Table 28 for normal plant operation and in Table 29 for operation with limestone injection. It should be noted that while these latter results are preliminary, they are based on actual tests at the Shawnee plant. One important point to note is that the Shawnee tests are based on a high calcium limestone containing very little magnesium. A high magnesium limestone (e.g., dolomite) would probably increase the dissolved solids since the magnesium compounds involved are more soluble than the calcium compounds.

FIGURE 51

THEORETICAL TOTAL ASH BURDEN AND SLUICE FLOW

LIMESTONE INJECTION

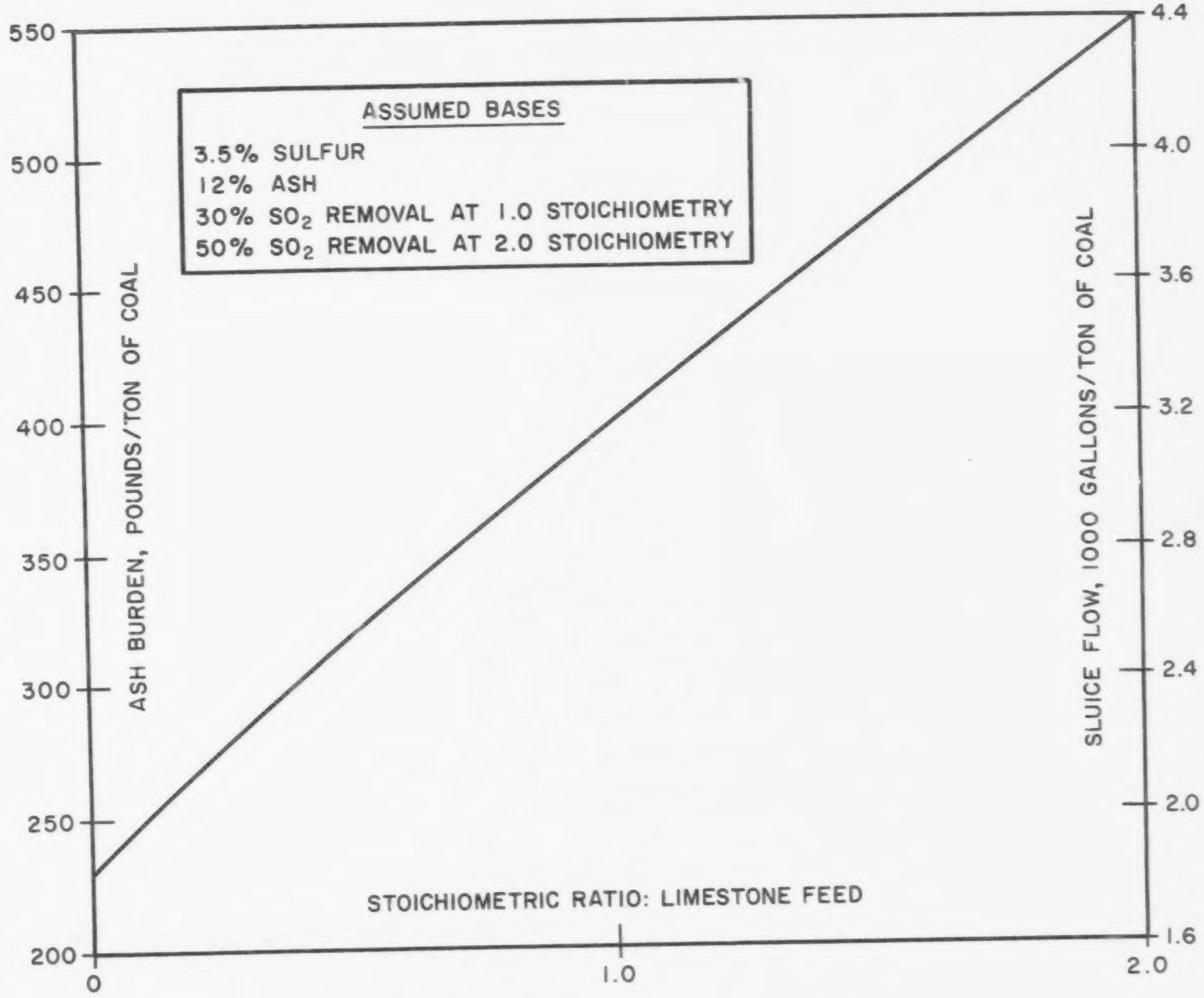

TABLE 27

RESULTS OF ANALYSIS OF ASH POND EFFLUENT FROM TYPICAL PLANTS

Constituents (mg/l except as noted)	Plant A	B	C	D	E
Average flow (mgd)	7.0	5.0	10.0	19.0	12.0
Dissolved oxygen	9.33	9.98	8.4	9.0	8.6
pH	11.8	12.0	9.6	11.0	9.0
Alkalinity (pheno)	259	186	14.0	-	5.0
Alkalinity (total)	279	204	40.0	163	74.0
Solids (total)	464	388	422	786	237
Hardness ($CaCO_3$)	296	276	183	338	128
Calcium	114	106	65.3	130	43.6
Magnesium	3.0	3.0	5.0	3.17	4.63
Iron (ferrous)	0.0	0.01	0.0	0.02	0.0
Iron (total)	0.21	0.10	1.12	0.50	0.55
Manganese (total)	0.08	0.03	0.17	0.03	0.02
Silica	6.9	13.7	4.94	51.9	1.91
Chloride	21.9	5.69	70.4	71.6	20.6
Sulfate	84.5	69.5	93.5	145	6.7
Specific conductance (umhos)	1260	1110	551	870	332

TABLE 28

SLUICE WATER QUALITY NORMAL PLANT OPERATION

Type of Sluice	Parameter	Mean Concen. (mg/l)	Range of Concen. (mg/l)
Mechanical	Ca	232	44-480
"	Mg	51	0-144
"	Hardness	790*	130-1700*
"	pH	120**	10.4-12.2**
"	Total Alkalinity	820	150-1700
"	SO_4	130	22-460
"	Total Dissolved Solids	2800	300-5600
Electrostatic	Ca	66	23-140
"	Mg	28	5-58
"	Hardness	282*	120-520*
"	pH	9.8**	7.5-11.5**
"	Total Alkalinity	125	44-270
"	SO_4	150	31-430
"	Total Dissolved Solids	450	150-900
Bottom	Ca	128	64-272
"	Mg	19	0-48
"	Hardness	400*	270-440*
"	pH	10.7**	7.3-11.6**
"	Total Alkalinity	180	92-340
"	SO_4	250	50-570
"	Total Dissolved Solids	700	380-1100
Pyrite	Ca	53	21-104
"	Mg	10	0-24
"	Hardness	176*	100-280*
"	pH	7.8**	7.5-8.1**
"	Total Alkalinity	55	50-62
"	SO_4	29	24-42
"	Total Dissolved Solids	132	120-150

---

* As $CaCO_3$

** Median Value; Units

TABLE 29

SLUICE WATER QUALITY
LIMESTONE INJECTION

Type of Sluice	Parameter	Mean Concen. (mg/l)	% of Mean Concen. of Normal Opera.
Mechanical	Ca	520	220
"	Mg	390	770
"	Hardness	2900*	370
"	pH	12.6**	Not applicable
"	Total Alkalinity	2900	350
"	SO_4	320	250
"	Total Dissolved Solids	16,000	570
Electrostatic	Ca	360	550
"	Mg	530	1900
"	Hardness	3100*	1100
"	pH	12.6*	Not applicable
"	Total Alkalinity	2400	1900
"	SO_4	620	410
"	Total Dissolved Solids	14,000	3100

---

* As $CaCO_3$
** Median Value; Units

The preliminary data from the Shawnee tests have been projected to an actual steam plant burning a large quantity of coal and having low receiving stream flows available for dilution. Figure 52 shows the effects on the receiving stream of limestone injection. The allowable loads are based on maximum concentrations in the stream of:

- dissolved solids - 500 mg/l
- SO_4 - 150 mg/l
- hardness - 50% rise in concentration above 100 mg/l
- ph - 8.5 units

The assumed available flow for dilution is one-half the average flow. These results, while of a preliminary nature, clearly show that further consideration must be given to the water quality aspects of the limestone injection process before the process can be considered ready for widespread commercial application. Indeed, water pollution ultimately may be the most severe problem facing the limestone injection process.

The above discussion and tables presented were extracted from the Morris paper and were based on preliminary Dry Limestone Process data from TVA's Shawnee plant. Additional process data have recently been made available in the TVA October-December 1970 Progress Report(34) on the Shawnee plant test results. Typical ash sluice water quality data from the mechanical and electrostatic collectors corresponding to the more recent information is presented in Table 30. The effect of the limestone injection tests on three water quality parameters is shown in Table 31. Comparison of these results with the earlier test data (Tables 28 and 29)

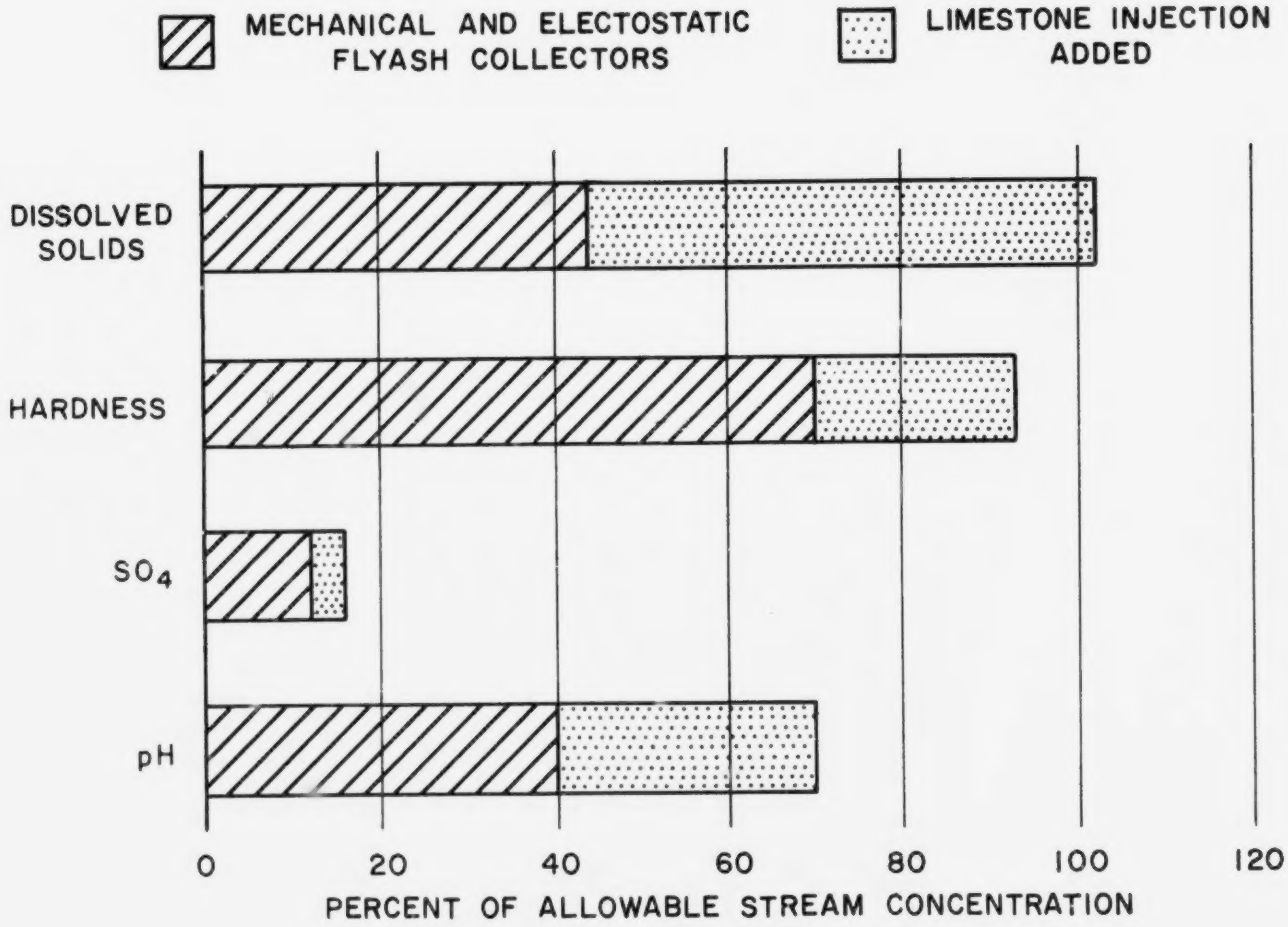

FIGURE 52

WATER QUALITY OF RECEIVING STREAM

AT

CRITICAL PLANT LOAD AND STREAMFLOWS

TABLE 30

SLUICE WATER QUALITY - NORMAL PLANT OPERATION

Type Sluice	Parameter	Concentration Mean	Concentration Med.	Standard
Mechanical	pH	11.5	11.6	6.0-9.0
Mechanical	Dis. Solids	2000	1550	500
Mechanical	Hardness	680	480	200
Electrostatic	pH	9.9	10.0	6.0-9.0
Electrostatic	Dis. Solids	610	525	500
Electrostatic	Hardness	300	265	200

TABLE 31

SLUICE WATER QUALITY - LIMESTONE INJECTION

Type Sluice	Parameter	Concentration Without Limestone	Concentration With Limestone	% Increase
Electrostatic	Calcium	200	1180	490
Electrostatic	pH	10.0	12.2	-
Electrostatic	Dis. Solids	300	11,500	3730
Mechanical	Calcium	430	1310	205
Mechanical	pH	11.5	12.4	-
Mechanical	Dis. Solids	680	12,100	1680

shows that a large increase in the total dissolved solids content is still being experienced. In fact, the reported values indicate that a high degree of dilution (~25 to 1) will be necessary to avoid excessive concentration in the receiving stream.

As cited previously, the overall solids disposal problem for the limestone injection process is a major one, and TVA studies in this area are continuing. Some aspects of the problem still under investigation are: the effect of heavy metal contaminants on effluent standards, the effect of limestone reaction products on ash pond settling characteristics, and overall effects on water recycle costs and problems. Firm design recommendations for the disposal system cannot be derived until the completion of the TVA Shawnee plant test program.

V. REFERENCES

(1) "Investigation of The Reactivity of Limestone and Dolomite for Capturing SO_2 from Flue Gas", Battelle Memorial Institute Final Report (November 20, 1970)

(2) "Additive Injection for Sulfur Dioxide Control - A Pilot Plant Study", The Babcock and Wilcox Company Final Report (March 27, 1970)

(3) "Pilot Plant Moving Grate Furnace Study of Limestone-Dolomite for Control of Sulfur Dioxide in Combustion Flue Gas", Peabody Coal Company Final Report (May 27, 1969)

(4) Borgwardt, R.H., "Isothermal Reactivity of Selected Calcined Limestones With SO_2", Paper presented at the Fourth Dry Limestone Process Symposium (June 22-26, 1970)

(5) Rootare, H.M., and Prenzlow, C.F. J. Phys. Chem., 71, 2733 (1967)

(6) TVA Fundamental Research Branch, Monthly Project Report, "Removal of Sulfur Dioxide from Stack Gases" (May 1968)

(7) Satterfield, C.N., and Sherwood, T.K., The Role of Diffusion in Catalysis, Addison-Wesley Publishing Co. Inc. (1963)

(8) Boynton, R.S., "Chemistry and Technology of Lime and Limestone", 148, Interscience Publishers (1966)

(9) Staley, H.R., and Greenfeld, S.H., Ind. Eng. Chem. 41, 520 (1949)

(10) Levenspiel, O., Chemical Reaction Engineering, John Wiley & Sons, Inc., New York, 43 (1962)

(11) Ishida, M., and Wen, C.Y., A.I.Ch.E. Journal, 14, 311 (1968)

(12) Ishida, M., and Wen, C.Y., Chem. Eng. Sci., 23, 125 (1968)

(13) Howard, J.B., M.I.T. Final Report to APCO under Contract No. CPA-22-69-44: "Mathematical Model of The Reaction Between Sulfur Dioxide and Calcine Particles", (Nov. 1970)

(14) Borgwardt, R.H., "Kinetics of The Reaction of SO_2 with Calcined Limestone", Environmental Science and Technology, 4, No. 1, 59 (1970)

(15) "Fundamental Study of Fixation by Lime and Magnesia", Battelle Memorial Institute Report (June 30, 1966)

(16) Drehmel, D.C., "Test to Evaluate The Overburning of Carbonate Rocks", Paper presented at the Fourth International Symposium on Dry Limestone for SO_2 Control, Paducah, Kentucky (June 22-26, 1970)

(17) Ohno, Y., "The Direct Adsorption of CO_2 by Quicklime", Gypsum and Lime, No. 28, 22-28 (1957)

(18) TVA Fundamental Research Branch, Monthly Project Report, "Removal of Sulfur Dioxide from Stack Gases" (July, 1968)

(19) Zenz, F.A., and Othmer, D.F., Fluidization and Fluid-Particle Systems, Reinhold Publishing Corp., New York, 421-436 (1960)

(20) "Investigation of The Reactivity of Limestone and Dolomite for Capturing SO_2 from Flue Gas", Battelle Memorial Institute Report (August 30, 1968)

(21) Johnstone, H.F., Pigford, R.L., and Chapin, J.H., "Heat Transfer to Clouds of Falling Particles", Trans. A.I.Ch.E., 37, 95 (1941)

(22) Leva, M., Fluidization, McGraw-Hill Publishing Co., New York (1959)

(23) Thomas, David G., "Dry Limestone Injection: Factors Affecting The Reaction of SO_2 with Limestone Particles", Oak Ridge National Laboratory, Oak Ridge, Tennessee (August, 1970)

(24) Kato, Kunio, Hiroshi, Kubota and Wen, C.Y., "Mass Transfer in Fixed and Fluidized Beds", Chemical Engineering Symposium Series, 66, Number 105 (1970)

(25) Borgwardt, Robert H., and Harvey, Richard D., "Physical Properties of Carbonate Rocks Related to SO_2 Reactivity" (1971)

(26) Harvey, R.D., Interim Report to APCO under Contract No. CPA 22-69-65: "Petrographic and Mineralogical Characteristics of Carbonate Rocks Related to Sorption of Sulfur Oxides in Flue Gas", (June 22, 1970)

(27) McClellan, G.H., "Physical Characterization of Calcined and Sulfated Limestones", Paper presented at the Fourth Dry Limestone Process Symposium (June 22-26, 1970)

(28) Pickett, J.L., TVA Report No. 54: "Electrostatic Fly Ash Collector Performance Test - Shawnee Steam Plant Unit 10" (July 9-August 6, 1969)

(29) McDonald, W.M., TVA Report No. 62: "Electrostatic Fly Ash Collector Performance With Limestone Injection - Shawnee Steam Plant Unit 10 Precipitator A" (June 9-July 15, 1970)

(30) Brown, R.F., Research-Cottrell Inc., Final Report Technical Memorandum CES 70-1: "Determination of Bulk Electrical Resistivity Characteristics of Boiler Flue Gas Desulfurization Additives and Their Reaction Products" (Jan. 19, 1970)

(31) Attig, R.C., and Duzy, A.F., "Coal Deposition Studies and Application to Boiler Design", Vol. 31, Proceedings of the American Power Conference (1969)

(32) Barnhart, D.H., and Williams, P.C., "The Sintering Test - An Index to Ash Fouling Tendency", Transactions of the ASME (August 1956)

(33) Morris, J.S., "The Dry Limestone Injection Process for SO_2 Control - Solid Waste and Water Quality Considerations", Paper presented at the Fourth Dry Limestone Process Symposium (June 22-26, 1970)

(34) Reese, J.T., TVA Quarterly Progress Report, October-December 1970, Dry Limestone Injection Project 2438 (Feb. 19, 1971)

(35) TVA Conceptual Design and Cost Study, "Sulfur Dioxide Removal from Power Plant Stack Gas - Sorption by Limestone or Lime - Dry Process", Prepared for the National Center for Air Pollution Control (1968).

(36) Chrusciel, R. T., "Investigation of American Coal and Limestone Shipped to Energopomiar", letter report to D. T. Clay (OAP), December 14, 1970.

(37) Womble, T. D., Jr., Reese, J. T., "The Dry Limestone Injection Process For SO_2 Control", Paper presented at the Fourth International Symposium on Dry Limestone Injection Process June 22-26, 1970.

BATTELLE MEMORIAL INSTITUTE, COLUMBUS
LABORATORIES: "FUNDAMENTAL STUDY OF
SULFUR FIXATION BY LIME AND MAGNESIA",
(June 30, 1966)

APPENDIX A

THERMOCHEMICAL VALUES FOR BASIC REACTIONS IN FLUE GAS SULFUR FIXATION

REACTIONS GIVEN IN TABLES

TABLE A-1. $CaO(c) + \frac{1}{2} S_2(g) + \frac{3}{2} O_2(g) = CaSO_4(c)$

$CaO(c) + SO_2(g) + \frac{1}{2} O_2(g) = CaSO_4(c)$

TABLE A-2. $MgO(c) + \frac{1}{2} S_2(g) + \frac{3}{2} O_2(g) = MgSO_4(c)$

$MgO(c) + SO_2(g) + \frac{1}{2} O_2(g) = MgSO_4(c)$

TABLE A-3. $CaMg(CO_3)_2(c) = CaCO_3(c) + MgCO_3(c)$

$CaMg(CO_3)_2 = CaCO_3(c) + MgO(c) + CO_2(g)$

TABLE A-4. $CaSO_3(c) + \frac{1}{2} O_2(g) = CaSO_4(c)$

$CaSO_4(c) = CaS(c) + 2O_2(g)$

TABLE A-5. $MgSO_4(c) = MgS(c) + 2O_2(g)$

$MgSO_3(c) + \frac{1}{2} O_2 = MgSO_4(c)$

TABLE A-6. $MgCO_3(c) + SO_2(g) = MgSO_3(c) + CO_2(g)$

$CaCO_3(c) + SO_2(g) = CaSO_3(c) + CO_2(g)$

TABLE A-7. $CaO(c) + SO_2(g) = CaSO_3(c)$

$CaO(c) + CO_2(g) = CaCO_3(c)$

TABLE A-8. $MgO(c) + SO_2(g) = MgSO_3(c)$

$MgO(c) + CO_2(g) = MgCO_3(c)$

REACTIONS GIVEN IN TABLES
(Continued)

TABLE A-9. $MgCO_3(c) + SO_3(g) = MgSO_4(c) + CO_2(g)$

$MgCO_3(c) + SO_2(g) + \frac{1}{2} O_2(g) = MgSO_4(c) + CO_2(g)$

TABLE A-10. $CaCO_3(c) + SO_2(g) + \frac{1}{2} O_2(g) = CaSO_4(c) + CO_2(g)$

$CaCO_3(c) + SO_3(g) = CaSO_4(c) + CO_2(g)$

TABLE A-11. $\frac{1}{2} S_2(g) + O_2(g) + SO_2(g)$

$SO_3(g) = SO_2(g) + \frac{1}{2} O_2(g)$

TABLE A-12. $CaO(c) + \frac{1}{2} S_2(g) = CaS(c) + \frac{1}{2} O_2(g)$

$MgO(c) + \frac{1}{2} S_2(g) = MgS(c) + \frac{1}{2} O_2(g)$

TABLE A-13. $4C(gr) + CaSO_4(c) = CaS(c) + 4CO(g)$

$4CO(g) + CaSO_4(c) = CaS(c) + 4CO_2(g)$

TABLE A-14. $4C(gr) + MgSO_4(c) = MgS(c) + 4CO(g)$

$4CO(g) + MgSO_4(c) = MgS(c) + 4CO_2(g)$

TABLE A-15. $2CaO(c) + SiO_2(c) = Ca_2SiO_4(c)$

$CaO(c) + SiO_2 = CaSiO_3(\alpha)$

TABLE A-16. $CaO(c) + H_2O(g) = Ca(OH)_2(c)$

$MgO(c) + H_2O(g) = Mg(OH)_2(c)$

REACTIONS GIVEN IN TABLES
(Continued)

TABLE A-17. $Na_2SO_4(c) = Na_2O(c) + SO_2(g) + \frac{1}{2} O_2(g)$

$Al_2(SO_4)_3(c) = Al_2O_3(c) + 3SO_2(g) + \frac{3}{2} O_2(g)$

TABLE A-18. $FeSO_4(c) = \frac{1}{2} Fe_2O_3(c) + SO_2(g) + \frac{1}{4} O_2(g)$

$FeSO_4(c) = \frac{1}{3} Fe_3O_4(c) + SO_2(g) + \frac{1}{2} O_2(g)$

TABLE A-19. $FeSO_4(c) = FeO(c) + SO_2(g) + \frac{1}{2} O_2(g)$

TABLE A-1. THE THERMOCHEMISTRY OF SULFUR FIXATION BY CALCIUM OXIDE

Temp, F	$CaO(c)+\frac{1}{2}S_2(g)+\frac{3}{2}O_2(g)=CaSO_4(c)$[a]		$CaO(c)+SO_2(g)+\frac{1}{2}O_2(g)=CaSO_4(c)$[a]		Temp, K
	ΔF°_R, cal $mole^{-1}$	Log_{10} K	ΔF°_R, cal $mole^{-1}$	Log_{10} K	
300	-170,095	88.045	-91,036	47.122	422.2
400	-165,381	75.644	-87,291	39.926	477.8
500	-160,683	65.846	-83,566	34.245	533.3
600	-155,987	57.887	-79,843	29.630	588.9
700	-151,317	51.317	-76,154	25.827	644.4
800	-146,658	45.787	-72,464	22.623	700.0
900	-142,023	41.077	-68,816	19.904	755.6
1000	-137,421	37.026	-65,185	17.563	811.1
1100	-132,839	33.496	-61,587	15.529	866.7
1200	-128,295	30.403	-58,018	13.749	922.2
1300	-123,776	27.664	-54,476	12.175	977.8
1400	-119,298	25.231	-50,977	10.782	1033.3
1500	-114,848	23.050	-47,496	9.532	1088.9
1600	-110,443	21.091	-44,073	8.416	1144.4
1700	-106,068	19.317	-40,658	7.404	1200.0
1800	-101,734	17.707	-37,311	6.494	1255.6
1900	-97,446	16.243	-33,985	5.665	1311.1
2000	-93,192	14.902	-30,711	4.911	1366.7
2500	-72,600[b]	9.648	-14,949[b]	1.987	1644.4
3000	-53,152	6.043	-276	0.031	1922.2

(a) Data based on Appendix References (1, 7).

(b) Melting point of $CaSO_4$ = 1723 K.

TABLE A-2. THE THERMOCHEMISTRY OF SULFUR FIXATION BY MAGNESIUM OXIDE

Temp, F	$MgO(c)+SO_2(g)+\frac{1}{2}O_2(g)=MgSO_4(c)$[a]		$MgO(c)+\frac{1}{2}S_2(g)+\frac{3}{2}O_2(g)=MgSO_4(c)$[a]		Temp,
	ΔF°_R, cal $mole^{-1}$	Log_{10} K	ΔF°_R, cal $mole^{-1}$	Log_{10} K	
300	-62,020	32.103	-133,867	69.293	422.2
400	-58,245	26.641	-130,091	59.502	477.8
500	-54,488	22.329	-126,299	51.756	533.3
600	-50,733	18.827	-122,483	45.453	588.9
700	-47,003	15.941	-118,660	40.242	644.4
800	-43,271	13.509	-114,827	35.849	700.0
900	-39,571	11.445	-112,787	32.621	755.6
1000	-35,885	9.669	-108,125	29.133	811.1
1100	-32,224	8.125	-103,486	29.094	866.7
1200	-28,588	6.775	-98,874	23.431	922.2
1300	-24,973	5.581	-94,281	21.072	977.8
1400	-21,392	4.524	-89,726	18.977	1033.3
1500	-17,823	3.577	-85,181	17.096	1088.9
1600	-14,306	2.732	-80,690	15.409	1144.4
1700	-10,793	1.966	-76,203	13.878	1200.0
1800	-7,339	1.277	-71,776	12.493	1255.6
1900	-3,903	0.651	-67,370	11.229	1311.1
2000	-511	0.082	-63,007[b]	10.075	1366.7
2500	15,985	-2.114	-41,962	5.577	1644.4
3000	31,332	-3.562	-21,738	2.471	1922.2

(a) Data based on Appendix Reference (2).

(b) $MgSO_4$ decomposes at 1397 K.

TABLE A-3. THE THERMOCHEMISTRY OF DOLOMITE DISSOCIATION

Temp, F	$CaMg(CO_3)_2(c) = CaCO_3(c) + MgCO_3(c)^{(a)}$		$CaMg(CO_3)_2(c) = CaCO_3(c) + MgO(c) + CO_2(g)^{(a)}$		Temp, K
	ΔF°_R, cal mole^{-1}	$\log_{10} K$	ΔF°_R, cal mole^{-1}	$\log_{10} K$	
300	2,602	-1.347	13,021	-6.740	422.2
400	2,558	-1.170	10,670	-4.880	477.8
500	2,513	-1.030	8,337	-3.416	533.3
600	2,469	-0.916	6,019	-2.234	588.9
700	2,424	-0.822	3,722	-1.262	644.4
800	2,380	-0.743	1,442	-0.450	700.0
900	2,336	-0.676	-817	+0.236	755.6

(a) Data based on Appendix Reference (11). Data estimated by Brewer's approximation, Appendix Reference (13).

TABLE A-4. THE THERMOCHEMISTRY OF CALCIUM SULFATE AND CALCIUM SULFIDE FORMATION

Temp, F	$CaSO_3(c) + \frac{1}{2} O_2(g) = CaSO_4(c)^{(a)}$		$CaSO_4(c) = CaS(c) + 2 O_2(g)^{(b)}$		Temp, K
	ΔF°_R, cal mole^{-1}	$\log_{10} K$	ΔF°_R, cal mole^{-1}	$\log_{10} K$	
300	-52,182	27.011	191,634	-99.195	422.2
400	-50,875	23.269	186,892	-85.482	477.8
500	-49,515	20.291	182,165	-74.649	533.3
600	-48,115	17.855	177,444	-65.849	588.9
700	-46,699	15.837	172,745	-58.585	644.4
800	-45,279	14.136	168,059	-52.468	700.0
900	-44,891	12.984	163,423	-47.269	755.6
1000	-43,726	11.781	158,809	-42.789	811.1
1100	-42,620	10.747	154,172	-38.875	866.7
1200	-41,675	9.876	149,573	-35.445	922.2
1300	-40,602	9.074	144,998	-32.407	977.8
1400	-39,568	8.368	140,498	-29.715	1033.3
1500	-38,560	7.739	136,048	-27.305	1088.9
1600	-36,785	7.026	131,599	-25.131	1144.4
1700	-35,848	6.528	127,168	-23.159	1200.0
1800	-34,954	6.084	122,834	-21.380	1255.6
1900	-34,077	5.680	118,536	-19.758	1311.1
2000	-33,258	5.318	114,225	-18.265	1366.7
2500	-29,845	3.966	93,600	-12.439	1644.4
3000	-24,293	2.762			1922.2

(a) Data based on Appendix References (1-3, 6, 7, 9). Data estimated by Brewer's approximation, Appendix Reference (13).
(b) Data based on Appendix References (1, 4, 7). Data estimated by Brewer's approximation, Appendix Reference (13).
Note: Melting point of CaS = 1123 K.

TABLE A-5. THE THERMOCHEMISTRY OF MAGNESIUM SULFIDE AND MAGNESIUM SULFATE FORMATION

Temp,	$MgSO_4(c) = MgS(c) + 2\ O_2(g)$(a)		$MgSO_3(c) + \frac{1}{2} O_2 = MgSO_4(c)$(b)		Temp,
F	ΔF°_R, cal mole^{-1}	Log_{10} K	ΔF°_R, cal mole^{-1}	Log_{10} K	K
300	185,710	-96.128	-53,711	27.802	422.2
400	180,870	-82.728	-52,224	23.887	477.8
500	176,053	-72.144	-50,719	20.784	533.3
600	171,236	-63.546	-49,199	18.258	588.9
700	166,452	-56.450	-47,662	16.164	644.4
800	161,665	-50.478	-46,117	14.398	700.0
900	158,011	-45.701			755.6
1000	152,051	-40.968			811.1
1100	147,348	-37.154			866.7
1200	142,821(c)	-33.845			922.2
1300	138,172	-30.882			977.8
1400	133,565	-28.249			1033.3
1500	128,968	-25.884			1088.9
1600	124,431	-23.762			1144.4
1700	119,897	-21.835			1200.0
1800	115,426	-20.090			1255.6
1900	110,973	-18.498			1311.1
2000	106,565	-17.040			1366.7
2500	85,085	-11.308			1644.4
3000	64,589	-7.343			1922.2

(a) Data based on Appendix Reference (2).

(b) Data based on Appendix References (1-3, 9).

(c) Melting point of MgS = 923 K.

TABLE A-6. THE THERMOCHEMISTRY OF SULFUR DIOXIDE FIXATION BY CALCIUM CARBONATE AND MAGNESIUM CARBONATE

Temp,	$MgCO_3(c) + SO_2(g) = MgSO_3(c) + CO_2(g)$(a)		$CaCO_3(c) + SO_2(g) = CaSO_3(c) + CO_2(g)$(b)		Temp,
F	ΔF°_R, cal mole^{-1}	Log_{10} K	ΔF°_R, cal mole^{-1}	Log_{10} K	K
300	2,110	-1.092	-12,453	6.446	422.2
400	2,091	-0.956	-12,103	5.536	477.8
500	2,056	-0.842	-11,806	4.838	533.3
600	2,016	-0.748	-11,539	4.282	588.9
700	1,957	-0.664	-11,298	3.832	644.4
800	1,908	-0.596	-11,051	3.450	700.0
900			-9,796	2.833	755.6
1000			-9,317	2.510	811.1
1100			-8,799	2.219	866.7
1200			-8,130	1.927	922.2
1300			-7,606	1.699	977.8
1400			-7,069(c)	1.495	1033.3
1500			-6,513	1.307	1088.9
1600			-6,766	1.292	1144.4
1700			-6,177	1.125	1200.0
1800			-5,601	0.975	1255.6
1900			-5,013	0.835	1311.1
2000			-4,409	0.705	1366.7
2500			-1,131	0.150	1644.4
3000			-801	0.091	1922.2

(a) Data based on Appendix References (1-3, 7, 9).

(b) Data based on Appendix References (1-3, 6, 7, 9).

(c) $CaCO_3$ thermochemically unstable in furnace atmosphere.

TABLE A-7. THE THERMOCHEMISTRY OF CALCIUM OXIDE WITH SULFUR DIOXIDE AND CARBON DIOXIDE

Temp.	$CaO(c) + SO_2(g) = CaSO_3(c)$[(a)]		$CaO(c) + CO_2(g) = CaCO_3(c)$[(b)]		Temp.
F	ΔF°_R, cal mole^{-1}	Log_{10} K	ΔF°_R, cal mole^{-1}	Log_{10} K	K
300	-38,854	20.112	-26,401	13.666	422.2
400	-36,416	16.656	-24,313	11.120	477.8
500	-34,051	13.954	-22,245	9.116	533.3
600	-31,729	11.775	-20,190	7.492	588.9
700	-29,454	9.989	-18,156	6.157	644.4
800	-27,185	8.487	-16,134	5.037	700.0
900	-23,925	6.920	-14,129	4.086	755.6
1000	-21,459	5.782	-12,143	3.272	811.1
1100	-18,967	4.783	-10,168	2.564	866.7
1200	-16,343	3.873	-8,213	1.946	922.2
1300	-13,874	3.101	-6,268	1.401	977.8
1400	-11,409	2.413	-4,340	0.918	1033.3
1500	-8,936	1.793	-2,423	0.486	1088.9
1600	-7,289	1.392	-523	0.100	1144.4
1700	-4,810	0.876	1,367	-0.249	1200.0
1800	-2,357	0.410	3,244	-0.565	1255.6
1900	92	-0.015	5,105	-0.851	1311.1
2000	2,548	-0.407	6,957	-1.112	1366.7
2500	14,896	-1.980	16,027	-2.130	1644.4
3000	24,017	-2.731	24,818	-2.822	1922.2

(a) Data based on Appendix References (1-3, 6, 9). Data estimated by Brewer's approximation, Appendix Reference (13).
(b) Data based on Appendix References (1, 7).

TABLE A-8. THE THERMOCHEMISTRY OF MAGNESIUM OXIDE REACTING WITH SULFUR DIOXIDE AND CARBON DIOXIDE

Temp.	$MgO(c) + SO_2(g) = MgSO_3(c)$[(a)]		$MgO(c) + CO_2(g) = MgCO_3(c)$[(b)]		Temp.
F	ΔF°_R, cal mole^{-1}	Log_{10} K	ΔF°_R, cal mole^{-1}	Log_{10} K	K
300	-8,309	4.301	-10,419	5.393	422.2
400	-6,021	2.754	-8,112	3.710	477.8
500	-3,769	1.544	-5,825	2.387	533.3
600	-1,534	0.569	-3,550	1.317	588.9
700	659	-0.223	-1,298	0.440	644.4
800	2,846	-0.888	938	-0.293	700.0
900			3,153	-0.912	755.6

(a) Data based on Appendix References (1-3, 9). Data estimated by Brewer's approximation, Appendix Reference (13).
(b) Data based on Appendix References (1, 7).

TABLE A-9. THE THERMOCHEMISTRY OF MAGNESIUM CARBONATE REACTING WITH SULFUR OXIDES

Temp. F	$MgCO_3(c) + SO_3(g) = MgSO_4(c) + CO_2(g)$[(a)]		$MgCO_3(c) + SO_2(g) + \frac{1}{2} O_2(g) = MgSO_4(c) + CO_2(g)$[(b)]		Temp. K
	ΔF°_R, cal mole^{-1}	Log_{10} K	ΔF°_R, cal mole^{-1}	Log_{10} K	
300	-37,615	19.470	-51,601	26.710	422.2
400	-37,389	17.101	-50,133	22.930	477.8
500	-37,151	15.224	-48,663	19.942	533.3
600	-36,898	13.693	-47,183	17.510	588.9
700	-36,625	12.421	-45,705	15.500	644.4
800	-36,331	11.343	-44,209	13.802	700.0

(a) Data based on Appendix References (2, 7, 9).

(b) Data based on Appendix References (2, 7).

TABLE A-10. THE THERMOCHEMISTRY OF CALCIUM CARBONATE REACTING WITH SULFUR OXIDES

Temp. F	$CaCO_3(c) + SO_2(g) + \frac{1}{2} O_2(g) = CaSO_4(c) + CO_2(g)$[(a)]		$CaCO_3(c) + SO_3(g) = CaSO_4(c) + CO_2(g)$[(b)]		Temp. K
	ΔF°_R, cal mole^{-1}	Log_{10} K	ΔF°_R, cal mole^{-1}	Log_{10} K	
300	-64,635	33.457	-50,649	26.217	422.2
400	-62,978	28.805	-50,234	22.976	477.8
500	-61,321	25.129	-49,809	20.411	533.3
600	-59,654	22.138	-49,369	18.321	588.9
700	-57,997	19.669	-48,917	16.589	644.4
800	-56,330	17.586	-48,452	15.127	700.0
900	-54,687	15.817	-49,208	14.232	755.6
1000	-53,043	14.292	-47,621	12.831	811.1
1100	-51,419	12.965	-47,216	11.905	866.7
1200	-49,805	11.803	-46,955	11.127	922.2
1300	-48,208	10.775	-46,552	10.404	977.8
1400	-46,637[(c)]	9.864	-46,176[(c)]	9.766	1033.3
1500	-45,073	9.046	-45,810	9.194	1088.9
1600	-43,551	8.317	-45,462	8.682	1144.4
1700	-42,025	7.653	-45,107	8.215	1200.0
1800	-40,555	7.059	-44,782	7.794	1255.6
1900	-39,090	6.516	-44,464	7.411	1311.1
2000	-37,667	6.023	-44,216	7.070	1366.7
2500	-30,976	4.117			1644.4
3000	-25,094	2.853			1922.2

(a) Data based on Appendix References (1, 7).

(b) Data based on Appendix References (2, 7, 9).

(c) $CaCO_3$ thermochemically unstable in furnace atmosphere.

TABLE A-11. THE THERMOCHEMISTRY OF SULFUR AND OXYGEN AS GASES

Temp.	$\frac{1}{2} S_2(g) + O_2(g) = SO_2(g)$(a)		$SO_3(g) = SO_2(g) + \frac{1}{2} O_2(g)$(b)		Temp.
F	ΔF°_R, cal mole^{-1}	$\log_{10} K$	ΔF°_R, cal mole^{-1}	$\log_{10} K$	K
300	-71,942	37.239	13,986	-7.239	422.2
400	-71,928	32.899	12,744	-5.829	477.8
500	-71,879	29.455	11,512	-4.717	533.3
600	-71,805	26.647	10,285	-3.817	588.9
700	-71,689	24.313	9,080	-3.079	644.4
800	-71,562	22.342	7,878	-2.460	700.0
900	-73,216	21.176	5,479	-1.584	755.6
1000	-72,240	19.464	5,422	-1.461	811.1
1100	-71,262	17.969	4,203	-1.060	866.7
1200	-70,434	16.691	2,850	-0.675	922.2
1300	-69,460	15.524	1,656	-0.370	977.8
1400	-68,490	14.485	461	-0.098	1033.3
1500	-67,520	13.551	-737	0.148	1088.9
1600	-66,552	12.709	-1,911	0.365	1144.4
1700	-65,582	11.944	-3,082	0.561	1200.0
1800	-64,614	11.246	-4,227	0.736	1255.6
1900	-63,647	10.609	-5,374	0.896	1311.1
2000	-62,681	10.023	-6,549	1.047	1366.7
2500	-57,867	7.691			1644.4
3000	-53,070	6.034			1922.2

(a) Data based on Appendix Reference (2).

(b) Data based on Appendix References (2, 9).

TABLE A-12. THE THERMOCHEMISTRY OF CALCIUM OXIDE AND MAGNESIUM OXIDE WITH SULFUR GAS

Temp.	$CaO(c) + \frac{1}{2} S_2(g) = CaS(c) + \frac{1}{2} O_2(g)$(a)		$MgO(c) + \frac{1}{2} S_2(g) = MgS(c) + \frac{1}{2} O_2(g)$(b)		Temp.
F	ΔF°_R, cal mole^{-1}	$\log_{10} K$	ΔF°_R, cal mole^{-1}	$\log_{10} K$	K
300	21,539	-11.149	51,748	-26.786	422.2
400	21,511	-9.839	50,697	-23.188	477.8
500	21,483	-8.804	49,686	-20.361	533.3
600	21,456	-7.962	48,698	-18.072	588.9
700	21,428	-7.267	47,760	-16.197	644.4
800	21,400	-6.681	46,832	-14.621	700.0
900	21,400	-6.189	45,224	-13.080	755.6
1000	21,388	-5.763	43,926	-11.735	811.1
1100	21,333	-5.379	43,862	-11.059	866.7
1200	21,278	-5.042	43,799	-10.379	922.2
1300	21,222	-4.743	43,739	-9.776	977.8
1400	21,200	-4.484	43,683	-9.239	1033.3
1500	21,200	-4.255	43,625	-8.755	1088.9
1600	21,156	-4.040	43,573	-8.322	1144.4
1700	21,100	-3.843	43,522	-7.926	1200.0
1800	21,100	-3.673	43,473	-7.567	1255.6
1900	21,090	-3.515	43,423	-7.238	1311.1
2000	21,033	-3.363	43,373	-6.936	1366.7
2500	21,000	-2.791	43,123	-5.731	1644.4
3000	21,000	-2.388	42,851	-4.872	1922.2

(a) Data based on Appendix Reference (4).

(b) Data based on Appendix Reference (2).

Note: Melting point of CaS = 1123 K; melting point of MgS = 923 K.

TABLE A-13. THE THERMOCHEMISTRY OF THE REDUCTION OF CALCIUM SULFATE BY CARBON AND CARBON MONOXIDE

Temp,	$4C(gr) + CaSO_4(c) = CaS(c) + 4CO(g)^{(a)}$		$4CO(g) + CaSO_4(c) = CaS(c) + 4CO_2(g)^{(a)}$		Temp,
F	ΔF°_R, cal mole^{-1}	Log_{10} K	ΔF°_R, cal mole^{-1}	Log_{10} K	K
800	1,939	-0.605	-43,821	13.681	700
1700	-81,432	14.830	-42,872	7.808	1200
2600	-160,228	20.598	-39,428	5.069	1700

(a) Data based on Appendix References (2, 4, 7).

TABLE A-14. THE THERMOCHEMISTRY OF THE REDUCTION OF MAGNESIUM SULFATE BY CARBON AND CARBON MONOXIDE

Temp,	$4C(gr) + MgSO_4(c) = MgS(c) + 4CO(g)^{(a)}$		$4CO(g) + MgSO_4(c) = MgS(c) + 4CO_2(g)^{(a)}$		Temp,
F	ΔF°_R, cal mole^{-1}	Log_{10} K	ΔF°_R, cal mole^{-1}	Log_{10} K	K
800	-4,207	1.313	-50,503	15.767	700
1700	-88,299	16.081	-50,631	9.221	1200

(a) Data based on Appendix Reference (2).

TABLE A-15. THE THERMOCHEMISTRY OF FORMATION OF CALCIUM SILICATES

Temp,	$2CaO(c) + SiO_2(c) = Ca_2SiO_4$ [illegible]		$CaO(c) + SiO_2 = CaSiO_3(\alpha)^{(a)}$		Temp,
F	ΔF°_R, cal mole^{-1}	Log_{10} K	ΔF°_R, cal mole^{-1}	Log_{10} K	K
300	-30,710	15.896	-21,249	10.999	422.2
400	-30,770	14.074	-21,243	9.716	477.8
500	-30,840	12.638	-21,236	8.702	533.3
600	-30,910	11.471	-21,229	7.878	588.9
700	-30,970	10.503	-21,223	7.198	644.4
800	-31,040	9.691	-21,216	6.624	700.0
900	-31,110	8.998	-21,209	6.134	755.6
1000	-31,170	8.398	-21,203	5.713	811.1
1100	-31,240	7.877	-21,196	5.345	866.7
1200	-31,310	7.419	-21,189	5.021	922.2
1300	-31,370	7.011	-21,183	4.734	977.8
1400	-31,440	6.649	-21,176	4.479	1033.3
1500	-31,510	6.324	-21,169	4.248	1088.9
1600	-31,570	6.028	-21,163	4.041	1144.4
1700	-31,640	5.762	-21,156	3.853	1200.0
1800	-31,710	5.519	-21,149	3.681	1255.6
1900	-31,770	5.296	-21,143	3.524	1311.1
2000	-31,840	5.091	-21,136	3.380	1366.7
2500	-32,173	4.276			1644.4

(a) Data based on Appendix Reference (5).

TABLE A-16. THE THERMOCHEMISTRY OF HYDRATION OF CALCIUM OXIDE AND MAGNESIUM OXIDE

Temp.	$CaO(c) + H_2O(g) = Ca(OH)_2(c)$ (a)		$MgO(c) + H_2O(g) = Mg(OH)_2(c)$ (b)		Temp.
F	ΔF°_R, cal mole^{-1}	Log_{10} K	ΔF°_R, cal mole^{-1}	Log_{10} K	K
300	-10,882	5.633	-4,165	2.156	422.2
400	-8,956	4.096	-2,197	1.005	477.8
500	-7,061	2.894	-261	0.107	533.3
600	-5,190	1.926	1,658	-0.615	588.9
700	-3,347	1.135			644.4
800	-1,526	0.476			700.0
900	272	-0.079			755.6
1000	2,042	-0.550			811.1

(a) Data based on Appendix References (1, 7).

(b) Data based on Appendix Reference (2).

TABLE A-17. THE THERMOCHEMISTRY OF DISSOCIATION OF SODIUM SULFATE AND ALUMINUM SULFATE

Temp, F	$Na_2SO_4(c) = Na_2O(c) + SO_2(g) + \frac{1}{2}O_2(g)$ (a)		$Al_2(SO_4)_3(c) = Al_2O_3(c) + 3SO_2(g) + \frac{3}{2}O_2(g)$ (b)		Temp, K
	ΔF°_R, cal mole^{-1}	Log_{10} K	ΔF°_R, cal mole^{-1}	Log_{10} K	
300	132,791	-68.736	120,881	-62.571	422.2
400	125,436	-57.373	109,371	-50.025	477.8
500	118,081	-48.388	97,967	-40.146	533.3
600	110,719	-41.088	86,628	-32.148	599.9
700	103,365	-35.055	75,389	-25.567	644.4
800	96,010	-29.974	64,210	-20.046	700.0
900	88,655	-25.642	53,106	-15.360	755.6
1000	81,300	-21.905	42,096	-11.342	811.1
1100	73,945	-18.645	31,134	-7.851	866.7
1200	66,591	-15.781	20,261	-4.801	922.2
1300	59,236	-13.239	9,431	-2.108	977.8
1400	--	--	-1,316	0.278	1033.3

(a) Data based on Appendix Reference (1). Data estimated by Brewer's approximation, Appendix Reference (13).

(b) Data based on Appendix References (1, 7).

TABLE A-18. THE THERMOCHEMISTRY OF FERRIC SULFATE TO FERRIC OXIDE AND FERRO-FERRIC OXIDE

Temp, F	$FeSO_4(c) = \frac{1}{2}Fe_2O_3(c) + SO_2(g) + \frac{1}{4}O_2(g)$(a)		$FeSO_4(c) = \frac{1}{3}Fe_3O_4(c) + SO_2(g) + \frac{1}{2}O_2(g)$(a)		Temp, K
	ΔF°_R, cal mole^{-1}	Log_{10} K	ΔF°_R, cal mole^{-1}	Log_{10} K	
300	27,551	-14.261	34,390	-17.801	422.2
400	24,399	-11.160	30,960	-14.161	477.8
500	21,252	-8.709	27,535	-11.284	533.3
600	18,099	-6.717	24,105	-8.945	588.9
700	14,953	-5.071	20,681	-7.014	644.4
800	11,800	-3.684	17,250	-5.385	700.0
900	8,648	-2.501	13,820	-3.997	755.6
1000	5,501	-1.482	10,395	-2.801	811.1
1100	2,348	-0.592	6,965	-1.756	866.7
1200	-799	0.189	3,540	-0.839	922.2
1300	-3,951	0.883	110	-0.024	977.8
1400	-7,098	1.501	-3,315	0.701	1033.3
1500	-10,251	2.057	-6,745	1.354	1088.9
1600	-13,397	2.558	-10,169	1.942	1144.4
1700	-16,550	3.014	-13,600	2.477	1200.0
1800	-19,702	3.429	-17,030	2.964	1255.6
1900	-22,849	3.809	-20,455	3.409	1311.1
2000	-26,002	4.158	-23,885	3.819	1366.7
2500	-41,747	5.548	-41,020	5.452	1644.4
3000	-47,499	6.537	-58,160	6.612	1922.2

(a) Data based on Appendix References (1, 7). Data estimated by Brewer's approximation, Appendix Reference (13).

TABLE A-19. THE THERMOCHEMISTRY OF DISSOCIATION OF FERROUS SULFATE TO FERROUS OXIDE

Temp, F	$FeSO_4(c) = FeO(c) + SO_2(g) + \frac{1}{2}O_2(g)$(a)		Temp, K
	ΔF°_R, cal mole^{-1}	Log_{10} K	
300	55,608	-28.784	422.2
400	51,600	-23.601	477.8
500	47,600	-19.506	533.3
600	43,592	-16.177	588.9
700	39,592	-13.427	644.4
800	35,584	-11.109	700.0
900	31,476	-9.133	755.6
1000	27,576	-7.430	811.1
1100	23,569	-5.943	866.7
1200	19,568	-4.637	922.2
1300	15,560	-3.478	977.8
1400	11,560	-2.445	1033.3
1500	7,552	-1.516	1088.9
1600	3,552	-0.678	1144.4
1700	-456	0.083	1200.0

(a) Data based on Appendix References (1, 7). Data estimated by Brewer's approximation, Appendix Reference (13).

REFERENCES FOR THERMOCHEMICAL CALCULATIONS

(1) Latimer, Wendell M., Oxidation Potentials, Second Edition, Prentice Hall, Inc., New York (1952).

(2) JANAF Thermochemical Data, issued by the Dow Chemical Company, Midland, Michigan.

(3) Stull, D. R., and Sinke, G. C., Thermodynamic Properties of the Elements, American Chemical Society, Washington, D. C. (1956).

(4) Elliott, J. F., and Gleiser, M., Thermochemistry for Steel Making, Addison-Wesley, Reading, Massachusetts (1960), Vol I.

(5) Kubaschewski, O., and Evans, E. L., Metallurgical Thermochemistry, Pergamon Press, New York (1958).

(6) Maslov, P. G., "Thermodynamic Characteristics of Calcium, Gallium, Indium, and Thallium Compounds", Journal of General Chemistry of the U.S.S.R., V 29 (5), 1387-1397 (1959).

(7) Kelley, K. K., "Contributions to the Data on Theoretical Metallurgy", U. S. Bureau of Mines Bull. No. 584 (1960).

(8) Kelley, K. K., and King, E. G., "Contributions to the Data on Theoretical Metallurgy", U. S. Bureau of Mines Bull. No. 592 (1961).

(9) Coughlin, J. P., "Contributions to the Data on Theoretical Metallurgy", U. S. Bureau of Mines Bull. No. 542 (1954).

(10) Wagman, D. D., Evans, W. H., Halow, I., Parker, V. B., Bailey, S. M., and Schumm, R. H., "Selected Values of Chemical Thermodynamic Properties", National Bureau of Standards Technical Note 270-1, Superintendent of Documents, Washington, D. C., 1965.

(11) Stout, J. W., and Robie, R. A., "Heat Capacity from 11 to 300°K, Entropy, and Heat of Formation of Dolomite", J. Phy. Chem., 67, 2248-2252 (1963).

(12) Halla, F., "Note on the Thermodynamics of Formation of Dolomite", J. Phys. Chem., 69 (3), 1065 (March, 1965).

(13) Quill, L. L., Ed., The Chemistry and Metallurgy of Miscellaneous Materials: Thermodynamics, Paper 4, McGraw-Hill Book Company, Inc., New York (1950).

(14) Wicks, C. E., and Block, F. E., "Thermodynamic Properties of 65 Elements – Their Oxides, Halides, Carbides, and Nitrides", U. S. Bureau of Mines Bull. No. 605 (1963).

(15) Kelley, K. K., and Anderson, C. T., "Contributions to the Data on Theoretical Metallurgy", U. S. Bureau of Mines Bull. No. 384, 1935.

(16) Kelley, K. K., "Contributions to the Data on Theoretical Metallurgy", U. S. Bureau of Mines Bull. No. 406, 1937.

ADDENDA

Desulfurizing Action of Hydrated Lime

Since issuing this report, information has been received suggesting that $Ca(OH)_2$ is being used with considerable promise in Germany for the fixation of SO_2 in flue gas. Slaked lime had been omitted from the original calculations here because of its instability above quite moderate temperatures. However, in light of this demonstrated ability of $Ca(OH)_2$ to capture SO_2, the same sort of calculations were made for the reaction

$$Ca(OH)_2 + SO_2 \rightarrow CaSO_3 + H_2O$$

as were included initially in the report for other lime and magnesia reactions.

Table A-20 gives the results of thermochemical calculations for this reaction. The free-energy change, ΔF°_R, suggests that there is a good likelihood for the reaction to occur, but Table A-16 shows that the upper temperature limits are clearly limited. As was shown in Table A-16, $Ca(OH)_2$ is thermodynamically unstable above 849 F in steam at 1 atmosphere pressure. How rapidly this dehydration will occur is not predictable, but the calculations definitely indicate that slaked lime should have only limited usefulness except in relatively cool flue gases. In fact, data from Table A-16 show that the dissociation temperature of $Ca(OH)_2$ in flue gas will be 682 F when the flue gas contains 7.1 percent water vapor. At higher temperatures, particularly with relatively long periods of exposure, $Ca(OH)_2$ would be converted to CaO, and although the physical state of the solid might be different, it would behave thermochemically as CaO.

TABLE A-20. THE THERMOCHEMISTRY OF CALCIUM HYDROXIDE REACTING WITH SULFUR DIOXIDE TO FORM CALCIUM SULFITE AND WATER VAPOR(a)

$$Ca(OH)_2(c) + SO_2(g) \rightleftarrows CaSO_3(c) + H_2O(g)$$

Temperature, F	ΔF°_R, cal mole^{-1}	$\log_{10} K$	Temperature, K
300	-27,972	+14.478	422.2
400	-27,460	+12.559	477.8
500	-26,990	+11.060	533.3
600	-26,539	+9.848	588.9
700	-26,107	+8.853	644.4
800	-25,659	+8.010	700.0
900(b)	-24,197	+6.998	755.6
1000	-23,501	+6.332	811.1

(a) Data calculated from Tables A-7 and A-16.

(b) $Ca(OH)_2$ is thermochemically unstable above 849 F in steam at 1 atmosphere pressure.

Both compounds are extremely good desulfurizing agents if equilibrium can be approached. However, $Ca(OH)_2$ has a lower thermodynamic efficiency than an equivalent amount of CaO, as is evident from the data in Table A-21. If $Ca(OH)_2$ proves to be more effective as a desulfurizing agent than CaO, the behavior can be explained best on the basis of a more reactive physical state of CaO resulting from dehydration of $Ca(OH)_2$, not one of greater thermodynamic efficiency.

The likely reaction product of CaO or $Ca(OH)_2$ with SO_2 is $CaSO_3$. As was shown in Table A-4, $CaSO_3$ will be thermochemically reactive with the excess O_2 in flue gas to form $CaSO_4$.

TABLE A-21. COMPARISON OF CALCULATED EQUILIBRIUM CONCENTRATION OF $SO_2(g)$, ppm IN FLUE GAS, IN THE PRESENCE OF EXCESS $Ca(OH)_2$ OR CaO

Temperature, F	$Ca(OH)_2 + SO_2(g) \rightleftarrows CaSO_3(c) + H_2O$ With 7.1% H_2O in Flue Gas and Unit Activity of Solids	$CaO(c) + SO_2(g) \rightleftarrows CaSO_3(c)$ Activity of Solids Assumed to be Unity
300	2.4×10^{-10}	7.7×10^{-15}
500	2.0×10^{-8}	1.1×10^{-8}
700*	1.0×10^{-4}	1.0×10^{-4}
800*	6.9×10^{-4}	3.3×10^{-3}

*Above dissociation temperature of $Ca(OH)_2$ in flue gas.

Reliability of Calculations

A question has been raised about the reliability of these thermochemical calculations. How precisely do they define the actual equilibrium concentrations, and how reliably can the calculations be used?

The thermodynamic working Tables A-1 through A-20 were compiled and calculated from the most reliable data given in recent sources, as listed under the references given on pages A-13 and A-14. Because of the need for arithmetical consistency in this type of study, the number of significant figures in the values reported is beyond that which actually exists.

In several of the tables, high-temperature heat-capacity data were not available. In these cases, Brewer's Approximation (Reference 13) was used. Brewer's Approximation gave data comparable with that reported in Table A-1, which is based on experimental values to 2000 F. It is believed that the calculations listed in the tables can be rated as "good" for evaluating practical temperature limits of the desulfurizing action of the compounds under consideration. By estimating the limits of error for several important cases, it was concluded that the SO_2 concentration calculated at a specific temperature should not vary from the actual value by more than 10 ppm SO_2. Considering that flue gas nominally contains 2000 ppm to 3000 ppm SO_2 and that a good desulfurizer would lower the SO_2 only to 200 ppm to 300 ppm, these calculations are considered to be well within reasonable practical limits.

APPENDIX B

SUMMARY OF EXPERIMENTAL STUDIES OF SO_2 REMOVAL SYSTEMS

I. TVA (Muscle Shoals, Alabama)
Small Coal Burning Pilot Plant (1955)

A. Conditions

1. Limestones: 87.3% CaO (Pelham)
   97.5% CaO (Rockwood)

2. Limestone passed 100% through a 200-mesh screen

3. SO_2 Concentration = 2900 ppm

4. Residence time = 1 sec.

5. Exit temperature range = 1150-1370°F (no temp. profile given)

B. A plot of SO_2 removal vs stoichiometry compares very favorably with the same plots of the B & W data (Port A injection, low coal firing rates - residence time = 1.6-2.4 sec., SO_2 concentration ~3500 ppm).

C. Also tests with synthetic stack gases (N_2, CO_2, O_2)

1. Limestone requirement much higher

2. No effect of humidity

D. Best correlation between reactivity with SO_2 and physical properties was related to pore volume of 17.5 to 0.035μ pores of the calcine.

II. APCO Studies

A. Fixed Bed Sorption Unit

1. Ten limestones and dolomites (not listed)

2. -10+28 mesh particles

3. Flue gas from burning natural gas

B. Results

1. Measured in terms of time required for sorbent saturation to the "breakthrough point" (point at which 20% of sulfur passes through)

2. Samples varied from 30-150 min. in breakthrough time

3. 1600°F and 1800°F optimum temperature

4. No correlation between chemical composition and reactivity

5. Very fast reaction rate (total SO_2 removal in 0.02 sec. up to the breakthrough point)

Standard Operating Conditions:

1. 20 SCFH through 1-1/4" dia. reactor
2. SO_2 conc. in gas = 2800 ppm
3. Flue gas from methane burned at 67% excess air
4. SO_2 content of flue gas by IR

III. Bergbau-Forschung (Essen, Germany)

A. Small scale tests on non-isothermal kinetics of decarbonization reaction

B. Results on non-isothermal study

1. Calcination and SO_2 sorption occur simultaneously

2. For actual injection conditions, only 50% conversion under the best conditions

3. Limestones vary widely in reactivity

C. Small pilot plant (isothermal)

1. Coal combusted (1.5-1.8% S)

2. SO_2 conc. = 1100-1400 ppm

3. Velocity = 1-4 meters/sec.

4. Hydrated dolomites tested

   a. At 900°C, much higher desulfurization than at lower temps down to 400°C.
   b. 80% SO_2 removal at 900°C and 300% stoichiometry.
   c. SO_2 removal 20% higher with particles <60μ.
   d. Residence times longer than 1.5 to 2.0 sec. do not influence degree of SO_2 removal.

D. Concluded that incomplete utilization of sorbent due to very rapid coating of injected particle with a dense sulfate coating.

E. Small pilot plant reactor.

   1. 7 meters high; 10 cm in diameter

   2. Electrically heated

   3. Constant temperature along length of reactor.

F. Pilot plant studies proved limestone to be the best desulfurizing additive, and dolomite the poorest.

IV. Landesanstalt (Essen, Germany)

   A. Small scale studies in fixed bed reactor with 97.4% CaO limestone and 59.9% CaO dolomite

      1. Sorption increased up to 900°C (highest temperature studied).

      2. Calcined limestone exhibited considerably higher utilizations than did the uncalcined stones.

      3. Both calcined and raw limestones gave better results than the corresponding dolomite.

4. Reducing the particle size by a factor of 2 almost doubled limestone utilization

5. O_2 essential to the sorption

6. H_2O vapor tends to depress loading capacity of calcined limestones.

B. Reactor Conditions

1. Quartz tube reactor - 21.5 mm I.D. with 50-350 liter/hr flow rate.

2. Artifically-produced flue gas.

C. Results

1. Reaction with uncalcined stone began at 700°C

2. Reaction with stones calcined for 13 hrs at 1000°C started at 500°C, but only 1% of lime utilized before breakthrough. Optimum SO_2 reactivity between 800 and 900°C.

V. Resources Research Institute (Kawaguchi-Saitama, Japan)

A. Fixed bed studies

1. Optimum calcination temperature about 1000°C.

2. Optimum SO_2 sorption temperature about 900°C.

3. Rapid decline in SO_2 sorption below 700°C.

4. Small particle size important.

B. Injection Tests

1. Residence time = 3 sec.

2. SO_2 concentration = 2000-2500 ppm.

3. Little or no sorption after 1.5 sec. retention time.

4. Graph showing effect of particle size and residence time.

C. Absorbents tested

1. Limestone with diameter = 1-2 mm
2. Tablet of limestone of 100-200 mesh binded by 1-2% magnesium stearate 1-2 mm diameter
3. Tablet of limestone under 200 mesh with same binder
4. Tablet of same size formed by slaked lime with same binder
5. Limestones used were calcined in an electric furnace for 3 hrs

D. Reactor conditions

1. Silica glass reaction tube of 34 mm diameter
2. Reaction tube put in electric furnace and temperature of absorbent was kept at desired value
3. Flue gas velocity = 2800-3100 HSV (hourly space velocity) at temperature of 900°C

E. Desulfurization tests showed that desulfurization rate is proportional to $d^{-1/6}$

F. Desulfurization by $CaCO_3$ found to be inferior to that by slaked lime

VI. Steinkohlen-Elektrizitat A.G. (Essen, Germany)

A. Boiler with steam production rate of 110 tons/hr

1. Coal with 1.5% S (1.4-2.2 stoich.)

2. Injection at 1500°C, 1325°C, 1150°C, 1075°C, and 920°C

3. Optimum temperature for hydrated dolomite - 1150°C

4. Other materials used

   a. Hydrated lime (150,000 cm^2/gm)
   b. Byproduct lime (107,000 cm^2/gm)
   c. Calcined limestone (8000 cm^2/gm)
   d. Raw limestone (4000 cm^2/gm)

5. Hydrated lime most efficient - calcined lime least efficient

6. Tests showed small particles of limestone more effective

B. Electrostatic precipitator operation

C. Reactor limestone distribution studied

VII. Technical University of Stuttgart, Institute of Process Technology (Stuttgart, Germany)

A. Boiler with maximum steam output of 54 tons/hr

1. Hydrated lime deadburned badly
2. Residence time = 4-5 sec. from 1000°C to air heater
3. Better results with injection between 950° and 1000°C
4. Hydrated lime considerably more effective than hydrated dolomite
5. Better sorption with oil firing
6. Sorbent reacted with CO_2 as well as SO_2

B. Three-part program

1. Precalcined lime mixed with pulverized coal
2. Injection of dolomite and lime hydrates into a pulverized coal firing power plant
3. Injection of dolomite and lime hydrates into the same plant with coal firing

VIII. Central Research Institute of Electric Power Industry (Tokyo, Japan)

A. Pilot plant studies (oil-fired)

1. Optimum limestone injection temperature 900-1200°C
2. Removal decreased inversely with the one-fourth power of particle size
3. Limestones with $>1\%$ ferric oxide were $\sim 50\%$ more effective than those with $<0.5\%$ (oil-fired boiler)

B. Plant tests (oil-fired boiler)

1. Injection at 1100-1200°C
2. Hydrated lime superior
3. Trend indicated on graph of SO_2 removal vs stoichiometry agrees with that of B & W data
4. Boiler consumed 18.5 tons of 2.17% sulfur fuel oil/hr

IX. Wisconsin Electric Power Company (Milwaukee, Wisconsin)

A. Plant consisting of five 80-megawatt units

1. Dolomitic limestone used
2. Coal with 2.8% S and 8% ash
3. Tests run at 130% and 65% stoichiometry
4. Coal-limestone mix about 65% -200 mesh
5. ~50% removal with 135% stoich.; no appreciable removal for 65% stoich.
6. Data on effect of limestone on ash fusion temperature

X. Combustion Engineering and Detroit Edison (Detroit, Michigan)

A. Twin 325-megawatt furnace

1. Coal ~3-4% Sulfur
2. Stoichiometric amount of dolomite injected into one side
3. Over 90% of the injected dust left the boiler with fly ash rather than bottom ash
4. A little data with coal burner tilt a variable
5. Dust loading in stack gas increased about 65% as a result of dolomite injection
6. High temperature and low temperature corrosion measurements made
7. No unusual slagging tendencies although a 14% ash coal was used
8. Optimum operating conditions
    a. Dolomite injection at 106-112% stoichiometric
    b. Dolomite injection at a burner tilt of +14 degrees
    c. Coal feed at a burner tilt of -15 degrees

XI. TVA Colbert Steam Plant

A. 200 megawatt boiler

B. Static tests

1. Lumps (3/8 in.) various lime materials held in boiler for 5 minutes
2. No SO_2 sorbed below 1200°F
3. Calcined and hydrated limestones sorbed CO_2 below 1200°F
4. Very little SO_2 sorption unless calcination was complete
5. Iron oxide promoted both decarbonation and SO_2 sorption
6. Occasional deadburning in samples exposed at 1900°F

C. Injection at part stoichiometry

1. One-sixth stoich. injected by sand-blasting machine
2. Erratic injection rates and dilution of recovered sample by fly ash - not much significant data
    a. Calcined lime more effective than raw limestone
    b. $<30\%$ of material was reacted
    c. Fine particles reacted to much higher degree than coarser ones

D. Injection at full stoichiometry

   1. Limestone mixed with coal

   2. Different feed arrangements used

   3. Degree of SO_2 removal determined

      a. Stack gas analysis
      b. Solids analysis
      c. Petrographic examination of solids

   4. Results

      a. Limestone ground as easily as the coal and more of it ground to -200 mesh
      b. Slag accumulation not excessive, but unusual stringy appearance
      c. Although solids load was doubled, dust removal equipment was not overloaded

XII. Central Research Institute of Electric Power Industry (Tokyo, Japan) - Later Studies

A. Experimental Set-up

   1. Furnace with inverse U-type reaction tower

   2. Fuel oil was burned, and SO_2 level was controlled by injecting SO_2 from a cylinder

   3. Pulverized limestone injected with air

   4. SO_2 removal determined by analysis of gas at various points

   5. Gas temperatures along with oxygen and carbon dioxide levels in the gas were measured

   6. Six different limestones and two hydrated limes were utilized

B. Effect of physical conditions

  1. Reaction determined to be first-order with respect to SO_2 concentration

  2. Particle size effect

     a. Initial reaction rate increased with decreasing particle size
     b. Reaction rate for finer particle sizes of limestone reduced more rapidly with progress of the reaction

  3. Effect of injection temperature

     a. Higher reaction rate was obtained at the beginning of the reaction at higher injection temperatures
     b. Decrease of reaction rate was more rapid in cases of injection at higher temperatures

  4. Effect of limestone used

     a. Sorption efficiency of Tokunoshima Limestone (coral reef rock) was about twice that of other limestones
     b. Due to a gentle decrease of reaction rate, sorption efficiency of the hydrated lime was much higher than that of the limestones

C. Conclusions regarding reaction mechanism

  1. Diffusion of SO_2 through gas-film boundary layer on CaO particle was considered not to be the rate controlling resistance

  2. At the beginning of the SO_2 reaction, rate controlling resistance was considered to be both the diffusion and chemical reaction in the pore of the calcine particle

APPENDIX C

SHRINKING CORE MODEL DEVELOPMENT

THE RATE OF A DIFFUSION-CONTROLLED REACTION BETWEEN A GAS AND A POROUS, SOLID SPHERE--

The reaction of SO_2 with $CaCO_3$

by

Robert L. Pigford
University of California
Berkeley, California 94720

June 1971

Summary

The reaction rate is assumed to be governed by two diffusional processes: the diffusion of SO_2 through the pores, and the diffusion of SO_2 through a layer of solid reaction product which forms on the active solid surface progressively as the reaction proceeds. One or the other predominates, depending on particle size, gas composition, and temperature. The theory accounts qualitatively for the observations of Borgwardt (1970) and Coutant et al. (1970).

Introduction

One of the major sources of atmospheric pollution in the United States is the coal-fire power plant, which frequently consumes sulfur-laden fuel and produces flue gas containing a few thousand parts per million SO_2. In recent years there has been increasing interest in chemical processes for the removal of sulfur compounds from the flue gas stream. Many of these involve treatment of the effluent gas stream from the plant with alkaline liquid reagents in large scrubbers before the gas is discharged. Such processes are capable of nearly complete recovery of gaseous sulfur but the equipment may be very costly and may be hard to add to many existing power plants. A process which can be applied to existing plants involves the injection of finely powdered limestone or Dolomite into the fire box of the boiler, where the solid particles decompose, forming calcium oxide. This reacts with sulfur dioxide and with excess oxygen, forming calcium sulfite and calcium sulfate. The reaction product must be collected with the fly ash in dust collection equipment.

In the evaluation of the limestone injection processes it is necessary to know the rates of the chemical reactions between the gas and the solid in order to determine the quantity of solid required, its particle size, the temperatures at the injection point and downstream, and the time of exposure of the solid to the gas. Previous studies of the rate phenomena have led to somewhat confusing results.

Borgwardt (1970) measured the rates of reaction using beds of solid particles of CaO through which the gas passed. His times of exposure were on the order of one to two minutes, much longer than those which are of practical interest. He assumed that the heterogeneous reaction rate was governed by the speed of a chemical reaction and evaluated an apparent first-order rate constant, which he found to vary with the particle size and with the elapsed time of the reaction. Such ambiguous results are cause for caution in the application of his data.

Coutant et al. (1970) carried out a more extensive and realistic series of experiments at the Battelle Memorial Institute, in which particles of limestone particles (type 2061, screened to average size about 0.00895 cm. diameter) were injected into a current of hot gas which flowed upward through an insulated tube. By varying the height of the particle injection point various times of exposure could be obtained, from a fraction of a second to about three seconds. The particles were collected and analyzed to determine the extent to which conversion to CaO and to $CaSO_3$ and $CaSO_4$ had occurred. The gas concentration of SO_2 varied between 0.0004 and 0.009 mole fraction and the temperature between 1600 and 2148 deg. F. Interpretation of the data was attempted using an equation apparently borrowed from classical corrosion theory, according to which the quantity of sulfur picked up should be proportional to the square root of the reaction time. Thus the rate was expected to vary inversely with $t^{1/2}$, evidently because of the changes in thickness of a layer of reaction product through which SO_2 had to diffuse to reach the active reagent underneath. It was noted, however, that several of the sets of data did not follow such a relationship and it was not possible to find a systematic relationship between the "rate constants" and gas composition, temperature, or particle size. Thus, application of the data to a variety of conditions may be difficult on the basis chosen.

The idea that the rate of the reaction is governed by diffusion is an appealing one and some aspects of the Battelle data suggest that the idea may be correct. For example, at comparable times or extents of reaction the rates did not appear to vary with temperature as rapidly as would be expected from typical chemical reaction activation energies. Moreover, the plots of amount of sulfur absorbed versus time were concave toward the time axis, as in most diffusion-controlled processes in which the build-up of concentration inside the particle reduces the driving force or the accumulation of a reaction product increases the resistance. Nevertheless, the process could not be represented as an ordinary, linear diffusion problem because the rate did not seem to be proportional to the gas concentration.

A diffusion-plus-reaction mechanism which suggests itself as potentially capable of accounting for the data is one in which each particle of solid is assumed to be made up of many smaller spherical particles of solid reagent, as indicated by the sketch in Figure 1. The sulfur dioxide diffuses through the pores separating these sub-particles and reacts on their surfaces. The speed of the reaction is determined by the thickness of a solid reaction product layer which forms on the surface of each

FIGURE 1. DRAWING OF POROUS PARTICLE CONTAINING SUB-PARTICLES OF SOLID REAGENT

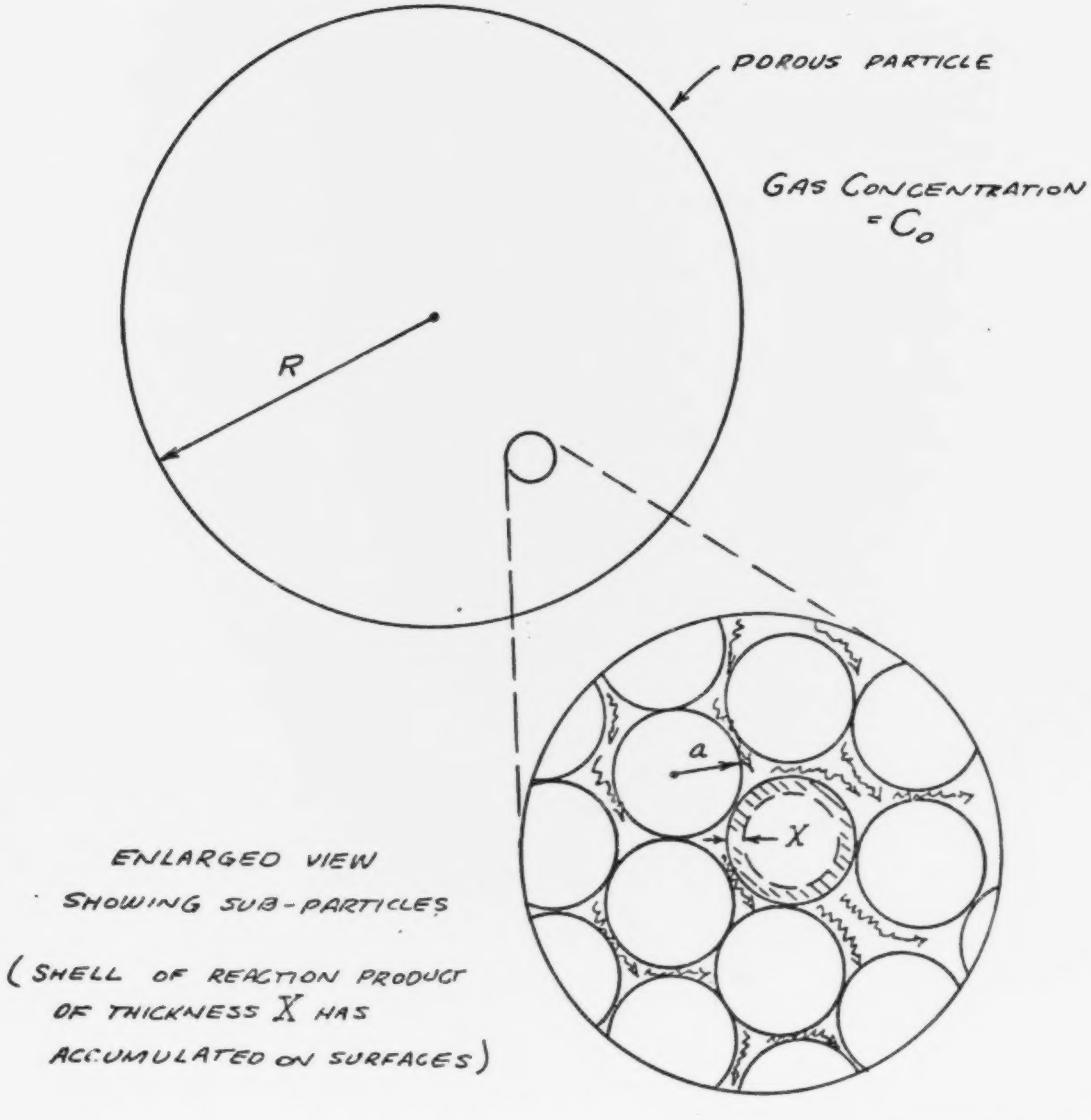
POROUS PARTICLE
GAS CONCENTRATION = C_0
R
a
X
ENLARGED VIEW SHOWING SUB-PARTICLES
(SHELL OF REACTION PRODUCT OF THICKNESS X HAS ACCUMULATED ON SURFACES)

sub-particle and by the local concentration inside the pores. The product layer thickness is, in turn, determined by the whole time history of the local concentration since it represents the accumulated product, i.e. the integral of the local reaction rate, at the particular position in the porous solid. Note that it is not necessary to assume that the SO_2 dissolves in the sulfite or sulfate layer for such a layer could easily develop cracks or fissures owing to a mismatch of solid density with the calcium oxide underneath.

Such a reaction mechanism is not wholly different from the simple one assumed by Coutant et al.; it is a logical extension of theirs, including an additional pore diffusion process which may be important if gaseous diffusion is slow, if the specific surface of the pores is large, or if the particles are large. Under these conditions the composite particles should react principally near their exterior surfaces, their interior regions being inaccessible to SO_2.

The following pages present an analysis of the proposed diffusion theory and compare its predictions with the two sets of available data.

The Theory of Diffusion Plus Reaction Between a Gas and a Porous Solid Sphere:

Consider the material balance representing the transient diffusion of a gas having concentration $C(r,t)$ through the pores of a spherical particle of radius R, reacting on the surface of the pores at a rate v per unit surface, as in Figure 1. Let the internal surface area per unit volume of the particle be S_v.

The equation which results is

$$\left(\frac{D\alpha}{\tau}\right) \frac{1}{r^2} \frac{\partial}{\partial r}\left(r^2 \frac{\partial C}{\partial r}\right) = \frac{\partial C}{\partial t} + S_v v \tag{1}$$

in which α represents the fraction by volume of pores, τ is their tortuosity, and D is the gaseous diffusivity.

The local reaction rate, v, can be computed by considering the diffusion of gaseous reactant through a spherical shell of reaction product of thickness X which forms on the surface of each sub-particle of solid reagent. We assume that such diffusion processes are always at steady state and we evaluate the diffusion flux in the following equation by multiplying the solid-phase diffusion coefficient, D_s, by the geometric-mean cross sectional area and the quotient of concentration difference by film thickness.

$$\Gamma_s \, 4\pi(a-X)^2 \left(\frac{dX}{dt}\right) = \frac{D_s}{X} 4\pi \, a(a-X) \, C(r,t) \tag{2}$$

If the gaseous reactant must dissolve in the surface of the reaction product layer we should include a Henry's Law coefficient as a factor on the right multiplying the solid diffusion coefficient; if the gas diffuses through cracks in the product layer the coefficient would be omitted. Equation (2) is an ordinary differential equation from which $X(r,t)$ can be found as a function of the sub-particle radius, a, the physical properties of the solid, and the local value of the integral of C with respect to time.

In order to find an expression for $v(r,t)$ we need to solve explicitly for X, in order to evaluate the diffusion flux into the sub-particle,

$$v(r,t) = \frac{a-X}{aX} D_s C(r,t) \tag{3}$$

It is difficult to obtain a simple expression for v except when the thickness of the product layer is small compared with the sub-particle radius, i.e. only when the fractional conversion of the solid is small. Then we may take $X \ll a$ and find

$$X^2 = (2D_s/\Gamma_s) \int_0^t C(r,p)\,dp \tag{4}$$

and

$$v(r,t) = \sqrt{\frac{D_s \Gamma_s}{2}} \frac{C(r,t)}{\sqrt{\int_0^t C(r,p)\,dp}} \tag{5}$$

Introducing this result into Equation (1), and setting $c = C/C_o$, $\theta = \beta t$, and $\xi = r/R$, we obtain

$$\nabla_{\xi}^{2} c = \left(\frac{\tau R^{2}\beta}{D\alpha}\right)\left(\frac{\partial c}{\partial \theta}\right) + \frac{S_{V}\tau R^{2}}{D\alpha C_{o}}\sqrt{\frac{D_{s}\Gamma_{s}C_{o}\beta}{2}}\;\frac{c}{\sqrt{\int_{o}^{\theta} c\,d\theta}} \qquad (6)$$

Now it is very likely that for the conditions of real interest the time-derivative term on the right will be insignificantly small, as in the classical problem of the effectiveness factor for a porous catalyst particle. We shall drop the term by assuming that $\tau R^{2}\beta/D\alpha \ll 1$, an assumption which we can justify a postiori. Now, if we choose

$$\beta = \frac{2C_{o}D^{2}\alpha^{2}}{D_{s}\Gamma_{s}S_{V}^{2}\tau^{2}R^{4}} \qquad (7)$$

our mathematical problem reduces to

$$\frac{1}{\xi^{2}}\frac{\partial}{\partial \xi}\left(\xi^{2}\frac{\partial c}{\partial \xi}\right) = \frac{c}{\sqrt{\int_{o}^{\theta} c\,d\theta}} \qquad (8)$$

with the boundary conditions

$$c(1,\theta) = 1 \; ; \; c_{\xi}(0,\theta) = o \; ; \; c(\xi,o) = 0 \qquad (9a,b,c)$$

Note that Equation (8) is not linear; as a result we can expect that the gas concentration will appear in a non-linear way in the solution. In fact, the characteristic time, β^{-1} , depends on the ratio of solid and gas molar concentrations. After we have obtained the solution, we shall want to find the instantaneous rate of passage of SO_2 across the exterior surface of the sphere, given by

$$N = \frac{\alpha D C_o}{\tau R} \left(\frac{\partial c}{\partial \xi}\right) (1,\theta) \tag{10}$$

where N(t) is the rate per unit of external surface area. Then, we shall want to compute the fraction of the total solid reagent contained in the particle which has been consumed at any time of exposure, F.

$$F = \frac{3}{R\Gamma_s(1-\alpha)} \int_0^t N dt = \gamma^{-1} \int_0^\theta c_\xi(1,p)dp \tag{11}$$

where

$$\gamma = \frac{R^2 \Gamma_s \tau(1-\alpha)}{3\, D C_o \alpha} \qquad \beta = \frac{2\, D\alpha(1-\alpha)}{3\, R^2 S_v{}^2 \tau D_s} \tag{12}$$

The solution of Equation (8) is presented in Appendix I. Table I gives a few selected values of numerical results, including instantaneous values of the dimensionless rate, $(\partial c/\partial \xi)(1,\theta)$, and the cumulative dimensionless fraction conversion $\int_0^\theta c_\xi(1,p)dp$, versus dimensionless time θ . Note that, for small θ , the instantaneous rate is very nearly proportional to $\theta^{-1/4}$ and the reaction fraction is proportional to $\theta^{3/4}$; for large θ the corresponding relationships are $\theta^{-1/2}$ and $\theta^{1/2}$, respectively. Thus, the theory provides a gradual transition from a situation at small θ , in which the reacting region of a particle is near its surface and very little SO_2 reaches the center, to a different situation at large θ in which the SO_2 is spread nearly uniformly through the pores and all the particle's interior reacts. Large θ therefore corresponds to the situation assumed by Coutant _et al_. (1970) and the calculated time dependence agrees with their assumption.

Figure 2 shows how the ratio of SO_2 concentrations at the center and the surface of the porous particle depends upon θ . Figure 3 is a plot of the instantaneous rate and Figure 4 shows the cumulative fraction reacted.

When the original expression for the rate of absorption is evaluated with the theoretical results we obtain

$$4\pi R^2 N = 13.6 \left(\alpha^{1/2} D^{1/2} D_s^{1/4} S_v^{1/2} \Gamma_s^{\frac{1}{2}} R^2 C_o^{3/4} \middle/ \tau^{1/2} t^{1/4} \right) \tag{13}$$

when pore diffusion is controlling at small θ and

$$4\pi R^2 N = 5.5 \left(D_s^{1/2} . S_v \Gamma_s^{1/2} R^3 C_o^{1/2} \Big/ t^{-/2} \right) \tag{14}$$

when the diffusional resistance of the pores is small and θ is large. Note that, depending on the time constant, β , the dependence of the rate on particle size can change from R^2 to R^3 , the effect of gas concentration from $C_o^{3/4}$ to $C_o^{1/2}$, and the effect of exposure time from $t^{-1/4}$ to $t^{-1/2}$, respectively. Moreover the effect of temperature, presumably contained in D and D_s and possibly also in S_v, can also vary. Under the assumption of small conversion which we have made the only effect of the size of the tiny sub-particles is through the specific surface as expressed by

$$S_v = 3(1-\alpha)/a$$

FIGURE 2
DEPLETION OF GASEOUS REACTANT AT THE CENTER
OF THE SPHERE OWING TO DIFFUSIONAL RESISTANCE IN THE PORES

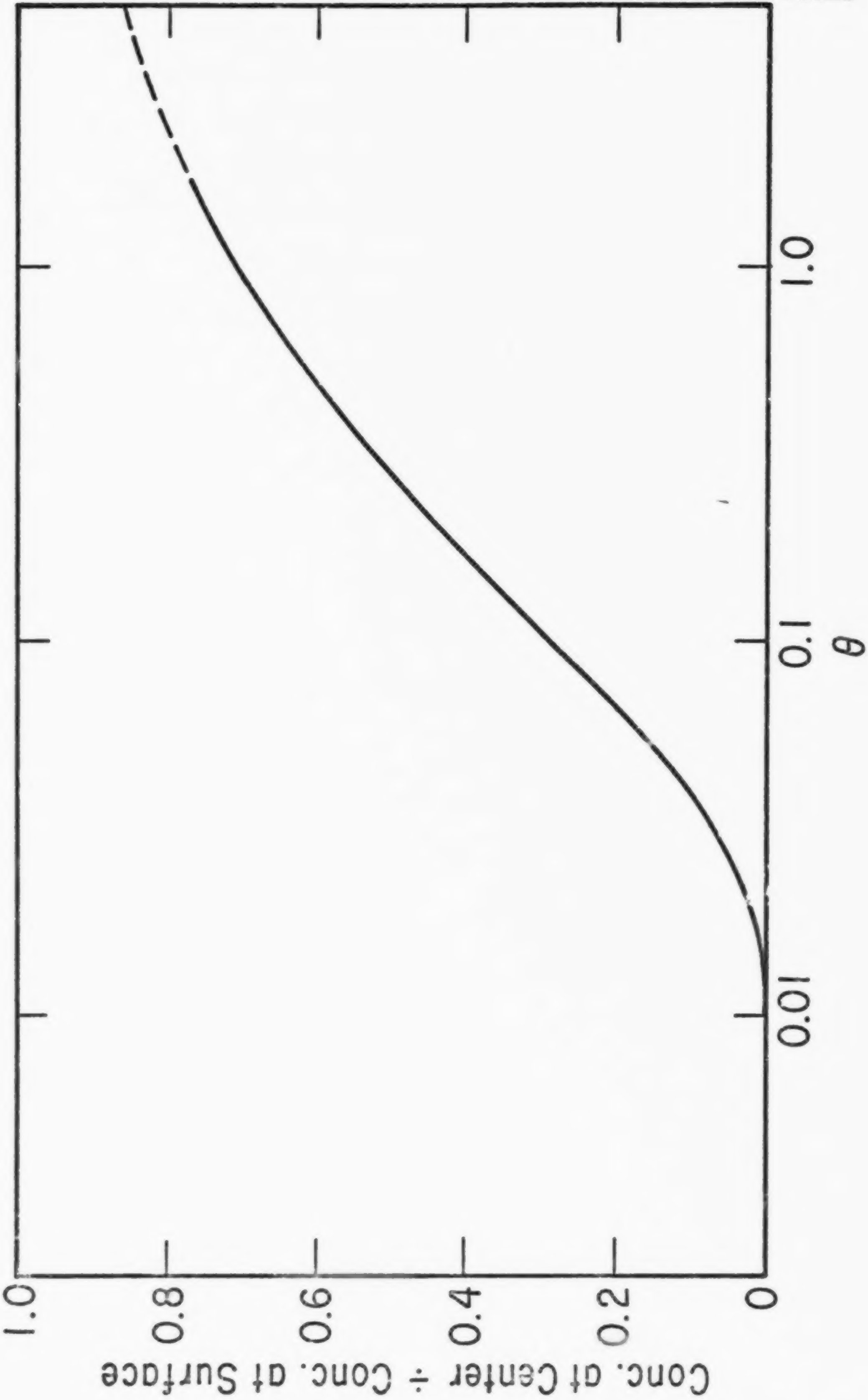

(THIS PAGE INTENTIONALLY BLANK)

(Former Figure 3--Theoretical Values of Rate of Transport Across Surface of Reacting Sphere--has been combined on following page with Figure 4.)

ENVIRONMENTAL PROTECTION AGENCY
NATIONAL AIR POLLUTION CONTROL ADMINISTRATION

Date:

Reply to
Attn of:

Subject:

To:

FIGURES 3 and 4

THEORETICAL VALUES OF RATE OF TRANSPORT ACROSS EXTERIOR SURFACE AND FRACTION CONVERSION OF SOLID, VARIATION WITH TIME OF EXPOSURE

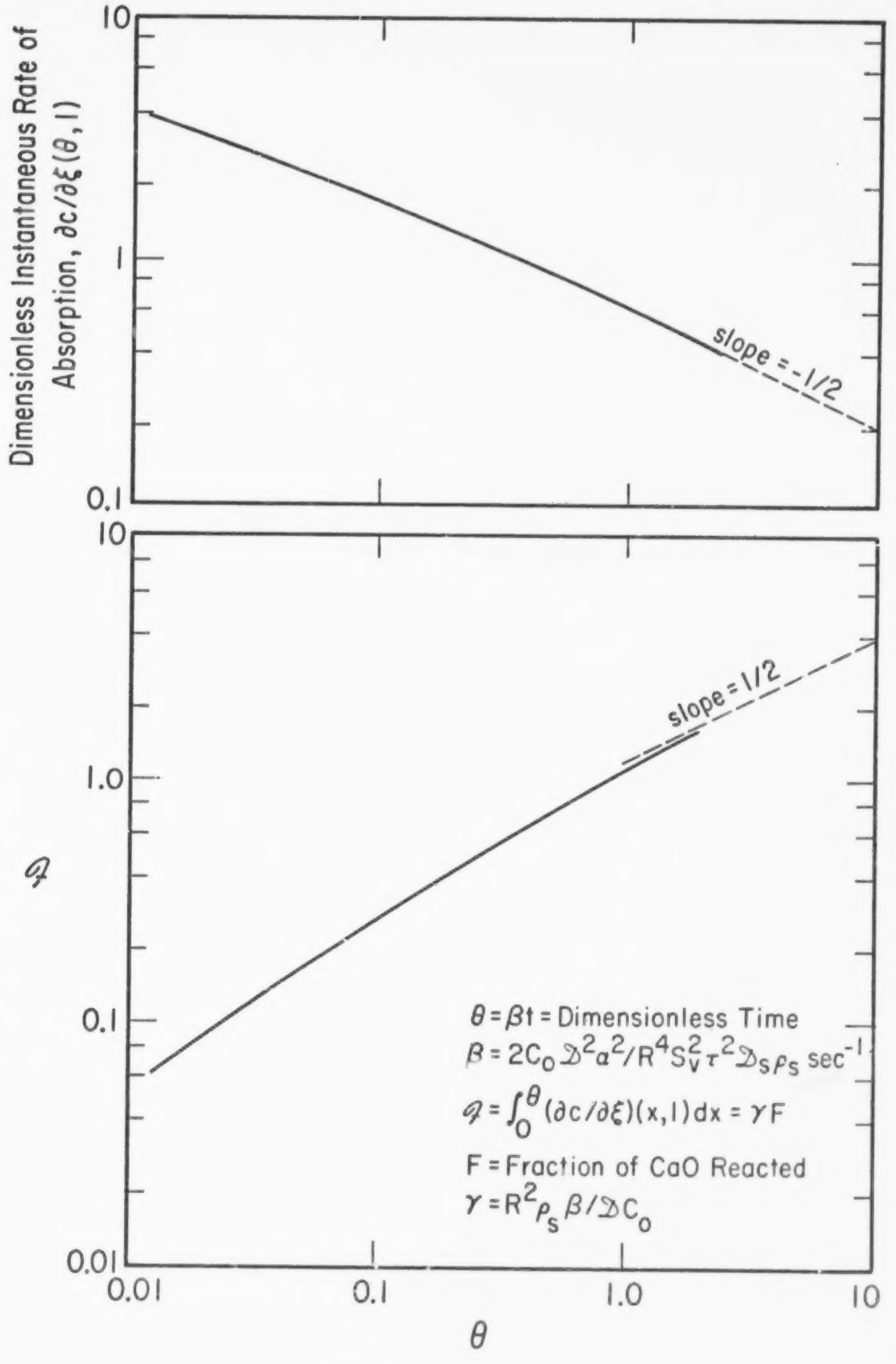

TABLE I

Numerical Values of Reaction Rate and Fraction Conversion from Diffusion Theory

$\theta=\beta t$	Dimensionless Rate			Dimensionless Total Quantity Absorbed, $\gamma F=\int_o^\theta c_\xi(1,p)dp$		
	$\frac{\partial c}{\partial \xi}(1,\theta)$	$\theta^{1/4}\ \frac{\partial c}{\partial \xi}(1,\theta)$	$\theta^{1/2}\ \frac{\partial c}{\partial \xi}(1,\theta)$	γF	$\theta^{-3/4}\gamma F$	$\theta^{-1/2}\gamma F$
0	∞	1.287		0	1.717*	
0.02	3.174	1.193		0.0879	1.65	
0.04	2.475	1.106		0.1435	1.606	
0.05	2.273	1.075		0.1683	1.592	
0.10	1.728	0.971		0.2666	1.589	
0.15	1.462	0.909		0.3447	1.430	
0.20	1.292	0.864		0.4144	1.382	
0.30	1.081	0.799		0.5322	1.310	
0.40	0.9517	0.757		0.6335	1.260	
0.50	0.8603	0.723		0.7239	1.218	
0.60	0.7911	0.696		0.8063	1.182	

TABLE I Continued

0.70	0.7362	0.673		0.8825	1.151	1.056
0.80	0.6933	0.656		0.9540	1.128	1.067
1.00	0.6244	0.624	.624	1.0855	1.085	1.085
1.2	0.5733	0.600	.628	1.205	1.050	1.100
1.5	0.5160	0.5613	.621	1.368		1.117
∞						1.188*

* By Extrapolation

Interpretation of the Data of Borgwardt (1970) and Coutant, et al. (1970):

The diffusion theory contains two combinations of physical constants, β and γ, defined in Equations(7) and (12). Each contains several quantities, such as the specific surface area and the solid diffusion coefficient, which are very difficult to estimate and which must be found from the data themselves. Note, however, that the combination β/γ contains constants that are readily accessible from independent measurement or can be estimated approximately.

$$\frac{\beta}{\gamma} = \frac{3D}{R^2}\frac{C_o}{\rho_s}\frac{\alpha}{\tau(1-\alpha)} \qquad (15)$$

Assuming that the gas diffusivity in the pores is equal to its bulk value, which varies with the 7/4 power of the absolute temperature, and taking $\alpha \sim 0.5$ and $\tau \sim 1.0$,

$$\beta/\gamma = 2.29\times10^{-4}(y/R^2)(T/273)^{3/4}\ \text{, sec.}^{-1} \qquad (16)$$

where y is the mole fraction of SO_2 in the gas, R is in cm., and T is in deg. K. Obviously if α is smaller than 0.5 and τ is larger than unity β/γ can be smaller. In the following, however, a value found from Equation (16) will be referred to as a "standard value."

The procedure for estimating the remaining parameter from the data, either β or γ, is to compute β/γ from Equation (16) (or from the same equation with a multiplying constant) and to determine β so as to minimize deviations from the theory. If βt is sufficiently small it will be possible to determine β by dividing each of the measured values of the fraction conversion, F, by $t^{3/4}$, taking an average value of the quotient, and referring to Table I to find the appropriate value of $F/\theta^{3/4}$ in the expression

$$F/t^{3/4} = \left[\theta^{-3/4}\gamma F\right] (\beta/\gamma)\beta^{-1/4} \qquad (17)$$

from which $\beta^{-1/4}$ and β can be computed. Similarly, if βt is sufficiently large, an equation like Equation (17) will give a value of $\beta^{-1/2}$. One sees that, following this procedure, the data at large values of $C_o t/R^4$, corresponding to large θ, should give a more reliable value of β and of the constants it contains, such as γ and S_v.

Note also that by choosing β/γ smaller than its "theoretical value" one can reduce the value of β to be found, causing the time dependence of the rate to be more nearly as $t^{-1/4}$ than as $t^{-1/2}$ and also changing the effects of R and C_o, as indicated in Equation (13) and (14). Thus, when data are available for various gas compositions and various particle sizes, as well as for varying times of exposure it may be possible to find best values of both γ and β when all the data are considered. In general the problem is one of non-linear curve fitting because of the changing functional behavior of the two constants, as shown in Table I.

The Effect of Particle Size on the Reaction Rate:

Figure 5 shows the data of Borgwardt (1970), plotted logarithmically as suggested by the diffusion theory. Note that the straight line drawn through the points representing the smallest particles has a slope just greater than 1/2, suggesting that for these particles there was not much difference in the SO_2 concentration at the center and at the surface and negligible diffusional resistance in the pores. The data for the largest particles, however, yields a slope approximately equal to 3/4, suggesting that these particles were large enough for their centers to be ineffective. The instantaneous rates of reaction, dF/dt, can be evaluated easily as a function of t and particle size. The results show that the rate at constant t is proportional to the -0.29 power of diameter at $t = 10$ sec. and to the -0.18 power at $t = 60$ sec. These numerical results should be associated with the intermediate particle size. The slope would be zero if all the interior of each particle were reacting equally and equal to minus one if there were major resistance to diffusion through the pores, as indicated in Equation (13) and (14). Evidently, particles about a quarter of a millimeter in diameter experience some influence of pore diffusion.

By fitting the theoretical results to the Borgwardt data, using Equation (16) to evaluate β/γ, the results shown in Table

II were obtained. The values of βt corresponding to $t = 60$ sec., the average time of exposure, show that only for the largest particles was there appreciable pore diffusion resistance. The last two columns in the table show that the derived values β and γ vary with particle radius approximately in the way expected from the theory.

Although it is possible to determine the product $S_v^2 D_s \sim 40 \text{ sec.}^{-1}$ from the empirically derived values of either β or γ, using estimated values of α and τ, neither S_v nor D_s can be determined separately. Nevertheless, if the pure guess is made that the elementary sub-particles were about 40 microns in diameter and $\alpha \sim 1/2$ and $\tau \sim 1$, D_s turns out to be about 10^{-6} cm^2/sec. Obviously this is a highly unreliable value because it is highly sensitive to the assumed value of a. If a were off by a factor of ten, D_s would be changed by a hundred.

Moreover, the values of β computed from the data are strongly affected by the assumed ratio of the true value of (β/γ) to its "nominal value" according to Equation (15). A non-linear least-squares procedure applied to the same data shows that the quality of fit of the data can be improved by taking β/γ equal to 0.11 times its nominal value, yielding smaller values of $R^4\beta$ and $S_v^2 D_s = 5000 \text{ sec.}^{-1}$, corresponding to $D_s \sim 10^{-5}$ cm^2/sec. if $a \sim 40$ microns.

The value of such highly speculative estimates lies in the possibility of attaching significance to the assumptions made in the derivations of the rate equations. Since none of the diffusivities estimated above for the penetration of the layer of product $CaSO_4$ by SO_2 are as small as expected for diffusion in the solid state it seems possible that the diffusional process in the accumulating layer of product is assisted by cracks or fissures.

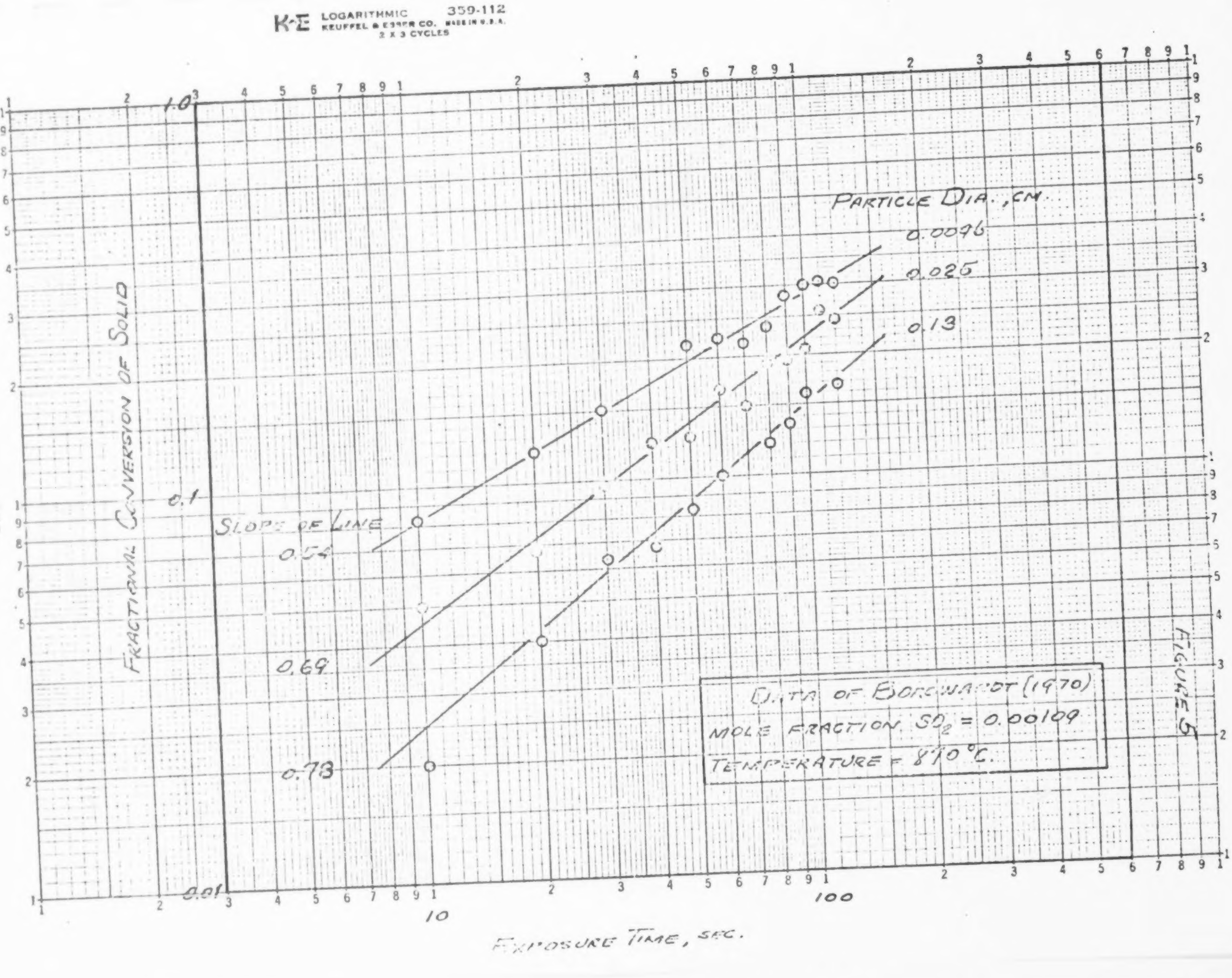
K-E LOGARITHMIC 359-112
KEUFFEL & ESSER CO. MADE IN U.S.A.
2 X 3 CYCLES
PARTICLE DIA., CM
0.0096
0.025
0.13
SLOPE OF LINE
0.54
0.69
0.78
1.0
0.1
0.01
10
100
FRACTIONAL CONVERSION OF SOLID
EXPOSURE TIME, SEC.
DATA OF BORGWARDT (1970)
MOLE FRACTION SO_2 = 0.00109
TEMPERATURE = 870 °C.

FIGURE 5

TABLE II

Values of Physical Constants Derived from Data of Borgwardt--
Effect of Particle Size

Particle	Derived Constants			βR^4	γR^2
Dia., cm.	β, sec.$^{-1}$	γ	βt at ave. t	sec.$^{-1}$ cm.^{4}	cm.^{2}
0.0036	14	156	820	$7\text{x}10^{-9}$	$3.6\text{x}10^{-3}$
0.025	0.6	48	37	$15\text{x}10^{-9}$	$7.5\text{x}10^{-3}$
0.13	$6\text{x}10^{-4}$	1.3	0.035	$11\text{x}10^{-9}$	$5.5\text{x}10^{-3}$
			averages:	$11\text{x}10^{-9}$	$4.1\text{x}10^{-3}$

If $\alpha = 1/2$, $\tau = 1$, $a = 40$ microns it follows that $D_s = 4\text{x}10^{-7}$ cm.^{2}/sec.

The Effect of Gas Concentration of SO_2 on the Reaction Rate:

The data of Coutant, et al. (1970) were taken at gas concentrations ranging from 0.0004 to 0.0095 mole fraction SO_2 and at various temperatures, although at only one value of the particle size, 0.009 cm. When the observed values of the fractional conversion of CaO are plotted logaritmically against times, as in Figure 5, it is once again possible to draw straight lines through the data, which extend from $t = 0.25$ to 3.2 sec. According to Equation (13) and (14) the logarithmic slope should vary from 0.75 if pore diffusion is limiting to 0.50 if the surface reaction rate is limiting. Table III gives values of dF/dt at 2 sec., a quantity proportional to the rate of reaction per unit mass of solid, at the four different gas compositions. It is seen that the slopes are very nearly within the range expected. The values imply that the reaction rate is small enough at the lowest concentration that pore diffusion easily keeps the interior of the particles fully supplied with the gaseous reactant, while, at the highest concentration pore diffusion is limiting. Figure 6 shows a plot of the slopes against the gas mole fraction. The straight line through the data has a slope of 0.64, nearly half way between the possible extremes expected, indicating that, at least at the intermediate concentrations, the data are in a transition region between limiting pore diffusion and uniform surface rate.

Values of β and γ derived from the Coutant data are listed in Table IV, which shows that β is nearly proportional

TABLE III

Effect of Gas Composition on the Slope of log F vs. log t ; data of Coutant *et al.* (1970) at T = 1700 deg. F., particles 0.009 cm. diameter

Mole Fraction SO_2 in Gas	d log F/d log t
0.0004	0.49
0.00302	0.68
0.00748	0.74
0.00954	0.75

FIGURE 6

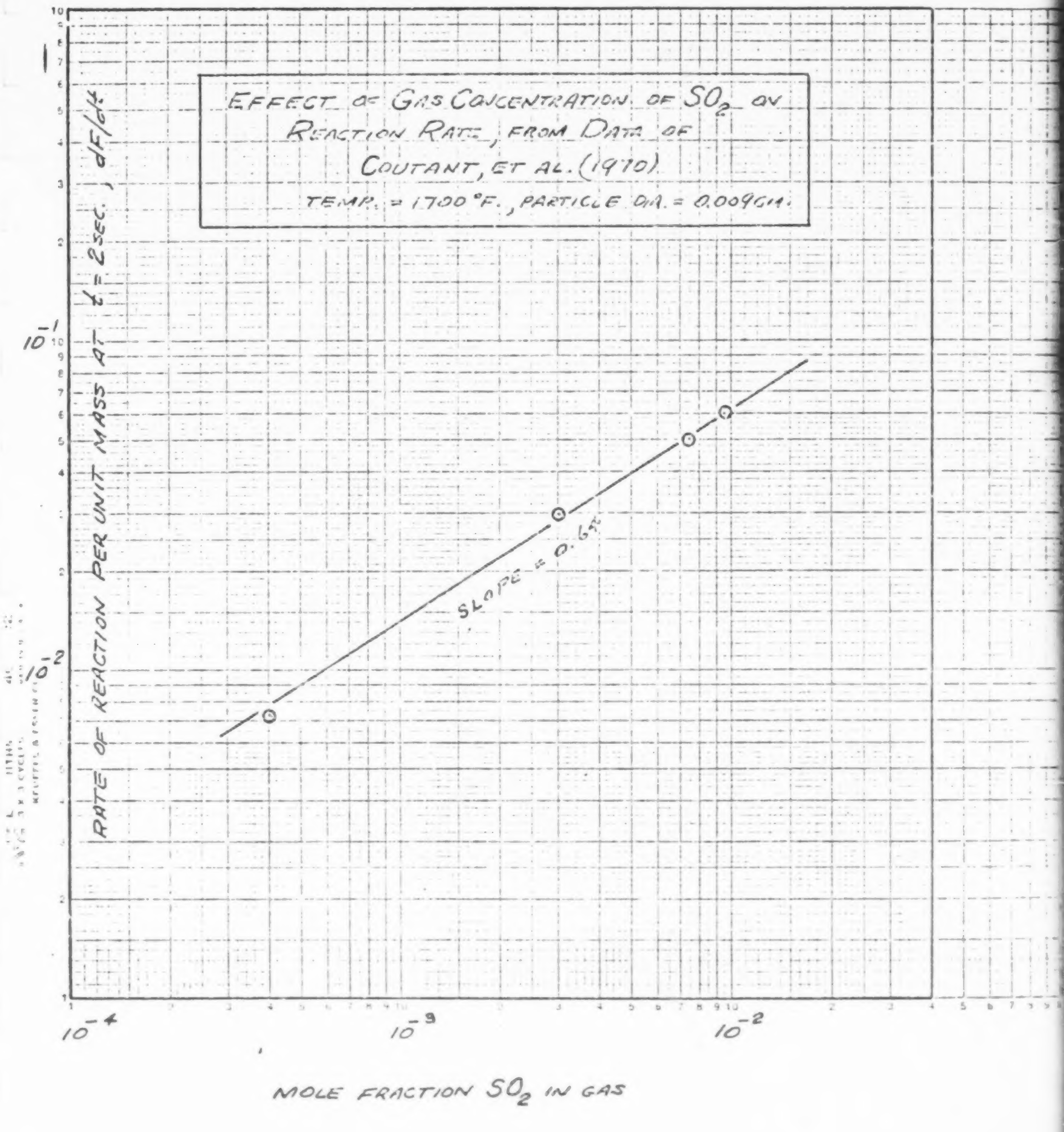
EFFECT OF GAS CONCENTRATION OF SO_2 ON
REACTION RATE, FROM DATA OF
COUTANT, ET AL. (1970)
TEMP. = 1700 °F., PARTICLE DIA. = 0.009 CM.
SLOPE = 0.65
RATE OF REACTION PER UNIT MASS AT t = 2 SEC., dF/dt
10^{-1}
10^{-2}
10^{-4}
10^{-3}
10^{-2}
MOLE FRACTION SO_2 IN GAS

TABLE IV

Values of Physical-Constant Groups, β and γ, Derived from Data of Coutant, *et al.*(Battelle)

Mole Fraction SO_2 in Gas	Gas Temp.,°F	β, $sec.^{-1}$	β/y	γ	βt_{av}
A. Effect of Gas Composition:					
0.0004	1692	0.32	800	23	0.55
0.00302	1692	6.0	2000	58	8.2
0.00748	1690	12.3	1600	48	19.7
0.00954	1703	16.2	1700	49	25.8
		ave. =	1500	45	
B. Effect of Temperature:					
0.00303	1600	8.2		81	
0.00302	1692	6.0		58	
0.00277	1845	2.5		25	
0.00305	2041	3.3		28	
0.00302	2109	6.9		57	
0.00306	2148	16		130	

to y , as expected from the theory. One exception is the point at the smallest value of y , at which the determination of β is least accurate. If the average value of β/γ is used, as before, to find an apparent value of $S_v^2D_s$, assuming $\alpha = 1/2$ and $\tau = 1$, the result is 190 sec.$^{-1}$, which is remarkably close to the value from the data of Borgwardt. Once again, as with the previously considered data, it is statistically possible to improve the quality of the comparison between theory and data concerning gas composition by choosing a value of (β/γ) equal to about 0.1 times the "nominal value." The result is that the values of β are reduced below those listed in Table IV and the time dependence of the observed conversion is matched much better. When the apparent value of $S_v^2D_s$ is computed from the results of the non-linear least squares procedure one obtains $S_v^2D_s$ 3 x 10^4 sec.$^{-1}$, which is substantially greater than the apparent value obtained from the Borgwardt data. Note, however, that the data of Coutant et al. were obtained in an experiment in which limestone particles were injected into the hot gas containing SO_2 whereas Borgwardt used limestone that had already been calcined to CaO. Thus, in the experiments which lead to the larger apparent value of $S_v^2D_s$, CO_2 evolution occurred simultaneously with SO_2 absorption.

Figure 7 shows a comparison of the measured values of the fraction of CaO converted versus time, based on the data of Coutant et al. at 1700 deg. F. and 2R = 0.009 cm., and theoretical lines based on the diffusion theory. The two parameters, β and γ , were adjusted to obtain the best fit of the data while

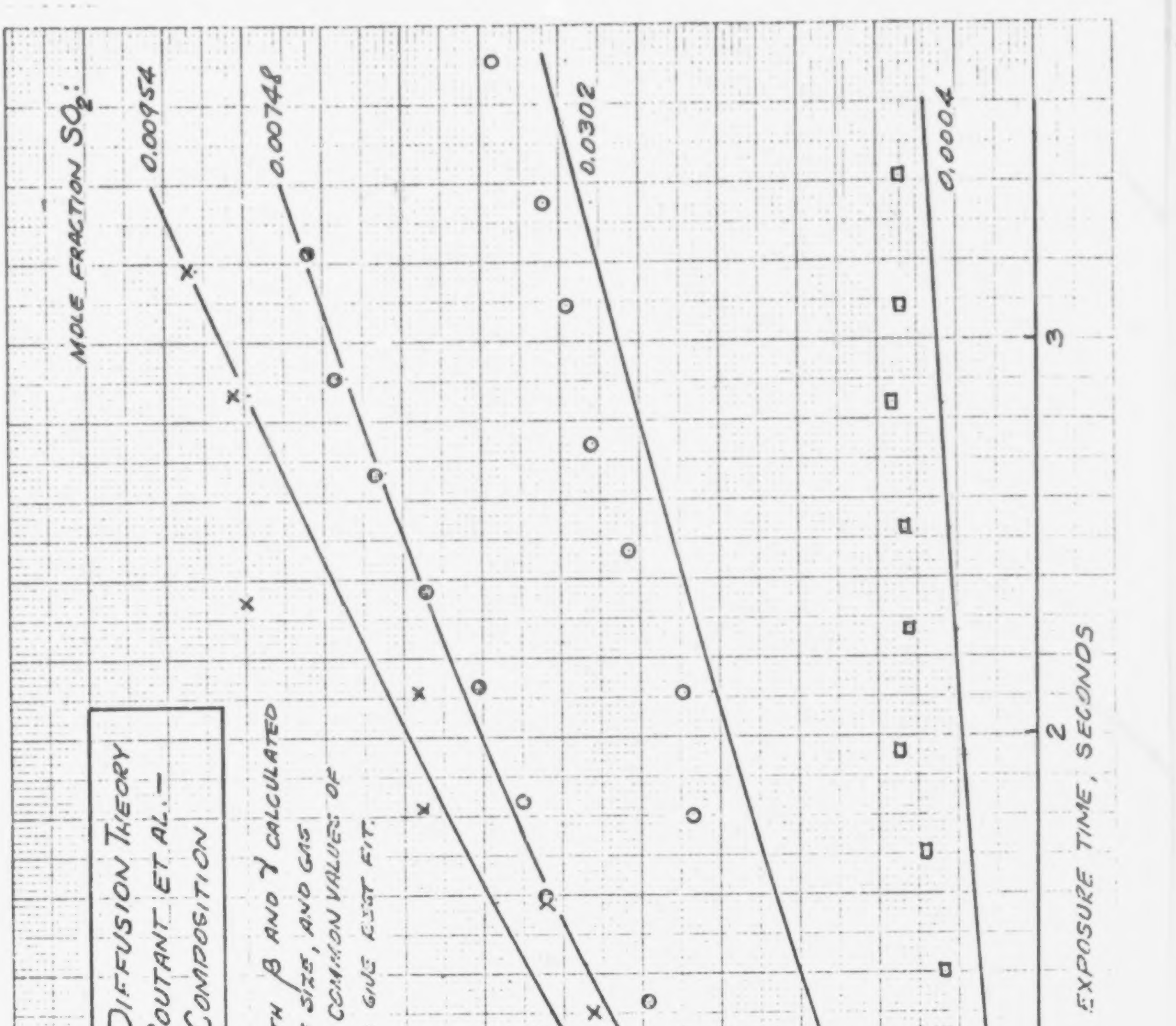

COMPARISON OF DIFFUSION THEORY WITH DATA OF COUTANT ET AL. — EFFECT OF COMPOSITION

LINES SHOW THEORY WITH β AND γ CALCULATED FROM TEMP., PARTICLE SIZE, AND GAS COMPOSITION USING COMMON VALUES OF OTHER PROPERTIES TO GIVE BEST FIT.

SQUARE 10 X 10 TO THE HALF INCH
GRAPHIC CONTROLS CORPORATION Buffalo, New York

maintaining the dependence of these quantities on particle size and gas concentration computed in the theory. The parameters used corresponded to (β/γ) equal to 0.12 times its nominal value and $\beta/y = 11$ sec.$^{-1}$. The smaller value of (β/γ) can easily be accounted for by a pore diffusion coefficient smaller than the bulk-gas value and tortuosity in the diffusion channels. One sees from the figure that the theory is capable of accounting for effects of composition and time on the conversion in these experiments.

The Effect of Temperature on the Reaction Rate:

Table IV shows some values of β and γ computed from data of Coutant *et al*. in which the particle size and the gas composition were held constant and the gas temperature was varied. One expects that an increase in temperature will decrease β because of the probably greater increase in D_s than in D^2C_o; similar changes should also occur in γ. The table shows, however, that both β and γ go through a minimum at a temperature of about 1845 deg. F., corresponding to the observed maximum reaction rate at this temperature. The increase in the parameters at higher temperature may be owing to sintering of the particles and a resulting decrease in S_v.

Conclusions:

The good qualitative agreement of the theory with data expressing the effects of particle size and gas concentration and the rough agreement of apparent values of physical constants with accepted ranges indicate that the pore-diffusion theory is capable of accounting for the main features of the reaction of gaseous SO_2 with porous limestone particles. The theory is not exact, however, and ought not to be used as a substitute for experiment. It can be used for estimates of the effects of changes in the particle size, the gas composition, and temperature in a narrow range on the rate of absorption of SO_2 for adjustment of experimental data. Thus, with the theory available, costly experimentation may be reduced, if not eliminated, and data taken under idealized laboratory conditions can be applied to the design of practical recovery systems.

References:

Borgwardt, R. H., Environmental Science and Technology, 4, (1970)

Coutant, R. W., Barrett, E. E., Simon, R., Campbell, B. E., and Lougher, E. H., "Investigation of the Reactivity of Limestone and Dolomite for Capturing SO_2 from Flue Gas," Battelle Memorial Institute, Columbus, Ohio, November 20, 1970.

Acknowledgement:

Assistance from technical discussions with L. Scotti and J. Bellott formerly of the M.W. Kellogg Company and with L. Hegedus is gratefully acknowledged. W. Tang assisted with the computations.

Appendix

Solution of the Differential Equation for Diffusion and Reaction

We wish to find the solution of the problem

$$\frac{1}{\xi^2}\frac{\partial}{\partial \xi}\xi^2\frac{\partial c}{\partial \xi} = \frac{c}{\sqrt{\int_0^{\theta} c(\xi,p)dp}} \qquad \text{(A-1)}$$

with the boundary conditions

$$c(\xi,0) = 0 \ , \ c(1,\theta) = 1 \ , \ c_{\xi}(0,\theta) = 0$$

$$\text{(A-2,a,b,c)}$$

If we let

$$u^2(\xi,\theta) = \xi \int_0^{\theta} c(\xi,p)dp \qquad \text{(A-3)}$$

we find that Equation (A-1) becomes the third-order equation

$$\frac{\partial}{\partial \theta}\left(\frac{\partial^2 u^2}{\partial \xi^2} - 2\xi^{1/2}\,u\right) = 0 \qquad \text{(A-4)}$$

(Note that $\xi^{1/2}\,u\,(\xi,\theta)$ is proportional to the thickness of the product layer, X .) Integrating Equation (A-4) with respect to time,

$$\frac{\partial^2 u^2}{\partial \xi^2} - 2\xi^{1/2} u = o; \; u(\xi,o) = o; \; u(1,\theta) = \theta^{1/2} \qquad \text{(A-5)}$$

Let

$$u^2(\xi,\theta) = \theta \, F^2(\xi,\theta)$$

so that

$$F(\xi,\theta) = (\xi/\theta) \int_o^\theta c(\xi,p)\,dp$$

(Note that this relationship makes $F(o,\theta) = o$.) The problem is now reduced to

$$\frac{\partial^2 F^2}{\partial \xi^2} - 2(F^2\xi,\theta)^{1/2} = o; \; F(o,\theta) = o; \; F(1,\theta) = 1 \qquad \text{(A-6)}$$

A numerical solution is possible as follows.

Obviously F depends on both ξ and θ, but one can start the integration of Equation (A-6) in the ξ- direction to obtain F vs. ξatθfixed θ. The integration begins at $\xi = o$, where $F = o$, regardless of θ, and continues to $\xi = 1$ where $F = 1$, regardless of θ. At intermediate points F depends on θ. To begin the integration one must supply a value of $\partial F/\partial \xi(o,\theta)$, say b ($\theta$). The correct value of c is the one that yields $F(1,\theta) = 1$.Near $\xi = o$, $F = \xi b(\theta)$ and

$$b(\theta) = \frac{1}{\theta} \int_o^\theta c(o,p)\,dp \qquad \text{(A-7)}$$

from which the concentration of the gaseous reagent at the center of the porous sphere can be found.

Nomenclature:

a	radius of sub-particle of solid reagent
C	concentration of reactant gas inside porous particle, mole/volume; subscript o refers to gas outside porous sphere
D	Diffusion coefficient of gaseous reactant in pores
D_s	diffusivity of SO_2 through solid product shell
F	dimensionless fraction conversion, equal to γF
F	fraction conversion of solid reagent in porous particle
N	rate of absorption of gaseous reagent per unit exterior surface of porous particle
r	radius in porous particle
R	radius of porous solid particle
S_v	surface area for reaction per unit volume of large particle
t	time following first exposure of porous particle to gas
T	gas temperature, deg. K.
v	reaction rate on interior surface of porous particle, moles/(sec)(sq.cm.)
X	thickness of solid product shell
y	mole fraction SO_2 in gas outside porous sphere

Greek Letters

α	fraction by volume of pores in large particle
β	time constant defined in Equation (7)
γ	combination of physical constants defined in Equation (12), used for expressing the fraction conversion of the solid reagent
Γ_s	molar concentration of solid reagent, moles/cc

θ	dimensionless time, equal to βt
ξ	dimensionless radial distance in porous sphere
τ	tortuosity of pores